UNIVERSITY OF DEBRECEN
Faculty of Engineering
Department of Mechanical Engineering

PROCEEDINGS OF THE 3rd INTERNATIONAL SCIENTIFIC CONFERENCE ON ADVANCES IN MECHANICAL ENGINEERING (ISCAME 2015)

19 November, 2015 Debrecen, Hungary

organized by

Department of Mechanical Engineering
Faculty of Engineering, University of Debrecen

and

Working Commission in Mechanical Engineering
Specialized Committee in Engineering
Regional Committee in Debrecen, Hungarian Academy of Sciences

PROCEEDINGS OF THE
3rd INTERNATIONAL SCIENTIFIC CONFERENCE ON
ADVANCES IN MECHANICAL ENGINEERING

Edited by **Sándor BODZÁS PhD**
Tamás MANKOVITS PhD

Publisher: **Department of Mechanical Engineering**
Faculty of Engineering
University of Debrecen
2-4 Ótemető str. Debrecen, Hungary
Phone: +36 52 415 155
Web page: www.eng.unideb.hu/gepesz

ISBN 978-963-473-917-3

PROCEEDINGS

3rd INTERNATIONAL SCIENTIFIC CONFERENCE ON ADVANCES IN MECHANICAL ENGINEERING (ISCAME 2015)

19 November, 2015 Debrecen, Hungary

Organizational Chairman of the ISCAME 2015

Tamás MANKOVITS PhD, University of Debrecen, HU
tamas.mankovits@eng.unideb.hu

Scientific Program Committee

István BUDAI PhD, University of Debrecen, HU
Sándor BODZÁS PhD, University of Debrecen, HU
Lajos FAZEKAS PhD, University of Debrecen, HU
Ferenc KALMÁR PhD, University of Debrecen, HU
Sándor PÁLINKÁS PhD, University of Debrecen, HU
Istvánné RÁTHY PhD, University of Debrecen, HU
Edit SZŰCS PhD, University of Debrecen, HU
Zsolt TIBA PhD, University of Debrecen, HU
János TÓTH PhD, University of Debrecen, HU
László TÓTH DSc, University of Debrecen, HU

Technical Assistance

Judit BAK, University of Debrecen, HU

CONTENTS

INTERNATIONAL SCIENTIFIC CONFERENCE ON ADVANCES IN MECHANICAL ENGINEERING

19 November 2015, Debrecen, Hungary

OPTIMIZATION OF SURFACE COOLING SYSTEMS WITH PHASE CHANGE MATERIAL ENERGY STOREING

ANDRÁSSY Zoltán, FARKAS Rita

Faculty of Mechanical Engineering, Budapest University of Technology and Economics
E-mail: zolee92@gmail.com, f.rita33@gmail.com

Abstract
In our paper we present phase change materials, as effective thermal energy storage due to their great latent heat storing possibility. We investigate a ceiling cooling system combined with phase change materials in an office environment with the aim of saving energy, lowering temperature oscillation and increasing inner thermal comfort. We discuss the thermal modelling of these materials and using of simulations we optimize the operation of the combined system. We present many different ways to lower the energy usage of offices, for example with lowering the mass flow in cooling pipes, or rearranging the operation time of refrigerator system. We also demonstrate an ANSYS Fluent CFD simulation which can validate our thermal model. To prove our results we built an experimental system, a miniature adiabatic room. With the measurement of temperature in different points inside the room we could get acquainted with the operation of the system in practice, and we could validate our models. We could specify the optimal properties of the phase change material which could be paired to the surface cooling system.

Keywords: *phase change material, thermal energy storage, surface cooling system, energy effectiveness*

1. INTRODUCTION

Phase change materials (PCM) are materials used for storing heat energy. To do that these materials use latent heat in the storing process, so PCMs store heat with higher density and release it, when it is necessary. The biggest advantage of these materials is storing huge amount of heat energy with low temperature difference, saving energy and space [1-3].
The most commonly used material for thermal energy storing purposes is water, let's see a quick example why an average PCM is better than water. Changing the temperature of 1 m^3 water with 10 °C, 42 MJ/m^3 energy could be stored. With an average PCM (latent heat capacity: 200-250 kJ/kg, density: 800 kg/m^3) just with the use of its latent heat capacity, so without changing its temperature 160-200 MJ/m^3 thermal energy could be stored. It means smaller storage space volumes.
Phase change materials has many advantages and disadvantages as well, it could be seen below.
Advantages:

- high density thermal energy storing capabilities,
- can lower heat oscillation,
- wide range of melting temperatures,
- simple storage,
- cheap (in material).

Disadvantages:

- thermodynamic properties are function of time and temperature,
- low heat conductivity,
- density change when changing phase,

- degradation after many cycles,
- supercooling,
- phase segregation,
- could be reactive, corrosive, flammable.

We used two types of PCMs in our research, BioPCM and savE® HS 22. Due to lack of material properties, we had to measure the heat capacity, the density and the heat conductivity of the materials, the results can be seen in *Table 1*. Column 4 contains the average properties of savE® materials. BioPCM was not appropriate for our system, and the melting temperature of savE® HS 22 was not suitable for cooling issues, but for the measurements we used this material with the change of operating conditions of the system. The average material was used for optimization issues.

Table 1 Properties of used PCMs

	BioPCM	savE® HS 22	avg. savE® PCM
Solidification temperature [°C]	19	22	
Melting temperature [°C]	23	25	
Latent heat of melting [kJ/kg]	160,7	185,0	185,0
Specific heat in solid phase [kJ/kg K]	2,37	2,5	2,4
Specific heat in liquid phase [kJ/kg K]	3,34	3,06	3,0
Density in solid phase [kg/m^3]	849,4	1840	1600
Density in liquid phase [kg/m^3]	834,7	1540	1500
Heat conductivity in solid phase [W/m K]	0,18	0,54	0,6
Heat conductivity in liquid phase [W/m K]	0,18	1,09	1

In our research we investigated the combination of PCMs with a ceiling cooling system (*Figure 4*). With surface cooling systems due to the low temperature of surfaces and the even distribution of temperature the heat transmission with radiation can grant pleasant inner heat comfort. Our goal is to lower the energy usage, lower the peak cooling needs and to improve inner heat comfort.

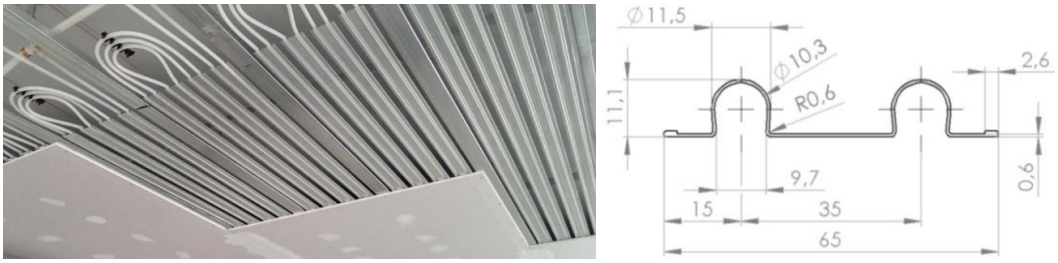

Figure 4 Ceiling cooling system [4]

2. METHODS

2.1 Thermodynamic model

We have not found similar problem solution methods in the technical literature, so we made up our own thermodynamic model. The problem could be modelled separately in 4 subsystems, could be solved separately and joined through others boundary conditions. The 4 subsystems:

- phase change material,
- ceiling cooling system,
- heat radiation inside the examined room,
- heat generation and heat loss of the examined room.

Due to page constraints we just present the essential parts of the model.
The modelling of PCM can be seen in our other article for the conference.
The modelling of ceiling cooling system consists of the calculations of the water temperature along the cooling pipes, the rib effect of the metal panel, the heat transfer to the PCM and the room. The temperature along the cooling pipes could be calculated from the following energy differential equation:

$$\dot{m}_w c_{p,w} T_w - \dot{m}_w c_{p,w} \left(T_w + \frac{\partial T_w}{\partial x} \Delta x \right) = k_{panel} K \Delta x \left(T_w - T_{panel} \right) + V_{pipe} c_{p,pipe} \frac{\partial T_{pipe}}{\partial \tau}, \quad (1)$$

where $\dot{m}$ is the mass flow, c_p is the specific heat, T is the temperature, x is the length size coordinate, k is the heat transfer coefficient, K is the perimeter, V is the volume and τ is the time, index w stands for water, index *panel* for the cooling panel and index *pipe* for the cooling pipe.
Without the deduction and using the definition of NTU, the temperature along the cooling pipes:

$$T_w{}^n = T_w{}^{n-1} - (T_w{}^{n-1} - T_{panel}{}^{n-1}) \cdot (1 - e^{-NTU}), \quad (2)$$

where index n is the n^{th} time step.
To model heat radiation properly we divided the walls into smaller surfaces and used the following equation to calculate the heat radiation between every surfaces using a matrix structure:

$$d\dot{Q}_{1,2} = \sigma_0 \cdot \varepsilon_1 \cdot \varepsilon_2 \cdot \frac{1}{\pi} \cdot \cos\gamma_1 \cdot \cos\gamma_2 \cdot \frac{A_1 \cdot A_2}{S^2} \cdot (T_1^4 - T_2^4), \quad (3)$$

where $\dot{Q}$ is the heat radiation performance, σ_0 is the Stefan Boltzman constant, ε is the emissivity, and the geometry dependent factors can be seen on *Figure 5*.

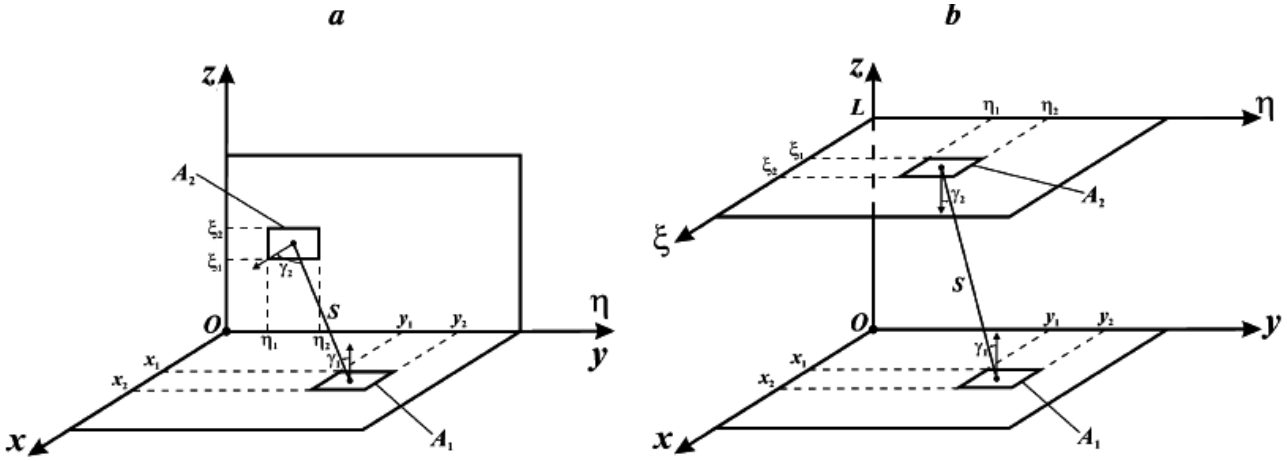

Figure 5 Geometry dependent factors of heat radiation

To model heat generation and heat loss we used different profiles for inner heat gain (*Figure 6*) and ambient temperature (*Figure 7*) in the function of time during a day.

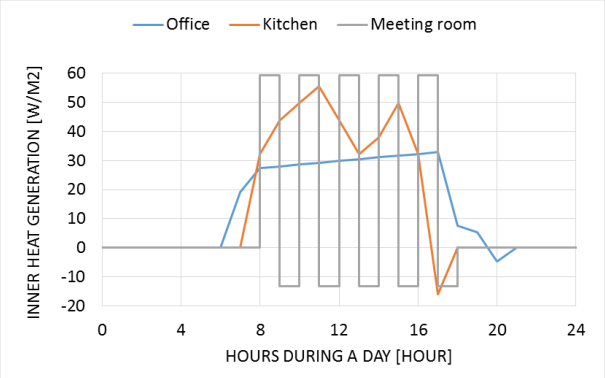

Figure 6 Inner heat generation

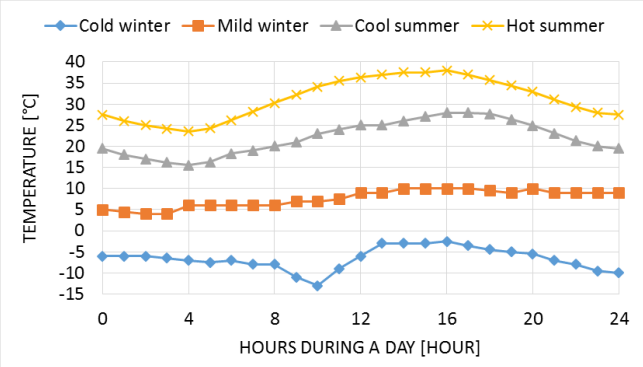

Figure 7 Ambient temperature

2.2 CFD model

To examine the system on a smaller scale and to validate the thermodynamic model we made a CFD model. The geometry can be seen on *Figure 8*. From top to bottom it consists of the PCM layer placed onto the surface cooling panel, under a gypsum board can be seen and at the bottom the air of the simulated room. The mesh can be seen on *Figure 9*, a fine mesh is needed to model the heat transfer and the difficult geometry properly. After mesh independence study we optimized the used models in ANSYS FLUENT. We used Realizable k-epsilon turbulence model with enchanced wall function and full Bouyancy effect. With the CFD simulation we could define some values that could not be defined with the measurement and the thermodynamic model. For example we could model the surface heat transfer coefficient inside the PCM and on the border of the air and the gypsum layer.

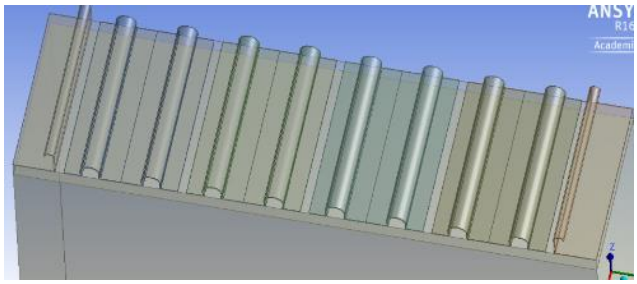

Figure 8 Geometry of CFD model

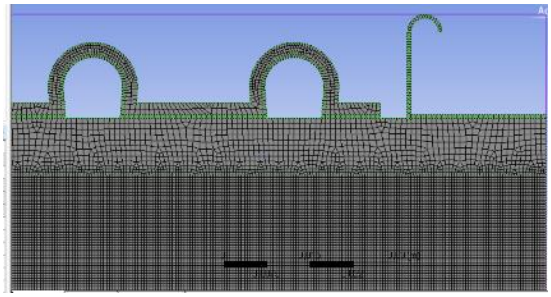

Figure 9 Mesh of CFD model

2.3 Experimental system

To validate our models and to see the processes in practice we built an experimental system. It is a good insulated (12 mm polystyrene) 1x0,8x0,7 meter adiabatic box with the ceiling cooling panel with PCM on the top and a 105 W light bulb. The size of the box is calculated according to the surface area to volume ratio, using the small sample model. With the bulb the inner heat generation can be modelled. We placed 8 temperature sensors inside the box to measure the distribution of the temperature and to measure the temperature of the PCM. The adiabatic box can be seen on *Figure 10* and *Figure 11*.

Figure 10 Adiabatic box

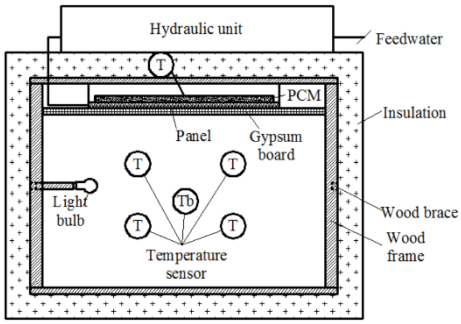

Figure 11 Section drawing of the adiabatic box

3. RESULTS

There are several possibilities to improve energy effectiveness with PCMs:

- reduction of the time of cooling,
- growth in the effectiveness of refrigeration system (EER),
- avoidance of partial loads,
- reduction of the mass flow of cooling water,
- cooling with ambient air at night.

Figure 12 presents the cooling time reduction in the function of PCM thickness. As the PCM layer thickness grows cooling time reduction grows as well, but after 2,5 mm the reduction effect decreases. The specific cooling time reduction depends on the mass of the material, it can be seen, that the 0,5 mm thickness shows the best result. It is a technical maximum, an economic calculation should be added to carry out the economical optimum and decide whether it is a worthy possibility.

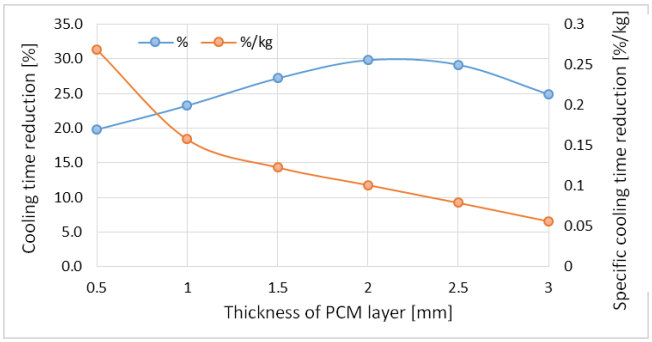

Figure 12 Cooling time reduction in the function of PCM thickness

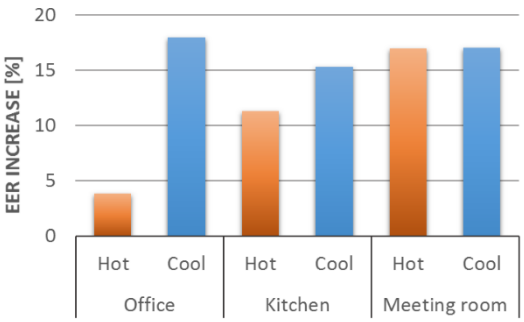

Figure 13 ERR increase in different room types

Figure 13 shows the EER increase of the cooling system in the function of different room types, on hot and cool summer days. The increase in the effectiveness of the cooling system can reach 15-18%. As the EER proportional to the electricity usage of the compressor of the cooling system, it is a direct way to reduce the electricity usage of the system.

The results of the CFD simulation can be seen on *Figure 14* and *Figure 15*. When there is no PCM in the system, the surface temperature is not ever, but with PCM its dispersion is lower. As the cooling performance is proportional to the surface temperature, the system containing PCM has bigger cooling performance.

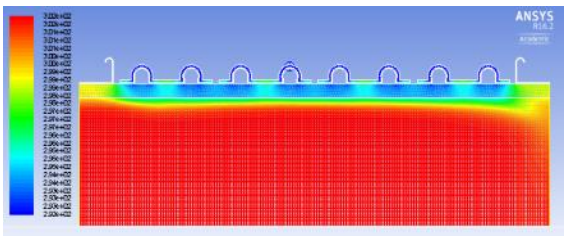

Figure 14 Temperature without PCM

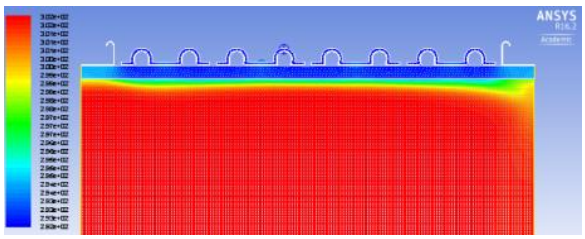

Figure 15 Temperature without PCM

The design value of the performance of the cooling system is 74 W/m^2 with 2 °C difference between the temperature of the inlet and outlet water temperature and 0,07 kg/s mass flow. With PCM with low temperature, the mass flow could be reduced with the same cooling performance. The temperature difference will not grow, as the PCM can locally cool the water in the pipes.
With the use of PCM the average heat performance of the panel can be 85 W/m^2, while the cooling system is working. When it is not working the *Figure 16* shows the performance of the PCM in the function of the temperature difference of the PCM and the inside air temperature of the room. The PCM itself can produce 30-40 W/m^2 cooling performance.

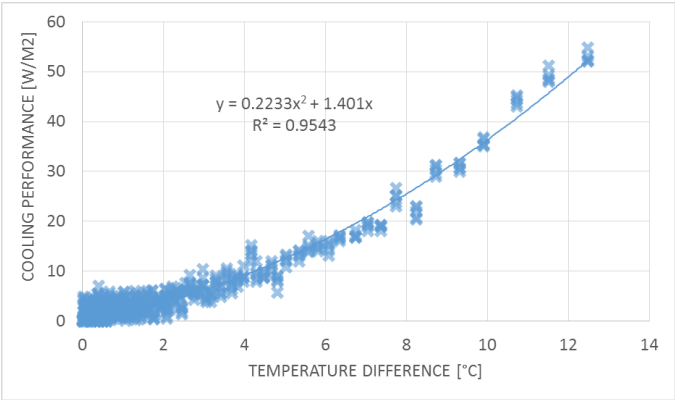

Figure 16 Temperature profile of the cooling panel

CONCLUSIONS

To sum up we combined a ceiling cooling system with phase change material. We investigated the combination with a thermodynamic model, with a CFD simulation and with an experimental system. The combined system holds several energy saving potential, the overall amount of energy saving can be 15-20% with the proper operation conditions. The cooling performance of the system can be higher than the design value and only the PCM without the cooling water can absorb 30-40 W/m^2 energy in the function of temperature difference. The system has many challenges and an economic calculation has to be done to decide that is it reasonable or not.

REFERENCES

[1] Andrássy, Z., Farkas, R.: *Fázisváltó anyagok alkalmazása falszerkezetekben*, TDK dolgozat, 2014.
[2] Ravikumar, M., Srinivasan, P.: *Phase change material as a thermal energy material for cooling of building*, Journal of Theoretical and Applied Information Technology, pp.: 503-511, 2007.
[3] Árokszállási, K.: *Hőtárolás, a jövő technológiája*, Roxa Kft.
[4] http://www.ngbsh.hu/

EVALUATION OF MATHEMATICAL MODELLING OF THIN-LAYER FREEZE DRYING

ANTAL Tamás PhD

Institute of Engineering and Agricultural Sciences, College of Nyíregyháza
E-mail: antalt@nyf.hu

Abstract
In this study, the influences of chamber pressure of freeze drier on the drying kinetics and five thin layer mathematical models fitting on drying curves were investigated. Lemon balm's freeze drying kinetics is described by a Newton, Page, Henderson & Pabis, Logarithmic and third-degree polynomial models. It was found that overall freeze drying (FD) carried out at high (FD-HP) and low pressure (FD-LP) settings consist of sublimation rate, first falling rate and second falling rate periods. Drying time of FD-LP samples was about 14% shorter than that of FD-HP material. Drying rate of FD-LP dried lemon balm leaves are higher than FD-HP dried samples, where the drying rates ranged from 0.063 to 0.449 g H_2O/ g DM. s and 0.0365 to 0.395 g H_2O/ g DM. s, respectively. Assessment of five mathematical models revealed that the third-degree polynomial model exhibited the best performance in fitting the experimental data.

Keywords: *Thin layer models, drying kinetics, freeze drying, pressure, lemon balm*

1. INTRODUCTION

Drying is one of the oldest methods of food preservation and represents a very important aspect of food processing [4]. Freeze drying (FD) is known for its ability to retain food quality such as minimising loss of flavour and aroma compounds as well as bio-active ingredients, reducing shrinkage and etc. through vacuum and low-temperature drying. According to Ratti [13], it is due to the absence of liquid water and low temperature deactivated most of the microbiological reactions and gives a final product of excellent quality.
The thin-layer drying models in the databases are empirical, semi-theoretical and theoretical types. The semi-theoretical and empirical models consider only the external resistance to moisture movement between the materials and surrounding air. The solution of Fick's second law of diffusion is used widely as a theoretical model in thin-layer drying of food. The developed models is the scientific literature are used for designing new drying methods as well as selection of optimum drying conditions and for accurate prediction of heat and mass transfer phenomena during the dehydration process. In addition, the thin-layer drying models can be used to predict drying kinetics of food materials [8, 11].
Lemon balm has been traditionally used for different medicinal purposes as tonic, juice or tea, for digestives, gastrointestinal disorders, catarrhs, migraines, high blood pressures, nerve pains, stiff necks, toothaches, earaches, sedative-hypnotics, strengthening the memory, stress-induced.
Currently, research related to freeze drying kinetics of lemon balm leaves is rather scarce. The objectives of this study are to investigate the influence of chamber pressure (high and low) of a freeze dryer on drying kinetics of lemon balm leaves which are described by mathematical models.

2. METHODS

2.1. Lemon balm leaves

Lemon balm (*Melissa officinalis* L.) samples were collected before flowering from an organic farm in Nyíregyháza (Hungary), in 15 June 2011. The samples were obtained by cutting the plant manually. After that, harvesting samples was stored in plastic bags and kept in a refrigerator (Husqvarna, QT 4609 RW, Hungary) at temperature, frozen duration and relative humidity of 5°C, 4 h and 88-92%, respectively. Prior to freeze drying process, lemon balm leaves were separated from the stems.

2.2. Freeze drying

About 50 g of lemon balm leaves were dried using a freeze drying method. The leaves were frozen at -28°C in a laboratory freeze dryer (FT33, Armfield Ltd., England). The samples were dried at pressure of 250-300 Pa for 14 hours (freeze drying at high pressure, FD-HP) and 50-80 Pa for 12 hours (freeze drying at low pressure, FD-LP). The self-temperature was set at temperature of 18 °C and –50 to –55°C as condenser temperature. Data collection was performed through weighing samples at 1 hour intervals using a digital balance (EMALOG, PAB-01, Hungary) with accuracy of 5000 ±0.1 g built in under a samples tray. Samples were freeze dried at high pressure (FD-HP) and low pressure (FD-LP) with three replications.

2.3. Determination of moisture content

The moisture content before and after freeze drying of the leaves was determined by the gravimetric method (105°C for 4 h) in triplicate and the average value was recorded. The experiments were conducted using a hot-air laboratory drier (LP-306, LABOR-MIM, Hungary).
In an environment containing moisture, dry material will absorb moisture until it is in equilibrium with the surrounding atmosphere. Similarly, saturated material, when placed in an atmosphere of lower relative humidity (RH), will lose moisture until equilibrium is attained. If the sample is placed in an environment where the RH is stable, it will attain constant moisture content (MC), known as the equilibrium moisture content (EMC) [1]. The EMC is usually determined by weighing the sample periodically until a constant weight is reached.

2.4. Mathematical modelling of freeze drying

There are several empirical approaches for modelling of the drying kinetics. Newton, Page, Henderson and Pabis (exponential), Logarithmic and third-degree polynomial models were used to fit the drying curves (MR versus drying time) in this study.
The moisture ratio (MR) of lemon balm leaves during the drying experiments was calculated using equation (1). The M_e values were a bit lower than final moisture content of dried samples. Such low values of M_e had a negligible effect on MR, which depended mainly on the values of M and M_o [3].

$$MR = \frac{M - M_e}{M_0 - M_e} \tag{1}$$

where *MR* = Moisture ratio, *M* = Moisture content (g H_2O/ g DM), M_e = Equilibrium moisture content (g H_2O/ g DM), M_0 = Initial moisture content (g H_2O/ g DM).

The final moisture content of samples (M) was determined using equation (2):

$$M = \frac{W_t - W_k}{W_k} \tag{2}$$

where W_t = Sample weight at a specific time (kg), W_k = Sample dry weight (kg).
The experimental data were fitted to the following a third-degree polynomial model (Eq. 3), Newton model (Eq. 4), Page model (Eq. 5), Henderson and Pabis model (Eq. 6) and Logarithmic model (Eq. 7) [6, 7, 10, 12, 17].

$$MR = at^3 + bt^2 + ct + 1 \tag{3}$$

The values of parameters *a*, *b*, *c* of the third-degree polynomial depend on the characteristics of the material, including variety, freezing rate, ripeness, and tendency to lose water [2].

$$MR = \exp(-kt) \tag{4}$$
$$MR = \exp(-kt^n) \tag{5}$$
$$MR = a\exp(-kt) \tag{6}$$
$$MR = a\exp(-kt) + c \tag{7}$$

where *MR* = Moisture ratio; *a*, *c* and *n* = constants in models, *k* = drying constant (h^{-1}), t= drying time (h).
To find the best fit model, two statistical indicators are used and shown in Equation (8) and (9). Model with the highest coefficient of determination (R^2) and the lowest Root Mean Square Error (RMSE) values indicate the best fit model.

$$R^2 = \frac{\sum_{i=1}^{N}\left(MR_{pre_i} - MR_{mean}\right)^2}{\sum_{i=1}^{N}\left(MR_{\exp_i} - MR_{mean}\right)^2} \tag{8}$$

$$RMSE = \sqrt{\frac{1}{N}\cdot\sum_{i=1}^{N}(MR_{\exp_i} - MR_{pre_i})^2} \tag{9}$$

where *i* = Sequence number of observation, $MR_{exp,i}$ = Experimental moisture ratio at observation, $MR_{pre,i}$ = Predicted moisture ratio at observation, *N* = Number of observations.

2.5. Data Analysis

The statistical package chosen for analysis was PASW Statistics version 18.0 (SPSS Inc., Chicago, Illinois, USA). In addition, non-linear regression analysis was performed using Excel Solver program (Microsoft Office Excel, 2007) in the numerical calculations.

3. RESULTS

3.1. Drying kinetics

Figure 1 shows the drying characteristics of lemon balm leaves dried using high pressure and low pressure settings. Drying rates of lemon balm leaves dried at lower pressure (FD-LP) are higher compared to high pressure (FD-HP), where the drying rates ranged from 0.063 to 0.449 g H_2O/ g DM. s (DM is dry matter) and 0.0365 to 0.395 g H_2O/ g DM. s, respectively. FD-HP lemon balm leaves samples required 2 hours longer drying time to achieve the same final moisture content compared to FD-LP lemon balm leaves samples. Antal *et al*. [2] reported that the FD-LP can reduce the drying time. On the other hand, the FD-HP samples need longer drying time. Liapis and Bruttini [9] reported that at high pressure, the mean free path of gas molecules within the void spaces of the dried layer become substantially less than the dimension of void space and vice versa. This is also in agreement with Rim *et al*. [14]. The authors reported that the sublimation rate is inversely proportional to the mass transfer resistance. Therefore, drying rate at higher pressure is lower compared to low pressure during freeze drying. In addition, Fissore *et al*. [5] reported that sublimation duration increased with pressure as a result of low driving force for mass transfer.
Typical freeze drying process starts with sublimation followed by desorption. Drying rate of lemon balm leaves samples dehydrated using the FD-LP method increased from 0.063 to 0.67 g H_2O/ g DM. s for the first 6 hours. At this stage, outer layer of ice of the samples was removed completely and formed a dry layer. Drying rate started to decrease after the critical moisture content due to removal of water vapor from the interior ice sublimation has to overcome the dry layer which is a barrier to the vapor transport [16]. Sagara and Ichiba [15] reported that drying rate decreased gradually with the increase of resistance of the dried layer to heat transfer.

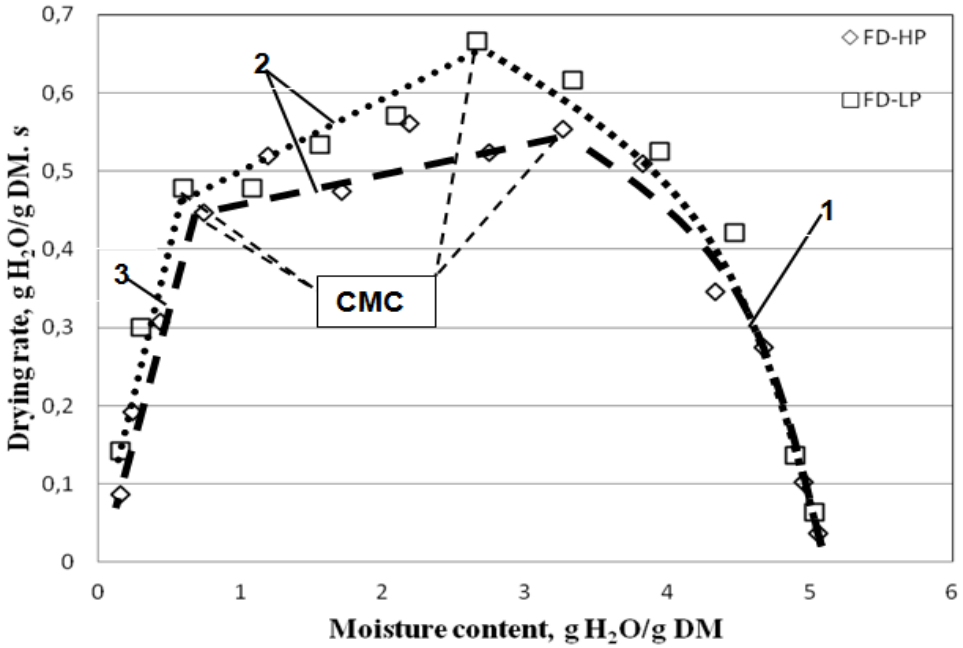

1 – increasing rate period; 2 – first falling rate period; 3 – second falling rate period; CMC- critical moisture content

Figure 1 Drying rate of lemon balm leaves

Figure 1 shows that both drying curves exhibit an initial transient period and two distinctive falling rate periods. The initial transient period is rather long if compared to typical drying curves obtained

from convective drying. During the initial transient period of FD-LP, drying rate increased from 0.03 to 0.68 g H_2O/ g DM. s while moisture content (MC) was dropped from 5.1 to 2.8 g H_2O/ g DM. Moisture content of 2.8 g H_2O/ g DM is the first critical point of falling rate period, it marks the beginning of falling rate. The drying rate decrease linearly to a second critical moisture content which is 0.8 g H_2O/ g DM. In the second falling rate period where the MC dropped from 0.8 to 0.1 g H_2O/ g DM, the drying rate dropped sharply if compared to the first falling rate period. According to Wang *et al.* [16], desorption occurred after complete removing of ice. Bound water is difficult to remove. It can be clearly observed from *Figure 1* where the drying rate decreases appreciably to 0.16 g H_2O/ g DM. s in the second falling rate of FD-LP. For samples dehydrated at the FD-HP setting, drying rate also increased at the first 6 hours from 0.0365 to 0.554 g H_2O/ g DM. s. The critical moisture content for the first falling rate period and second falling rate period are 3.27 and 0.83 g H_2O/ g DM, respectively.

3.2. Thin-layer drying modelling

The dimensionless moisture content also known as moisture ratio (MR) changes during freeze drying. The moisture ratio profile (moisture ratio versus time) is similar to moisture content profile (moisture content versus time). The moisture ratio profile is presented in *Figure 2*.
The equilibrium moisture content (EMC) of dried lemon balm leaves is obtained when the profile becomes flat at the end of the drying process. From *Figure 2*, the EMC is 0.157 g H_2O /g DM for both FD-LP and FD-HP samples, after drying for 12 and 14 hours, respectively.
The drying kinetics was modelled using third-degree polynomial model, Newton model, Page model, Henderson and Pabis model and Logarithmic model. The high values of R^2 and low values of RMSE are indicative of good fitness of empirical models.

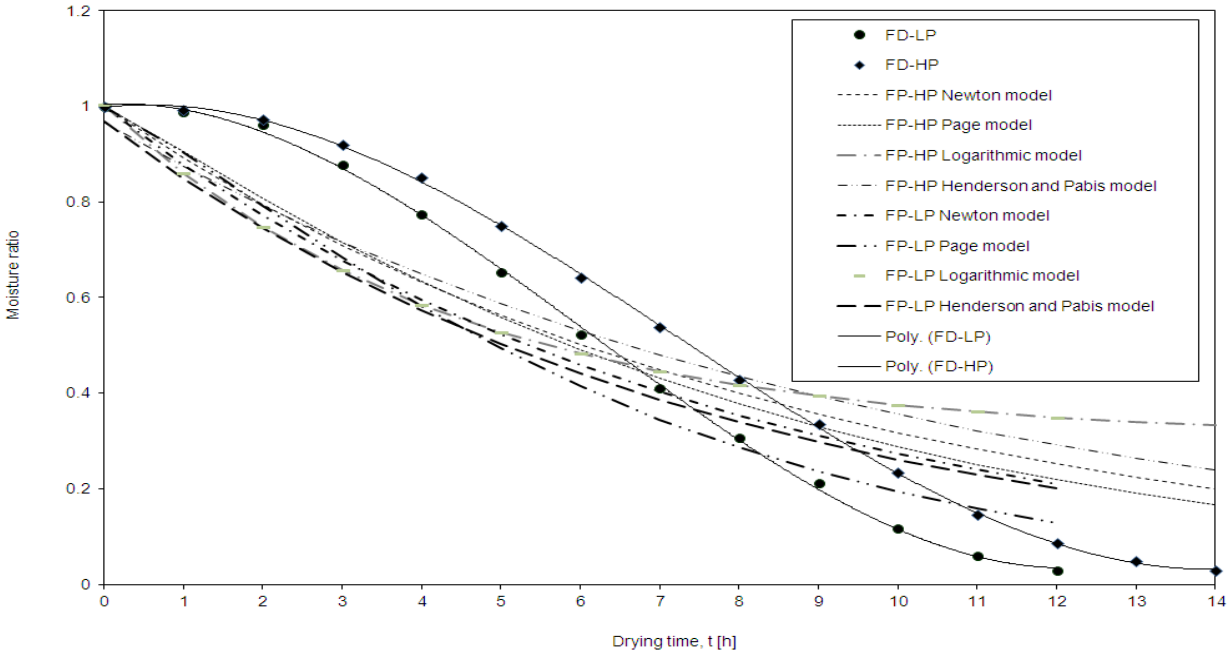

Figure 2 Variations of moisture ratio as a function of drying time for FD of lemon balm

Table 1 shows the models coefficients and R^2 and RMSE coefficient obtained from statistical analysis when fitting the experimental data to the selected drying models. The best fit model is the third-degree polynomial model where the R^2 and RMSE values are 0.9998 and 0.9994, 5.24×10^{-3} and 1.022×10^{-2}, for both samples dehydrated by FD-HP and FD-LP methods. Based on the

statistical parameters (R^2<0.99; RMSE>1.1×10^{-2}) other thin-layer equations are not suitable for modelling of freeze drying kinetics.

Table 1 Coefficients and evaluations of the thin layer drying models

Models	Model coefficients and statistical parameters					
	a	*b*	*c*		R^2	*RMSE*
Polynomial [hp]	0.0008	-0.0177	0.0187	-	0.9998	0.00524
Polynomial [lp]	0.0012	-0.0213	0.0089	-	0.9994	0.01022
	k	*n*	*a*	*c*	R^2	*RMSE*
Newton [hp]	0.1147	-	-	-	0.9163	0.1494
Newton [lp]	0.1298	-	-	-	0.9245	0.1399
Page [hp]	0.1000	1.0947	-	-	0.9270	0.1384
Page [lp]	0.1000	1.2151	-	-	0.9432	0.1320
Logarithmic [hp]	0.2268	-	0.6981	0.3035	0.7907	0.2085
Logarithmic [lp]	0.7000	-	0.3035	2.55e10	0.8349	0.1836
Henderson & Pabis [hp]	0.9676	-	0.1000	-	0.9295	0.1390
Henderson & Pabis [lp]	0.9676	-	0.1310	-	0.9236	0.1405

[hp] means Freeze drying at high pressure
[lp] means Freeze drying at low pressure

CONCLUSIONS

The effect of chamber pressure on drying characteristics of lemon balm leaves under freeze drying was studied. A decrease in drying chamber pressure decreased the freeze-drying time. It was stated that drying rate of freeze drying consist of three periods, viz. increasing rate, first falling rate and second falling rate. In order to explain the drying behaviour of lemon balm leaves, five different thin layer mathematical models were compared to their coefficient of determination (R^2) and root mean square error (RMSE). It was found that the third-degree polynomial model gave the best fitting of the experimental data. This model is suitable to estimate the moisture content during freeze drying in order to determine drying time.

REFERENCES

[1] Akyildiz, M.H., Ates, S.: *Effect of heat treatment on equilibrium moisture content (EMC) of some wood species in Turkey*, Research Journal of Agriculture and Biological Sciences, 4(6): 660-665., 2008.
[2] Antal, T., Figiel, A., Kerekes, B., Sikolya, L.: *Effect of drying methods on the quality of the essential oil of spearmint leaves (Mentha spicata L.).* Drying Technology, 29(15): 1836-1844., 2011.
[3] Calín-Sánchez, Á., Figiel, A., Lech, K., Szumny, A., Carbonell-Barrachina, Á.A.: *Effects of drying methods on the composition of thyme (Thymus vulgaris L.) essential oil*, Drying Technology, 31: 224-235., 2013.
[4] Doymaz, I., Tugrul, N., Pala, M.: *Drying characteristics of dill and parsley leaves*, Journal of Food Engineering, 77: 559-565., 2006.
[5] Fissore, D., Velardi, S.A., Barresi, A.A.: *In-line control of a freeze-drying process in vials*, Drying Technology, 26: 685–694., 2008.
[6] Henderson, S.M., Pabis, S.: *Grain drying theory, II: Temperature effects on drying coefficients*, Journal of Agricultural Engineering Research, 6: 169-174., 1961.

[7] O'Callaghan, J.R., Menzies, D.J., Bailey, P.H.: *Digital simulation of agricultural dryer performance*, Journal of Agricultural Engineering Research, 16: 223–244., 1971.
[8] Kucuk, H., Midilli, A., Kilic, A., Dincer, I.: *A Review on thin-layer drying-curve equations*, Drying Technology, 32 (7): 757-773., 2014.
[9] Liapis, A.I., Bruttini, R.: *Freeze drying*, In Mujumdar, A.S. (Ed.). Handbook of industrial drying, 5th Eds., New York: CRC press, USA, 275-278. p., 2007.
[10] Liu, Q., Bakker-Arkema, F.W.: *Stochastic modelling of grain drying, part 2: model development*, Journal of Agricultural Engineering Research, 66: 275-280., 1997.
[11] Midilli, A.: *Determination of pistachio drying behavior and conditions in a solar drying system*, International Journal of Energy Research, 25(8): 715-725., 2001.
[12] Page, G.E.: *Factors influencing the maximum rates of air drying shelled corn in thin layers*, M.Sc. thesis, Department of Mechanical Engineering, Purdue, USA., 1949.
[13] Ratti, C.: *Hot air and freeze-drying of high-value foods: a review*, Journal of Food Engineering, 49: 311-319., 2001.
[14] Rim, D., Séverine, V., Julien, A., Oliver, M.: *Sublimation kinetics and sublimation end-point times during freeze drying of pharmaceutical active principle with organic co-solvent formulations*, Chemical Engineering Research and Design, 87: 899-907., 2009.
[15] Sagara, Y., Ichiba, J.: *Measurement of transport properties for the dried layer of coffee solution undergoing freeze drying*, Drying Technology, 12: 1081-1103., 1994.
[16] Wang, R., Zhang, M., Mujumdar, A.S., Sun, J.: *Microwave freeze-drying characteristics and sensory quality of instant vegetable soup*, Drying Technology, 27: 962-968., 2009.
[17] Yagcioglu, A., Degirmencioglu, A., Cagatay, F.: *Drying characteristic of Laurel leaves under different conditions*, In: Proceedings of the 7th International Congress on Agricultural Mechanization and Energy, Faculty of Agriculture, Adana, Turkey, 26–27 May, 565–569., 1999.

INTERNATIONAL SCIENTIFIC CONFERENCE ON ADVANCES IN MECHANICAL ENGINEERING
19 November 2015, Debrecen, Hungary

GEOMETRIC ANALYSIS AND MODELLING OF SPIROID HOBS HAVING TWO DIFFERENT TYPE FACE SURFACE

[1]BODZÁS Sándor PhD, [2]DUDÁS Illés DSc

[1]Department of Mechanical Engineering, University of Debrecen
E-mail: bodzassandor@eng.unideb.hu
[2]Institute of Production Science, University of Miskolc
E-mail: illes.dudas@uni-miskolc.hu

Abstract
We have worked out two type of hobs having different face surface for the manufacturing of the face gear of an our designed spiroid worm gear drives having arched profile [5]. The face surface of one of the hob is a planar surface. The face surface of the other hob is an Archimedean thread surface which has a reverse lead of thread than the thread surface of the hob. We determined the equations of the main surfaces and edges of the hob which are necessary for the computer aided design (CAD) of the tools. After these we design the models of the tools for our other analysis (for example FEM and TCA analysis, etc.).

Keywords: *hob, face surface, spiroid, model*

1. INTRODUCTION

Knowing the main characteristics and production geometry of hob is important for the correct and appropriate quality production [4].

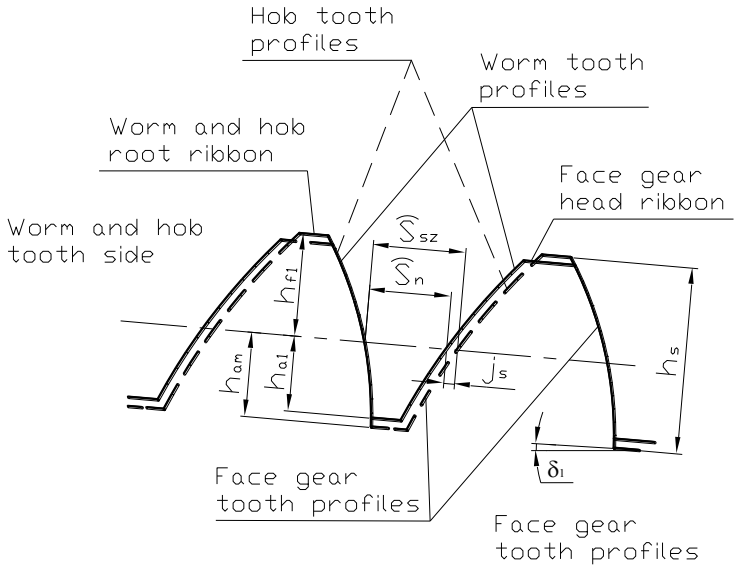

Figure 1 The base profile of the spiroid worm, face gear hob and face gear [1]

The elements of the face gear hob is equal with the elements of the worm co-operating as a gear drive with the face gear by direct motion mapping [4].

The thread pitch of the hob is equal with the thread pitch of the worm. The addendum circle diameter is varied because of the resharpening provision [4], that is why it is higher than the addendum circle diameter of worm connecting with the face gear (Figure 1).

2. SPIROID HOB HAVING PLANAR FACE SURFACE

In this case the face surface of the hob is the plane intersecting the axis of the hob.
Derivation: the hob is intersected by a $x_{1F}=0$ axial section plain, then the equation of the plain is the same as the equation of the face surface (Figure 2) [3, 4].
The common solution of the equations of the face surface of the hob and the two parametric vector – scalar function of the conical thread surface [1] are given the equation of the cutting edge of the hob [1, 4]:

$$\left.\begin{aligned} x_1^V &= 0 \\ y_1^V &= \eta \cdot \cos(\vartheta + \varphi_1) + p_r \cdot \vartheta \cdot \cos\varphi_1 \\ z_1^V &= p_a \cdot (\vartheta + \varphi_1) + \sqrt{\rho_{ax}^2 - (K_e - \eta)^2} + z_{axe} \end{aligned}\right\} . \tag{1}$$

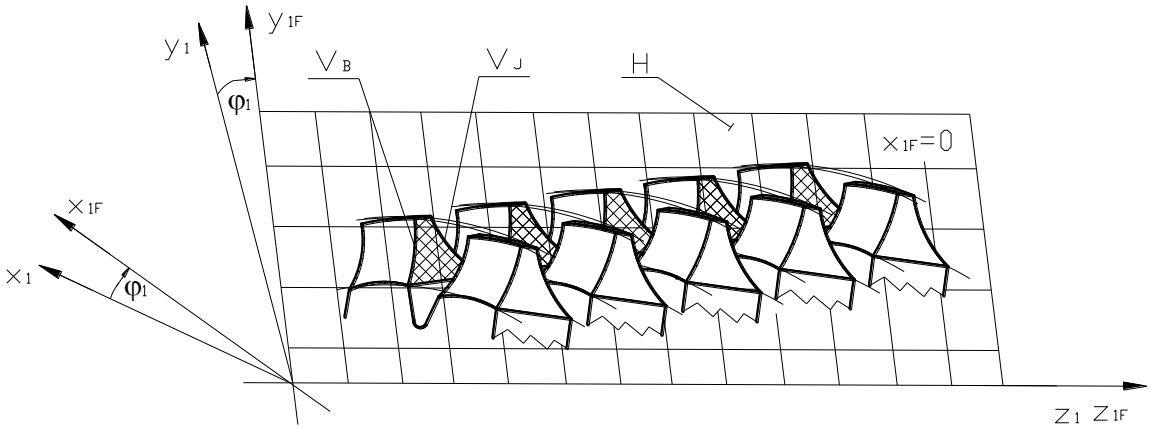

Figure 2 Defining H face surface and $V_{J,B}$ cutting edges in case of planar face surface

The equation of the backward turned surface is the following:

$$\left.\begin{aligned} x_{hre} &= -\eta' \cdot \sin\left[\frac{p_a}{p_{ae}'} \cdot (\vartheta + \varphi_1)\right] - p_r \cdot \vartheta \cdot \sin\left[\frac{p_a}{p_{ae}'} \cdot (\vartheta + \varphi_1) - \vartheta\right] \\ y_{hre} &= \eta' \cdot \cos\left[\frac{p_a}{p_{ae}'} \cdot (\vartheta + \varphi_1)\right] + p_r \cdot \vartheta \cdot \cos\left[\frac{p_a}{p_{ae}'} \cdot (\vartheta + \varphi_1) - \vartheta\right] \\ z_{hre} &= p_{ae}' \cdot (\vartheta + \varphi_1) + \sqrt{\rho_{ax}^2 - (K_e - \eta')^2} + z_{axe} \end{aligned}\right\} . \tag{2}$$

In case of the other tooth side electing the appropriate indications the equations of the face surface, the backward turned surface and the cutting edge could be defined by similar way.
Using the received equations the computer aided model of the spiroid hob has been designed in case of planar face surface for a concrete geometry by SolidWorks 2012 designer software (Figure 3) [1, 2].

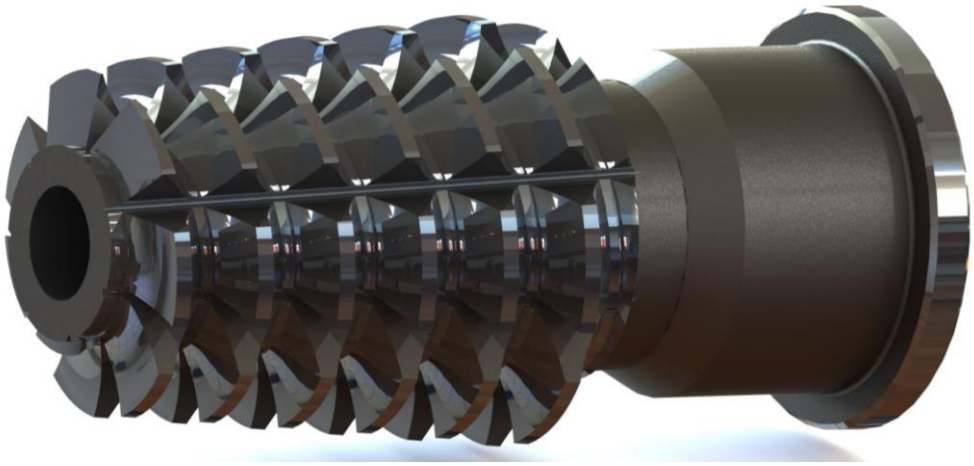

Figure 3 The CAD model of spiroid hob having planar face surface

3. SPIROID HOB HAVING ARCHIMEDEAN THREAD FACE SURFACE

In this case the face surface of the hob is an Archimedean thread surface which has a reverse lead of thread than the thread surface of the hob [4].
Derivation: the half-line perpendicular to the axis of the helicoid makes a moving motion of p_h face surface axial helicoidal parameter, and p_r radial helicoidal parameter, while also rotating (Figure 4) [3, 4].
Based on this the equation of the face surface of the hob is [1]:

$$\left.\begin{aligned} x_1^H &= -\eta \cdot \sin(\vartheta + \varphi_{oh}) - p_r \cdot \vartheta \cdot \sin\varphi_1 \\ y_1^H &= \eta \cdot \cos(\vartheta + \varphi_{oh}) + p_r \cdot \vartheta \cdot \cos\varphi_1 \\ z_1^H &= -p_h \cdot (\vartheta + \varphi_{oh}) \end{aligned}\right\} \qquad (3)$$

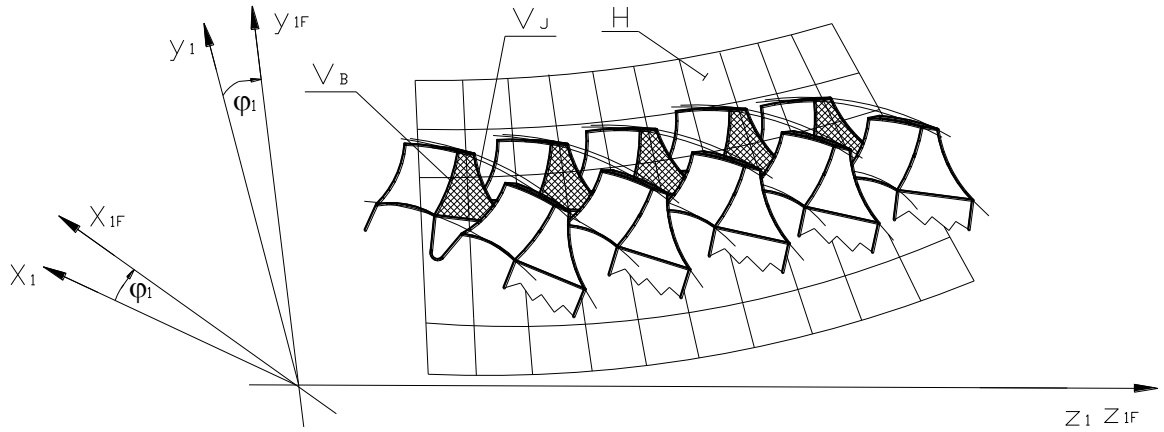

Figure 4 Defining H face surface and $V_{J,B}$ cutting edges in case of Archimedean thread face surface

The common solution of the equations of the face surface of the hob (3) and the two parametric vector – scalar function of the conical thread surface [1] are given the equation of the cutting edge of the hob [1, 4]:

$$\left.\begin{aligned} x_1^V &= -\eta\cdot\sin\left[-\frac{p_a}{p_h}\cdot(\vartheta+\varphi_1)-\frac{1}{p_h}\cdot\sqrt{\rho_{ax}^2-(K_e-\eta')^2}-\frac{z_{zaxe}}{p_h}\right]-p_r\cdot\vartheta\cdot\sin\varphi_1 \\ y_1^V &= \eta\cdot\cos\left[-\frac{p_a}{p_h}\cdot(\vartheta+\varphi_1)-\frac{1}{p_h}\cdot\sqrt{\rho_{ax}^2-(K_e-\eta')^2}-\frac{z_{zaxe}}{p_h}\right]+p_r\cdot\vartheta\cdot\cos\varphi_1 \\ z_1^V &= p_a\cdot(\vartheta+\varphi_1)+\sqrt{\rho_{ax}^2-(K_e-\eta')^2}+z_{axe} \end{aligned}\right\} \quad (4)$$

The equation of the backward turned surface is the following:

$$\left.\begin{aligned} x_{hre} &= -\eta'\cdot\sin\left[\frac{p_a}{p_{ae}'}(\vartheta+\varphi_1)\right]-p_r\cdot\vartheta\cdot\sin\left[\frac{p_a}{p_{ae}'}(\vartheta+\varphi_1)-\vartheta\right] \\ y_{hre} &= \eta'\cdot\cos\left[\frac{p_a}{p_{ae}'}(\vartheta+\varphi_1)\right]+p_r\cdot\vartheta\cdot\cos\left[\frac{p_a}{p_{ae}'}(\vartheta+\varphi_1)-\vartheta\right] \\ z_{hre} &= p_{ae}'\cdot\left[\frac{p_a}{p_{ae}'}(\vartheta+\varphi_1)\right]+\sqrt{\rho_{ax}^2-(K_e-\eta')^2}+z_{axe} \end{aligned}\right\} . \quad (5)$$

In case of the other tooth side electing the appropriate indications the equations of the face surface, the backward turned surface and the cutting edge could be defined by similar way.
Using the received equations the computer aided model of the spiroid hob has been designed in case of Archimedean thread face surface for a concrete geometry by SolidWorks 2012 designer software (Figure 5).

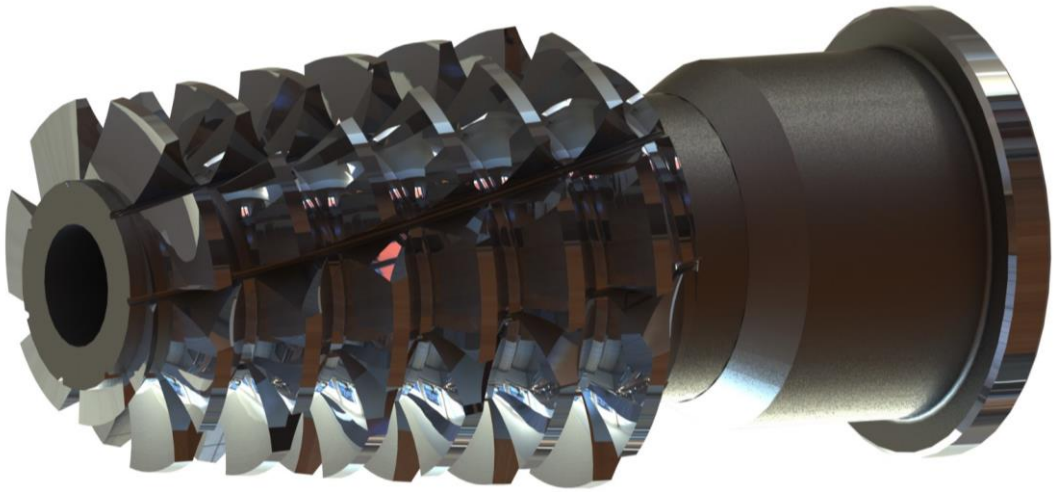

Figure 5 The CAD model of spiroid hob having Archimedean thread face surface

CONCLUSIONS

We have carried out two type of hobs having planar and Archimedean face surface for the manufacturing of the face gear of the our designed spiroid worm gear drives having arched profile [5].

We have determined the equations of edges and surfaces of the manufacturing tools. Based on these we have designed the CAD models of these manufacturing tools for our other research works (for example FEM, TCA analysis).
It could be seen these hobs have complicated geometry and expensive tools that is why considering the profile accuracy of the face gear the assurance of repeated resharpening is important on designing.
The geometric aspects of cutting the hobs having Archimedean thread face surface are more favourable. At the same time the manufacturing costs, manufacturing process, sharpening and measurement of these are more complicated than the hobs having planar face surface.

REFERENCES

[1] Bodzás, S.: *Connection analysis of surfaces of conical worm, face gear and tool,* Ph.D. dissertation, University of Miskolc, 2014., p. 154., Research Leader: Prof. Dr. Illés Dudás, DOI 10.14750/ME.2014.006

[2] Bodzás, S. Dudás, I.: *Mathematical description and modelling of a tooth surface of spiroid face gear having arched profile in axial section,* International Journal of Advenced Manufacturing Technology, Springer, ISSN 0268-3768 (Online), 2015. 04. 17. (Online), 2015. 08. 31. (Online), Volume 80, Numbers 5-8 (2015), (IF 1.779)
DOI 10.1007/s00170-015-7798-3
http://link.springer.com/article/10.1007/s00170-015-7798-3
http://www.springer.com/home?SGWID=0-0-1003-0-0&aqId=2914160&download=1&checkval=d2c51f8f54ea90ba551e7f0cff61d47c

[3] Dudás, I., Bodzás, S.: *Production geometry analysis, modeling and rapid prototyping production of manufacturing tool of spiroid face gear*, International Journal of Advenced Manufacturing Technology, Springer, ISSN 1433-3015 (Online), 2012.07.19. (Online), ISSN 0268-3768 (Print), Volume 66, Issue 1 - 4., pp. 271 – 281., 2013. 04. (Print), (IF 1.779),
DOI 10.1007/s00170-012-4323-9,
http://www.springerlink.com/content/t12l4xh51g664266/?MUD=MP
http://www.springer.com/home?SGWID=0-0-1003-0-0&aqId=2362785&download=1&checkval=5131188b9d22673b4f7f1f6eb76f3a2e

[4] Dudás, I.: *The Theory and Practice of Worm Gear Drives* Penton Press, London, 2000., ISBN 1877180295

[5] Dudás, I., Bodzás, S., Dudás, I. Sz., Mándy, Z.: *Konkáv menetprofilú spiroid csigahajtópár és eljárás annak köszörüléssel történő előállítására*, The day of the patent registration: 2012.07.04., Patent number: 229 818

[6] Hegyháti, J.: *Untersuchungen zur Anwendung von Spiroidgetrieben*. Dissertation, TU Dresden, 1988.

IMPLEMENTATION OF AN AUTOMATIC POSITIONING FUNCTION FOR AUTOMATED TRANSPORT VEHICLES

BOHÁCS Gábor PhD, RÓZSA Zoltán, RÁCZ-SZABÓ András

Department of Materials Handling and Logistic Systems; Faculty of Transportation Engineering and Vehicle Engineering; Budapest University of Technology and Economics
E-mail: gabor.bohacs@logisztika.bme.hu

Abstract
Automatic guided vehicles (AGVs) for material flow systems in logistics gain more and more importance. One typical application field is the transfer of various materials inside of buffer areas. Such an application can be in manufacturing facilities or material depots in construction yards. This paper aims to present an intended accessorial function with easy teach-in, which serves for positioning. A comparison to similar systems from the literature is also presented.

Keywords: *AGV, logistics, visual servo, neural network.*

1. INTRODUCTION

Automated guided vehicles are used for various transportation tasks for decades. There exist many different solutions for sensors, navigations, hardware construction. Regarding navigation most common solutions are following of a passive (magnetic tape or painted line) or active line. Advanced and more expensive solutions apply virtual navigation lines, such as rotating laser navigation or contour following. So the question arise, what kind of development is needed here at all?
The industry requires however not only high-tech solutions but these should be economic, reliable and flexible as well. In recent years camera technology became inexpensive so related AGV development seems reasonable.

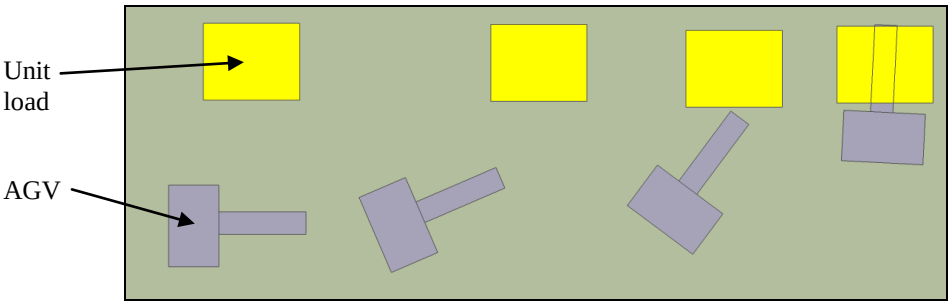

Figure 1 Visualization of the proposed task

Our goal is to implement an automated function based on cameras image processing functions to execute manipulation movement. This navigation differs from the main navigated movement of the AGV. That means, first the vehicle approaches the appropriate loading-/unloading position, afterwards the intended navigation takes over and guides the AGV under the loading unit.

2. METHODS FROM THE LITERATURE

Above described functionality may look similar to automatic parking aids, which are used in premium cars (e.g. [1], [2]). Main difference of these systems from our case that the cars park under supervision of the driver who can override the automatic function.
The parking problem has been researched widely in the research community as well. Zhao and Collins Jr. present in their paper [3] a fuzzy controller based function to help the test mobile robot parking at tight places. The test vehicle is equipped with several sensors, such as ultrasonic, CCD and laser range finder. The task has been decomposed for three steps (1. reach a ready-to-reverse position, 2: reversing, 3: adjust forward inside the space). During the navigation the vehicle calculates only angle difference from the actual target (see Fig. 2.).

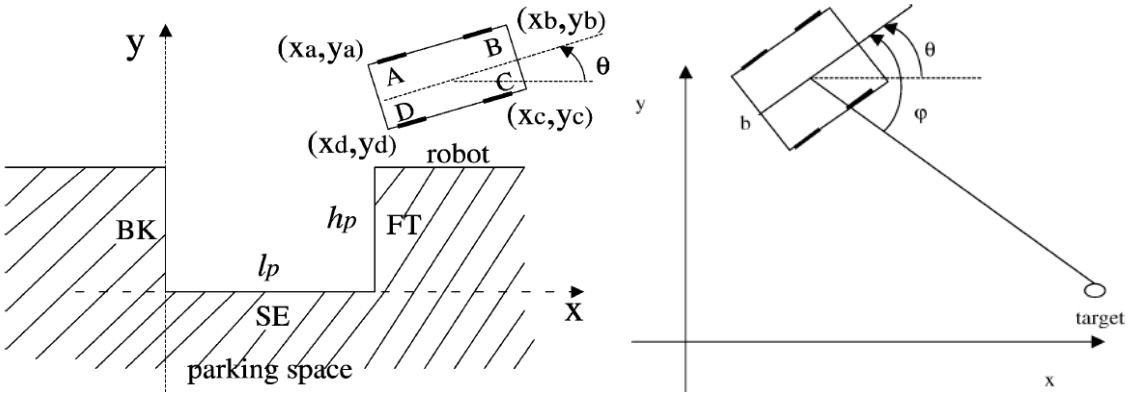

Figure 2 Robust automatic parallel parking in tight spaces via fuzzy logic [3]

Demirli and Khoshnejad in their paper [4] present Autonomous parallel parking of a car-like mobile robot by a neuro-fuzzy sensor-based controller. Thanks to the neural network the car can be taught directly in manual mode for various situations. The test vehicle was equipped with ultrasonic sensors. The inputs to the controller are the three distances, d1, d2, and d3, acquired by the ultrasonic sensors (S1,S2,andS3) as well as the difference, d4, of the previous and the new distances measured by S3. The output of the controller is the turning angle which is a first order function of the inputs. Authors claim an error of the system ca. 7-8 cm. It may seem much for a navigation, however it must always be considered in connection with he application.

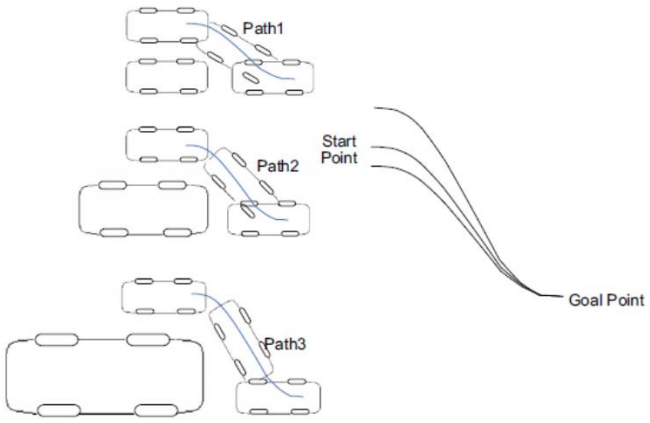

Figure 3 Paths used for training [4]

3. DESCRIPTION OF THE TEST SYSTEM

The experiments are carried out on a test system. As an image processing device an Omron F210 industrial vision system was used. It should be remarked that this choice is only for test, on a final AGV a less expensive sensor is sufficient. The camera system recognizes markers of the goal and of the AGV (both position and orientation) and transmit the coordinates via RS232. Information is processed in Matlab, neural network is also implemented here. This software takes over both the teaching and testing tasks. Commands are transferred via WiFi to a LEGO Mindstorms EV3 robot with differential drive.

Figure 4 Test system [5]

4. NEURAL NETWORK DESIGN AND RESULTS

The proposed structure of the neural network was certainly unknown. We tried out several structures, finally, on seeing the results, a feedforward network with 40 hidden neurons in one layer was accepted. Results were even better than for the case of two hidden layer networks, however there were only 20 hidden neurons in one layer.
The network has two inputs: relative angle to the goal and the distance to it. It has 3 outputs: 100 means left turn, 010 means go forward and 001 means right turn.
The network has been taught in using approximations of the goal from different starting points and orientations. After some teaching paths test were carried out. First tests resulted sometimes in false directions, therefore a re-teach function was implemented where new correct manual data could have been taught in as well. That made continuous improvement of the robot over time.

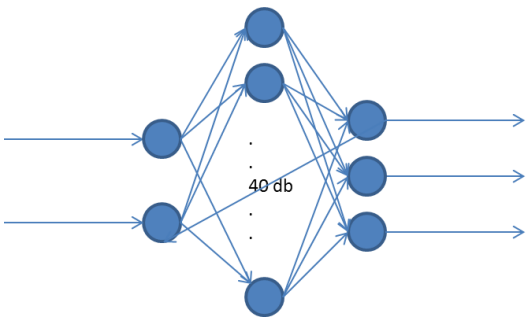

Sorszám	Szögeltérés a kamera x tengelyéhez képest [fok]	Távolság a célterülettől [egység]	Megadott parancs	Megadott parancs kódja		
0	0	437.1041	-	0	0	0
1	9.2110	429.5326	b	1	0	0
2	12.5288	425.5925	b	1	0	0
3	16.9908	421.8048	b	1	0	0
4	21.8014	417.6389	b	1	0	0
5	27.9795	413.5048	b	1	0	0
6	34.1145	409.1021	b	1	0	0
7	32.8285	378.6070	e	0	1	0
8	37.1847	371.2226	b	1	0	0

Figure 1 Implemented neural network and example data

CONCLUSIONS, FURTHER RESEARCH

Test resulted an accuracy of 2% of the whole area which is normal regarding the inaccurate image processing of the camera, and the hardware's small inaccuracy. We deemed the tests altogether successful because the main goal was to determine if such a system can work at all. The continuous improvement of the neural network was extremely advantageous and promising for practical applications.

REFERENCES

[1] Technology that Supports Parking: http://www.toyota-global.com/innovation/safety_technology/safety_technology/parking/
[2] Stress-free Parking. http://www.bmw.com/com/en/insights/technology/connecteddrive/2013/driver_assistance/intelligent_parking.html.
[3] Zhao, Y., Collins, E.G.: *Robust automatic parallel parking in tight spaces via fuzzy logic*; Robotics and Autonomous Systems 51 (2005) 111–127 S., 2009.
[4] Demirli, K., Khoshnejad, M.: *Autonomous parallel parking of a car-like mobile robot by a neuro-fuzzy sensor-based controller*; Fuzzy Sets and Systems 160, 2876–2891., 2009.
[5] Rácz-Szabó, A.: *Kísérleti vezetőnélküli targonca modell neurális hálózat alapú navigációjának fejlesztése*. TDK dolgozat, BME, 2015.

INTERNATIONAL SCIENTIFIC CONFERENCE ON ADVANCES IN MECHANICAL ENGINEERING
19 November 2015, Debrecen, Hungary

INVESTIGATION OF EN AW 5754 ALUMINIUM ALLOY'S FORMABILITY AT ELEVATED TEMPERATURES

BUDAI Dávid, TISZA Miklós DSc, KOVÁCS Péter Zoltán PhD

Institute of Material Science and Technology, University of Miskolc
E-mail: david.budai@uni-miskolc.hu, tisza.miklos@uni-miskolc.hu, metkpz@uni-miskolc.hu

Abstract
Application of aluminium in car body manufacturing has already some decades of history. This innovation is forced by the strict emission rules and low consumption efforts. This design direction appeared in the middle of the last century as the technology of the future. However, the aluminium – due to its significantly different properties compared to steel – creates limits for the production technology and tasks for the researchers to solve it. Due to these developments, today the economical production of a full aluminium body car is not a privilege of the premium segment anymore. With the recent developments, economic production of a medium category aluminium car in mass production volume has become available. The goals of the next decades are to increase the number of the aluminium car manufacturers and to find economical solution to product small size aluminium cars. Increasing the formability of aluminium and developing the joining technologies are the most relevant tasks in recent research topics. If the research area finds solutions to these problems, it makes the manufacturers think about the aluminium car technology, since using these solutions makes the production costs much lower and finally supports to start a new era in aluminium car production. In this paper an investigation of the formability of the EN AW 5754 aluminium alloy at elevated temperatures will be described. In these tests, the specimens formed at higher temperatures to obtain the FLC curves at different temperatures. These results are useful for the industry to develop forming processes and make the aluminium car production easier and more economical.

Keywords: *aluminium, formability, FLC, 5754, temperature*

1. INTRODUCTION

The low CO2 emission rules are big challenges for the automotive researches [1][2]. To pass these requirements the automotive designers have to rethink the conventional car design and production methods to reduce the fuel consumption. Nowadays, every part of a car is designed by these principles: tyres with low rolling resistance, plated wheels and air openings, low air resistance body design, hybrid drive line, downsized engines, high gear ratios, gearboxes with 8-9 gears and lightweight car body. Light-weighting of automotive vehicles helps reduce the CO2 emissions by reducing fuel consumption. This is the most efficient way to pass the emission rules, because the engine developments have reached their limits and there is no way to reduce the fuel consumption without power loss. Using high stress steels the weight reduction of a car is about 10-25% [3], using aluminium this value is about 30-40% [4]. Compared to steel, aluminium has different characteristics, which causes difficulties for the steel based automotive industry. To produce an aluminium car, the production process needs new manufacturing methods and new forming tools, because producing an aluminium car is more than changing the base material from steel to aluminium. The altered material does not have the same formability and mechanical properties as steel this is why the aluminium car production requires new tools for a successful production. We

can demonstrate this problem through a simple test. We performed numerical simulations with the same part geometry, but with different materials. By using S350 steel (Figure 1.), the part successfully formed, but by using EN AW 5754 alloy (Figure 2.), there were failures in the lower corner of the part because of lower formability. This test showed spectacularly the problem of the lower formability of aluminium.

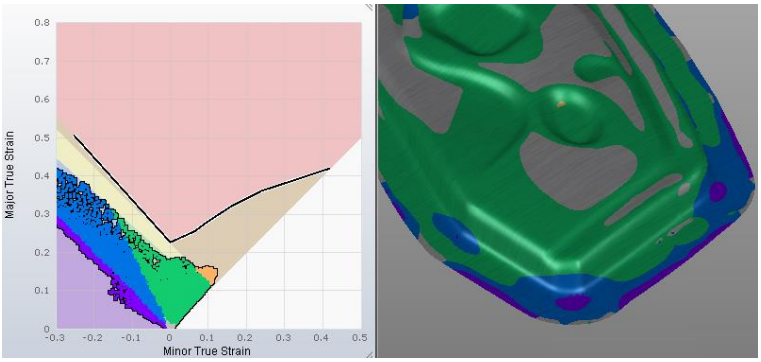

Figure 1.: Numerical simulation with S350 material

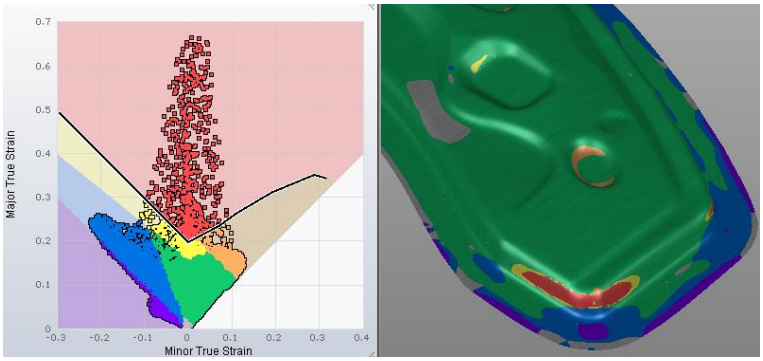

Figure 2.: Numerical simulation with EN AW 5754 material

Sometimes, the part also needs geometry changes, because the designed geometry can be hardly manufactured from aluminium. That is why the base material circumscribes the design steps. The most spectacular result of these limitations is the present aluminium car's exterior design with its large, planar shapes Figure 3. Increasing the formability of aluminium would be the solution for the car production which has to make compromises if it wants to product aluminium cars. Basically, there are two possibilities to achieve this. The first one is to increase the strain rate. This method is not applicable at the industry, where the developments are to speed up the production process. The second option is to increase the forming temperature. Taking the advantages of the changed mechanical properties at elevated temperatures, we could increase the aluminium's formability. The formability-temperature correlation would be useful for the industry that is why these researches are promoted by the automotive industry.

Beside the production, the assembly of aluminium car parts also requires special solutions. The spot-welding technology, which is used in the steel based car production, is not suitable for the aluminium car production because of the aluminium's high heat conductivity. The car makers use the riveting and adhesive bonding technology of the airplane industry Figure 4. Using these technologies, the aluminium car industry is able to produce mechanical joints with high strength.

Figure 3.: Large, planar shapes on the aluminium cars – Range Rover

The quality of a part is featured by the possibility of assembly. The part's cost depends on the geometry, the size tolerance, mechanical properties, etc. Some manufacturing methods need an additional technology to complete the part, which makes it more expensive. The applied technology also has a great effect on the costs. A part made by 3D bending or hydroforming is much expensive than the one made by cold forming or casting. It is clearly shown that the aluminium car production requires different rules compared to the steel based car production. To reduce the cost of a car the industry has to produce cars in large quantities, because this is the only way to keep the piece cost in a low level. High volume production looks for minimum material (part) cost and low assembly cost, but can afford relatively high capital investments (both in tools and manufacturing equipment). In contrast, low volume production asks for minimum capital expenditures whereas component and assembly costs play a less important role. Sheet designs are primarily directed towards higher production volumes because of the high investments in stamping tools and presses. On the other hand, sheets are relatively inexpensive product forms.

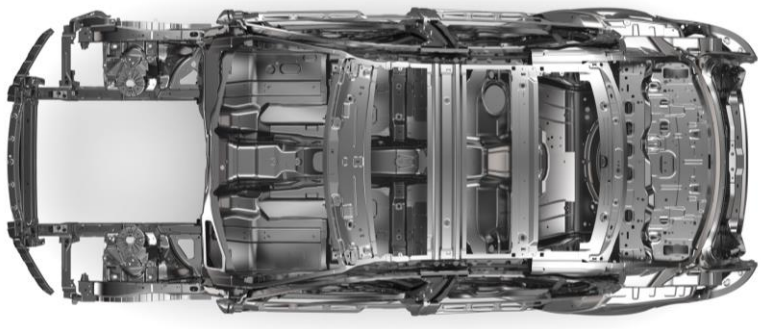

Figure 4.: More than 2400 Self Pierce Rivet joins in the Jaguar XE

2. ALUMINIUM IN AUTOMOTIVE APPLICATIONS

In the aluminium car history, the first car was Panhard Z1, which was made by mass production. This car was built from EN AW 5754 (AlMg3) aluminium alloy in 1953. The automotive industry has continuously investigated the applicability of the aluminium in cars. Until the 80's, it was only an experimental technology to build a car from aluminium alloy. In 1981, the Porsche presented an

aluminium and a steel 928 type at the Frankfurt Car Show, to demonstrate the possibilities of the aluminium car technology. The aluminium car was made from EN AW 6016, and its weight was 106 kilograms lower than of the steel one. Using aluminium, the total body weight was 161 kilograms. After the demonstration, the Audi wanted to give an answer, and the brand started its own aluminium car program. Its first aluminium car was an Audi 100. In the early 90's, the Alcan Aluminium Ltd. and Ford Motor Company developed their own aluminium car prototypes. The result of the cooperation was the Ford P2000 build by EN AW 5754. The Jaguar adopted the Ford's aluminium technology, and built the XJ220 super sport car. Using the AVT technology which was developed by Ford and Alcan, the Jaguar used EN AW 6111 for outer panels, and EN AW 5182 for inner panels. The great invention was the front and rear cross member built by EN AW 7108-T6, and the side panel built by EN AW 6082-T6. The Land Rover also used the Jaguar Land Rover's aluminium technology to create the Range Rover luxury SUV. The roof was made from EN AW 6181A and 6451 alloy. This alloy has high strength and good polishing level.

The EN AW 6014 alloy is commonly used in safety elements. Beside Jaguar Land Rover, only Audi has a well-developed aluminium car technology. The first aluminium Audi, which was produced in large quantities, was the Audi A8 in 1994. The brand used EN AW 6060 alloy for stamped parts, EN AW 6016 for exterior parts, EN AW 6009 for interior parts, EN AW 5182 for structure parts, and A356 (7Si-0,3Mg) for castings. The next step was the Audi A2. The Audi wanted to achieve the 3 l/100 km combustion level with their new car. The outer parts were made from EN AW 6016, the structured parts were made from EN AW 6181A, and the others were made from EN AW 6014. The next generation A8 used the EN AW 6181A for structure elements. The castings were made from GD-AlSi10Mg, GD-AlMg3Mn and AlSi7Mg alloys. The Lamborghini which is part of the Volkswagen group used the Audi aluminium technology. For example, the Lamborghini Gallardo's stamped parts were made from EN AW 6060 alloy. The great example about the technology transfer in the VW group is the body of the Audi R8, which is from the Lamborghini and built from EN AW 6181A. In the newest Audi A8, the usage of the EN AW 6181A decreased. The used materials are shown below:

- Audi A8 (D2): 7 alloys strength range: 100-200 *MPa*
- Audi A8 (D3): 10 alloys strength range: 120-240 *MPa*
- Audi A8 (D4): 13 alloys strength range: 120-280 *MPa*

In the evolution of the A8, the number and the strength of the used materials increased. This shows the process of the development of the aluminium technology. Thanks to the developments, the production technology is able to form aluminium alloys of higher strength, and the material technology is able to produce new and special alloys for special applications. The Audi and Jaguar Land Rover make cars by mass production that is why they are using a small number of alloys. On the contrary, a car which is produced in small quantities is using a large number of alloys. For Example, the Ferrari 548 Italia uses C65K T7 and C611 T6 alloy for castings, 6005 T6, 6260 T6 and H0682 T6 for extrusions and 6181A T6, 6082 T6 and 6022 T6 for sheet forming.

The BMW also has an aluminium car, the Z8. The extruded parts are made from EN AW 6060, 6063 and 6082. The structure parts are made from EN AW 5754 and 5182. In 2010, the BMW presented the 5 and 6 series, which had a full aluminium front built from EN AW 5042, EN AW 5182 and EN AW 6008 sheets. For extrusions, the BMW used EN AW 6060 and EN AW 6082 alloy. The Rolls-Royce which is a brand of the BMW Group, has the largest luxury car in the field, the Phantom. The Rolls-Royce Phantom with its 6 meter length, is the longest car in the luxury field. To provide the strength of the car, the designers created massive elements, which does not means additional weight, because the whole body is built from aluminium alloys. The extruded parts are built from EN AW 6060, 6063 and 6082 alloys. The brand used 6016 for outer parts, 5182 and 5454 for inner parts [5].

3. INVESTIGATIONS

During our tests, the specimens were formed at higher temperatures to obtain the FLC curves at different temperatures. The used material was the EN AW 5754 H22. In our investigations we created industrial circumstances to obtain useful data for the possible industrial application.

3.1. Material

The EN AW 5754 (AlMg3) alloy is used in sports cars like the Jaguar XK, Lotus Evora and Chevrolet Corvette. This alloy has medium strength among the aluminium alloys. Composition: 95,8% Al, 2,78% Mg, 0,29% Si, 0,36% Fe, 0,37% Mn. Temper: H22. Mechanical properties: $R_{p0,2}$=180 MPa; R_m=243MPa; $A_{50\%}$=17 (Alcoa).
The specimens have different geometries with a thickness of 1.0 mm. The different pieces are connected to the FLC's special strain paths.

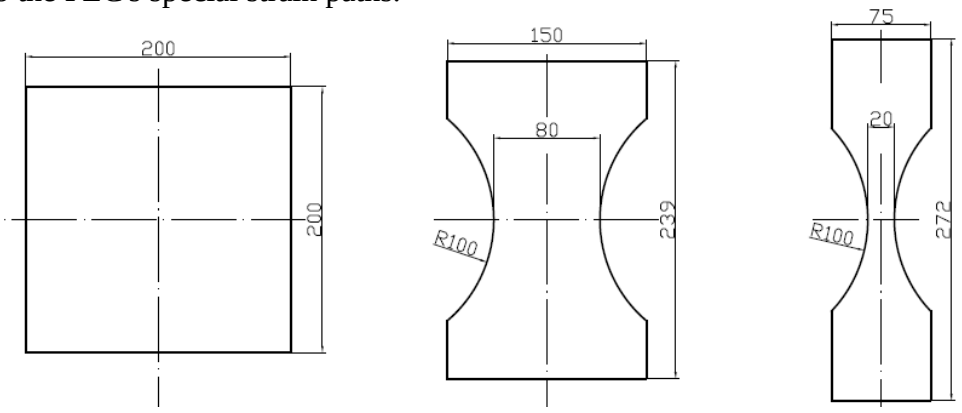

Figure 5.: Test specimens

3.2. Equipment

In our tests, a computer controlled universal sheet formability testing machine was used. This is able to perform Erichsen, Nakazima, Bulge, FLD, FLC tests. The equipment has electrohydraulic powertrain and it is suitable to test 3 mm maximum sheet thickness of steel, or 6 mm maximum thickness of aluminium. The forming tool geometry is a hemisphere with a diameter of 100 mm. The maximum load is F_{max}=600kN, the speed interval of the tool is between v=0 mm/s and v= 5 mm/s. The equipment includes an optical strain measurement system, which records the distortion of the grid which is painted on the sheet before the tests. The system has 4 CCD cameras to obtain the 3D point cloud from the mesh. From the measurements, the Vialux-AutoGrid software determines the deformation and strain distribution along the curved surface. With these data, the FLC and FLD can be determined [6].

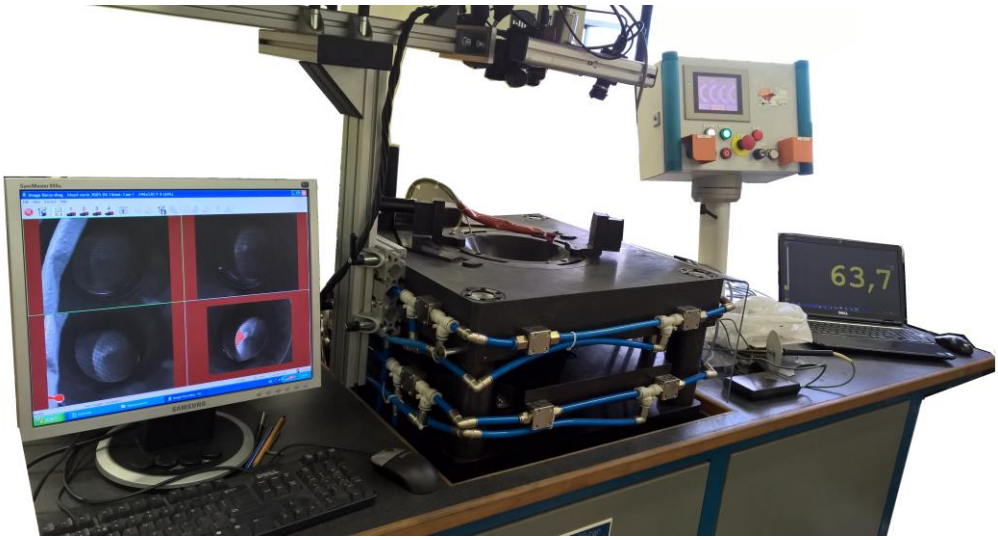

Figure 6.: Universal sheet formability testing machine

3.3. Parameters

During the tests, we simulated industrial environment where no preheat system is applied to heat the sheet to the forming temperature. The sheet only gets heat from the tool, which is preheated by the previous forming applications. If the production line uses a preheat system it would make the process more complicated. To achieve the equivalent product quality, the preheat temperature and time has to be the same, and it is a great challenge to fit a preheat system next to the press line. We only heated the sheet with the forming tool. The test was carried out at the following temperatures: 130°C, 200°C and 260°C. For a reference test, we performed a test at room temperature. Table 1. shows the temperatures of the tool and the sheet. The large differences between the temperatures are caused by the good heat conductivity of the aluminium.

Table 1.: Temperature of the tool and the sheet

Tool	250°C	400°C	600°C
Sheet	130°C	200°C	260°C

The speed of the forming tool was 0,5 mm/s in every measurements. We did not use any lubricant, so, the lubrication condition was the same in every measurements.

4. RESULTS

During the experiments, we measured the tool displacement, the forming force and the temperature of the sheet. With the mesh and the optical system we collected the maximum elongation before the failure of the sheet.

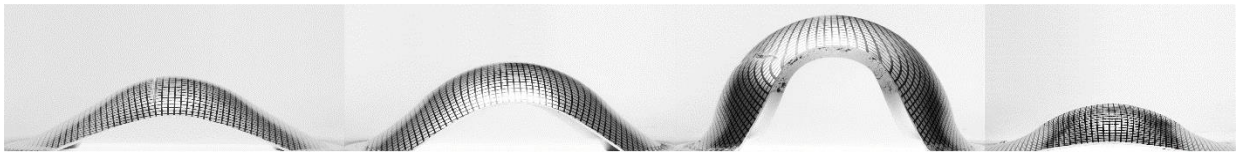

Figure 7.: Formed specimens at different temperatures

The dome height increased when we raised the temperature until 200°C. At 260°C, the dome height was much lower, and in some cases, it was lower than the result at room temperature. The results show that the optimal forming temperature of the EN AW 5754 is between 200°C and 260°C, possibly close to 200°C. To obtain the correct value we have to do more experiments.

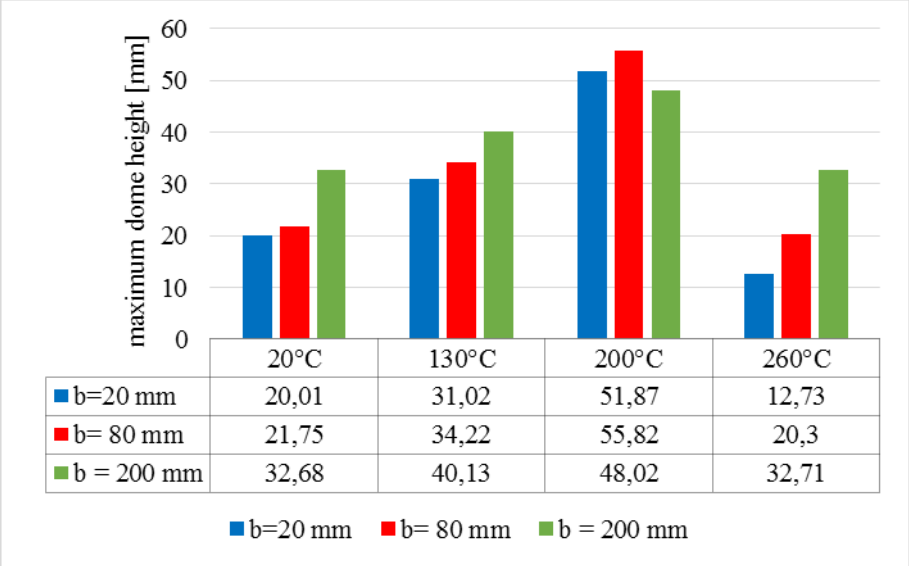

	20°C	130°C	200°C	260°C
b=20 mm	20,01	31,02	51,87	12,73
b= 80 mm	21,75	34,22	55,82	20,3
b = 200 mm	32,68	40,13	48,02	32,71

Figure 8.: Maximum dome height at different temperatures

We achieved a great formability at 200°C, which is twice as high as the result at room temperature. The FLC curves show the same trend. The forming limit curves are shifted up, which means the increase of the formability (Figure 9.).

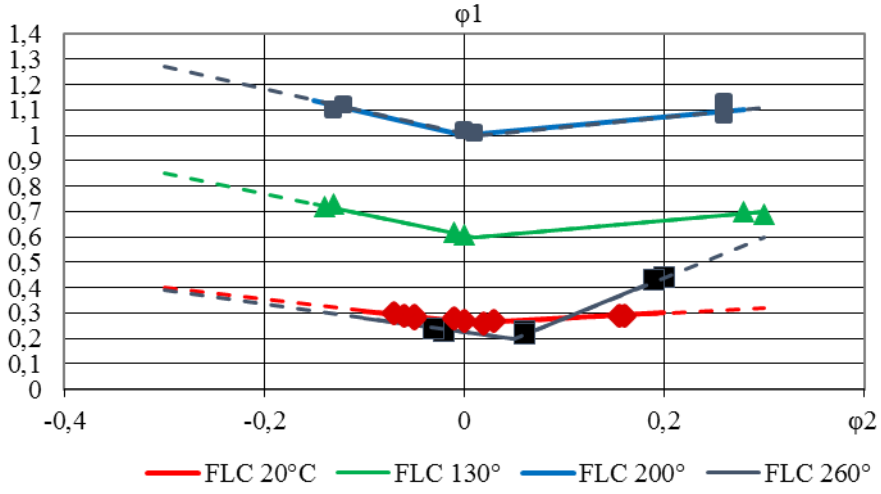

Figure 9.: FLC curves at different temperatures

The force vs displacement diagram (Figure 10.) includes useful data about the forming process. When the force achieved the maximum level, it went down while the dome height was continuously increasing. In this area, local contractions appeared which causes the same effects as in tension test.

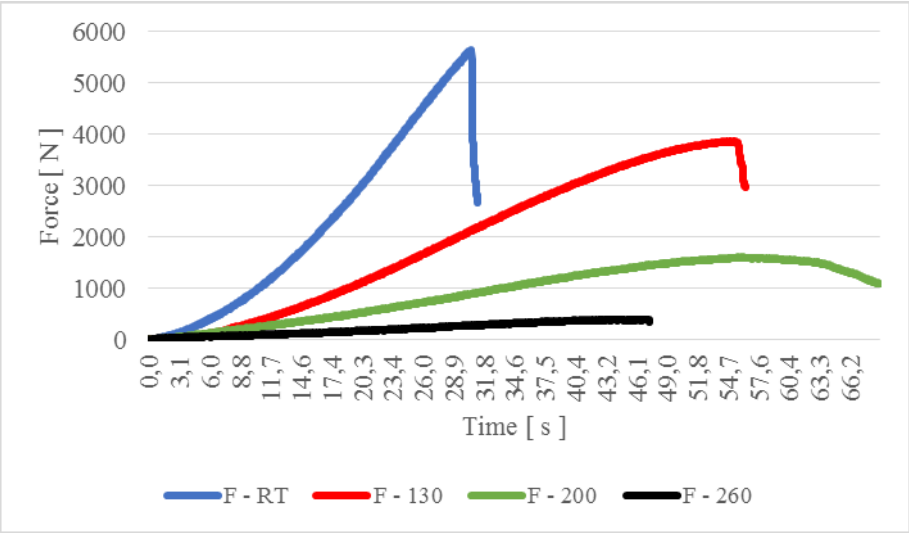

Figure 10.: Force-time diagram of the 200 width specimen

In this phase, the part is able to be formed, but the sheet is close to the failure point. With the investigation of this phase, the local contraction area would be well analysed. Increasing the forming temperature, the forming force was decreased. The lowest force was needed at 260°C. It shows, that for the elongation, less force is enough, because the yield strength decreased with the gaining temperature. It is unambiguous that material and crystal structure changes started at these temperatures, which causes the change of the formability.

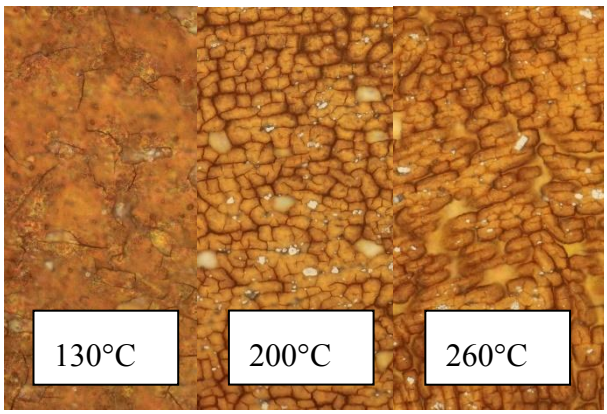

Figure 11.: Grain structure after forming at different temperatures

In the microscopic photos it is shown that the size of the grains are gained at the 200°C forming, but at the 260°C, the grain size is much bigger, and the structure is more different than the previous ones. In this study, we will not analyse the material structure changes (Figure 11.).

CONCLUSIONS

The investigations of the selected EN AW 5754 aluminium alloy were completed successfully: the formability increased when the temperature was elevated. Furthermore, we found the optimal forming temperature area of the alloy. The obtained FLC curves should be useful for the numerical modelling and for the technology planning. During the investigation, we could see, that a considerable formability growth only appeared above 130°C. This phenomenon indicates that we have to elevate the temperature from a defined value, to activate new slip planes. The new activated

slip planes cause formability growth until the recrystallization temperature (The recrystallization temperature of the EN AW 5754 is 240°C.), where the formability breaks down.

REFERENCES

[1] Európai Bizottság Kommunikációs Főigazgatóság, *Közérthetően az Európai Unió szakpolitikáiról - Éghajlat-politika*, Belgium, ISBN: 978-92-79-24716-3, 2014.
[2] International Council for Clean Transportation (ICCT); *Global Comparison for Passenger Car and Light Commercial Vehicle Fuel Economy/GHG Emissions Standards*; February 2014 Update; http://www.theicct.org
[3] Tisza, M.; *Képlékenyalakítás a járműiparban*; ISBN 978-963-358-082-0; Miskolci Egyetem 2015.
[4] *The Alu-maximised Car Study*, ika-RWTH-Aachen University, Germany, 2003.
[5] European Aluminium Association: *The Aluminium Automotive Manual*, (2002) http://www.alueurope.eu/aam/
[6] Kovács, P.Z.: *Alakítási határdiagramok elméleti és kísérleti elemzése*, PhD értekezés; Miskolci Egyetem 2015.

CONSIDERATION REGARDING THE IMPLEMENTATION OF RISC BASED MAINTENANCE ON MAIN COMPONENTS OF HIGH POWER DIESEL ENGINES

COROIAN Olimpia

Technical University of Cluj-Napoca
E-mail: olimpiatutas@yahoo.com

Abstract
The impetuous development of our country's economy has led over the years increased transportation tasks, raising questions regarding the ordinary course of production and supply of various industries. An important role in transportation owns railway, although the share of shipments made through the transportation has significantly decreased in recent years in favour of road transportation which is presently over 60% of all shipments carried out in Romania.
Repair and modernization of rolling stock is an important objective for each company in order to have an effective cooperation with companies working in rail transport, so that the transport company that can offer a higher degree of comfort, safety and quality of transport services.
The studies that we undertake, we propose to research the current situation of performing maintenance activities on some parts of the diesel engine in one of the companies, that has clearly this activity, and provide a plan maintenance based on risk, plan which provides improved services in the present.

Keywords: *maintenance, diesel engine, malfunctions*

1. INTRODUCTION

The diesel engine was designed by the German engineer Rudolf Diesel (who gives its name) between 1893-1897, for the purpose of service of the various means of transport - ships, trucks, locomotives, agricultural tractors, etc. The first diesel locomotive in the world was built and run in the summer of 1912, on the rail Winterhur-Romanshorn in Switzerland, but has proven to be a failure in terms of commercial, failing to apply new technology in a profitable manner. After several attempts in the United States by General Electrics, diesel engines specially designed for use in the case of locomotives, began slowly but surely, to beat the dominance of steam locomotives, due to increased efficiency in the manufacture and operation process.
For the successful implementation of a plan of maintenance on a diesel engine is impetuous need to know its components and their Tribology. Positive economic effects of applying tribological knowledge occur due to the following aspects [14] to extend the operation of engines, reducing outages and replacements of worn, reducing energy lost through friction, reducing the consumption of lubricants and materials.
The diesel engines are made from mobile and fixed parts. The main elements fixed diesel engine crankcase (lower engine that supports other parts thereof) cylinder block (the engine comprising cylinders), cylinder head (motor side care close cylinder TDC, respectively upper cylinder), pump housings, reduction gears, etc.
The main elements of the mobile are called as the diesel engine crank. Crank mechanism consists of many moving parts: the piston, connecting rod, crankshaft and piston and connecting rod assembly consisting of (completely assembled) called crankshaft.

Since the state of wear of the crank mechanism determines the intervals between repairs of locomotives, we study below this device.

2. DIAGNOSIS PRINCIPLES ON DIESEL ENGINES AND RESTORATION METHODS ON THE TECHNICAL STATE OF PARTS

An important step in the maintenance process, which can be determined, consists in identifying the potential defects as an early reforming of components would lead to an increase in the consumption of spare parts and hence the production spending and the use over the limit wear allowance would lead to an increase in energy consumption, failure to comply with the technical requirements and the reconditioning possibilities, even high possibility of accidents affecting the safety and security of personnel work.
Operational conditions of different equipment lead to wear and tear of different component parts that can change the lifetime of the equipment. The current trend is to use a system that reduces maintenance of involved costs. The intervention refers to maintenance, overhaul and repairs.
When it comes to repairs we refer to dismantlement, finding technical condition, washing components, replacement or refurbishment of parts, reassembly, testing and running. Reconditioning is a process that applies a single part in order to rebuild the technical condition. Technological reconditioning processes for compensating wear include: soldering charge, cold or hot micro pulverized alloys deposits, metallization, electroplating, plastic deformation, gluing, grouting, etc.
Checking the technical condition and then the possible solutions towards bringing equipment in normal operating condition and avoiding risks can be achieved by [12]: checking the technical condition without dismantling, checking the technical condition after the dismantle and control of hidden defects.

3. RISK BASED MAINTENANCE SYSTEM

The maintenance strategies have witnessed a continuous development starting from repairs in cases of emergency and developing based on the need to reduce costs, a maintenance strategy based on measurement and assessment of equipment during operation, in order to prevent adverse events. The risk-based maintenance system has as main pawn, the risk. Based on risk regular analyzes are carried out and a maintenance plan is established. An important step in the process, which can be determined step, consists in identifying the possible defects because a premature reorganization of the components would lead to an increase in the consumption of spare parts and consequently the production and use of government spending over the wear limit admissible would lead to an increase in energy consumption, failure technical conditions, prevention and reconditioning opportunities even to an accident affecting the safety and security of personnel work.

4. THE CRANKSHAFT

The crankshaft is the most important and expensive piece of the diesel engine, which is subject to the most complex applications. By means of the forward movement or the mechanical energy from the engine's cylinders by transmitting locomotive, being driven in rotation by the rod.
Taking into account the working conditions and its importance, the crankshaft must meet several requirements: to provide resistance and high stiffness, friction surfaces exhibit good resistance to wear, to avoid resonance oscillation of twisting, are balanced static and dynamic.

Characteristic malfunctions are deposits of debris in lubricating channels, cracks and crevices, bending, twisting, wear bearings and spindles crankpins, thread damage, wear mansions up and holes in the flange [14].
Deposits of impurities in the lubrication channels are cleaned with compressed air and oil installation or detergent under pressure of 12 daN / a rate of 15 / h.
Cracking of trees, unnoticed at the time, it causes serious damage (Figure 1). For this reason, after disassembling and cleaning is executed with strict control electromagnetic flaw detection, the ferromagnetic powder or solution, an ultrasonic crack or fluorescent liquid, and then checking the hardness spindles.

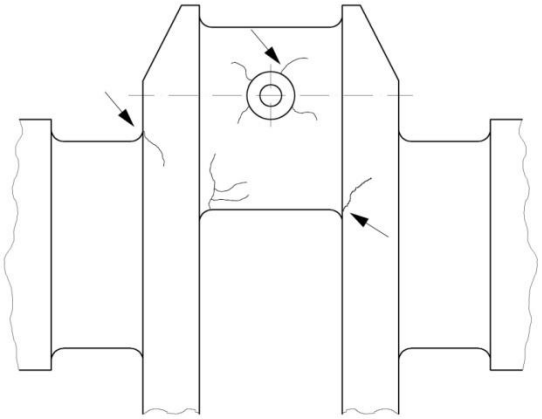

Figure 1 The cracking areas of crankshafts [14]

The crankshafts which show cracks are being reformed and only in case of force majeure, welded and then cut.
Bending crankshaft bearings are due to coaxially levels or the existence of unequal games between levels spindles and bearings.
Bending control is achieved using a dial comparator control board with prisms placed in the tree. The longer crankshaft and check the front to establish the beating of the axial flange. Control is performed by placing the probe flange comparator, and if the axis beating is greater than 0.05 mm, the front face of the flange is lathed.
Crankshaft torsion is usually insignificant if the engine suddenly blocking, gripping the shaft in bearings, pistons in the cylinder liners, etc. The torsion shaft is established by placing the light, and verifying the relative positions of spindles by rotating the shaft toward a designated location.
Wear due to friction spindles crankshaft gas under pressure and inertial forces pistons and spindles of the rod. Reconditioning of spindles waste processing is done either by size (speed) repairing or compensating the input material wear.
Processing dimensions repairs are performed at different stages and conditions of dimensional accuracy, shape and roughness of repair dimensions similar to the original is preserved. Wear compensation can be achieved by chrome plating, welding and plating. After deposition of metal to compensate for wear, follows the cutting processing and the dynamic balancing shaft.

5. THE ROD

The connecting rod is a component which connects the piston and the shaft, transforming the translational movement of the piston into rotary motion of the crankshaft. It is hinged at both ends and has a whole movement plane.

Severe working conditions require strong and rigid rod to have higher assured by design, materials and manufacturing
Damages that can occur during operation of the rod are: bending and torsion rod, wear alloy bush, wear housing for bearings, wear or damage threads, surface contact with the heads of the screws fastening the lid, or cracks in the body of the connecting rod [14].
Cracks can lead to rupture or damage the drive, so that both before and after reconditioning, all the rods can be controlled by flow, with the purpose of discovering cracks.
Bending and twisting of the connecting rod, is due mostly to inertial forces. A deformed rod bearing produces additional tasks, the piston rings and cylinder liner (Figure 2) which greatly accelerates the rate of wear.

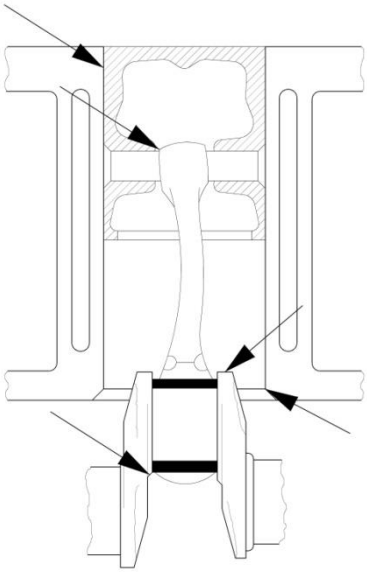

Figure 2 Sites for wear due to deformation of rods

Straightening of rods run cold on some special devices. The maximum permissible deviations are 0.05 mm over a length of 100 mm, and the rotations are the same lengths of 0.1 mm. Connecting rods that have undergone large deformation after straightening undergo a heat treatment, tempering by heating at 670-720 K and slow cooling with the furnace.
Wear head and foot rod bore (roundness) occurs due to weakening raise the rod or sleeve between bearing bronze. It is accepted that the maximum camber big bore -0.05 mm and -0.04 mm the smallest.
Refurbishment is done by turning the connecting rod bores fine on special boring machine connecting rod, or a universal car with a suitable device.
The head bore an elongated rod sometimes suffers in the longitudinal direction as a result of varying loads, mechanical and thermal. In this case, rebuild the original size of the bearing surfaces is achieved by processing the combination of rod cover and then bore the initial dimensional.

6. THE PISTON

The piston is the moving part which, under the action of the expanding gas in the cylinder, performs linear motion which is transmitted to the crankshaft via connecting rods. It provides the back and forth movements which carry the successive phases of the motor cycle.

Besides this main role, the mounted piston provides the air tightness of in the bottom of the cylinder engine, it prevents the penetration in the oil's firing chamber and discharges the quantity of received heat.
While choosing the material the piston is made, following have to be considered: resistance to mechanical and thermal pressure, light weight, to lower the inertial forces, easy and low-cost technology, low coefficient of superficial heat exchange in the cylinder. At the same time it is required high thermal conductivity for heat transfer reduced deformability in order to maintain the limits of the commutation between the piston and the cylinder.
During verification at the diesel engine pistons can be found these defects: wear segment channels, wear recesses for the piston pin, piston skirt wear, galling and cracks [14].
Wear of the channel segments occurs mostly in the axial direction and especially the first compression aid because alternatives shocks caused by forces of friction with gas cylinders under pressure and inertial forces.
Worn sofas are reconditioned in a correct geometric shape, size increased by about 0.5 mm in width, the initial accuracy and the rings are assembled with increased accordingly. Some units with a spacer ring compensates for wear, heat-treated, Fig. 3, and the piston assembly is done with new segments.
Reconditioning of segment channels are made by turning, with reliance on the inner surface, processed piston and support the tip of the tailstock with a knife shape (Fig. 4) [14].

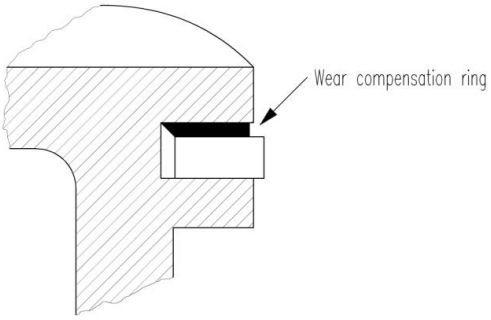

Figure 3 Channel segment wear compensation with a ring [14]

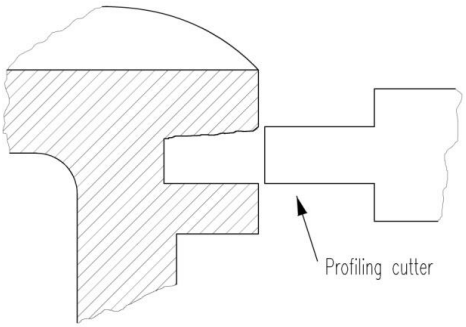

Figure 4 Reconditioning of channels with shaped knife segment [14]

Wear seat for bolt segment occurs due to gas pressure and inertial forces that produce camber, whole enlargement and weakening of tightening. Reconditioning of worn bores next step is to repair increased by 0.2 and 0.5 mm, assembly being made with the majority bolts.
Repair does not require a processing piston seized until complete disappearance of the tread pattern on the lateral surface. The point is to remove metal particles that were welded piston surface after seizure. Welded prominent particles must be removed by fine grinding with a grinder and there is no risk of damage to the piston cylinder surface. [17].
Due to considerable temperature and pressure being put on the piston head can crack it. Cracks may be shallow (superficial) or can cross the entire thickness of the piston head. Cracked engine pistons must be replaced always fast and slow engines will recondition or by sealing cracks with screws copper by oxyacetylene welding or by replacing the bottom [17].

CONCLUSION

Until it reached a state of failure, a diesel engine passes through certain phases / states of wear / degradation of its components. Reconditioning the components detected improper based on a risk maintenance plan, reduces operational costs up to 40%. Cost savings result from a better use of

energy, using high yield of raw materials and more effective control of inventory and quality of the parts in the process of manufacturing and of finished goods.
Knowing the potential faults that may occur during the functioning of diesel engines and their effects it can easily be established a general maintenance plan but without a more accurate risk analysis, full maintenance plan is compromised. I believe that removing the subjectivity of the human factor would lead to an improved quality of analysis. The challenge for any engineer maintenance is to prepare a maintenance plan based on possible risks to ensure the safety of both the team work and the environment, in terms of maximizing the availability of production equipment in terms of efficiency and to minimize total operating costs.

REFERENCES

[1] Blebea, I., Mocan, B., Steopan, A.,: *Reliability, maintainability and safety production systems*, U.T.PRESS, Cluj Napoca, 2013.
[2] Bonta, D.: *060-DA diesel electric locomotive of 2100 HP, construction, maintenance and operation*, Publisher ASAB, Bucharest, 2003.
[3] Cîmpan, M., ARGHIR, M.: *Studies and researches of equipment maintenance*, The 13th National Conference on Multidisciplinary, Sebes, 2013.
[4] Cîrstoiu, A.,: *Reliability, maintainability, availability*, Valahia University Press, Targoviste, 2008.
[5] Fulop, I.: *Theoretical and experimental research related to the application of risk-based maintenance in the cellulose and paper industry*, PhD Thesis, Cluj Napoca, 2010.
[6] Gyenge, C., Fraţila, D.: *Manufacturing Engineering*, course, Cluj Napoca, 2004.
[7] Gyenge, C.: *Technologies of auto manufacturing components, courses*, Cluj Napoca, 2010.
[8] Gramescu, T., Chirila V.: *Quality and reliability of products*, Technical Publishing House, Chisinau, 2001.
[9] Ionuţ, B., Rus, I.: *Maintenance, maintainability, tribology and reliability*, Publisher Sincron, Cluj-Napoca, 2003.
[10] Isac, C., Popoviciu, G.: *Diesel Electric Locomotive Technical Book, Vol. I*: Mechanical and thermal, Ministry of Transport and Telecommunications, Technical publications and documentation center, Bucharest, 1973.
[11] Moldovanu, I.: *The repair Tehnologia technology of farm machinery*, Didactic and Pedagogic Publisher, Bucuresti, 1976.
[12] Muresan, A.: *Contributions to the development of modern technologies for reconstructing some parts of the engine-transmission ensemble for diesel locomotives*, PhD Thesis, Cluj Napoca, 2010.
[13] Pisoschi, A.G., Popa, Gh., Constantinescu, A.: *Elements of durability, reliability and maintainability*, Universitaria Publishing House, Craiova, 2006.
[14] Praporgescu, G.: *Tribology. Lecture notes*, Petrosani 2010.
[15] Taraboi, V.: *The technology of repairing diesel engines*, Technical Publishing House, Bucuresti, 1956.
[16] Suteu, V.: *Technology maintenance and repair of machines and equipment*, Dacia Publishing Cluj Napoca, 1984.
[17] *Diesel hydraulic locomotive of 1250 HP, book*
[18] [*Rail freight in Romania*, Market Study, March 2013
[19] www.remarul.eu

DYNAMICS EXPERIMENTS APPLYING NI DEVICES AND LABVIEW

[1]DARAI Gyula, [2]FILEP Gábor, [3]NAGY-KONDOR Rita PhD, [4]SZIKI Gusztáv Áron PhD

[1,2]Department of Electrical Engineering and Mechatronics, Faculty of Engineering, University of Debrecen
E-mail: darai@eng.unideb.hu, filep95@gmail.com
[3,4]Department of Basic Technical Studies, Faculty of Engineering, University of Debrecen University of Debrecen
E-mail: rita@eng.unideb.hu, szikig@eng.unideb.hu

Abstract
Our program module "The Language of Mechanics" in the framework of TAMOP -4.2.3-12/1/KONV-2012-0048 project is recommended mainly to graduating secondary school students, but it can also be a useful practical supplement for college and university students in the subject Dynamics. In the program module a rolling motion problem is studied by students – supervised by teachers –theoretically and experimentally, applying a set-up which has been recently developed at the Faculty of Engineering the University of Debrecen. In the present work we describe measurement technique developments which had been made on the set-up applying NI devices and LabVIEW.

Keywords: *Mechanics, Teaching Physics, NI devices, LabVIEW.*

1. INTRODUCTION

In the last few years a lot of publications reported on the rapid decreasing of the mathematical knowledge and in general the educational level of students in higher education. It is also alarming that the skill to apply mathematics, physics and also the fundamental mathematical knowledge of graduated engineers show a decline. [2, 8]
Our course book „Mathematical tools in engineering applications" demonstrates the use of the different mathematical tools that are included in the syllabus of Mathematics (vectors, matrices, linear functions, differential and integral calculus, differential equations) in problems which are typical in Physics, Engineering Mechanics, Thermodynamics and Economics [4, 5, 6, 7]. We also elaborated a program module "The Language of Mechanics", which can be a useful practical supplement for secondary school students, college and university students to the subject Dynamics. The role of the course book and program module: help students understand the engineering aspects of the problems and make the connection between the mathematical, physical and engineering content of the problems clearer.

2. MEASUREMENT TECHNIQUE DEVELOPMENTS

In the frame of the TAMOP -4.2.3-12/1/KONV-2012-0048 project we elaborated a program module "The Language of Mechanics", which is recommended mainly to graduating secondary school students, but it can be also a useful practical supplementary help for college and university students for the subject Dynamics. [3, 9] During the program module we are studying a rolling motion problem theoretically and experimentally, applying a set-up which has been recently developed at the Faculty of Engineering University of Debrecen. (*Figure 1*)

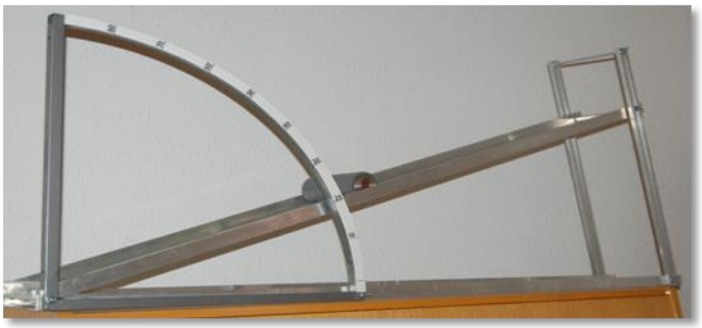

Figure 1 The experimental set-up before the measurement technique developments

The set-up is an incline, built up of aluminium profiles, on which a stainless steel cylinder is rolling. The rolling resistance of the cylinder can be increased by pulling a polyfoam tube on the cylinder. In the recent work we present measurement technique developments which had been made on the set-up applying NI devices and LabVIEW. [1, 10] *(Figure 2)*

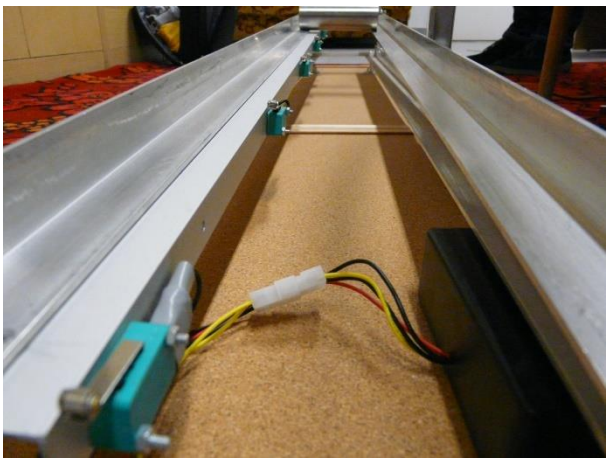

Figure 2 Measurement technique developments on the experimental set-up

The aim of the developments was to measure the time of rolling of the cylinder more accurate and also to determine the cylinder's kinematic functions (covered distance-, velocity- and acceleration-time functions of its centre of mass) experimentally. The above aim was realised applying six micro switch of MSW-0 type. *(Figure 3)*

Figure 3 Micro switch of MSW-0 type

The switches were mounted on the set-up as it is shown in *Figure 2*. For signal processing an NI USB-9234 data acquisition (DAQ) module *(Figure 4)* was used, which is a 4-channel C Series dynamic signal acquisition module specifically designed for high-channel-count sound and vibration applications.

Figure 4 NI USB-9234 data acquisition (DAQ) module

This instrument has an AC/DC analog input and 51.2 kS/s per channel maximum sampling rate.
The electric contact between the different parts of the measuring system was realised in an electric box. *(Figure 5)*

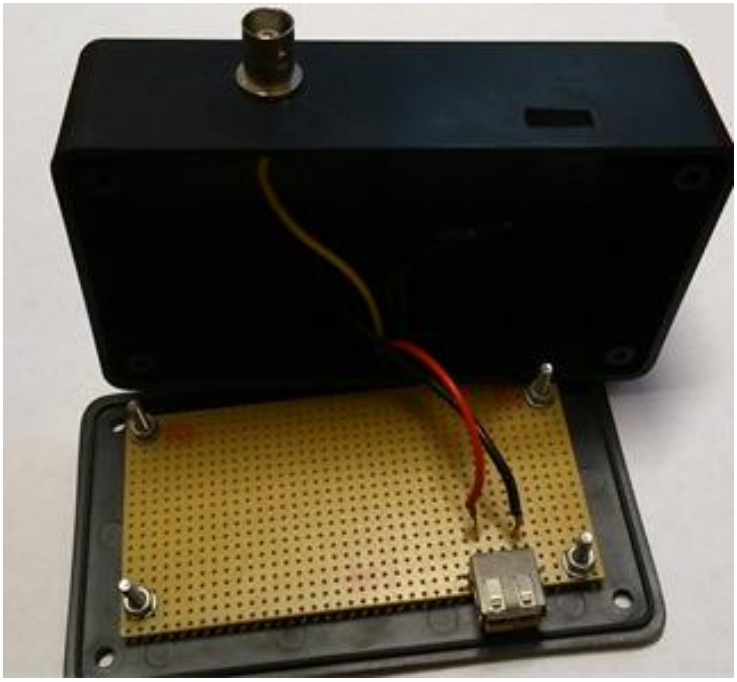

Figure 5 The electric box

The detailed circuit diagram of the measuring system is shown in *Figure 6*.

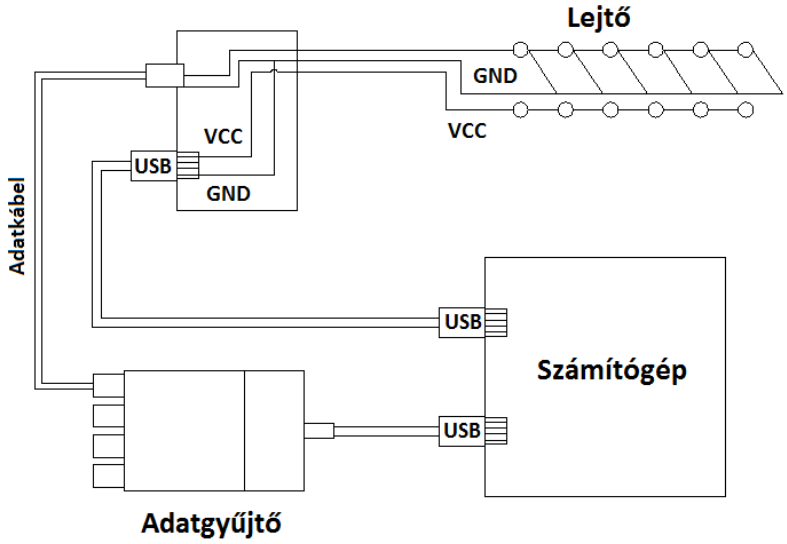

Figure 6 Circuit diagram of the measuring system

After we have built up our measuring system we created a program with LabVIEW 2012 software. The program is capable of measuring the elapsed time between the start of the cylinder and the switch on each switch. The block diagram of the program is shown in *Figure 7*.

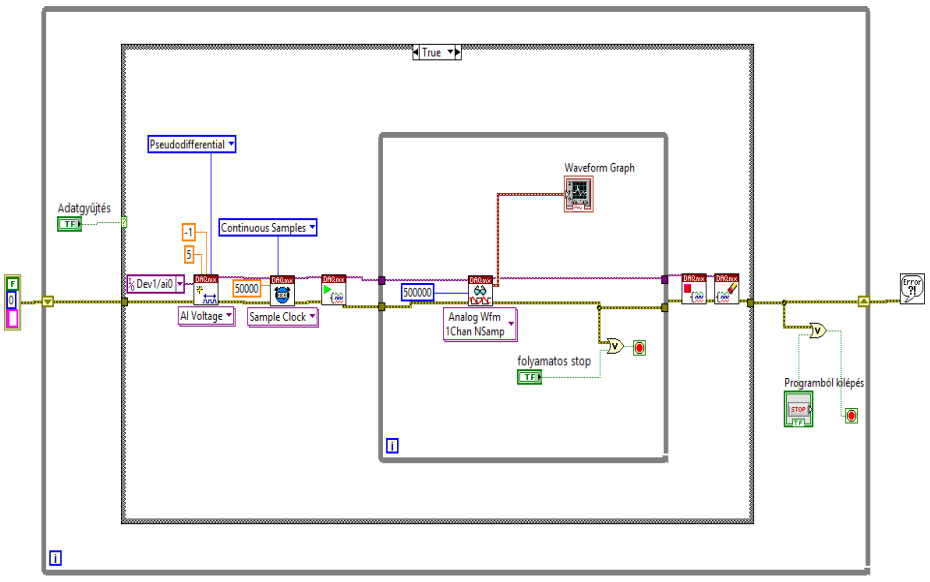

Figure 7 The LabVIEW program

Measuring the distance between the initial position of the cylinder and each switch we could plot the covered distance-time function of the cylinder. Figure 8 and 9 shows the measured values (single ticks) together with calculated ones (continuous line) in case of a cylinder without and with a polyfoam tube on it.

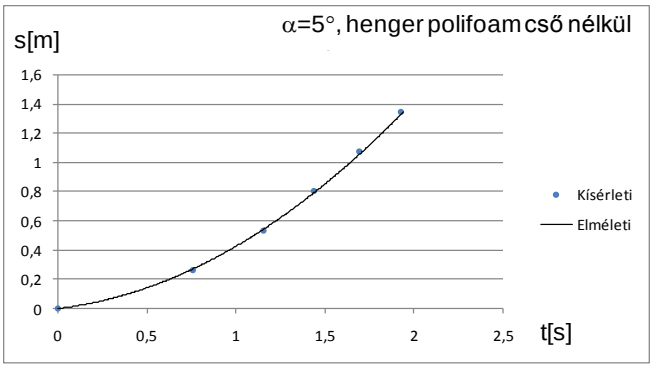

Figure 8 Comparison of experimental and theoretical position-time functions of the cylinder. (Polyfoam tube wasn't applied on the cylinder, α=5°)

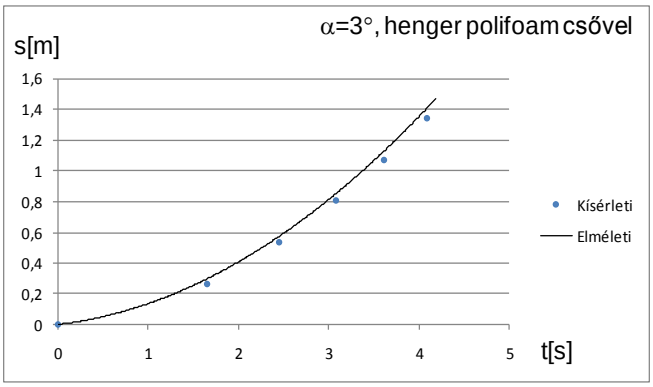

Figure 9 Comparison of experimental and theoretical position-time functions of the cylinder. (Polyfoam tube was applied on the cylinder, α=3°)

CONCLUSIONS

At the Department of Basic Technical Studies of the Faculty of Engineering, University of Debrecen we elaborated a program module "The Language of Mechanics", which is recommended mainly to graduating secondary school students, but it can be also a useful practical supplementary help for college and university students for the subject Dynamics. During the program module we are studying a rolling motion problem theoretically and experimentally, applying a set-up which has been recently developed at the Faculty of Engineering University of Debrecen.

In the program module students have to calculate the time of rolling of a stainless still cylinder (with and without a polyfoam tube pulled on it) applying their knowledge in mathematics, physics and informatics combined. Subsequently, they have to perform the experiment and compare the calculated and measured values.

In this article we described measurement technique developments which had been made on the set-up applying NI devices and LabVIEW. We believe that these modern devices and software will gather ground in secondary schools and also in higher education. We hope that our program module help to reach this aim.

REFERENCES

[1] *Bevezetés a mérnöki gyakorlatba, http://hungary.ni.com/akademia/oktatasi-teruletek/bevezetes-a-mernoki-gyakorlatba*
[2] Csákány, A., Pipek, J.: *A 2009. szeptemberében a műszaki és természettudományos szakokon tanulmányaikat kezdő hallgatók által írt matematika felmérő eredményeiről,* Matematikai Lapok, 1, 1-15.
[3] M. Csizmadia, B., Nándori, E.: *Mechanika mérnököknek: Mozgástan,* Nemzeti Tankönyvkiadó Rt.
[4] Nagy-Kondor, R., Síki, G. Á.: *GeoGebra animations for the course book "Mathematical tools in engineering applications"* (In: Report of Meeting Researches in Didactics of Mathematics and Computer Sciences). Teaching Mathematics and Computer Science, 12/1, 130., 2014
[5] Nagy-Kondor, R., Síki, G. Á.: *Engineering Applications in the Teaching of Mathematics II.* Debreceni Műszaki Közlemények, 1, 2014, pp. 57-60.
[6] Nagy-Kondor, R., Síki, G. Á.: *Mathematical tools in engineering applications.* 33rd International Congress of Teachers of Mathematics, Physics and IT, Conference Volume, pp. 50-54., 2009
[7] Nagyné Kondor, R., Síki, G. Á.: *Matematikai eszközök mérnöki alkalmazásokban* I. DE MK, Ceze Kft., 2009, ISBN 978-963-88614-0-5
[8] Radnóti, K., Pipek, J.: *A fizikatanítás eredményessége a közoktatásban,* Fizikai Szemle, 3, 107-113.
[9] Síki G., Á., Nagyné Kondor, R., Vinczéné Varga, A.: *Méréssel és számítógéppel támogatott mozgástani programelem középiskolásoknak és egyetemistáknak.* Proceedings of the Conference on Problem-based Learning in Engineering Education, 2013, ISBN 978-963-473-628-8, 24-28.
[10] *http://hungary.ni.com/labview*

MANUFACTURING OF TAPERED ROLLER BEARINGS, DEFECTS AND FAULT DETECTION

[1]DEÁK Krisztián, [2]KOCSIS Imre PhD

[1]Department of Mechanical Engineering, Faculty of Engineering, University of Debrecen
E-mail: deak.krisztian@eng.unideb.hu
[2]Department of Basic Technical Studies, Faculty of Engineering, University of Debrecen
E-mail: kocsisi@eng.unideb.hu

Abstract
Rolling bearings are one of the most important parts of the rotary machines. The most breakdowns derive from bearing defects. That is why so important to manufacture the bearings in outstanding quality. In this paper bearing manufacturing process is overviewed from the raw material handling to the end product. Typical steps are the cutting operations, grinding, finishing, heat treatment of the inner ring, outer ring and the rolling elements. Raw material rod could have inner cracks that should be investigated with Eddy current test. Pulling operation can cause traces on the roller surface which are parallel with the axis of the roller. Squeezing can cause irregular dents on the roller surfaces. If deburring is not perfect, shivers are pressed into the surface causing dents on the roller surfaces. During manufacturing several faults could emerged because of the grinding operation, grinding stone wear processes and chatter vibration. Inproper handling of the bearing parts because of the collosion to each other and the storing box. For further analysis Nitric acid 1-2% was used to initate the finished surface of the roller. Then 6-10% natrium-carbonate was used to nautralize the elements. They were washed in clean water, dryed under compressied air, finally greased with Castrol DW30X material. 240 rollers were analyzed from the previously Eddy current investigated rollers which were identified as bad quality rollers with inner cracks. 87% of the rollers had cracks inside. The average size of the cracks is 240,78 um from 138,7 um to 442,9 um.

Keywords: *bearing, manufacture, defects, fault, detection*

1. INTRODUCTION

Bearing, especially roller bearings are applied in every domestic and industrial applications. They are crucial part of machines and responsible for the most breakdowns. Condition monitoring helps to keep clear to unexpected failures and able to act before the problems happen. For reducing machinery downtime and maintenance time supervision is necessary during manufacturing.
Bearing defects have two main groups:
Manufacturing defects: material problems, cracks inside the material, grinding problems, pulling difficulties, improper handling of the bearing parts
Operational defects:
Wear, impact marks, smearing, spalls, fatigue cracks, corrosion, electric faults.
In this paper we focus on investigating the manufacturing defects.

2. PRODUCTION OF TAPERED ROLLER BEARINGS

Tapered roller bearings made of high tensile carbon steels, such us AISI 52100 and 100 Cr 6. Steel is handed by rigorous purification process when all impurities are removed by vacuum degassing.

Hardening of the steel is performed by heat treating process when microstructure of the steel is manipulated by cyclic heating and quick cooling processes to get 60…64 Rockwell C Hardness ratio. Finally penetration hardness test is made in order to determine the actual hardness of the bearing steel [1].

2.1. Production of inner and outer rings

1. First, raw material is arrived to production in form of forged rings. They are not separated thus inner ring and outer ring is one piece it is called tower-ring.

Figure 1 Raw material (left) and tower rings (right)

2. In second step tower ring is machined in its soft condition by turning operation with a single cutting tool.

Figure 2 Laterial grinded tower ring (left) and separated rings (right)

3. Next step is heat treatment of the bearing elements. Quenching is a process of cooling a metal at a rapid rate. This is most often done to produce a martensite transformation. In ferrous alloys, this will often produce a harder metal, while non-ferrous alloys will usually become softer than normal. To harden by quenching, a metal (usually steel or cast iron) must be heated above the upper critical temperature and then quickly cooled. By the heat treatment, hardness of the bearing steel is increased greatly and exceed 60 Rockwell Hardness ratio.

Figure 3 Heat treatment furnace (left) and heat treated rings (right)

4. In the fourth step grinding is applied to ensure the exact geometrical dimension both inner ring and outer ring. At first, sides of the rings are grinded, then lateral surfaces.

Figure 4 Side grinded rings (left) and lateral surface grinded rings (right)

5. After lateral surface grinding the races of the outer rings are machined. Firstly the races are grinded, then they are superfinished, finally stamped with identical numbers and letters on the sides of the rings. Identical information should contain the type of the bearing, brand, date of production, origin of the bearings.

Figure 5 Superfinished rings (left) and after stamping with ID characters (right)

2.2. Cage production

Cage of the bearing is manufactured from colled rolled sheets IS 4379, colled annealed sheets. Blanking, punching, forming, rivet hole making are made during the machining. The operational

sequence is blanking and piercing, forming pockets and piercing rivet holes. After surface treatment and cleaning, the cage is coated with preservative and transported to the assembly plant.
Another method in production of the cage of tappered roller bearings is to cut sections from the steel sheets then they are pressed to obtain smooth surfaces. Windows are cut from the piece of sheet according to the number of rollers of the bearing. Window geometrical dimensons are frequently measured. Finally they are washed and deburred before greasing and wrapping.
Plastic cages are not manufactured in the plant but they are purchased.

Figure 6 Cage under production

2.3. *Production of rollers*

Rollers are manufactured from cooled machined steel rods. They are purchased in 5 tonnes quantities. At first rod is cut then pressed to the tool.

Figure 6 Pressed rollers

Next step is the heat treatment of the rollers when the metallurgical condition of the material is enhanced by cyclic warming and cooling.

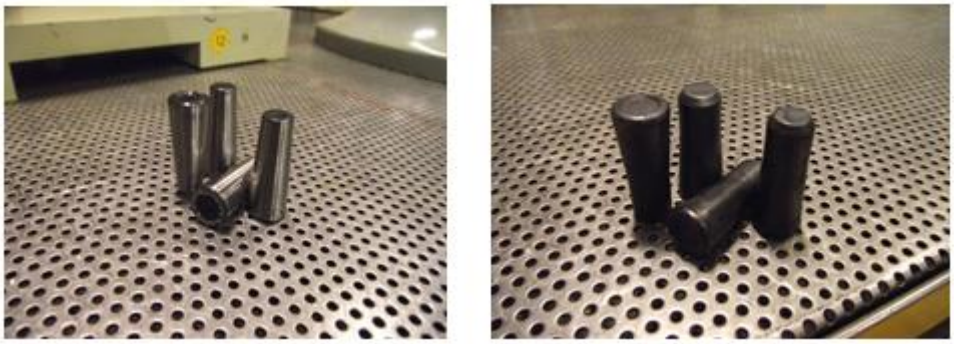

Figure 7 Finished rollers (left) and grinded rollers (right)

Lateral surfaces of the rollers are grinded, then face surfaces of the rollers are grinded. Smooth machining is necessary to ensure the standardized smoothness parameters. Superfinishing is applied to get very precise rollers. Rollers are visually inspected and dented rollers are separated from the health ones. It is important to classify the same diameter rollers before applying to the bearings. Precision of the sortiment is 0,003 mm. Rollers are not taken immediately into the bearing but only after further geometrical inspection in the measurement room.

2.4. Construction of the bearing

1. Final step is the construction of the bearings. All bearing parts should be placed to the construction section. Construction is separate from production so the efficiency does not depend on it.
2. Construction section are at the end of the production lines created construction cells. The advantage of this arragment that no storehouse necessary but bearing parts can be mixed which is the disadvantage of the process.
Construction has the steps: 1. Rollers are placed to the cage and the inner ring. 2. Cage pulling in order to ensure the exact size of the cage. In case of plastic cages there is no pulling movements. 3. Pairing with the outer ring 4. Washing and cleaning 5. Measurement of the construction height 6. Vibration measurement of the bearing 7. Greasing 8. Wrapping

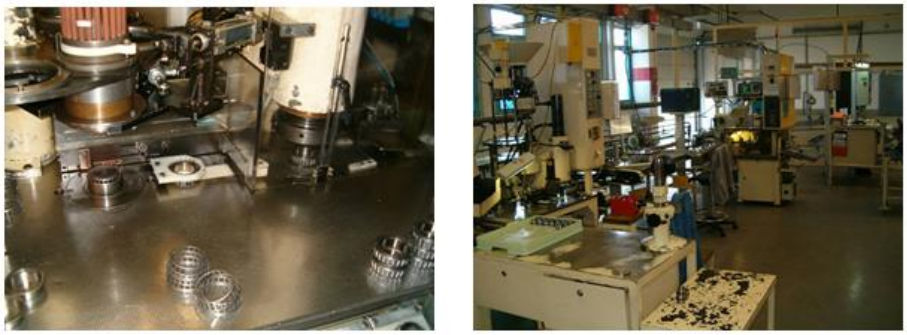

Figure 8 Stamping and pulling of the cage (left) and construction operation (right)

3. ISHIKAWA METHOD FOR ROOT CAUSE ANALYSIS

In this paper we focus on only the technical factors of the process. We do not focus on human and enviromental factors. Remaining useful lifetime is greatly influenced by manufacturing and operational defects [2,3].

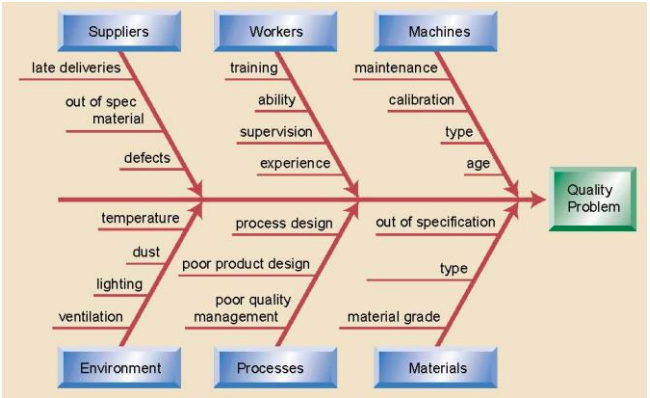

Figure 9 Ishikawa analysis for revealing root causes

Machine problems
Grinding problems due to grinding wheel wear process and misaligment of the wheel. Chatter vibration could have source of machining defects as well.

Figure 10 Misgrinded roller

Process and technology problems
Pulling operation can cause traces on the roller surface which are parallel with the axis of the roller.

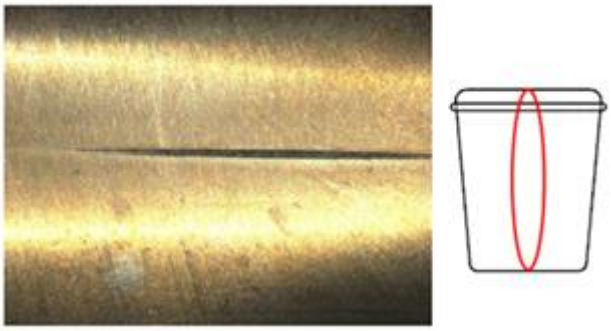

Figure 11 Pulling traces

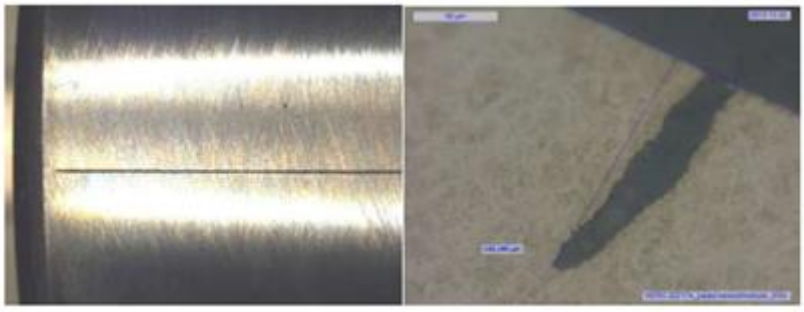

Figure 12 Pulling traces magnified under optical microscope

Squeezing can cause irregular dents on the roller surfaces. If deburring is not perfect, chips are pressed into the surface causing dents on the roller surfaces. Dents are placed mostly near to the radius of the rollers.

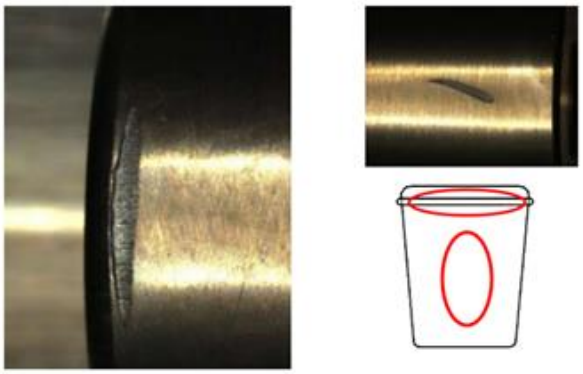

Figure 13 Chip injuries on the rollers I.

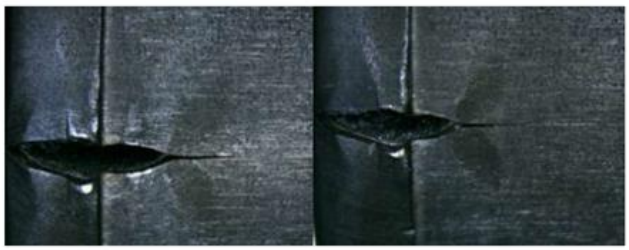

Figure 14 Chip injuries on the rollers II.

Inproper handling

Inproper handling of the bearing parts because of the collosion to each other and the storing box. On the surface of the rollers and inner rings dents are usually placed because of the unproper handling of the bearing elements. Mechanical damages and impacts are minimalized by using rubber plated storing boxes.

Figure 15 Storing box covered with rubber layer

Figure 16 Dents on the rollers due to mishandling

Material problems

Raw material rods sometimes have tiny cracks inside. If these cracks are not revealed properly they can cause operational problems. Eddy current measurements are generally used to investigate crack problems. Eddy currents are loops of electric current induced within conductors by a changing magnetic field in the conductor, due to Faraday's law of induction. Eddy currents flow in closed loops within conductors, in planes perpendicular to the magnetic field. Eddy current techniques are commonly used for the nondestructive examination (NDE) and condition monitoring of a large variety of metallic structures, including heat exchanger tubes, aircraft fuselage, and aircraft structural components.

4. DEFECTS ANALYSIS WITH OPTICAL AND SEMI-CONTACT METHOD

Dents on the rollers are measured under microscope generally 50x magnification. Size and form of the dent is determined.

Cracks are analyzed both with microscope and Eddy current testing. For deeper analysis rollers are sometimes further investigated. Rollers should be cleaned in ultrasonic bath. They are submerged into hydrochloric acid P3 UPON 5805 4-6% to emphasize the crack initiation. 5-10 minutes are necessary to the process but longer times can cause corrosion of the 100Cr6 bearing steel.

Nitric acid 1-2% was used to initiate the finished surface of the roller. Then 6-10% natrium-carbonate was used to neutralize the elements. They were washed in clean water, dryed under compressed air, finally greased with Castrol DW30X material.

Rollers can be cut to see the inner cracks of the rollers. It is sometimes analysed and measured under optical microscope. After cutting the roller surface should be finished to get a very smooth surface topography. Finishing is in three steps: 80 size grinding wheel is used, then 500 size wheel, finally 1200 size wheel. One cycle is about 5 minutes with 50 N pushing force. Final step is to place them in special DuroFast bacelit powder that is heat treated to get solid state.

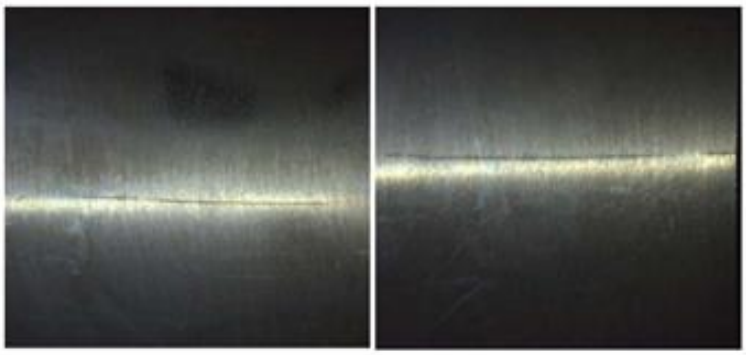

Figure 17 Cracks on the roller surface

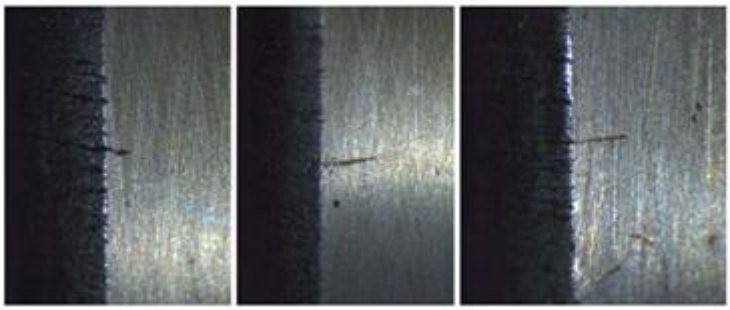

Figure 18 Cracks in the radius of the roller

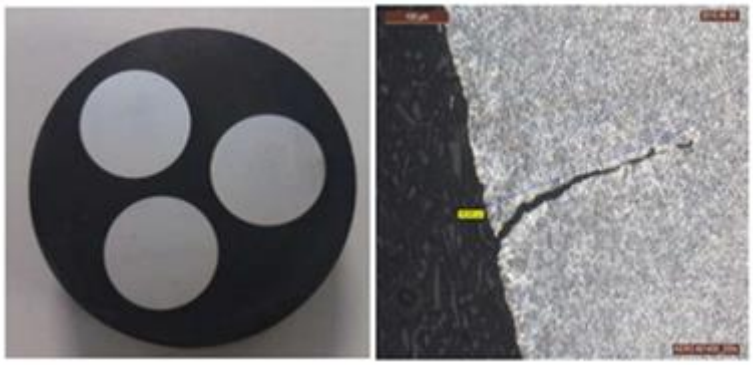

Figure 19 Embedded rollers (left) and cracks of the roller under 50x optical microscope (right)

Leica optical microscope was used in our experiment to measure the inner crack size. 240 rollers were analyzed from the previously Eddy current investigated rollers which were identified as bad quality rollers with inner cracks. 87% of the rollers had cracks inside. The average size of the cracks is 240,78 um, from 138,7 um to 442,9 um. Mahr Perthometer was used to measure the surface injuries.

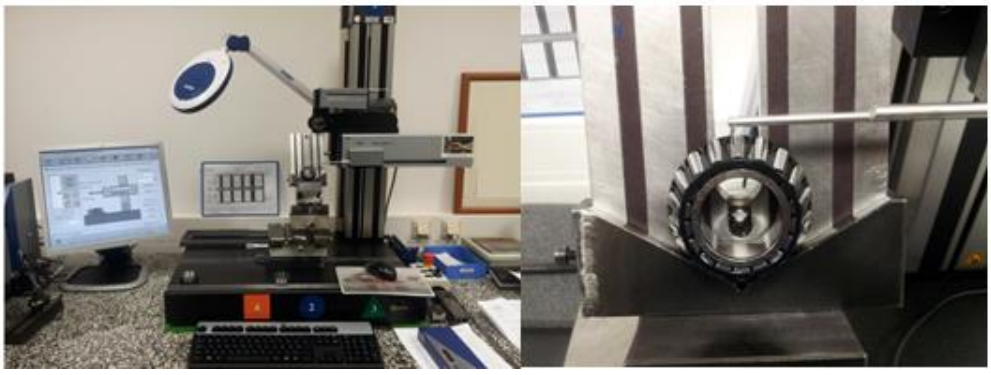

Figure 20 Mahr Perthometer (left) and semi-contact measurements of surface faults (right)

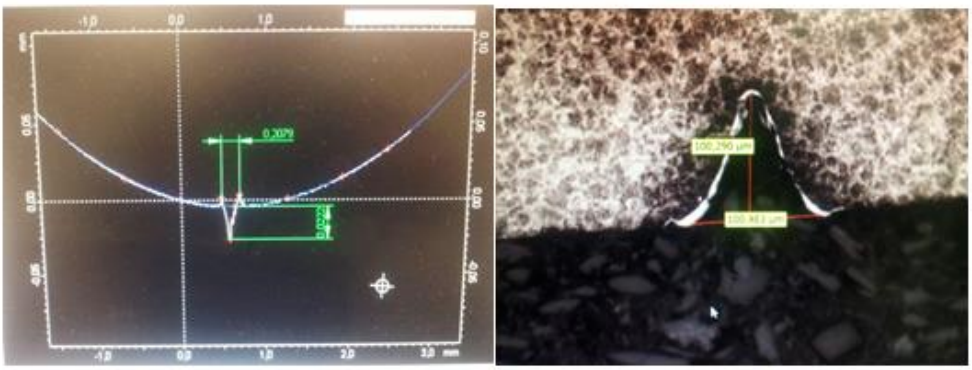

Figure 21 Inner crack dimension measurement with Mahr Perthometer (left) and optical microscope (right)

Mechanical injuries of the machine parts cause excessive vibration of the bearing. Bearings are further measured with vibration transducers and DAQ systems with Fourier transform in bearing manufacturing. These measurements are presented other papers of the authors.

CONCLUSIONS

In this paper tapered roller bearing faults were overviewed. These faults can be classified as production and operational faults. Manufacturing faults are investigated from the raw material handling to the end product. Sometimes raw material consists of inner crack that cause further problems. Eddy current testing in one method to reveal inner cracks but the process in not sure so other additional supervisions are applied. Manufacturing problems are from grinding defects, chatter vibration, irregular shape of grinding stone due to tool wear process and tool misalignment, pulling and squeezing operations. Improper handling of bearing elements could emerge when rings and rolling elements suffer plastic deformation such us dents and mechanical irregularities. Sources were revealed and analyzed by Ishikawa diagram. It is clear that beside human and environmental factors, machine and technology have a great influence on bearing quality. Visual inspection by optical devices can be efficiently applied to validate the outside faults. For analyzing inner cracks it was good result by cutting the rollers then handled by acids and placed, reinforced in test specimens. Cracks average dimension during manufacturing was determined by investigating 240 pieces of previously tested rollers. It is clear that constant development of technological processes is absolutely necessary in bearing manufacture.

REFERENCES

[1] Harncy, A.: *Bearing Design in Machinery – Engineering Tribology and Lubrication*, Marcel Dekker Inc, New York, 323-329., 2003.
[2] Medjaher, K., Tobon-Mejia, D.A., Zerhouni, N.: *Remaining useful life estimation of ctritical components whit application to bearings* IEEE Transactions on Reliability pp.292-302., 2012.
[3] Sutrisno, E., Hyunseok, B., Sarathi Vasan, A.S., Pecht, M.: *Estimation of Remaining Useful Life of Ball Bearings using Data Driven Methodologies*, Center of Advanced Life Cycle Engineering (CALCE), 2012.

AN EFFICIENT KINEMATIC SURFACE SIMULATION SYSTEM

DUDÁS László PhD

Department of Information Engineering, University of Miskolc
E-mail: iitdl@uni-miskolc.hu

Abstract
The paper introduces the well known Surface Constructor kinematical development and simulation program shortly, then presents some results achieved using it. Among the demonstrated examples the grinding wheel generation for exact grinding of a tapered worm, the determination of the mating members of a hypoid gear set, designing a new type of twice modified worm gearing, modelling and determination of the contact pattern of a worm gear pair having elliptical profile in the axle plane and modelling the parts of a new type internal combustion engine will be introduced. These results demonstrate the versatility and efficiency of the Surface Constructor software application.

Keywords: *gear development, Surface Constructor, internal combustion engine.*

1. INTRODUCTION

The quality of gears and efficiency of gear connections has been a major interest of gear designers and manufacturers from the start. The special characteristics and requirements of this goal have resulted in special software tools for aiding the processes of design and technology. There are many unique software programs for design of a given type or a narrow set of types of commonly applied gearings. These programs are created and used by the gear manufacturing machine tool providers or gearing design offices. There are fewer applications for helping with the innovation of new gearing types.
In the followings the well known Surface Constructor kinematical surface modelling and motion simulation application well be refreshed and its effectiveness in designing and analysing new gear and conjugate surface constructions will be demonstrated through examples.

2. SURVEYING METHODS FOR OPTIMUM GEAR DESIGN

The design of teethed parts or more generally of conjugate surface pairs has become a matured area these days. In the very beginning the researchers set a goal of determining the shape of an unknown surface contacting with the given surface in a line. The kinematical method and differential geometry were successfully used to solve this task. These tools made it possible to discover deviances, namely local under-cuts, and to give the border of points connecting in an enveloped manner [1].
Later the bettering of quality of contact became conspicuous. The form and the position of contacting lines, the angle relative to the direction of sliding velocity and the curvature relations were optimised to achieve loadable oil film and better lubrication.
Modificated contact areas were applied. Still, applying local methods initiated research into the effect of errors of the kinematical system on the suitable formation of surfaces and connection. Using multi- motion parametric kinematical models or intermediary generating surface in the examinations, the analysis of conjugate surface pairs was followed by discussion of point-type

contact. The effects of transmission error and the angle speed error characterising these types of gearings were detailed. The trace of the contacting line or contacting point was optimised, taking into consideration the transmission of force or driving moment.
As a result of powerful computer technology it has become possible to analyse real contact using 3D computer simulation. Moreover it is possible to simulate the manufacturing and cutting process for producing gear surfaces. This computational power is enough to carry out global examinations to detect global cut that depends on the used space or time interval. Models combining local and global computing theory were also published. A compact model was introduced by the author [2]. Determination of bearing patterns, ease-off topography and transmission error are common features of today's programs.

3. THE THEORY AND THE SOFTWARE REALISATION

The Reaching Model was discussed in detailed form by Dudás, L. [2]. The model resolves the well known task of gearings, the determination of the F2 conjugate surface if the generating F1 surface and the generating motion are given.
The main advantage of the model is its simplicity. In this model the generation of one of the points of the F2 surface is equal to solving a simple minimum value problem. The model can give all the types of local undercuts simply by discussing the minimum value problem in a local tangential point and can produce global cuts using the time and appropriate space interval given by the kinematical task. Though the theory works with analytical expressions and partial derivatives, a robust, surface-independent software for realisation of the theory was developed on a discrete numerical basis. This software realises the advances of the theory and is named Surface Constructor (SC). All the details of the algorithm are presented by Dudás, L. [3].
The system applies a two-level structure – symbolic and numerical representation of the objects. The embedded symbolic algebraic computation makes the use of the program convenient and flexible. SC starts as an empty kinematical modelling shell and models the kinematical modelling process itself. The system sketched in Fig. 1 has three main representation levels:

- the symbolic level, which uses a symbolic algebraic representation of the objects in the kinematical model,
- the numerical level, which stores the given and computed objects using numerical form, and
- the visualisation level, which allows the analysis of views and motion of the objects.

The selection and visualisation options are as follows:

- *F2glob*: global computational method and appropriate result
- *F2lok*: local computational method and appropriate result
- *F2al*: computation and visualisation of the occurrences of local undercuts
- *Φ :* computation and visualisation of moving path of selected points
- *R-Φ* : computation and visualisation of *R=R(Φ)* functions as a special feature of this software
- *v_a*: computation and visualisation of the space of relative speed and acceleration
- *PT* : computation and visualisation of axoids.

Most of these notions are discussed in detailed form by Dudás, L., [4]. The application can envelope different *F2i* surfaces by the same generating *F1* surface, modelling point-like connections in such a way.

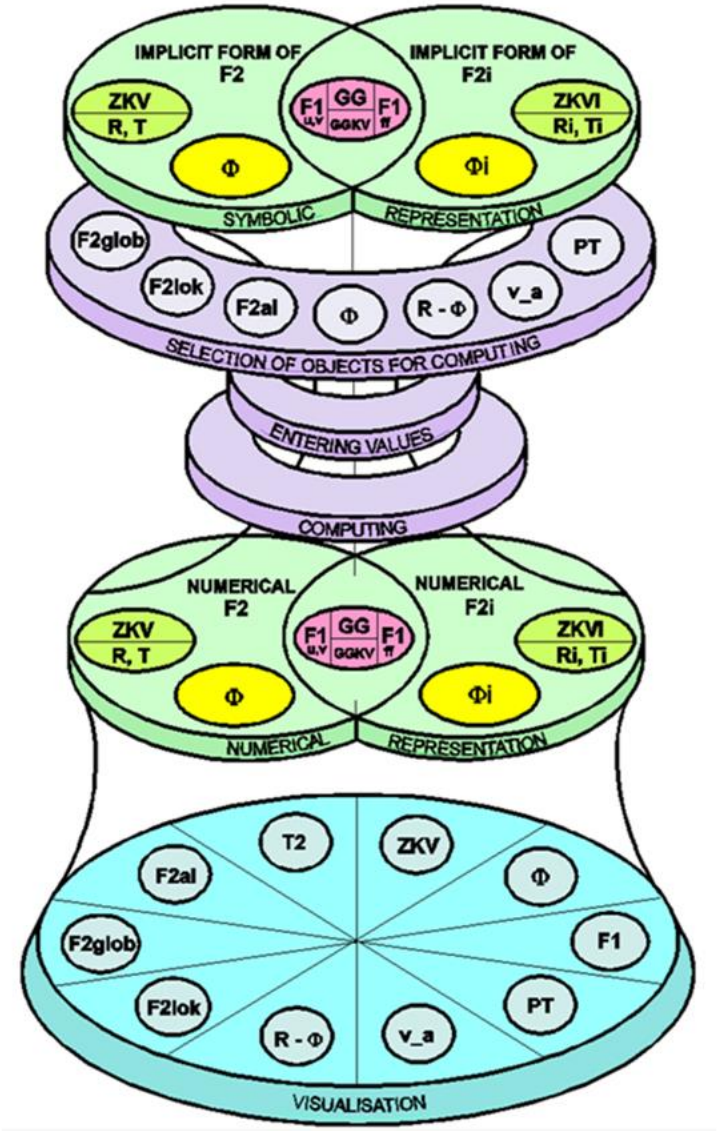

Figure 1 Structure of the gear development system

4. DEMONSTRATIVE EXAMPLES OF TASKS MODELLED BY SC

In the followings the paper presents some examples that demonstrate the power, versatility and efficiency of the SC kiematical modelling and simulation system.

4.1. Grinding wheel generation for theoretically exact grinding of tapered worms

In this example the surface of the worm functioned as the F1 generator surface and enveloped the working surface of the grinding wheel. This wheel is a very special and new type requiring special grinding machine and technology that is similar to Reishauer type grinding. The machine is special beacause applies a 1:1 revolving ratio. See Fig. 2.

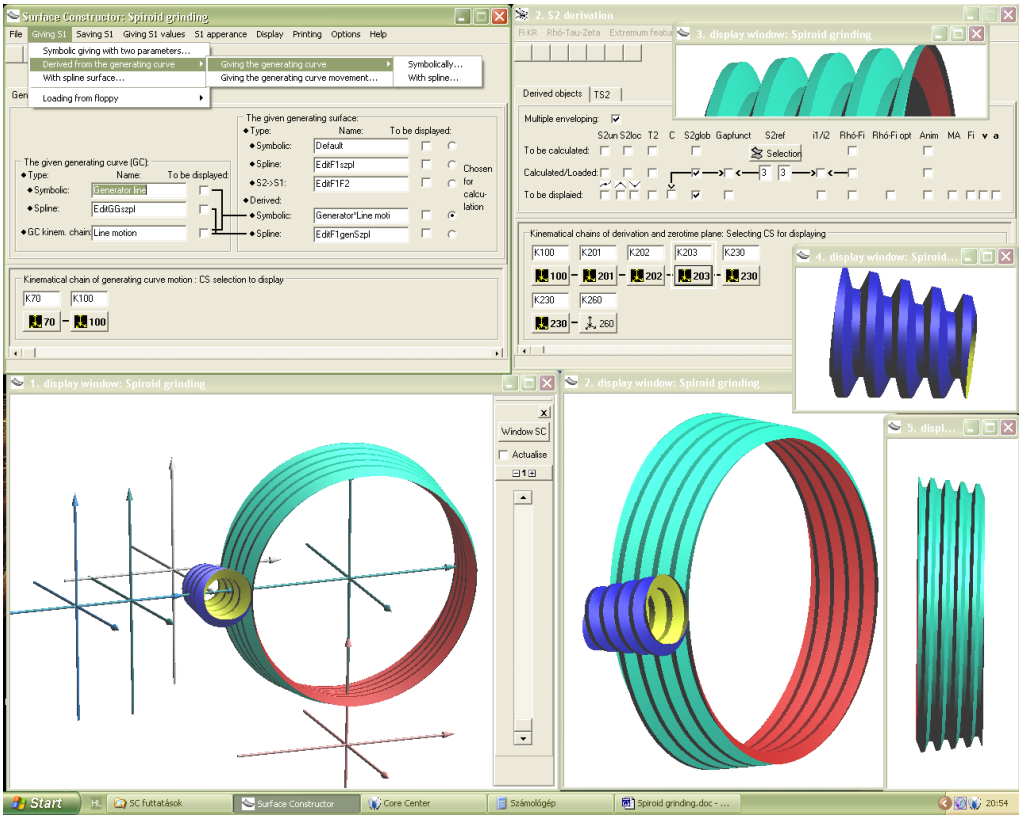

Figure 2 The analysis of theoretically exact grinding of a conical worm in the SC system

4.2. Determination of the mating members of a hypoid gear set

The hypoid generation method applies an intermediary generating surface for enveloping the two gear members. As a result, this method produces point-like contact between the gears. It is advantageous to avoid problems caused by manufacturing and assembly errors. Figure 3 shows the generated gear surface segments, the generator surface, the contact curve between larger gear and the generator surface and the quasi elliptical localised point-like contact pattern.

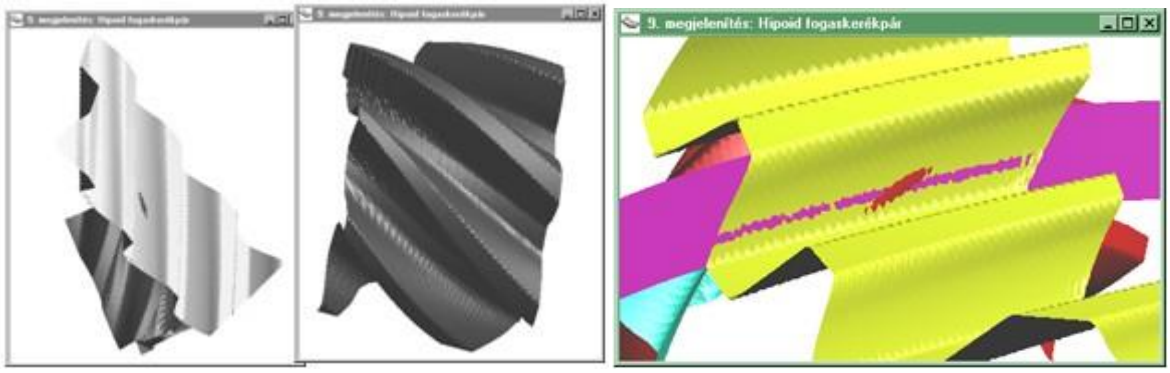

Figure 3 Spiral bevel gear segments and the ellipse contact pattern

4.3. New type of twice modified worm gearing

The next example will introduce the use of SC for investigating a new modification method for worm gearing with an elliptical generating curve in the axle plane of the worm.
The modification of gearing members is usually applied to achieve smooth starting and finishing of

connection when the teeth enter or exit from the meshing. Though these transitions are smoother in the case of helical gearings than with the connection of spur gears, the effect of elastic deformation because of the load or manufacturing and assembly errors causes deviance from the designed exact conditions. The goal of the modification is to achieve a point-like contact pattern instead of the exact line form of connections having one motion parameter. See Fig. 4.

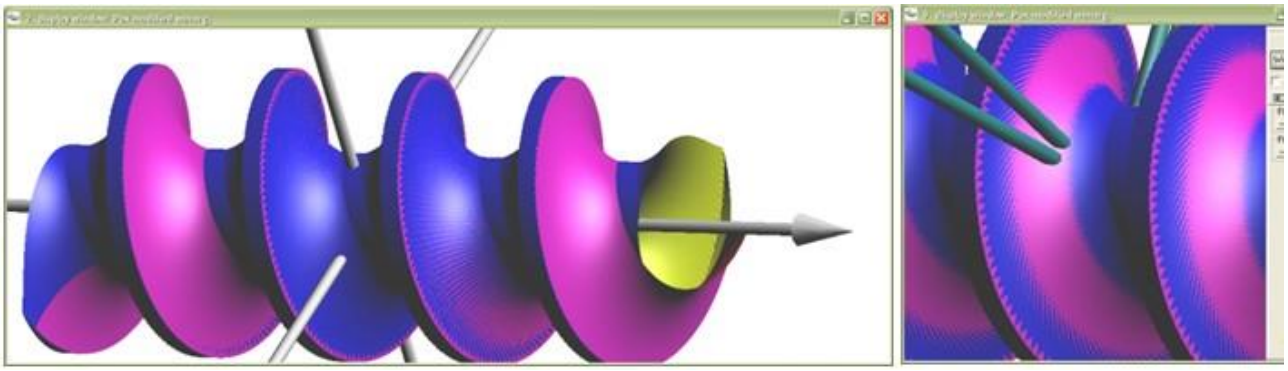

Figure 4 The worm with axially modified tooth surfaces and the lighter reference helicoid (to the left), and the second modification that localises the contact pattern in radial direction.

To make visible the very small axial modification, the non-modified helical surface is also drawn using a different, lighter colour. This surface stands out from the modified surface, showing that the modification results in larger differences at the two ends of the worm. This method is applied for visualisation of the effect of the second, radial modification. Fig. 5 shows the summated result of the two modifications on the contact patterns.

4.4. Modelling and determination of the contact pattern of a worm gear pair having elliptical profile

The elliptical profile gives one more degree for setting the form of the worm surface relatively to the circle profile. This worm gearing has an X form of the contact pattern in the muddle of mating process as demonstrated in Fig. 6. Moreover the curves of the pattern have an advantageous radial direction.

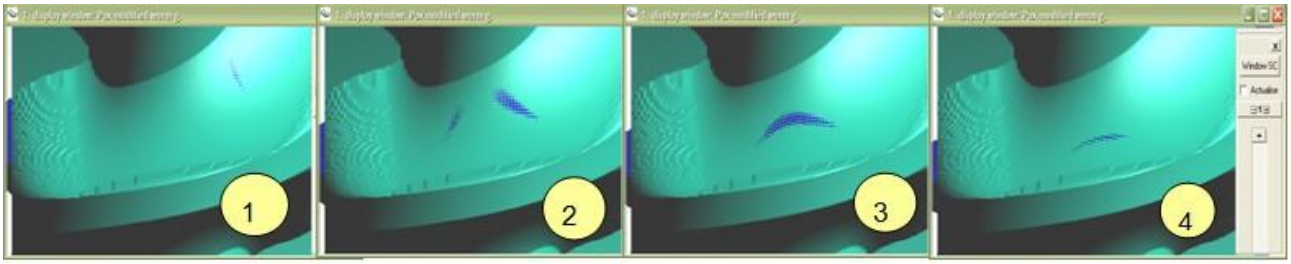

Figure 5 Contact patterns of the twice modified worm gearing

4.5. Modelling the parts of a new type internal combustion engine

For the modelling of the rotor and the rotary house of the engine the Surface Constructor was used. The rotor surface is a swept surface where the generator curve is an ellipse. The sweeping motion is a helical motion with changing pitch along the length of the rotor. Then the rotor is used in the enveloping process to generate the rotary house. The two parts are shown in Fig. 7.

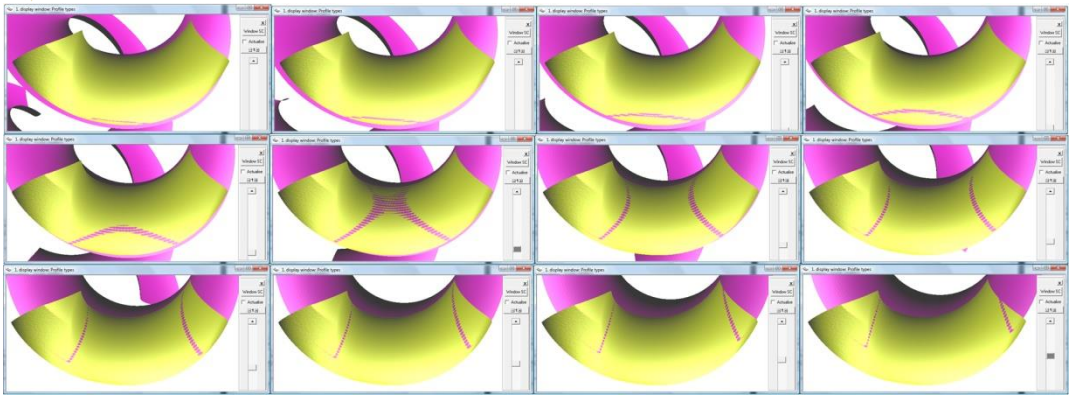

Figure 6 Contact lines of the worm gearing having elliptical profile

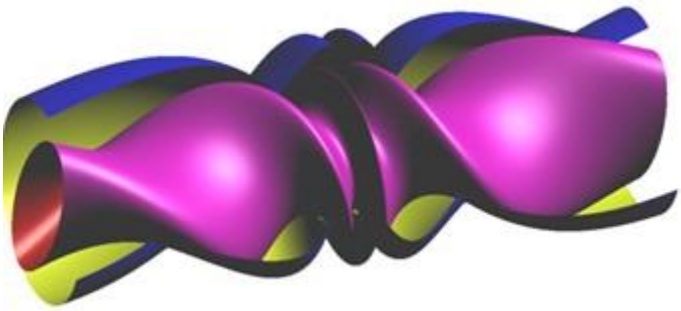

Figure 7 The opened rotary housing and the rotor

CONCLUSIONS

The paper refreshed the theory and the application of the Surface Constructor software system then demonstrated its versatility and efficiency through examples. The system proved its power many times.

ACKNOWLEDGMENTS

This research was partially carried out in the framework of the TÁMOP-4.1.1.C-12/1/KONV-2012-0002: "Cooperation between higher education, research institutes and automotive industry". The Project is supported by the Hungarian Government and co-financed by the European Social Fund.

References

[1] Litvin, F.L.: *Theory of Gearing*, p. 478, NASA Publication RP-1212 U.S.A., Washington, DC., 1989.

[2] Dudás, L.: "*A Consistent Model for Generating Conjugate Surfaces and Determining All the Types of Local Undercuts and Global Cut*"; Proceedings of UMTIK'96 International Machine Design and Production Conference, Ankara, pp. 467-476., 1996.

[3] Dudás, L.:*"Resolution of Geometrical Problems of Contacting Surfaces Using the Reaching Model"* (in Hungarian), PhD Thesis, Hungarian Academy of Sciences, Budapest, 1992.

[4] Dudás, L.: "*Surface Constructor - a Tool for Investigation of Gear Surface Connection*", Proceedings of CIM 2003 Advanced Design and Management Conference, Wisla, pp. 140-147., 2003.

INTERNATIONAL SCIENTIFIC CONFERENCE ON ADVANCES IN MECHANICAL ENGINEERING

19 November 2015, Debrecen, Hungary

OPTIMIZATION OF BUFFER TANK FILLED WITH PHASE CHANGE MATERIAL

FARKAS Rita, ANDRÁSSY Zoltán, SZABÓ János PhD, SZÁNTHÓ Zoltán PhD

Faculty of Mechanical Engineering, Budapest University of Technology and Economics
E-mail: f.rita33@gmail.com, zolee92@gmail.com

Abstract
In our paper we present phase change materials, as effective thermal energy storage due to their great latent heat storing possibility. The main substance used for thermal energy storage purposes is water. Storing the energy with water is not that effective as with phase change materials, because the temperature of water has to change, and it worsen the heat exchange intensity. On the other hand, with phase change materials the temperature of the material does not have to change due to the latent heat storage possibilities. We investigate a buffer tank with two pipe coils, filled with phase change materials with the aim to reduce the storage volume. We present an own thermodynamic model, a CFD simulation and an experimental system. We could validate our models and could examine the process of phase change. We could calculate the performance of heat absorption and release of the phase change material in the function of inlet water temperature and mass flow.

Keywords: *phase change material, thermal energy storage, heat storage tank*

1. INTRODUCTION

Energy is one of the most fundamental parts of our world. Our goal is to reduce the energy demand by increasing the efficiency of energy usage. About three-quarter of the energy consumption utilized in Hungary for heating and cooling in residential and commercial buildings. In our paper we want to find a solution for this problem with using phase change materials (PCM).
PCMs are a type of thermal energy storage materials, which use the latent heat hereby they can store energy with higher density. PCMs can be organic compounds like paraffin and fatty acids or inorganic like salts hydrates [1], [2].
We made an essay about the using of PCMs for the Scientific Student Conference on 2013. We investigated a storage tank filled with PCM and a gas boiler of a residential building cooperation. We proved that 4,63% efficiency improvement could be achieved during the heating period, which means 4,3% fuel saving. This improvement can only be achieved, when the PCM can absorb and release the optimal quantity of heat. In this summer we got the opportunity from the Department of Building Services and Process Engineering to make an experimental system in the Department's laboratory. In this paper we investigate the process of phase change and the heat capacity of the tank. Paraffin was used as phase change material, which physical properties is summarized in the *Table 1.*

Table 1 Physical properties of paraffin

Physical property	**Volume**
Solidification temperature	52 °C
Melting temperature	54 °C
Latent heat	145,3 kJ/kg
Solid specific heat	2 kJ/kg K
Liquid specific heat	2,3 kJ/kg K
Solid density	802 kg/m3
Liquid density	743 kg/m3
Heat transfer coefficient	0,7 W/m K

The solidification and melting temperature, the latent heat of fusion and the solid and liquid specific heat were measured with a DSC equipment, solid and liquid density were calculated from the volume and the weight, and the heat transfer coefficient was measured with Laser flash method.

2. METHODS

The process of phase change was investigated with measurement, numerical calculations and ANSYS simulation.

2.1. Measurement

On the *Figure 1* the Process flow diagram and on the *Figure 2* the measurement station can be seen.

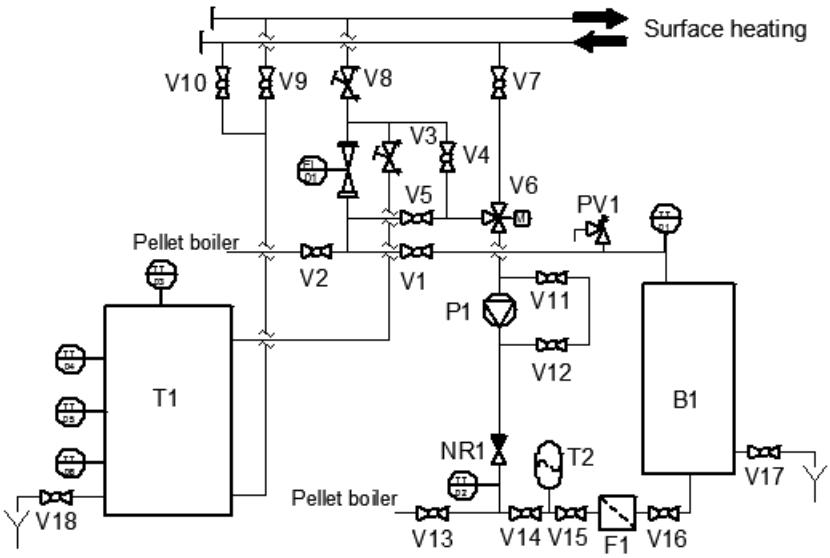

Figure 1 Process flow diagram

Notation: B: boiler, T: tank, V: valve, NR: non return valve, P: pump, F: filter, TT: temperature transporter, FI: flow indicator

Figure 2 Measurement station

The solid fuel boiler was signed with B1, the tank filled with PCM was signed with T1 and the heat consumer was the surface heating system of the laboratory. The hot water came from the boiler and it could be controlled to go to the surface heating or to the tank with the valve V8 and V3. The

return water from the tank could continue its way to the surface heating and to the boiler too. It could be controlled with the valve V10 and V9.
The dimensions and the inside shape of the tank is shown on the *Figure 3, Figure 4.*

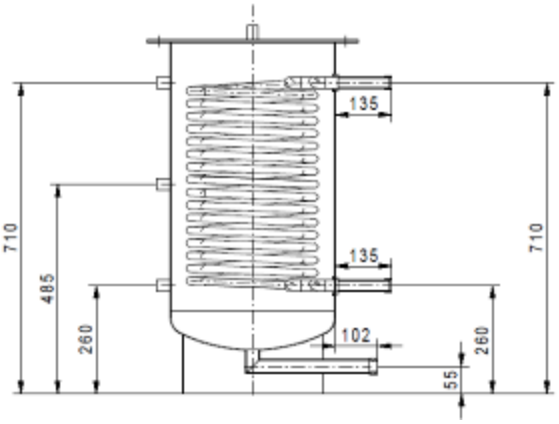

Figure 3 The dimensions of the tank

Figure 4 The double pipe coil inside the tank

2.2. Physical model

The main equation of the physical model is the calculation of the liquid fraction and the temperature of the PCM.
The fraction of liquid phase, which is the ratio of the mass of the liquid phase and the mass of the whole material, must be defined. The value of the fraction of liquid phase was calculated from the value of the enthalpy with the help of specific heat capacity and latent heat capacity.

$$y_n = \begin{cases} 0, & H_{PCM,n} < H_s \\ H_{PCM,n} - c_{p,s} \cdot m_{unit} \cdot \left(T_m + 273{,}15\right) \cdot \dfrac{100}{L_m \cdot m_{unit}}, & H_s < H_{PCM,n} < H_l \\ 100, & H_{PCM,n} > H_l \end{cases} \quad (1)$$

where y is the fraction of liquid phase, H is the enthalpy, c_p is the isobaric specific heat, m is the mass, T is the temperature, L_m is the melting heat, n is the nth time step, s is the solid phase and l is the liquid phase.
The other main equation is the determination of the temperature of the PCM. For this we can use the fraction of liquid phase and the enthalpy.

$$T_{PCM,n} = \begin{cases} \dfrac{H_{PCM,n}}{c_{p,s} \cdot m_{unit}} - 273{,}15, & y_n = 0 \\ T_m, & 0 < y_n < 100 \\ \dfrac{\left(H_{PCM,n} - L_m \cdot m_{unit} - H_s\right)}{c_{p,l} \cdot m_{unit}} + T_m, & y_n = 100 \end{cases} \quad (2)$$

2.3. ANSYS simulation

The ANSYS simulation was made in ANSYS Workbench R16.2 Academic software. The geometry was made in AutoCAD and was imported to ANSYS DesignModeller and after some small conversions the mesh was created in Workbench Mesher. The boundary conditions and physical models was defined in FLUENT, and its solver was used to calculate the results. For evaluation ANSYS CFD Post was used.
The used boundary condition were:

- Outside: The tank was insulated well, so the heat exchange with the outside is negligible.
- Water inlet/outlet: The Recirculation boundary condition was used to the inlets and outlets, points so the fall and rise of temperature could be modelled between the rows.
- Symmetry: The tank is symmetrical, so the simulation of eighth of it was enough.
- Interface: Between the bodies interfaces should be defined to avoid the heat dissipation.

After a mesh independence study we made the simulation with using the SIMPLEC scheme, and took account of Bouyancy effect and the proper turbulent model.

3. RESULTS

3.1. Measurement

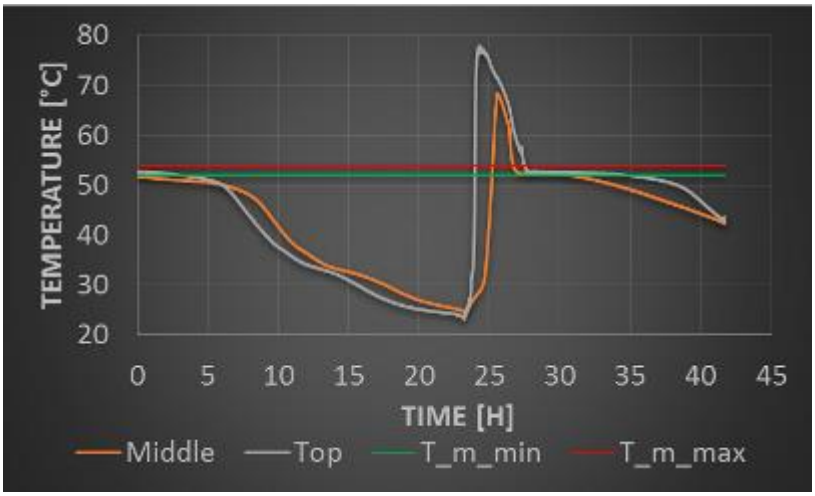

Figure 5 PCM's temperature

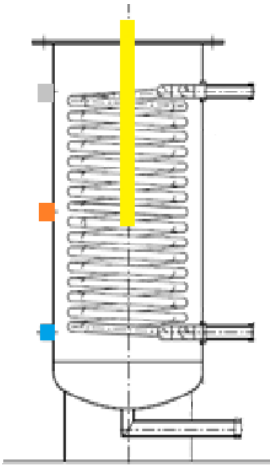

Figure 6 Temperature register points

The temperature of the PCM can be seen on *Figure 5*. The PCM temperature was measured on the side of the tank, as it can be seen on *Figure 6*. The PCM near to the water inlet has higher temperature, and its temperature rises more quickly in the melting process, and falls down more quickly in the freezing process than the lower layers of PCM. In the first session the phase change can be seen, because the temperature is steady. After that the freezing and the melting is represented. After the temperature fall, another phase change session can be seen, than the temperature begins to fall down.

3.2. Physical model

With the numerical model the best running condition was determined. The temperature and the mass flow of the inlet water temperature were investigated.

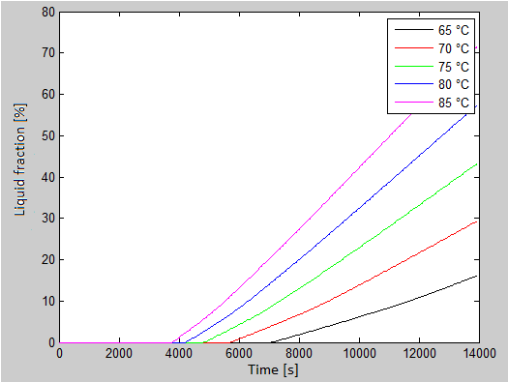

Figure 7 The effect of the inlet water temperature

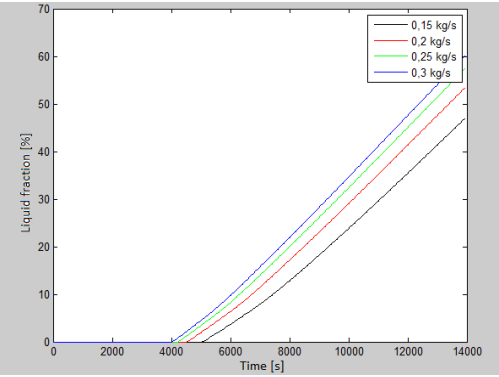

Figure 8 Liquid fraction in the function of water mass flow

On the *Figure 7* and *Figure 8* the changing of the liquid fraction can be seen. The liquid fraction rise more quickly, when the temperature and the mass flow of the inlet water is higher.

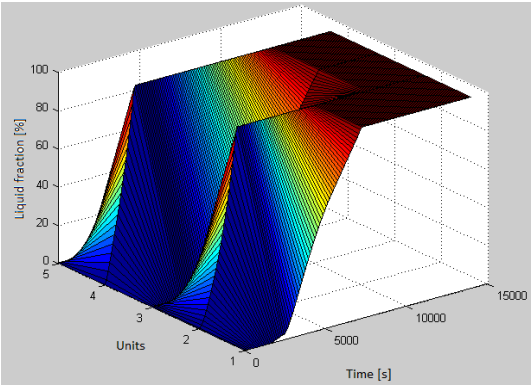

Figure 9 Liquid fraction in the function of time

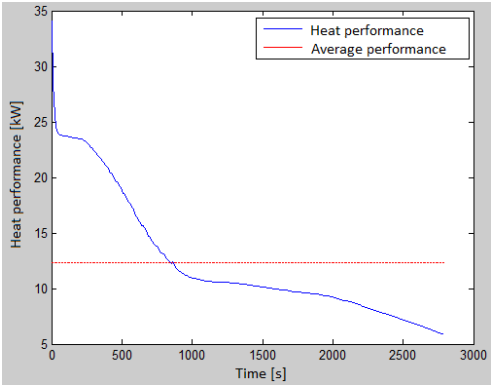

Figure 10 Take up heat performance in the function of time

In the best case the liquid fraction was investigated on the *Figure 9.* The PCM first melted near the pipe coil. On the *Figure 10* the heat performance can be seen. It is bigger in the beginning of the simulation, and reduces slowly. The average heat performance is 12,5 kW.

3.3. ANSYS simulation

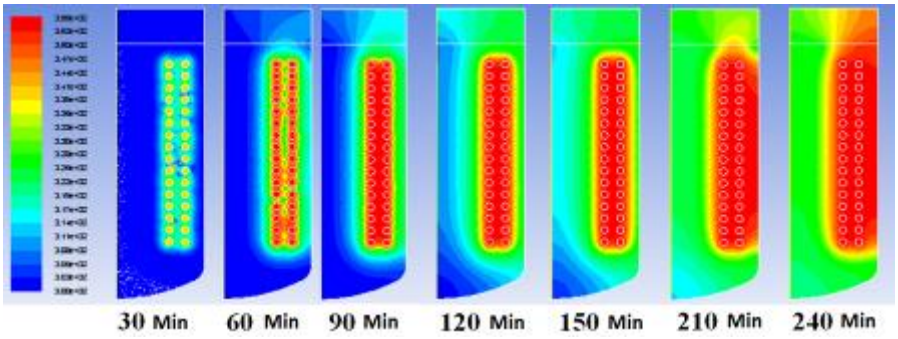

Figure 11 Temperature of the PCM in the function of time

The temperature of the PCM can be seen on the *Figure 11*. The currently phase changing part's temperature shown with yellow. The temperature first rises near the pipe coil, and in the middle of the tank lastly.

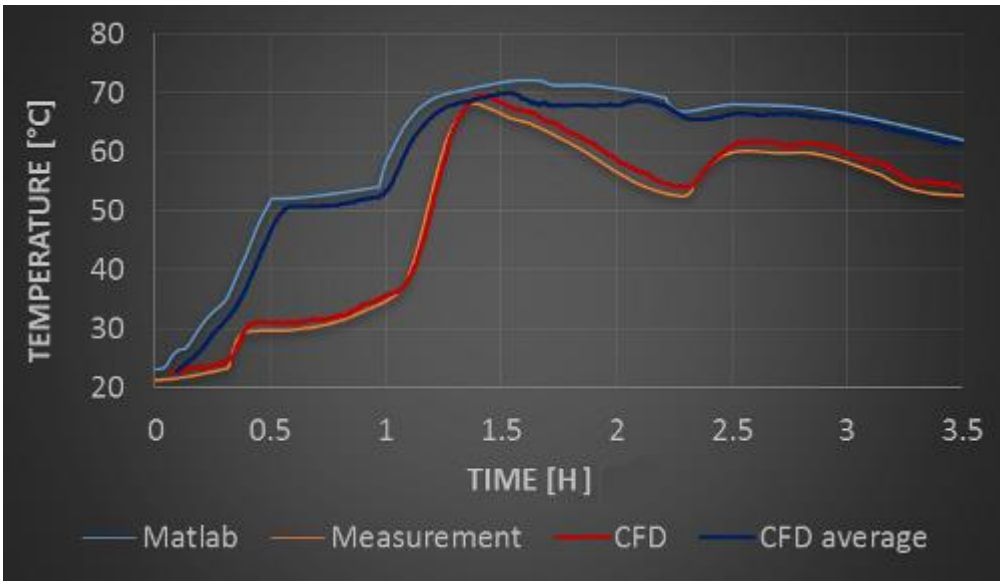

Figure 12 Comparison of the measure, the model and the simulation

On the *Figure 12*, the PCM's temperature, which was measured in one point can be seen with orange. In the CFD simulation monitor points can be defined, which showed the temperature in the same point as the measure. The correlation between the measure and the CFD simulation is 99.8%. The physical model calculated the temperature in a part of the volume. The CDF simulation can average the temperature on the same part as the model. The average temperatures are blue colour in the figure. The correlation between the model and the CFD is 99.5 %.

CONCLUSIONS

With the measures the phase change period was investigated. It is cleared up, that the PCM can absorb the amount of the heat, and can release it too. With the physical model the best operating

conditions were determined and with the help of CFD the model was validated with the measure. It was proved, that the PCM's performance is depend of the temperature and mass flow of the inlet water, and it can be changed to follow the needs of the customer.

REFERENCES

[1] N. Soares et al.: *Review of passive PCM latent heat thermal energy storage systems towards buildings' energy efficiency*, Buliding and Environment, pp. 82-103, 2012
[2] Andrássy Z., Farkas R.: *Fázisváltó anyagok alkalmazása fűtéskorszerűsítésre,* TDK dolgozat, 2013

INTERNATIONAL SCIENTIFIC CONFERENCE ON ADVANCES IN MECHANICAL ENGINEERING
19 November 2015, Debrecen, Hungary

THE CONNECTIONS BETWEEN DIFFERENT TYPES OF COLD FLAME-SPRAYED DISTANCES ON MECHANICAL SURFACE

[1]FAZEKAS Lajos PhD, [2]MENYHÁRT József, [3]MOLNÁR András, [4]HORVÁTH Csaba PhD

[1,2]Department of Mechanical Engineering, Faculty of Engineering, University of Debrecen
E-mail: fazekas@eng.unideb.hu, jozsef.menyhart@eng.unideb.hu
[3]Institute of Materials Sciences and Technology, University of Miskolc
E-mail: a.molnar2007@gmail.com
[4]Institute of Media Technology and Light Industry, Óbuda University
E-mail: horvath.csaba@rkk.uni-obuda.hu

Abstract
Nowadays one of the most important research areas of maintenance and surface treatment is the cold flame-spray technology. The research trend shows a lot of potential in cold flame-spray technology. This kind of technology is used by vehicle, aviation, and shipping industry and we can also find it in many other mechanical areas. Companies have spent (considerable) amounts of money on repair costs to find out which could be the best repairing method. Different powders, spraying guns, methods etc. are available from different firms. The study presents the influence of the spraying standoff distance on a normal and shear component of coating bond strength. The authors give guidance on the possibilities of cold flame-spray technology.

Keywords: *metal spraying, sprayed layers, cold-flame spray, normal and shear strength*

1. INTRODUCTION

The flame spraying technology is a member of the thermal spraying technology group. This technology is in fact a technique or method of surface engineering. This is quite a cheap technology and it is easy to use compared with any other spraying method. We call this technique cold flame spraying because it needs a relatively low thermal input. The preheating temperature is about 100 ^{o}C and the system temperature is not more than 250 ^{o}C.
The relatively mild conditions can have good bonding properties between substrate materials and different types of alloys especially if we use intermediate bonding films on the surfaces. Nowadays, cold flame spraying of surfaces can be the final step in the production process or we can consider it to be a new surface restoration technology. The cold flame spray technology is used by different engineering areas as we can read about it in the abstract.

2. METHODS

Cold spraying is the newest method of thermal spray processes. This technology is technically not a true thermal spray process because it does not use thermal energy as its primary energy source to melt materials, it only uses kinetic energy to project particles onto a mechanical surface. We can see the schematic figure of the cold spray process in Figure 1. [1]

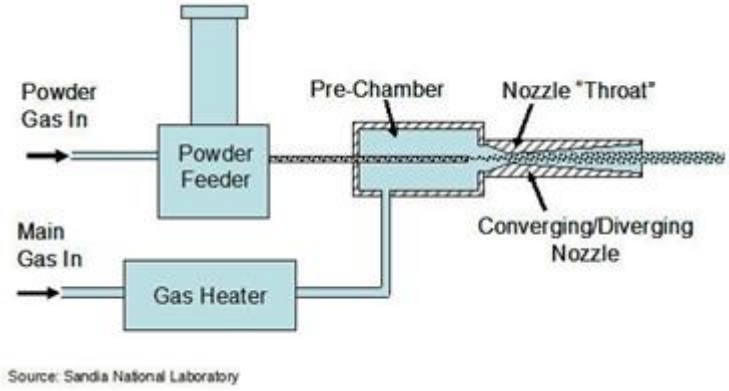

Figure 1 Schematic drawing of the cold spray process [1]

We used a RotoTec-80 equipment (Castolin Eutectic) during our research program. The main parameters of this equipment were the following:

- oxygen pressure: 4.0 bar
- acetylene pressure: 0.7 bar
- standoff distances: 100, 140, 180, 220, 260 [mm]
- spraying angle: 0^{o}

In the first step we preheated the experimental samples by an oxygen-rich flame. The temperature of the samples was about 50-100 ^{o}C. The thickness of the bonding layer was 0.2 mm. The coating was 1.5 mm on the samples which were prepared to tests of the normal component of coating bond strength.

3. MATERIALS OF THE EXPERIMENT

We selected 3 different powder alloys which have different characteristics for the extreme technological application of the cold flame-spraying metal powder spraying technology. These alloys are characteristically distinguished by their chemical compositions.

We used the following powders:

- HardTec 19400 – hard coating, protection against abrasive effects,
- LubroTec 19955 – excellent sliding requirements,
- DuroTec 19910 – tough and hard coating utilization of the dynamic loadability

Table 1 Results of the measurement

Alloy	C	Ni	Cr	Fe	Mn	Mo	Co	B	Si	S	Al
Xuper Ultra Bond 51000		89,5				5,4					5
DuroTec	0,1	84,6	9,4	2,1	0,02	0,3	0,05	1,1	4,8	0,015	
HardTec	0,1	1,1	15,8	78,1	0,08			1,0		0,018	
LubroTec	0,03	74,7	15,4	8,4	0,11	0,1	0,1			0,01	

We had to pay special attention during the standoff spraying because flame spraying is usually

performed by hand, during which it is impossible to keep the normal SOD, proposed by the manufacturer, precisely. The standoff spraying distance has a strong influence on the mechanical surfaces. This is the reason why we had to check our work with different SODs.
The research team checked the self-lubrication ability of the porous coating with oil uptake and release measurement and analyzed the change of surface energy components and the final chemical composition of the sprayed surface.
The main variables of our test are the following:

- spraying distance generally suggested by the producer (180 mm),
- increasing the spraying distance with 40% in extreme value,
- reducing the spraying distance with 40% in extreme value, and
- Using further spraying distances between extreme values.

4. NORMAL STRENGTH INVESTIGATION

We can define stress as a strength of a material per unit area in unit strength. It is in fact the force on a member divided by area, which carries the force or forces (N/mm^2; Mpa). [4]

$$R_{\perp} = \frac{F_{\perp}}{A} \tag{1}$$

- $R^{\perp}$ = Normal bonding strength (MPa)
- $F^{\perp}$ = Normal force acting on the sprayed surface (N)
- A = the sprayed area subjected to the normal force (mm2).

We can see a figure about normal stress in Figure 2.

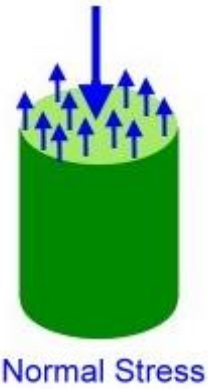

Figure 2 Normal stress [2]

We found a number of methods, techniques and literature for our research. We selected the Nádasdi – method from these activities. We can see a picture of it in Figure 3.

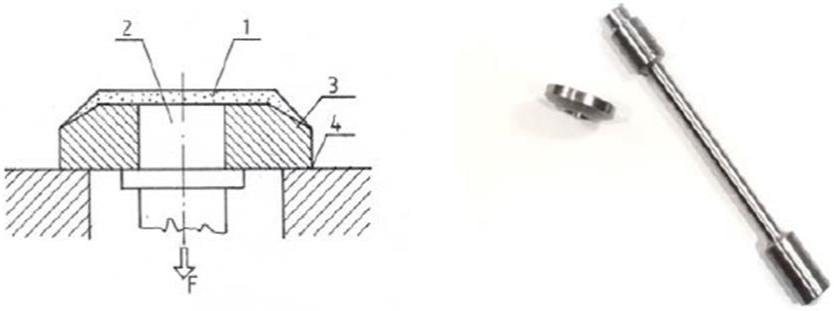

Figure 3 Test combination for normal strength tests

1 – Porous sprayed layer, 2 – tested substrate part, 3 – mating ring part, 4 – fixed base

5. SHEAR STRESS INVESTIGATION

Forces parallel to the area resisting the force cause shearing stress. It differs to tensile and compressive stresses, which are caused by forces perpendicular to the area on which they act. Shearing stress is also known as tangential stress. [5]

$$R_{\parallel} = \frac{F_{\parallel}}{A} \tag{2}$$

- $R_{\parallel}$ = shear strength (MPa)
- $F_{\parallel}$ = acting shear force (N)
- A = surface subjected to shear force (mm^2)

We can see an illustration of shear stress in Figure 4.

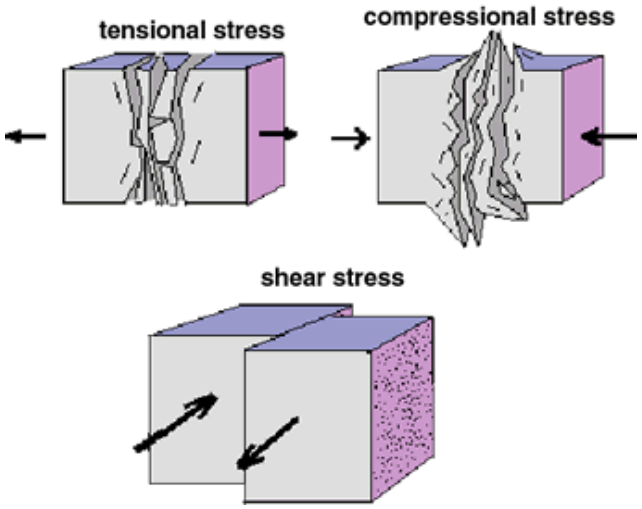

Figure 4 The difference between stresses [3]

During our research we chose the METCO method. This method is part of the DIN 50161. The applied test sample can be seen in Figure 5.

Figure 5 Shear test samples

1 – substrate part having sprayed and notched layer, 2 – shearing ring

6. RESULTS

The dependence of normal component of coating bond strength ($R^{\perp}$) on the standoff distance for the various coatings is shown in Fig. 6.

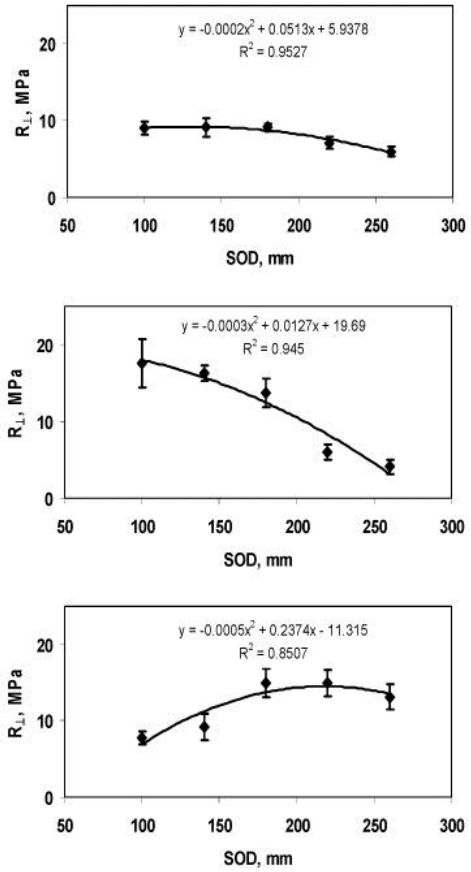

Figure 6. Normal component of coating bond strength, $R^{\perp}$
From top to bottom: DuroTec, HardTec, LubroTec

If the normal and shear components of coating bond strength are compared, the normal component was always much smaller than the shear one which is the effect of the standoff distance on mechanical strength of cold flame-sprayed porous metallic coating 100 HardTec and LubroTec,

respectively. As we can read in the previous chapter, flame spraying is usually made by hand, this is the reason why the normal SOD cannot be kept precisely on the surfaces. Figures 6 and 7 present the measuring results.

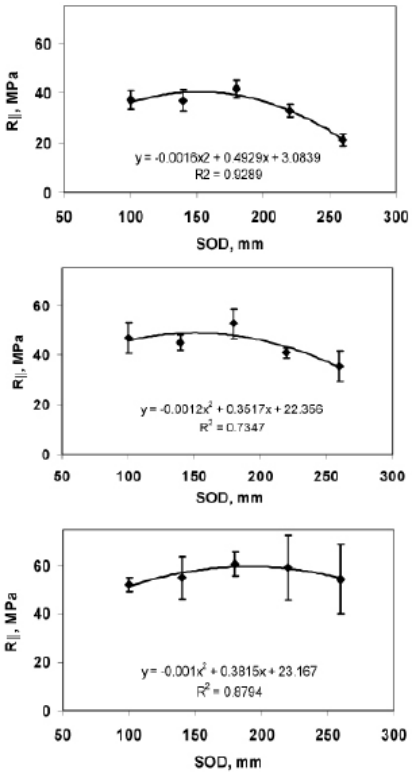

Figure 7. Shear component of coating bond strength, R⊥
From top to bottom: DuroTec, HardTec, LubroTec

The maximum available values of $R_{\parallel}$:

- 40 MPa
- 50 MPa
- 60 MPa

for DuroTec, HardTec and LubroTec. This trend is positive, which can be explained by the hindered diffusion of B in HardTec and B and Si in DuroTec upon cold flame spraying. Comparing the normal and shear components of coating bond strength, the normal component was always much smaller than the shear one.

CONCLUSIONS

The development of flame-sprayed technologies continues nowadays. This kind of method can be used in a lot of different areas, like renewing, or repairing parts. Nowadays the cold flame spraying technology gets a high priority in modern maintenance life. The main advantage of the technology is that it can be used in low heat range (200-3000^{o}C). This is the reason why we can avoid the texture change on mechanical surfaces.

The paper describes the results of the laboratory test in connection with the analysis of interlaminar strength, which is of great assistance when choosing the most suitable thermal spraying technology. The author tries to give some information about the advantages of the cold-flame spray technology.

REFERENCES

[1] *TST Engineered Coating Solutions – A Fisher Barton Company,* Cold Spray url: http://www.tstcoatings.com/cold_spray.html Downloaded: 2015.09.13.
[2] *www.pt.ntu.edu.tw,* Force and Strength, url: https://www.google.hu/search?q=shear+stress&source=lnms&tbm=isch&sa=X&ved=0CAcQ_AUoAWoVChMIs8antNqLyQIVQvNyCh26YQKv&biw=1366&bih=627#tbm=isch&q=normal+stress&imgrc=-nT1p_rW6vAe9M%3A Downloaded: 2015.10.12.
[3] *USGS science for a changing world,* Earthquake Hazards Program, Earthquake Glossary – shear stress, url: http://earthquake.usgs.gov/learn/glossary/?term=shear%20stress, Downloaded: 2015. 10. 12.
[4] *α MATHalino.com, Normal Stresses,* url: http://www.mathalino.com/reviewer/mechanics-and-strength-of-materials/normal-stresses Downloaded: 2015.10.12.
[5] *α MATHalino.com, Shear Stress,* url: http://www.mathalino.com/reviewer/mechanics-and-strength-of-materials/shear-stress Donwloaded: 2015.10.12.
[6] Fazekas, L.: *Tartósságnövelés módszereinek vizsgálata körszimmetrikus alkatrészek felújításakor,* Műszaki doktori értekezés, Budapest 1987.
[7] Szűs, S.: *Fémporszórási eljárások alkalmazásainak szemponjtai az alkatrész felújításban,* MTESZ "Borsodi" Műszaki Gazdasági Élet. Vol. XL., Nr3. 1995. p. 73-76.

INTERNATIONAL SCIENTIFIC CONFERENCE ON ADVANCES IN MECHANICAL ENGINEERING
19 November 2015, Debrecen, Hungary

BENDING STIFFNESS MEASUREMENT OF STRINGS

HORVÁTH Péter PhD, NAGY Attila

Department of Mechatronics and Machine Design, Széchenyi István University
E-mail: horvathp@sze.hu, anagy@gmail.com

Abstract
In this paper a measuring procedure of bending stiffness of wrapped piano bass string is presented. Up to now true data on this field are not known. The aim of the study is to determine the effect of wrapping on the bending stiffness. The measurement was performed under real operational conditions of the string. In the knowledge of true data found in this experiment, one can develop a process to decrease inharmonicity of strings, making clear and mellow tone of piano bass strings.

Keywords: *Bending stiffness, wrapped string, measurement, inharmonicity*

1. INTRODUCTION

Bending stiffness plays crucial role in engineering mechanics when calculating lateral displacement of beams or eigenfrequencies of vibrating beams. In most cases the material is homogenous and its Young's modulus is known, as well as the geometry of cross-section is simple enough to calculate inertia moment without difficulty. In contrast to it there are some cases when determination of bending stiffness IE uneasy. An example for this is the case of overwound strings applied in pianos. To highlight the problem recall the formula (1) of eigenfrequency of an ideally elastic string of length L, tensile force H and mass per unit length q

$$f_0 = \frac{1}{2L}\sqrt{\frac{H}{q}} \tag{1}$$

Applying real data, the length of strings in bass region of piano would reach about six meters. As dimensions of a piano are limited, the mass per unit length of the string should be increased. The widely used method is applying overwound strings, where a high density copper wire is turned tightly around the base steal string, as can be seen in Figure 1. It must be noted, that the outer dia-

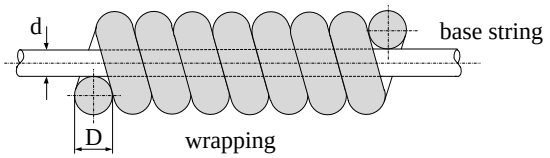

Figure 1. Overwound string

meter of the wrapping can reach even 5-6 millimetres. The wrapping increases the bending stiffness of string but its measure unfortunately is not known.. Some papers [1, 2] state without evidence, that the increase of bending stiffness is not considerable**,** but they do not supply with numerical data. New trends in piano development need more and more accurate parameters regarding especially strings as the most important sound generating elements of the piano. Bending stiffness

of strings is related to sound quality, inharmonicity of overtones and piano tuning. Correct knowledge of bending stiffness of overwound strings would make possible to develop new solutions decreasing inharmonicity of overtones, as proposed in [3]. As calculation of contact forces among turns of wrapping and base string by FEA would be difficult, consequently a measuring procedure is proposed in this paper.

2. MEASURING PROCEDURE

Special care was taken to ensure real operation conditions of the string. The string in piano is subject to about 700 N tensile force, while its transverse deformation runs to some millimetres during vibration. In the measurement procedure similar tensile force was applied in order to make contact force among turns close to real operation conditions. The overwound string was pulled by a tensile test machine with tensile force *H*. After that a frame was attached to the string and at last the midpoint of the string was moved to a given value δ by a micrometer, while the force *2F* was measured by a force sensor attached to the micrometer tip (Figure 2).

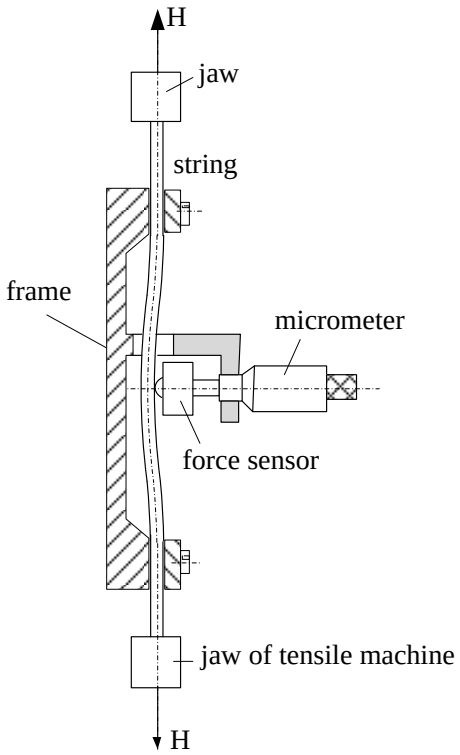

Figure 2. Measuring setup

Knowing the magnitude of tensile force *H* and the speaking length of the string *2L*, bending stiffness of the overwound string can be calculated as presented in the following. For symmetry reasons let us examine only the left hand side portion of the string (Fig.3).

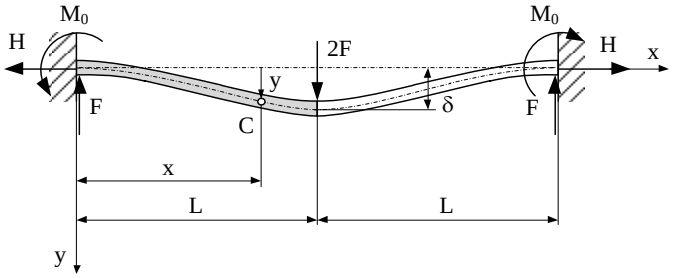

Figure 3. Force system acting on the string

Bending moment at any arbitrary cross-section *C* can be written as

$$M(x) = Fx - M_0 - Hy = -IE\frac{d^2y}{dx^2} \tag{2}$$

Applying the following boundary conditions y(0)=0, $y'(0) = 0$, $y'(L) = 0$, differential equation (2) can be solved. Do not specifying details of solution, the deflection of the midpoint of string holds

$$\delta = y(L) = \frac{F}{H}L + \frac{2F}{H\alpha}\left(\frac{1}{\sinh(\alpha L)} - \frac{1}{\tanh(\alpha L)}\right) \tag{3}$$

where parameter α is defined as

$$\alpha = \sqrt{\frac{H}{IE}}\ . \tag{4}$$

Deflection y(x) of the string of different bending stiffness under constant load can be seen in Fig. 4.

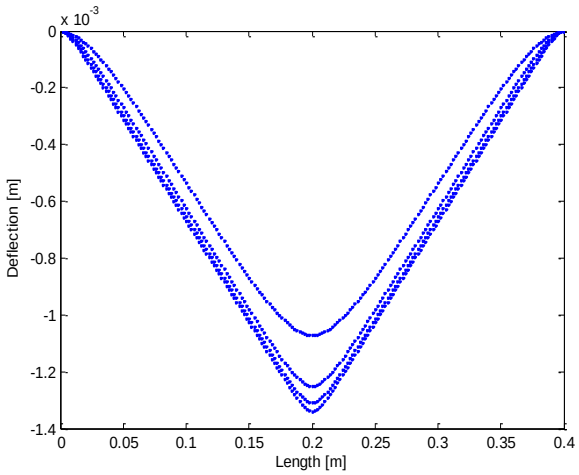

Figure 4. Deflection of string of parameter α=20, 40, 60, 80 1/m under load 5N.

Analysing expression (3), one can realise that the first term equals to the displacement of the ideally elastic string and the second term is due to the finite stiffness. From this transcendent equation α

can only be determined with numerical methods, but in case of small bending stiffness ($\alpha L>20$) $\sinh^{-1}(\alpha L)$ tends to zero and $\tanh^{-1}(\alpha L)$ tends to unity. In that case α can simply be determined by algebraic method and it holds

$$\alpha \approx \frac{2F}{H\delta - FL} \tag{5}$$

At last one can express bending stiffness from equation (4).

3. RESULTS OF MEASUREMENT

Measuring procedure has been done by the following data:

Tensile force	H=549 N
Half-length of string	L=0.2 m
Base string diameter	d=1,1 mm
Diameter of copper wire	d=1.5 mm
Mass per unit length	q=0.0888 kg/m
Displacement at midpoint	δ=1 mm

Measured force was 2F=5.86 N. Applying these data the following result turned up:

$$\alpha = \frac{2F}{FL - H\delta} = \frac{5.86}{2.93 \cdot 0.2 - 549 \cdot 0.001} = 158.3 \ \text{m}^{-1} \tag{6}$$

Verifying condition for simplified solution one receives $\alpha L = 156.2 \cdot 0.2 = 31.24 > 20$, consequently simplified expression (5) can be really applied. At last the bending stiffness is calculated from (4)

$$IE = \frac{H}{\alpha^2} = \frac{549}{158.3^2} = 0.022 \ \text{Nm}^2 \tag{7}$$

As the bending stiffness of circular core string of diameter 1.1 mm and of Young's modulus $2 \cdot 10^{11}$ N/m^2 can be found easily (IE_b=0.0143 Nm^2) the increase in bending stiffness caused by wrapping is

$$\frac{0.022 - 0.0143}{0.0143} \cdot 100 = 53{,}8\%. \tag{8}$$

CONCLUSIONS

The presented measuring procedure proved to be applicable to determine bending stiffness of structures of very low rigidity. The process accordingly needs high resolution force measurement system and accurate fixed-end constraints of the string in order to guarantee exact results. In the example of wrapped piano string it was established that a medium size wrapping causes about only 54 per cent increase in bending stiffness of the base string, but a circular cross section of the same mass per unit length would have about 250 times bending stiffness! Related work will be continued by measuring bending stiffness of overwound strings with both different core string diameters and wire diameters.

REFERENCES

[1] Chaigne, A, Askenfelt, A: *Numerical simulation of piano strings*. J. Acoust. Soc. Am. 95 (3), 1994. pp1631-1640.

[2] Stulov, A: *Piano string scale optimization on the basis of dynamic modelling of process of the sound formation.* Proceedings of the Twelft International Congress on Sound and Vibration. Lisbon, 2005. pp.1-8

[3] Franklin M.: *A proposed loading of piano strings for improved tone.* J. Acoust. Soc. Am. 21 (4), 1949. pp 318-322.

MODELLING OF FRACTIONAL CRYSTALLIZATION

HUMMEL Kristóf, HÉGELY László PhD, LÁNG Péter DSc

Department of Building Services and Process Engineering, Budapest University of Technology and Economics
E-mail: hummelkristof@gmail.com, hegelyl@hotmail.com, lang@mail.bme.hu

Abstract
The purification of an industrial wastewater containing sodium chloride and sodium sulphate with fractional crystallization is modelled. For the solid-liquid equilibrium calculations a free source software is used applying the Pitzer model for calculating the activity coefficients. Two technological versions are studied (without and with recycle of the final waste solution.)

Keywords: fractional crystallization, modelling, solid-liquid equilibrium, wastewater, technological calculations

1. INTRODUCTION

The crystallization is one of the most widespread separation and purification processes in the chemical industry. The process is really popular in the pharmaceutical industry, the wastewater processing and in the food industry. Its popularity and application area are still increasing. There is a serious need for the up-to-date treatment of wastewaters with high salt content. [1]
The common process simulators and conventional equation solvers are not suitable for modelling the process of fractional crystallization. Therefore, we had to look for a free source software, with which the equilibrium composition can be determined and which can help to design the crystallization operation. For testing the program, we used measurement data from literature sources and our own laboratory experimental results, as well.
The goals of this paper:

- to model the purification of an industrial wastewater containing sodium chloride and sodium sulphate with fractional crystallization,
- to propose technology for the fractional crystallization,
- to investigate two technological versions (without and with recycle of the final waste solution.),
- to suggest types of equipment for performing the process.

2. METHODS

The aqueous mixture to be processed (48.075 t/h) contains: sodium chloride (NaCl, 4 mass %) and sodium sulphate (Na_2SO_4, 7 %). The dependence of the solubilities of the salts on the temperature is really important to design a crystallization process.
The solubility characteristics of the solution studied: sodium chloride, sodium sulphate - water are shown in a common figure in *Figure 1.*

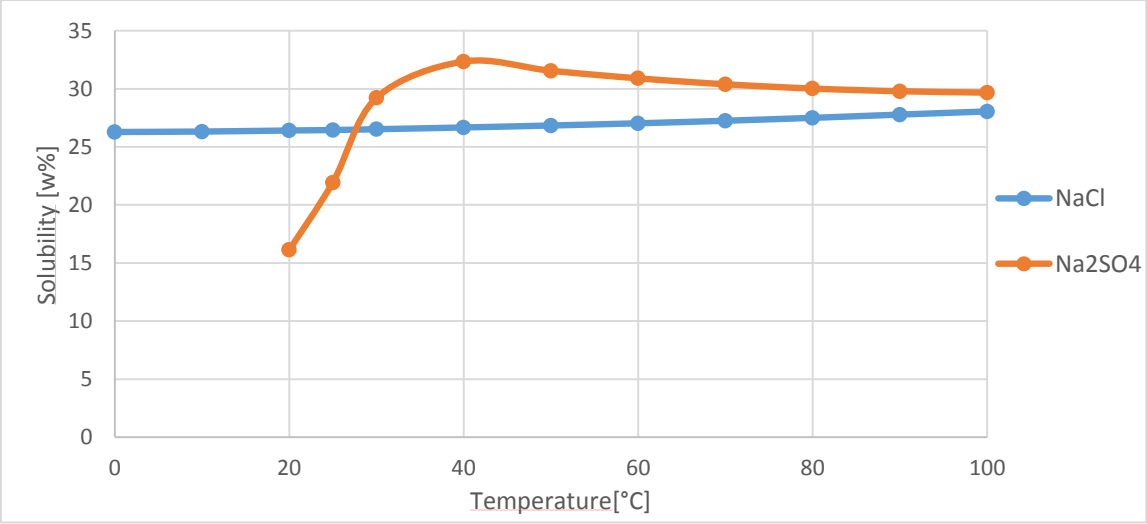

Figure 1. Dependence of the solubilities of the salts on the temperature [2]

We can see, that the two curves have different shapes. We can conclude that the solubility of NaCl is high even at lower temperatures, and it hardly increases with the temperature. However the solubility of sodium sulphate is much lower at low temperatures than that of sodium chloride. It strongly increases from 20 to 40 °C, where the solubility has a maximum. When designing the crystallization process for the separation of the two salts, we can take benefit of this difference in behaviour.
Solubility measurement data for the mixture NaCl-Na_2SO_4-H_2O at 25°C are shown in *Figure 2.*

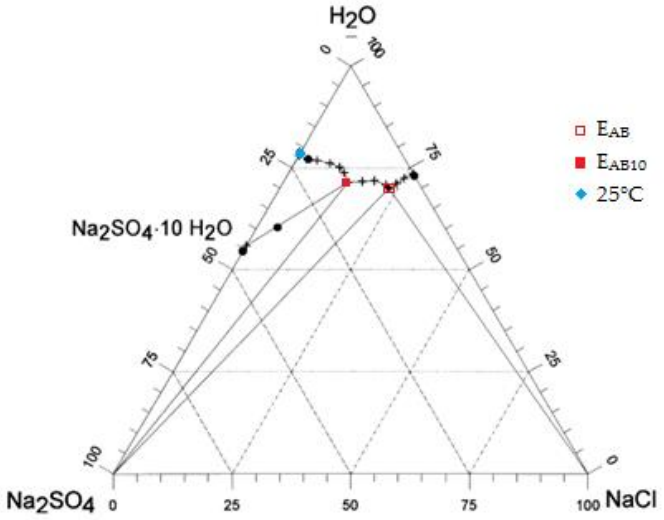

Figure 2. Solubility measurement data of the mixture NaCl-Na_2SO_4-H_2O (T=25°C) [3]

Two invariant points can be seen. E_{AB} represents the solution saturated for sodium-chloride and sodium sulphate, while E_{AB10} shows the composition where the solution is saturated for sodium-chloride and the hydrate of sodium sulphate ($Na_2SO_4 \cdot 10H_2O$). During the crystallization process two different modifications can crystallize.
The common flow-sheet simulators are not suitable for modelling the crystallization process, therefore we applied a free source software (EQ3/6) for the solid-liquid equilibrium calculations [4].
The solubility of the salts in water at a given temperature can be determined from their solubility product (Ks), which is the product of the ion activities.

$$Ks = [A^+]^x \, [B^-]^y \tag{1}$$

The activity is the product of the activity coefficient and the ion concentration. In the program the activity coefficients are calculated by the Pitzer model [5].

$$a_i = \gamma_i x_i \tag{2}$$

The calculation method and the software were validated with measurement data at 25 °C before the technological calculations. The measured and calculated data were in good agreement. However we had to complete the database of the program with data for 60 and 100°C.
The evaporation of water is treated as a fictive reaction in the software. For each equipment, the temperature is selected, then the reaction coordinate (ξ) is determined in an iterative way. With the reaction coordinate the solvent content of the solution can be varied. ξ must be progressively increased (decreasing the water content of the solution) until the solution became saturated for one of the salts.

3. RESULTS

The aim of the fractional crystallization is to crystallize the two salts separately. By taking into account the different solubility characteristics of the two salts, we suggested four equipment. Two versions of the technological process were studied by simulation. The technological process without recycle can be seen in *Figure 3*. The first equipment is a common evaporator. Since in this equipment there is no crystal segregation, the solution is only evaporated until it becomes saturated for sodium sulphate.
The second equipment is an evaporator crystallizer, where one part of the sodium sulphate is crystallized. At the end of this step, the solution becomes saturated for both salts at cca. 100 °C, therefore we had to change the operating parameters according to the dependence of the solubilities on the temperature.
In the third equipment, sodium chloride is crystallized at 40 °C in vacuum in an evaporator crystallizer. At the end of this step, the solution is saturated for both salts.
The temperature of the fourth equipment agrees with that of the second equipment. After this equipment the remaining solution is still rich in salts, that is, there is a considerable loss for both salts. The mass flow rate of NaCl in this solution is cca. 60% of the original quantity. The solution leaving this equipment is a waste, which must be still treated.
We also studied how the quantity of the waste can be decreased or even eliminated. The compositions of the solutions after the second and fourth equipment are equal, therefore they can be mixed and processed together in the third and fourth equipment. The flow-sheet and calculation results for the technological process with recycle are shown in *Figure 4*.

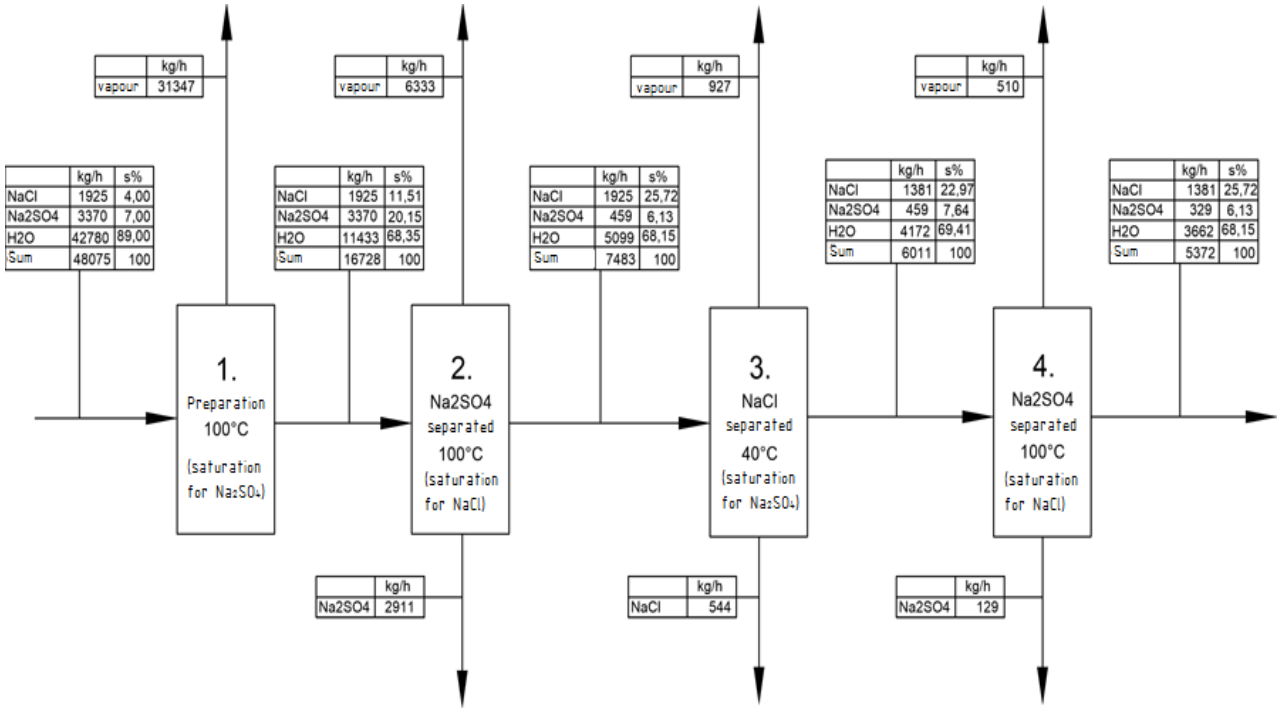

Figure 3. The technological process (without recycle)

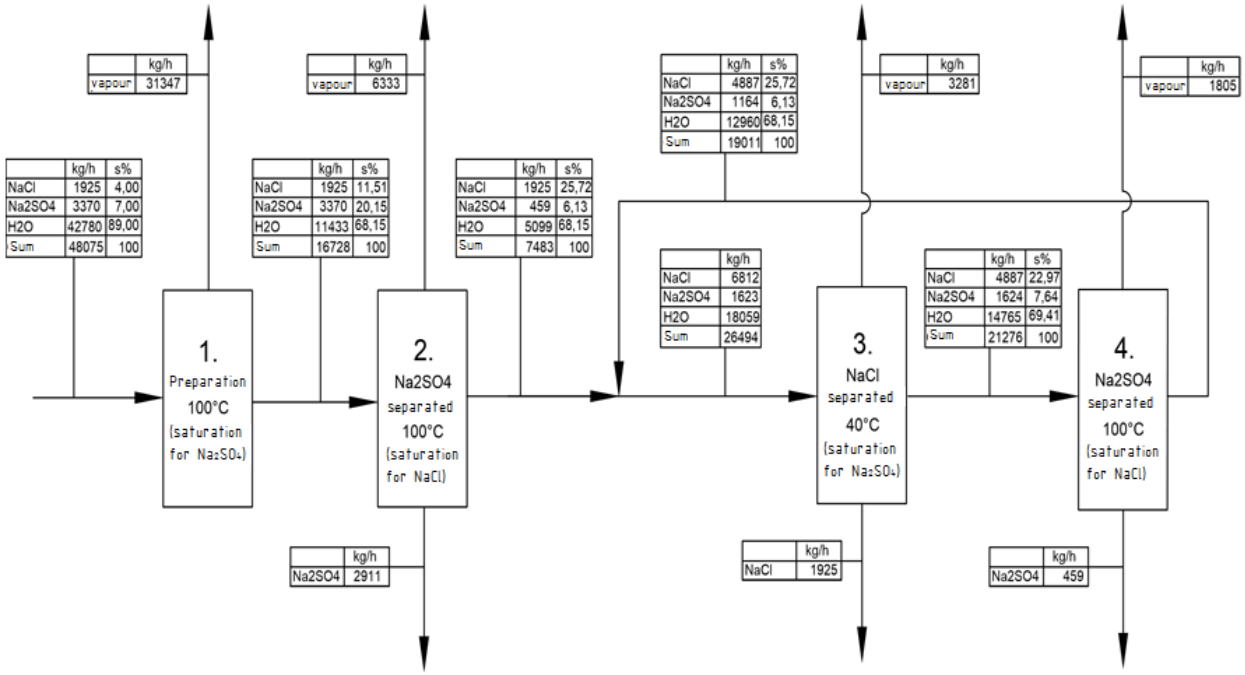

Figure 4. The technological process (with recycle)

By this solution the whole quantity fed of both salts could be crystallized separately. However, in this case all mass flows in the recycle loop would be more than 3.5 times greater than those without recycle. This would mean a huge increase in both the investment and operation (energy) costs.
We also suggested types of equipment which befits the technological processes. The first one is a common falling film evaporator.

The second and fourth ones are forced-circulation evaporation crystallizers, shown in *Figure 5*. The equipment consists of a vessel with a conical bottom. Recycling is provided by a circulating pump. The feed is introduced before the pump. The product slurry is withdrawn from the recirculation piping after the crystallizer outlet and before the feed inlet. When supersaturation is generated by evaporation, as shown here, the solution recirculating is passed through a shell-and-tube heat exchanger. Supersaturation is generated at the vapour-liquid interface [6].

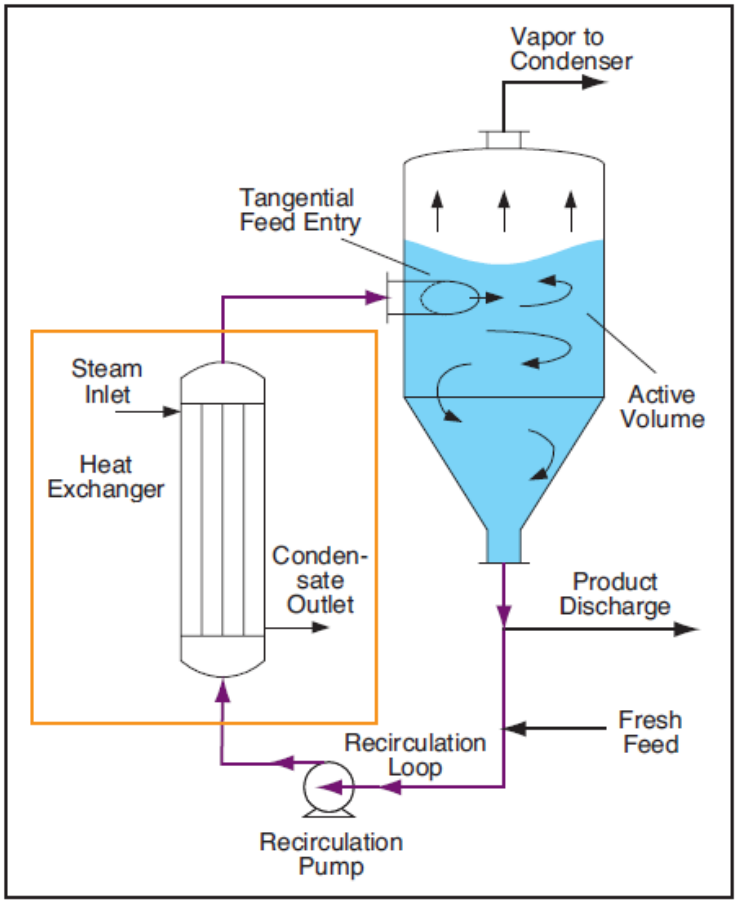

Figure 5. Forced-circulation evaporation crystallizer

The third equipment is a Swenson-type draft-tube crystallizer, which can be seen in *Figure 6.*

A closed vessel contains an internal skirt baffle positioned so that it provides a partitioned settling zone. Inside the baffle is a vertical draft tube, centred by support vanes. A slowly rotating agitator is located concentrically at the bottom of the draft tube. The feed inlet is located at the base of the bottom cone and is directed into the draft tube. The agitator induces the flow, circulating the liquor and crystals from the bottom of the unit to the top liquid surface. Supersaturation is produced with adiabatic evaporative cooling. It is closed and it can be operated in vacuum [6].

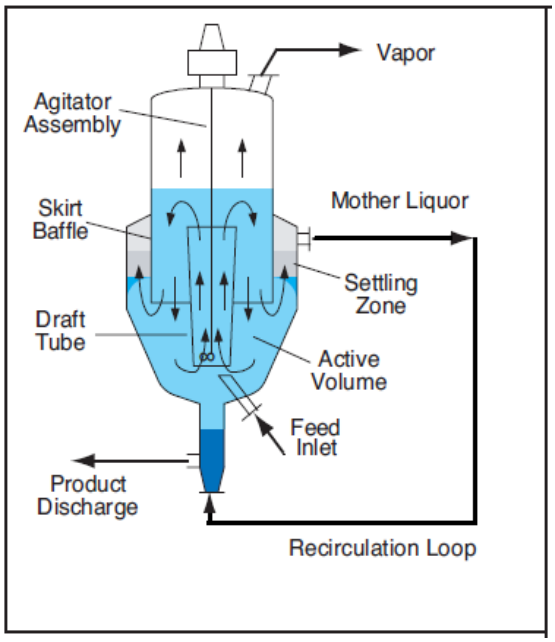

Figure 6. Swenson-type draft-tube crystallizer

CONCLUSIONS

The fractional crystallization of an industrial wastewater containing sodium chloride and sodium sulphate was investigated. For the solid-liquid equilibrium calculations a free source software (EQ3/6) was used. The activity coefficients was calculated by the Pitzer model. Two technological versions consisting of four steps were studied: common evaporation, crystallisation of Na_2SO_4, crystallisation of NaCl under vacuum, crystallisation of Na_2SO_4. We stated that without recycling the solution remaining after the last step the loss of both salts was considerable (71,7 % for the NaCl, 9,8 % for the Na_2SO_4). Furthermore this solution is a waste, which must be treated. With recycling this solution (mixing it with the solution leaving the second equipment) the losses can be decreased or even eliminated. However the recycle strongly increases the mass flow rates within the cycle and hence the energy need of the process.

REFERENCES

[1] Cséfalvay E., Deák A.: *Vegyipari művelettan II.*, BME Kémiai és Környezeti Folyamatmérnöki Tanszék, Budapest, 2012, pp. 430-475.
[2] Hégely L., Láng P.: *Collection of Solubility Data for the System NaCl-Na_2SO_4- $Na_2B_4O_7$.* Research report. BME Épületgépészeti és Gépészeti Eljárástechnika Tanszék, 2014.
[3] Edilson C. T., Susana I. S., Osvaldo C. F., Carlson P. S.: *Determination of salt solubility data for ternary aqueous systems with aquasiisothermic thermometric technique*, Thermochimica Acta, 328, 1999, pp. 25-258
[4] Wolery, T.J.: *EQ3/6 - Software for Geochemical Modeling, Version 8.0*, UCRL-CODE-2003-009, Lawrence Livermore National Laboratory, Livermore, California, 2002.
[5] Marliacy P., Hubert N., Schuffenecker L., Solimando R.: *Use of Pitzer's model to calculate thermodynamic properties of aqueous electrolyte solutions of Na_2SO_4 + NaCl between 273.15 and 373.15 K.*, Fluid Phase Equilibria 148, 1998, pp. 95–106.
[6] Samant K. D., O'Young L.: *Understanding Crystallization and Crystallizers*, Chemical Engineering Progress Magazine, 10/2006, 1996, pp. 28-37.

INTERNATIONAL SCIENTIFIC CONFERENCE ON ADVANCES IN MECHANICAL ENGINEERING
19 November 2015, Debrecen, Hungary

MULTIPLE REGRESSION ANALYSIS IN TIME MANAGEMENT

[1]KOCSIS Imre, PhD, [2]KRAKKÓ Béla, [3]VÁMOSI Attila, [4]DEÁK Krisztián

[1,3]Department of Basic Technical Studies, Faculty of Engineering, University of Debrecen
E-mail: kocsisi@eng.unideb.hu, vamosi.attila@eng.unideb.hu
[2]Diehl Aircabin Hungary Kft.
E-mail: bela.krakko@diehl.com
[4]Department of Mechanical Engineering, Faculty of Engineering, University of Debrecen
E-mail: deak.krisztian@eng.unideb.hu

Abstract
Time data management nowadays plays a central role in strategic and operative planning and decision making in manufacturing companies. Time and motion studies constituted the basis of Taylor's production theory at the beginning of the 20th century and now, a century later companies recognised again the significance of time in process improvement. When the variance of the manufacturing times is high the estimation of precise process times becomes difficult and costly. A customized approach is needed to define manufacturing times and to schedule the production, the standardized process times have to be defined on the basis of different parameters or characteristics. Regression analysis is a tool for the estimation of the time requirement of job elements. In this paper an application of regression analysis in standard time calculation is presented, and the applicability of multiple regression models is posed.

Keywords: *time management, manual work, standard time, regression*

1. INTRODUCTION

Time data management plays a central role in strategic and operative planning and decision making [3]. Time study is a work measurement technique for recording the times and rates of working for job elements. It is an analysis of a worker's performance against a time standard which is normally performed on short repetitive production types of tasks.
Time data are determined and utilised during product development, process planning and production phases. During production phase time data is essential in monitoring production processes and in continuous improvement.
The basic steps in a time study are the definition of the job to be analyzed; breaking the job into discrete tasks; measurement of the actual time required for each task; and the statistical evaluation of data.
Standard times are used to compare alternative processes, evaluate individual worker performance, cost the labour component of products; schedule and plan required resources. Standard time is the length of time a qualified worker needs to complete a specific job, allowing time for personal fatigue, and unavoidable delays. To determine standard times choose the specific job to be studied; break the job into easily recognizable units; time each element; rate the worker's performance; compute the normal time (*Normal time = Elemental average time × Rating factor*); compute the standard time (*Standard time = Normal cycle time × (1 + Allowance factor)*).
Actual times are specified by an observer measuring tasks directly at a work place. Target times are derived from actual times and their time-influencing factors. Target times are derived from actual times through statistical evaluations.

Standard data specifies target times for work elements describing work processes and their duration by means of time-influencing factors. REFA distinguishes the significant influencing factors into changeable and fixed. Furthermore the changeable influencing factors are subdivided into quantitative and qualitative [2].
A job element can be *repetitive* (occurs in every work cycle), *occasional* (occurs at regular or irregular intervals, *constant* (constant time whenever it is performed), *variable* (time varies with the products, equipments or processes); from another aspect it can be *manual, machine, governing* and *foreign* (not necessary) element.
In a hierarchic time category structure by REFA there are five levels of time categories for humans and machines. *Level I* represents the order time for humans or the holding time for machines, in *Level II* time is subdivided into setup and run time referring either to quantity units or orders, time per unit is also assigned to this level, in *Level III*, besides basic time for performing a work process also rest and allowance time are considered, the segmentation in several categories of basic time and allowance time is performed in *Level IV, Level V* finally depicts a segmentation of basic time into influential and non-influential working time [3].
In a time study the following must be taken into consideration. *Controllability of manual task* is the opportunity for employees to influence the way of performing a task and therefore the time of this task. It has a significant impact on the choice of the time determination method. *The extent of work content* specifies the duration of recorded work. *Type of time* can be actual time, target (planned) time, normal time and standard time [3].

2. STANDARD TIME CALCULATION IN AIRCRAFT CABIN ELEMENT PRODUCTION

In this study the Time Management System of Diehl Aircabin Hungary Kft, as a part of the Diehl Production System, is investigated. Diehl Aerosystems, a leading partner for aircraft cabin design and integration as well as first tier supplier for avionics solutions. Diehl Aircabin Hungary Kft. operates as a subsidiary of Diehl Aircabin, based in Laupheim, Germany, one of currently four operating units under the Diehl Aerosystems umbrella.
The main characteristics of the aircraft cabin element production in Diehl Aircabin Hungary Kft:

- high quality requirements (aircraft manufacturing standards, Diehl Production System);
- high variability of the size and geometry of products;
- frequently changing products (small batch production);
- high rate of manual work;
- high variability of time requirement of operations (from a few minutes to several hours);
- high productivity requirements.

Because of high variability of products and high rate of manual work the standard time calculation has crucial role in manufacturing processes planning and control. In time management the REFA methodology is used.
The REFA-methodology is an industrial proven instrument for time determination in repetitive manufacturing processes that gives a general overview how process times can be determined. REFA gives suggestions about how this time determination could be successfully applied where products and components are changing often from project to project [2].
In repetitive manufacturing production is generally paced at a certain takt time. When the variance of manufacturing times is high the estimation of precise process times becomes difficult and costly. Human workers have varying physical, mental, and emotional conditions and work under varying environmental circumstances. This variety makes standardized process times difficult to determine.

Other factors influencing the accuracy of determined process times could be the operator specificity and qualification; the firm-level or operator-level experience; environmental conditions; and the technology used.

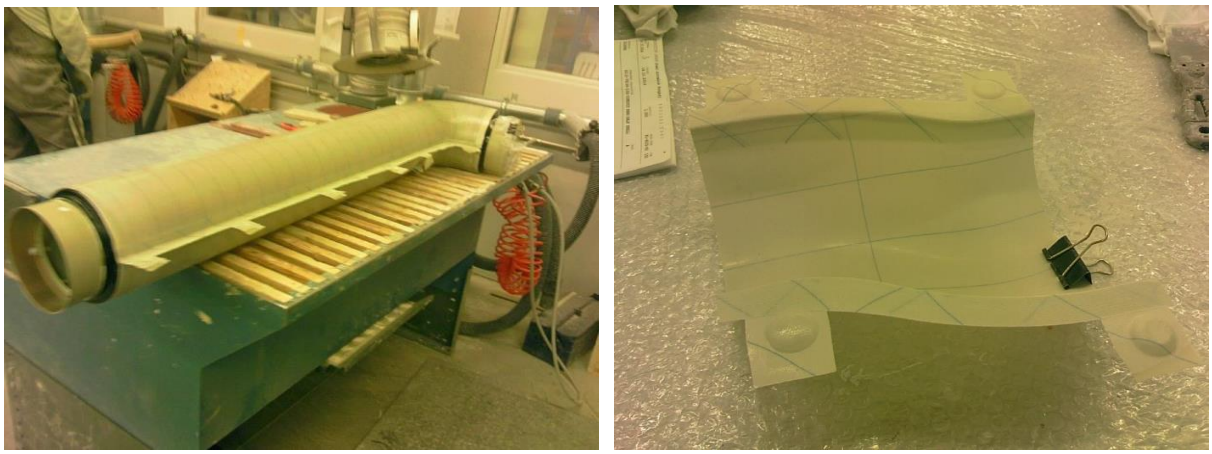

Figure 1. Air duct for an Airbus air conditioning system.

Determination of manufacturing times and scheduling of the production needs a customized approach, the standardized process times have to be defined on the basis of suitable parameters or characteristics. REFA-methodology describes three generally applicable ways for the determination of standardized process times [1]:

- calculation of process times through mathematical functions;
- comparison through historical data and product information in the archive (suitable only for repetitive products or similar products);
- estimation of production times by experienced personnel.

Table 1. Bonding length – time requirement data

	Length of bonding line (mm)						
Time requirement (min)	500	750	1000	1100	1300	1400	3000
apply adhesive	1.212	2.172	1.272	1.716	2.076	1.875	4.176
clip install/remove	1.109	1.116	1.344	1.311	2.940	1.472	1.068
remove adhesive	1.092	0.794	1.035	0.219	0.840	0.552	3.156

Process time includes all the needed activities for determined manufacturing activity. The three different process time categories [1]:

- parameterizable process times (calculate),
- categorizable process times (compare),
- non-definable process times (estimate/measure).

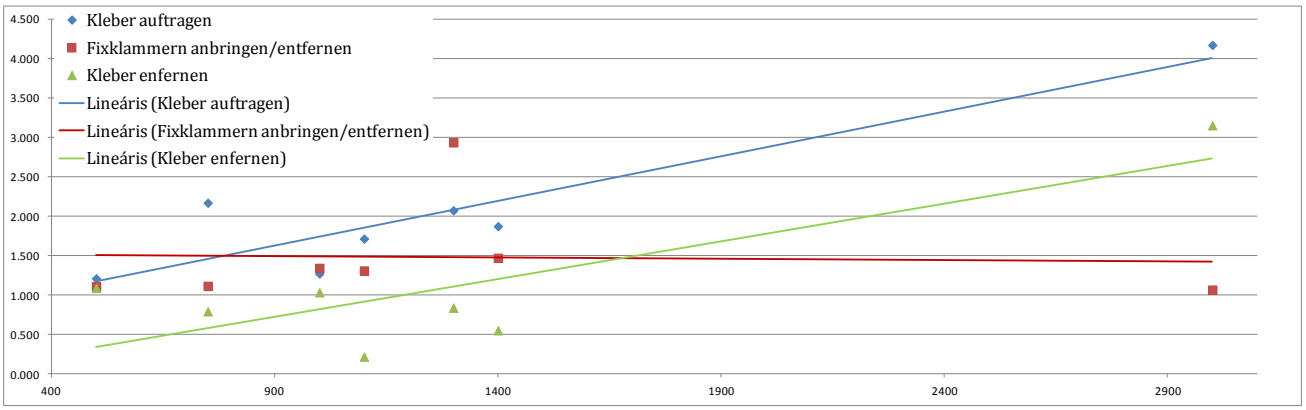

Figure 2. One variable linear regression functions regarding to three operations of bonding (time [min] vs. length of bonding line [mm]).

For calculation of the standard times for new products a database of the time requirements of the standard job elements is being built and connections between the parameters of the product (part) and the time of operations are analyzed.
In the bonding process the length of bonding line is the most influential parameter. The mapping between the length of bonding line and time requirement is analyzed and regression functions are determined for the operations. Table 1 shows the time requirement of three operations of bonding as a function of the length of bonding line (data refer seven different parts).
The analysis is currently based on a one-variable linear or non-linear regression model. Regression functions regarding the standard elementary operations, got from the regression analysis of measured data, are gathered in software and used for the estimation of standard times for production planning of the new products.
In Figure 2 linear regression functions are presented for the time requirement of three above mentioned operations (see Table 1).

3. APPLICATION OF MULTIPLE REGRESSION

The goal of the ongoing research project is to determine further variables influencing the time requirement of operations, and to apply linear, non-linear or non-parametric multiple regression models for estimation of standard times.
Possible parameters for calculation of standard time of bonding are

- the length of the bonding line;
- the diameter of the part (maximum distance between the points of the part);
- surface area of the part;

furthermore parameters characterizing the complexity of the bonding line (curve), namely

- the ratio of non-straight curve segments in the total bonding length ;
- the ratio of segments different from straight line and circle in the total bonding length;
- the ratio of non-plane curve segments in the total bonding length.

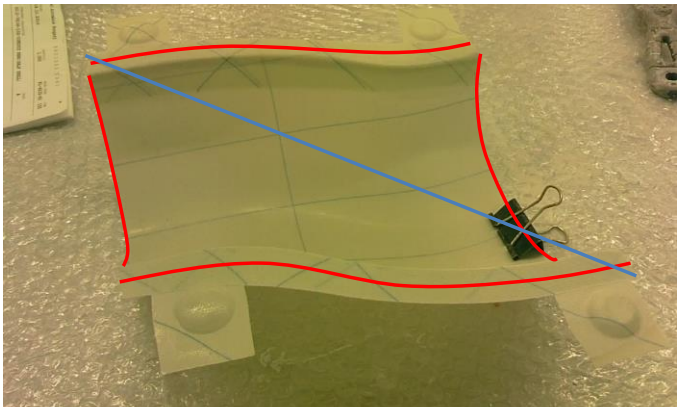

Figure 3. Parameters for a multiple regression model.

REFERENCES

[1] Matt, D.T., Ilmer, P., Rauch, E.: *Methodology for the determination of manufacturing process times in the ETO (Engineer-to-order) sector – a case study*, 11st AITeM Conference, At San Benedetto del Tronto, Italy, Volume: Enhancing the Science of Manufacturing, 2013

[2] REFA, *1997. REFA-Methodenlehre der Betriebsorganisation. Teil Datenermittlung*, Carl Hanser Verlag, Munich.

[3] P. Kuhlang et al.: *Morphology of time data management – systematic design of time data management processes as fundamental challenge in industrial engineering*, Int. J. Industrial and Systems Engineering, Vol. 16, No. 4, 2014

THE FUNCTION OF THE REPLENISHMENT TIME IN THE PURCHASING

[1]KORPONAI János, [2]BÁNYAINÉ TÓTH Ágota PhD, [3]ILLÉS Béla PhD

[1]József Hatvany Doctoral School, University of Miskolc
E-mail: janos.korponai@gmail.com
[2,3]Department of Materials Handling and Logistics, University of Miskolc
E-mail: altagota@uni-miskolc.hu, altilles@uni-miskolc.hu

Abstract
During the definition of the optimal stock level of purchased parts, the expenses related to procurement and stock management are important aspects beside the stock level. By using the economic order quantity model, we can define the optimal order quantity, along which our stock management can be guaranteed by the most favourable cost level. The basic model assumes a deterministic operational environment, where the future demands are known for us, the lead times are calculable and observable, and the stock replenishment can be performed any moment. In practice however, we have we have more complicated tasks to solve. The aim of our analysis is to choose and modify one factor from the initial conditions of the basic model, and to present its impact on the relations. We examine its impact on the timing of procurement, in case the stock replenishment is not immediate. We distinguish two versions in the light of the relation between the stock replenishment time and the procurement cycle, which is derived from the calculation of the economic order quantity. In the case of the first version, the stock replenishment can happen in the cycle of the order placement, while in the case of the second version the stock replenishment requires a longer cycle than the order cycle. As a result, we show the difference between the two versions, and define the latest date of order placement.

Keywords: *economic order quantity, replenishment time, costs, stock*

1. INTRODUCTION

The stock level of a company's purchased parts is the consequence of the joint action of several factors. It is influenced by the quantitative and temporal calculability of each phase of the supply chain, the features of the continuity of production and supply, and to a great extent, by the frequency of purchases and the individual order quantities as well. The balance between the stock level and the costs can be defined with the economic order quantity model, the initial conditions of which are as follows [1] [2]:

- The supply is immediate, thus the stock replenishment time is zero.
- The frequency of supplies is scheduled for identical periods.
- The demand is known and pre-definable with absolute certainty.
- Utilization is continuous and with uniform intensity.
- Stock shortage is not accepted.
- The ordering costs are independent from the order quantity.
- The holding costs per unit are constant and they change linearly with the stock quantity [1].

Since the economic order quantity model assumes an environment with deterministic features, which occurs very rarely in practice, two important tasks must be performed during the establishment of the stock management strategy [3]:

- The minimum of the total cost function, thus the economic order quantity, must be defined in the knowledge of the ordering cost, the holding cost and the planned demand
- By adjusting to practice, the cover strategy, thus the optimal level of the safety stock, must be defined by considering the stochastic features related to the replenishment time and the change of demands.

During our analysis, we assume deterministic demands and environment, and we start from a stock management strategy that does not allow a stock shortage, and a cost-minimizing rational behaviour.

2. METHODS

We perform a further analysis by leaving every condition of the economic order quantity model unaltered and by choosing and modifying the stock replenishment time. During our analysis, we want to see the changes of the relations defined in the basic model, if the stock replenishment is not immediate.
We must emphasize that these are theoretical analyses, which describe relations functioning in an abstracted environment, thus their practical application requires further modifications of the model's initial conditions.

3. RESULTS

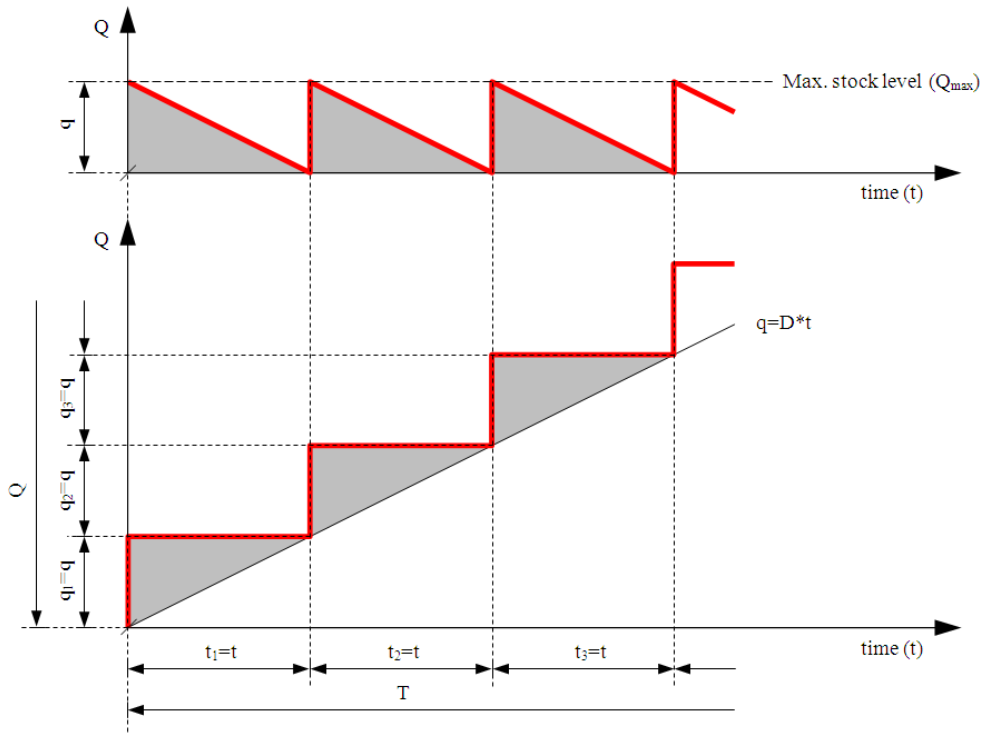

Figure 1 Optimal stock level in case of regular stock replenishment and a demand with uniform intensity

Basic model. The basic model of the economic order quantity starts from the relation that the purchase cost and the stock level change according to the order quantity, and the holding cost

changes as well. Accordingly, the more rarely orders are made, the more favourable the purchase costs are per unit, and at the same time, the holding costs are linearly increasing [4].
The purchase and holding costs can be derived from the relation of the stock level and the demands illustrated as a function of time. Figure 1 shows a stock management strategy that does not allow a stock shortage. The figure illustrates that during the complete *T* period it is necessary to purchase a *Q* amount of parts [5].
According to the model illustrated by figure 2, the optimal order quantity for a company is at the point, where the total cost, made of the holding cost and the purchase cost, reaches its minimum, thus the cost function is the minimum of the total cost [6].

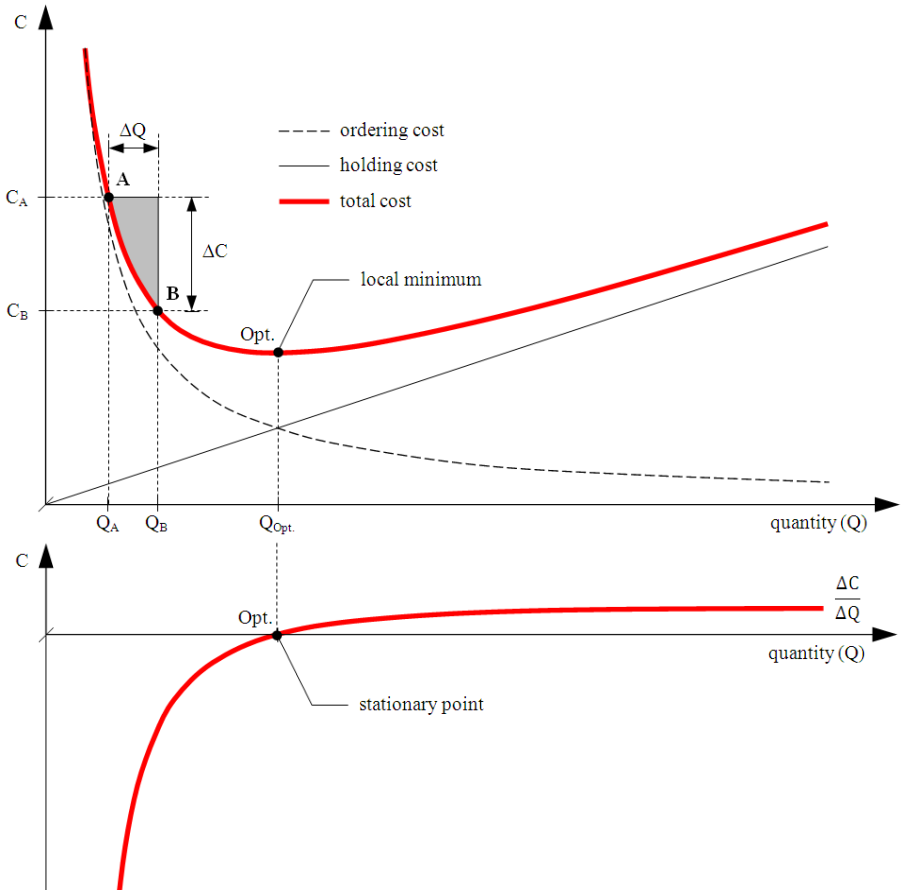

Figure 2 Purchase and holding costs in relations to stock levels

In case we purchase a *q* quantity covering the demand of a period with a *t* duration, the number of purchases can be expressed with the time factor:

$$\frac{Q}{q} = \frac{T}{t} \tag{1}$$

where

Q – total purchase demand for the examined period,
q – purchase demand for a single period,
T – the length of the complete period,
t – the length of a single period

In case we purchase a "q" quantity once, the purchase cost for a total *Q* quantity is:

$$C_1 = \frac{Q}{q} \cdot c_1 \tag{2}$$

where

C_1 – total purchase cost for the examined period,
c_1 – cost of a single purchase.

The holding cost can be derived from the area limited by the saw tooth diagram:

$$C_1 = \frac{1}{2} \cdot q \cdot t \cdot \frac{Q}{q} \cdot c_2 \tag{3}$$

where

C_2 – total holding cost for the examined period,
c_2 – holding cost per time unit.

Accordingly, the total cost made of the holding cost and the purchase cost is:

$$C = \frac{Q}{q} \cdot c_1 + \frac{1}{2} \cdot q \cdot t \cdot \frac{Q}{q} \cdot c_2 = \frac{Q}{q} \cdot c_1 + \frac{1}{2} \cdot q \cdot t \cdot \frac{Q}{q} \cdot c_2 \rightarrow \min \tag{4}$$

Figure 1 shows that the optimal order quantity is given, where the total purchase and holding cost function is at its minimum value, which can be defined by calculating the extreme values of formula no. (4):

$$q = \sqrt{\frac{2 \cdot Q}{T} \cdot \frac{c_1}{c_2}} \tag{5}$$

Introduction of replenishment time. In case of the basic model, we start from the assumption that the supply is immediate, thus the replenishment time is zero. In practice however, this condition is only rarely fulfilled, so we modify the model and introduce the replenishment time with arbitrary duration (*Figure 3*).
Figure 3 shows the case, where there is a replenishment time of a τ duration, which can be divided into the lead times of further part-activities. In case of the modified model, we have to emphasize that the replenishment time means the total lead time at the end of which the stock is freely available to satisfy further utilization demands. This is not identical with the arrival date of goods, as shown by the figure, since there are several other activities to be executed after the receipt of goods [7].

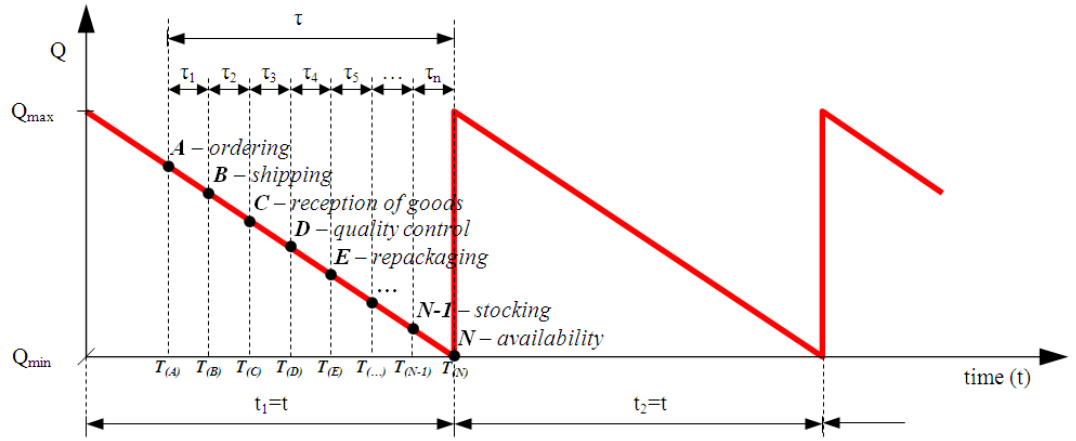

Figure 3 Stock management mechanism from the aspect of the freely available stock entered into storage; stock replenishment can be realized within the ordering period

Relation of replenishment time and periodical time. We have to examine the relation between replenishment time τ and cycle time t derived from the economic order quantity model.
During the development of the model, we distinguish two versions:

- Replenishment time τ is shorter than or the same as the cycle time t, so that $\tau \leq t$ (Figure *3*).
- Replenishment time τ is longer than the cycle time t, it means $\tau > t$ (Figure *4*).

The differentiation between the two versions is justified by the fact that for the first version we have to calculate only with the demand of the next cycle, and there is only a single freight on the road at a time. In the case of the second version, we do not plan the demand of the next period, and there are several freights on the road at a time, thus we must consider both the planned demands and the transit stocks during the order placement [5].

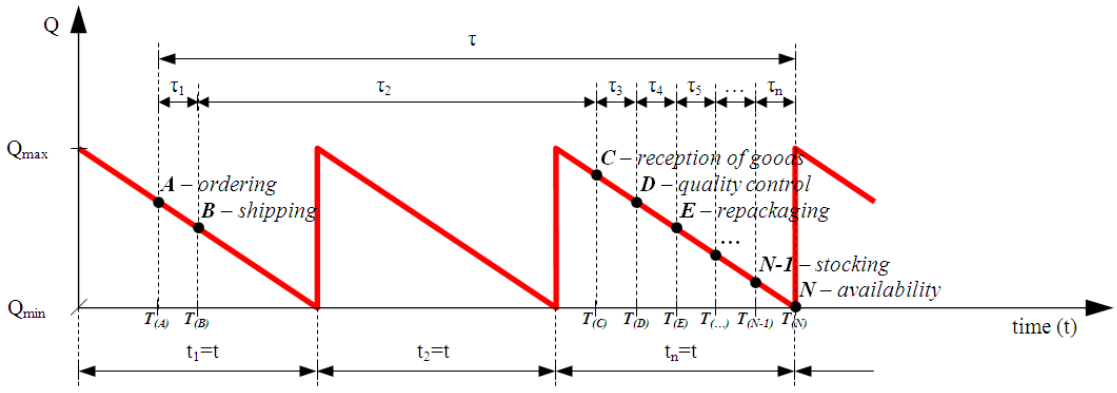

Figure 4 Stock management mechanism from the aspect of the freely available stock entered into storage; stock replenishment cannot be realized within the ordering period

The shortest planning time horizon is identical with the replenishment time in the case of both versions. It is clear that a lead time shorter than the replenishment time would result in the exhaustion of stocks before the availability of the newly arriving stocks, which would lead to an inadmissible stock shortage.

We can also see that, if we only modify the replenishment time from all initial conditions of the basic model, the task will not be the definition of the order quantities, but the calculation of the order placement date. The order quantity corresponds for both versions to the optimal order quantity.
The latest date of order placement can be calculated as follows:

$$T_{(A)} = T_{(N)} - \tau \tag{6}$$

where

$T_{(A)}$ – the date of order placement,
$T_{(N)}$ – the date of the free availability of the stock entered into storage.

CONCLUSIONS

During our analysis, we concluded that the relation between the length of replenishment time and the length of the order period defines the number of freights on the road at the same time, and the factors that have to be observed during the order placement. Among deterministic starting conditions, the only question is the definition of the order placement date in relation to the alteration of the replenishment time, while the ordered quantity is derived from the formula applied for the economic order quantity. In order to develop the basic model into a model that can be used in practice, we must analyse the impact of the alteration of the other initial conditions, and the relations must adapted to the real stochastic operational environment.

ACKNOWLEDGEMENTS

This research was partially carried out in the framework of the Centre of Excellence of Mechatronics and Logistics at the University of Miskolc.

REFERENCES

[1] Kummer, S., Grün, O., Jammernegg, W.: *Basics of purchasing, production, logistics (in German: Grundzüge der Beschaffung, Produktion, Logistik)*, Published by Pearson Studium, München, 2009, ISBN 978-3-8273-7351-9
[2] Szegedi Z., Prezenszki J.: *Logistics Management (in Hungarian: Logisztika-menedzsment)*, Published by Kossuth Kiadó, Budapest, 2003, ISBN 963 09 4434 0
[3] ILLÉS I-né.: *Companies' financial affair (in Hungarian: Társaságok pénzügyei)*, Published by SALDO Kiadó, Budapest, 1998, ISBN 963 621 872 2
[4] Kovács Z.: *Logistics (in Hungarian: Logisztika)*, Published by Veszprém Egyetemi Kiadó, Veszprém, 1998
[5] Kulcsár B.: *Industrial logistics (in Hungarian: Ipari logisztika)*, LSI Oktatóközpont, Budapest, 1998, ISBN 963 577 242 4
[6] Knoll I.: *Logistics in the 21th century (in Hungarian: Logisztika a 21. században)*, Published by KIT Képzőművészeti Kiadó, 1999, ISBN 963 336 873 1
[7] Vörös J.: *Production Management (in Hungarian: Termelésmenedzsment)*, Published by Jannus Pannonius Kiadó, Pécs, 1991, ISBN 963 641 284 7
[8] Körmendi L., Pucsek J., *The Logistics in theory and practice (in Hungarian: A logisztika elmélete és gyakorlata)*, Published by SALDO Kiadó, Budapest, 2008, ISBN 978 963 638 275 9, ISSN 1789-5103

INTERNATIONAL SCIENTIFIC CONFERENCE ON ADVANCES IN MECHANICAL ENGINEERING
19 November 2015, Debrecen, Hungary

SIMULATION STUDY OF AMINE-BASED CO_2 ABSORPTION

[1]LÁNG Péter DSc, [2]HÉGELY László PhD, [3]NAGY Dávid, [4]DÉNES Ferenc PhD

[1,2,3]Department of Building Services and Process Engineering, Budapest University of Technology and Economics
E-mail: lang@mail.bme.hu, hegelyl@hotmail.com, alfayadd@gmail.com
[4]Department of Energy Engineering, Budapest University of Technology and Economics
E-mail: denes@energia.bme.hu

Abstract
For the capture of CO_2 the most promising method is the chemical absorption in aqueous amine solutions. The most common solvent recycled in the absorber-stripper system is the aqueous monoethanolamine. The equilibrium model of the flow-sheet simulator is validated with vapour-liquid equilibrium measurement data. The simulation model created with a professional flow-sheet simulator is validated with pilot plant experimental data. Two flow-sheet modifications are studied by simulation and optimized by a genetic algorithm for the purification of the flue gas of a natural gas fired power plant. The objective function is the reboiler duty of the stripper.

Keywords: CO_2 capture, optimization, absorption, monoethanolamine, stripping, GA optimization

1. INTRODUCTION

From all the greenhouse effect gases, the atmospheric concentration of carbon dioxide shows the most significant increase. Several methods exist for the capture of CO_2 from flue gases, such as water or amine scrubbing, or membrane separation. The most promising method seems to be the chemical absorption in aqueous amine solutions. The most common solvent recycled in the absorber-stripper system is aqueous solution of monoethanolamine (MEA). Though the absorption process is efficient but the energy demand of the stripping is very high and this considerably decreases the efficiency of power plants.
In order to decrease the energy demand of the process several flow-sheet modifications were suggested [1]. By splitting the rich solvent stream into two streams ("rich-split"), and thus feeding it into the stripper at two different locations, the heat duty of the stripper was reduced by 10.3 %. By withdrawing a fraction of the liquid phase from the middle section of both columns, and feeding them to the middle section of the other column ("split-flow"), a reduction of 11.6 % was reported.
The goals of this paper:

- to create the ChemCAD model of the absorber-stripper system,
- to validate the vapour-liquid equilibrium model ("Amine") of the simulator,
- to validate the model with pilot plant measurement data,
- to study and optimize the "rich-split" and "split-flow" flow-sheet modifications.

2. VAPOUR-LIQUID EQUILIBRIUM CONDITIONS

The vapour-liquid equilibrium conditions were described by the "Amine" model of the professional flowsheet simulator ChemCAD [2,3], which can be applied for systems containing certain organic amines (such as MEA), CO_2, H_2S and water. The model solves seven reaction equations to obtain

the free concentration of CO_2 and H_2S in the liquid phase, on the basis of which the partial pressures are calculated by the Henry's constants. The solubility of O_2 and N_2 are also calculated by Henry's constants. The vapour enthalpy is obtained from the SRK equation of state. The liquid enthalpy with heat of absorption of H_2S and CO_2 in amine solution is calculated by the method of Crynes and Maddox [4]. The model was validated with vapour-liquid equilibrium measurement data from [5]. The partial pressure of CO_2 was calculated at different CO_2/MEA ratios for a mixture containing 30 mass% MEA. The calculations were performed for 40 °C and 120 °C, as these are temperatures of the absorber and stripper columns, respectively. The calculated and measured partial pressures show a good agreement (*Figures 1a&b*).

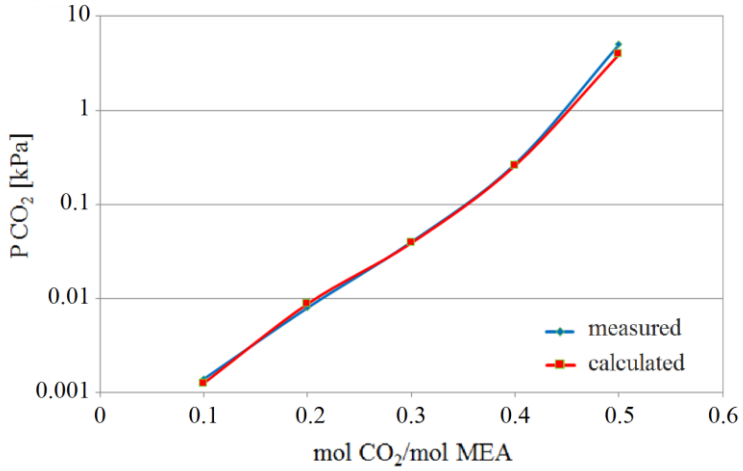

Figure 1a. Partial pressure of CO_2 in the mixture CO_2-water-MEA at 40 °C

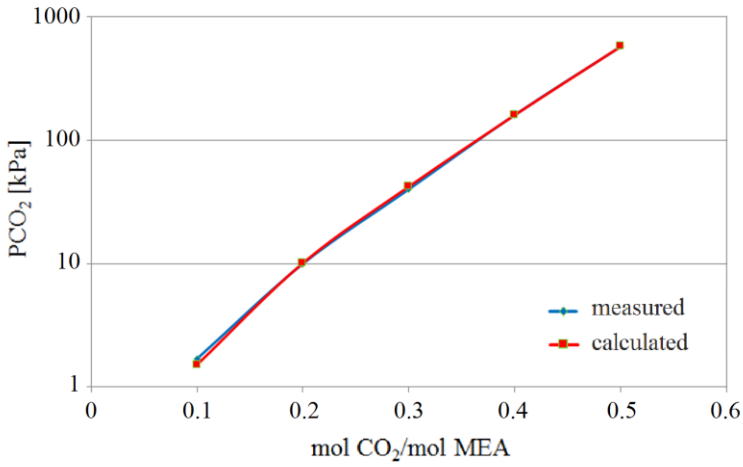

Figure 1b. Partial pressure of CO_2 in the mixture CO_2-water-MEA at 120 °C

3. PROCESS MODELS

The removal of CO_2 from the flue gas is performed in an absorber-stripper system (*Figure 2*). The CO_2 is absorbed from the flue gas by the solvent lean in CO_2 in the absorber, operating at nearly atmospheric pressure. The gas leaving the column is washed by water in a washing section, in order

to reduce solvent loss. The water make-up fed to the washing section compensates the water loss of the system. The solvent rich in CO_2 leaves the bottom of the absorber and, after being preheated by the lean solvent, enters the stripper, which is operated under pressure. The vapour generated in the reboiler strips the CO_2 out of the solvent, which is cooled down by the rich solvent and in an aftercooler then recycled to the absorber. The stripped gas is washed in a washing section, after which its water content is condensed. The condensate serves as the washing liquid.

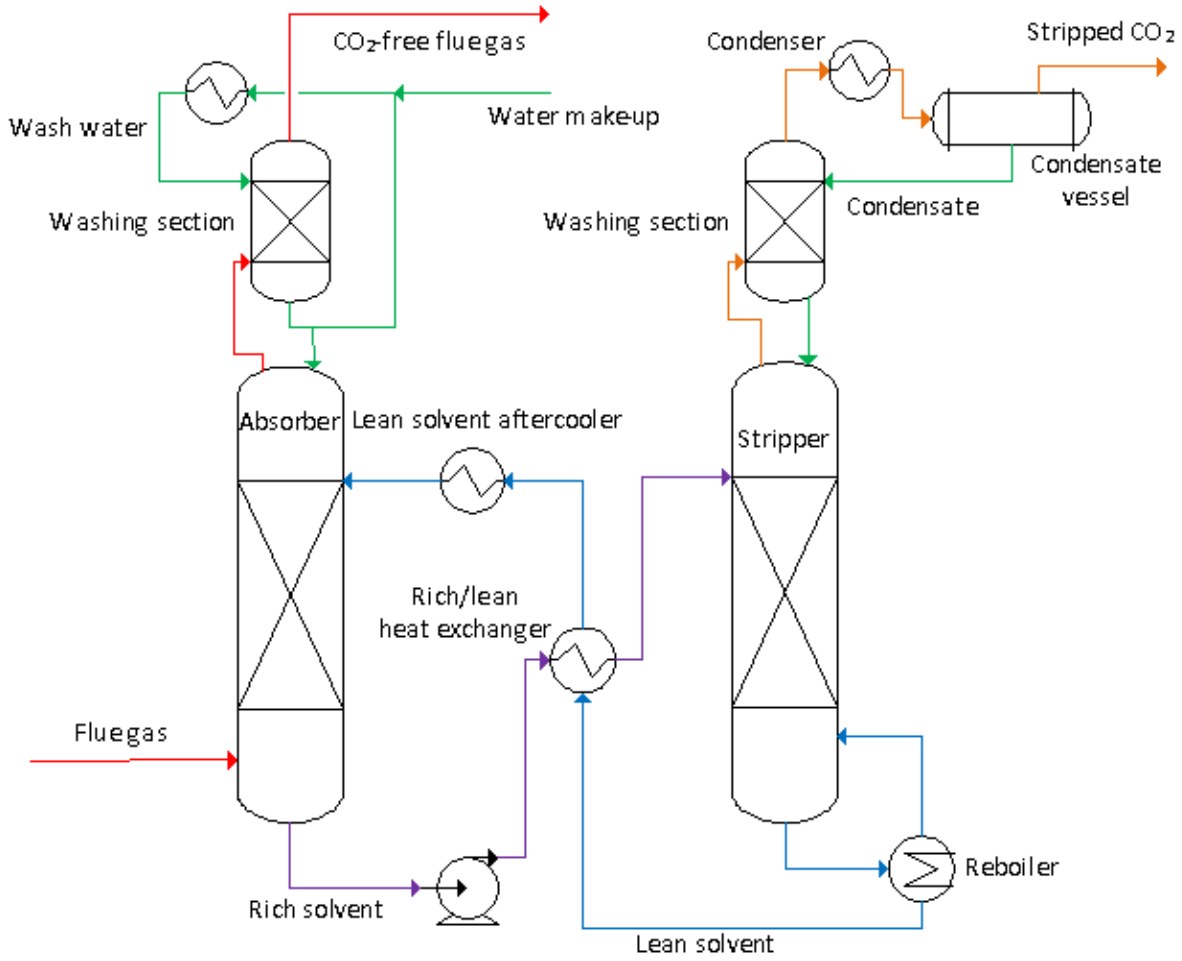

Figure 2. The basic absorber-stripper system

By the rich-split process modification (*Figure 3*) the rich solvent is split into two streams. One is fed into the top of the stripper without preheating, while the other one is preheated and fed into the middle section of the stripper. The steam formed in the middle section of the column preheats and strips the solvent in the upper section, thus making possible to reduce the heat duty of the reboiler. Additional degrees of freedom compared to the basic system are the location of side feeding and the ratio of the streams split.

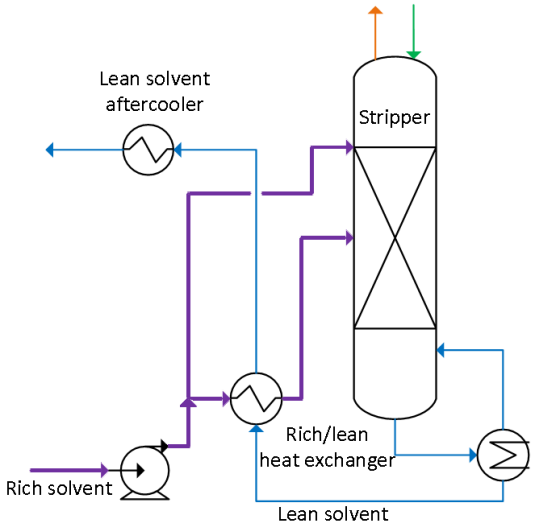

Figure 3. Rich-split process modification

By the split-flow process modification, a fraction of the liquid phase is withdrawn from the middle section of both columns and introduced to the middle section of the other column (*Figure 4*). In this way, although the capacity of the solvent is only partially utilized (semi-saturated and semi-stripped solvent), the temperature profiles are significantly improved. The average driving forces are increased and both absorption and stripping become more efficient. Appropriate preheating and cooling is important, in order not to induce warming up in the absorber or cooling up in the stripper. The additional degrees of freedom are: locations of both side products and both side feeds, withdrawal ratios in the absorber and in the stripper.

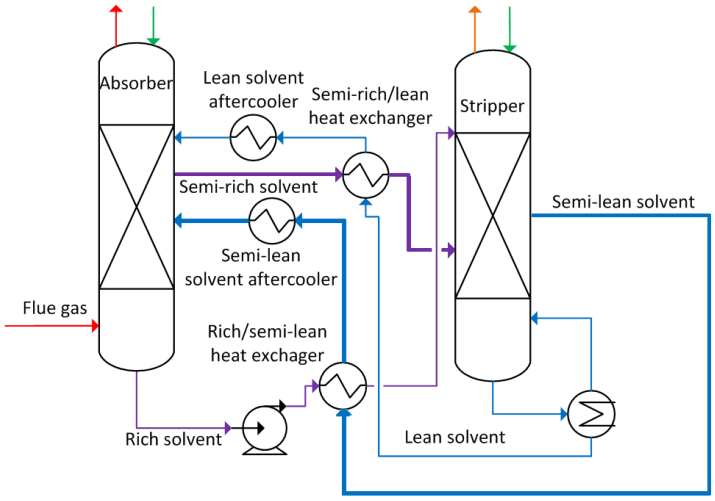

Figure 4. Split-flow process modification

4. VALIDATION OF THE SIMULATION MODEL WITH PILOT PLANT EXPERIMENTAL DATA

Mangalapally and Hasse [6] performed pilot plant experiments using the basic absorber-stripper system. We built up its model in ChemCAD and simulated their experiments in order to validate the simulation model for further calculations. The inlet flue gas consists of 8.2 mass% CO_2, 73.7 % N_2,

11.8 % O_2, 6.3 % H_2O. Both columns had the same diameter (125 mm) and were filled by Sulzer Mellapak 250.Y structured packing: for the absorber the packing height was 4.20 m (+0.42 m of washing section), for the stripper 2.52(+0.42), respectively. In the simulation the number of theoretical trays is 17 for the absorber and 11 for the stripper. The MEA content of the absorbent is 33 mass%. The experimental and simulation results are in good agreement (Table 1), that is, the ChemCAD model is adequate.

Table 1. Experimental and calculated parameters of the top products of the pilot plant system

		ChemCAD simulation	Pilot plant experiment
Absorber	Mass flow rate [kg/h]	71.9	70.7
	Temperature [°C]	48.7	48.0
	CO_2-content [m/m%]	2.0	1.6
Stripper	Mass flow rate [kg/h]	4.79	5.11
	Temperature [°C]	14.0	15.3
	CO_2-content [m/m%]	99.7	99.6
Recovery of CO_2 [%]		77	82

5. OPTIMIZATION

The optimization of the two process modifications is performed for the purification of the flue gas of a natural gas fired power plant, and the results are compared to that of the unmodified system. The following input data are the same for all the calculations, and were determined by a preliminary parameter study investigating the effect of the operational parameters. The data of the flue gas: 1400.5 t/h, 46.3 °C and 1.034 bar. The flue gas composition is the same as in the earlier simulations. The CO_2-free solvent's flow rate is 921.4 t/h, its MEA content is 33 mass%. The recovery of CO_2 is fixed at 85 %. The data of the two columns are shown in Table 2. The temperature of the lean solvent entering the absorber is 39.8 °C. The flow rate of the wash water recycled to the washing section of the absorber is 681.8 t/h.

The objective function is the reboiler duty of the stripper, which is evaluated by rigorous simulation using different modules of the flowsheet simulator ChemCAD. Given this black box approach of the evaluation, GA is chosen as optimization method. A real-coded elitist variant of the algorithm is written in VBA under Excel. The parameters of the GA: mutation probability: 5 %, population size: 30, crossover probability: 70 %. The optimization variables for the rich-split variant and their ranges are: the side feeding location (integer variable, counted from the top): $3 \leq f_{rs} \leq 10$ and solvent split ratio (flow rate of side feed/total flow rate of rich solvent): $0 \leq \eta_{rs} \leq 50$ %. In the case of the split-flow variant, two simplifying assumptions are applied. The first one is that the side feeds are located just below the side withdrawals. The second one is that the mass flow rates of the side withdrawals are equal, to assure the smoothness of liquid load profiles in the columns. In this way, there are only three optimization variables: the location of the side withdrawals (integer): $2 \leq f_{s,abs} \leq 13$, $2 \leq f_{s,str} \leq 10$, and their flow rates: $0 \leq F_s \leq 500$ t/h.

Table 2. Input data of the columns

	Absorber	Stripper
Number of theoretical plates	13	10
Top pressure (bar)	1.005	2
Pressure drop (bar)	0.029	0.02
Outlet temperature of heat exchanger (°C)	15	14

The reboiler duty of the basic system is 966.5 GJ/h. For the rich-split, we got zero as optimal solvent split ratio, that is, by the rich-split modification the energy need did not decrease. The optimal results for the split-flow process: $f_{s,abs}$=4, $f_{s,str}$=2, F_s=59.15 t/h. Both side streams have a flow rate of 59.15 t/h (this is 5.8 % of the flow rate of the total feed of the stripper). The side streams are fed to the columns on plate 5 in the absorber and plate 3 in the stripper, respectively, just below the locations of side withdrawals. The optimal reboiler duty is 938.9 GJ/h, which means a decrease of 2.76 %.

CONCLUSIONS

The removal of CO_2 from flue gas by aqueous monoethanolamine in an absorber-stripper system was investigated by rigorous simulation and optimization. The equilibrium model of the flow-sheet simulator applied was validated by using VLE measurement data. The absorber-stripper system was modelled for the purification of the flue gas of a natural gas fired power plant. Two flow-sheet modifications (rich-split and split-flow) were optimized by a genetic algorithm coded in VBA under Excel with the flow-sheet simulator performing the modelling calculations. The objective function was the reboiler duty.
For the rich-split the optimal solvent split ratio was zero, that is, the optimal result was given by the basic system. For the split-flow, a slight decrease (2.8 %) of the energy demand was achieved.

ACKNOWLEDGEMENTS

This work was supported by OTKA, project No.: K-106286 and TÁMOP - 4.2.2.B-10/1-2010-0009.

REFERENCES

[1] Cousins, A., Wardhaugh, L. T., Feron, P. H. M.: *Preliminary analysis of process flow sheet modifications for energy efficient CO_2 capture flue gases using chemical absorption*, Chemical Engineering Research and Design, 89, 2011, pp. 1237-1251.
[2] *CHEMCAD Version 6 User Guide*, Chemstations, 2012.
[3] Kent, R. L. and Eisenberg, B.: *Better Data for Amine Treating*, Hydrocarbon Processing, 1976, pp. 55, 87.
[4] Crynes, B. L. and Maddox, R. N.: *How to determine reaction heat from partial pressure data*, Oil & Gas Journal, 1969, pp. 65-67.
[5] Aronu, U. E., Gondal, S., Hessen, E. T., Haug-Warberg, T., Hartono, A., Hoff, K. A., Svendsen, H. F.: *Solubility of CO_2 in 15, 30, 45 and 60 mass% MEA from 40 to 120 °C and model representation using the extended UNIQUAC framework*, Chemical Engineering Science, 66, 24, 2011, pp. 6393-6406.
[6] Mangalapally, H. P. and Hasse, H.: *Pilot plant study of post-combustion carbon dioxide capture by reactive absorption: Methodology, comparison of different structured packings, and comprehensive results for monoethanolamine*, Chemical Engineering Research and Design, 89(8), 2011, pp. 1216-1228.

INTERNATIONAL SCIENTIFIC CONFERENCE ON ADVANCES IN MECHANICAL ENGINEERING
19 November 2015, Debrecen, Hungary

COMPARATIVE ANALYSIS OF THE COMPLIANT MECHANISM MOVEMENT WITH 2 DOF USING CIRCULAR, RECTANGULAR, ELLIPTICAL JOINTS

[1]LATEŞ Daniel PhD, [2]CIOLOCA Flaviu

[1] "Petru Maior", University of Târgu Mureș
E-mail: ddan005@gmail.com
[2]Mechanical Designer, IRUM, Târgu Mureș
E-mail: cioloca.flaviu@irum.ro

Abstract
In this work there will be presented three compliant mechanisms with 2 DOF, which differs through the utilised joints. There will be utilised three types of compliant joints, namely circular, rectangular and elliptical joints. In the introduction there will be presented a small description of the compliant mechanisms and then will be described the realisation of the joints for the three types mentioned above. The work will continue with the presentation of the compliant mechanism and then the mechanisms will be analysed through the finite element method. In the end will be presented the results and the comparative analysis of the three mechanisms from the movements point of view. The conclusions of the work present future directions of research.

Keywords: *compliant mechanism, circular joints, elliptical joints, rectangular joints, finite element method.*

1. INTRODUCTION

The compliant mechanisms are mechanisms which ensure the wanted movement through elastic deformation. These mechanisms are reversible and they are maintained in the availability limit of Hook's law. The particularity of these mechanisms it is given by their joints. The joints are flexible and they are made of the same mechanism material, the cinematic elements from those areas are being thinned for achieving the relative rotation between two adjacent elements.
In the figure 1 you can see some examples of obtaining the profiles for different flexible joints. In figure 1a you can see the obtaining of the rectangular joint, circular joint in figure 1b and in figure 1c elliptical joint towards a desired outcome.

a. b. c.

Figure 1. Examples of obtaining the profiles for different flexible joints.

Figure 2 outlines the general shape of the profile of a compliant joint. With *l* it is noted the length of the joint, *t* marks the thickness of the joint and *r* is the radius connection between the cinematic element and the joint.

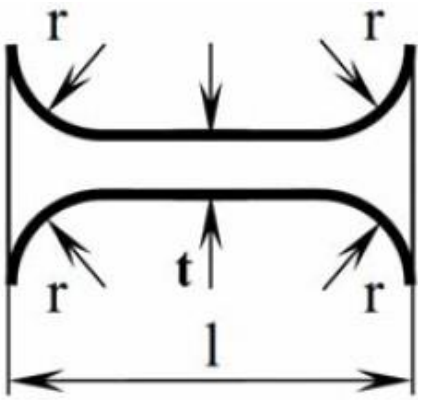

Figure 2. The general shape of the profile of the flexible joint

2. THE DESCRIPTION OF THE COMPLIANT MECHANISM WITH 2 DOF

The plan positioning mechanism it is formed by a structure with total compact compliance having elastic joints and elements. The rigid elements of this structure are the bold areas and the flexible joints consist of the thinned areas just to be able to achieve the compliation phenomenon. The micropositioning mechanism presented in the work it is formed from a parallel five-bar with two degrees of freedom. The structure can be seen in figure 3, where you can see the size and the dimensions of the flexible joints. The joints have the longitudinal section of a rectangular profile in this figure, with a 0.5 mm connection.

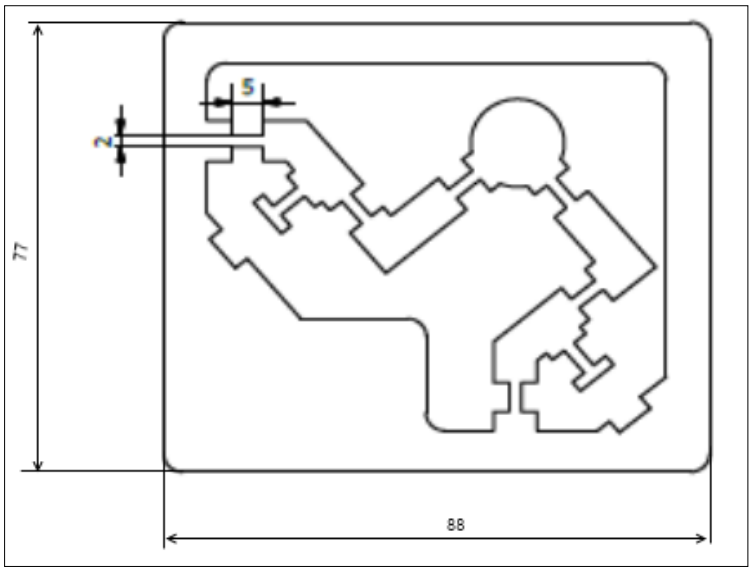

Figure 3. The technical drawing of the positioning mechanism with rectangular joint

For the realisation of the finite element analysis, the three mechanisms from the figure 4 have been projected and modelled 3D. The material chosen in this case is polycarbonate.

a b c

Figure 4. Compliant mechanisms with the rectangular, elliptical and circular joints profile

3. RESULTS

All the three mechanisms have been analysed through Finite Element Method (FEM), using the special module of the Inventor program. At first it was studied the joints mechanism with the rectangular profiles section. Figure 5 presents the forces which are acting upon the mechanism, enforcing movement on the final effector.

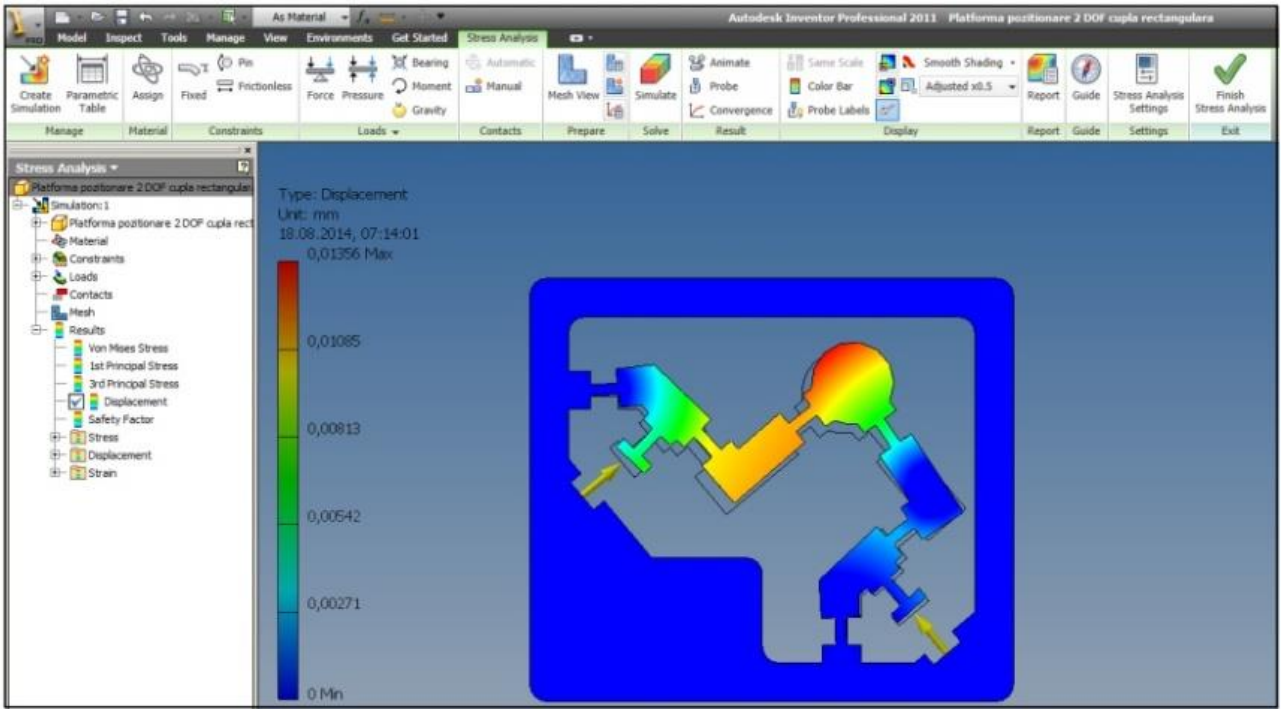

Figure 5. The determination of the mechanism displacement with the rectangular profiles section of the joints

The actuator displacement was of micrometer order. In table 1 it can be seen the results obtained of the final effector with the help of the actuator 1 and 2 movement for the mechanism with rectangular joints.

Table 1

No. test	Actuator 1 (Left)	Actuator 2 (Right)	Force on actuator (N)	FEM Analisis Displacement (μm)		
				x	y	comp.
1.	x	-	0.038	1.3	0.4	1.4
2.	x	-	0.116	4.0	1.5	4.1
3.	x	-	0.194	6.5	2.6	7,0
4.	x	-	0.272	8.7	3.9	9.6
5.	x	-	0.350	12	4.8	13
6.	-	x	0.07	-0.5	0.8	0.9
7.	-	x	0.210	-1.5	2.4	2.9
8.	-	x	0.350	-2.6	4.1	4.8
9.	-	x	0.490	-3.7	5.7	6.8
10.	-	x	0.650	-4.9	7.6	9.1

For the compliant positioning mechanism with joints of circular section, this can be seen in figure 6 during the simulation.

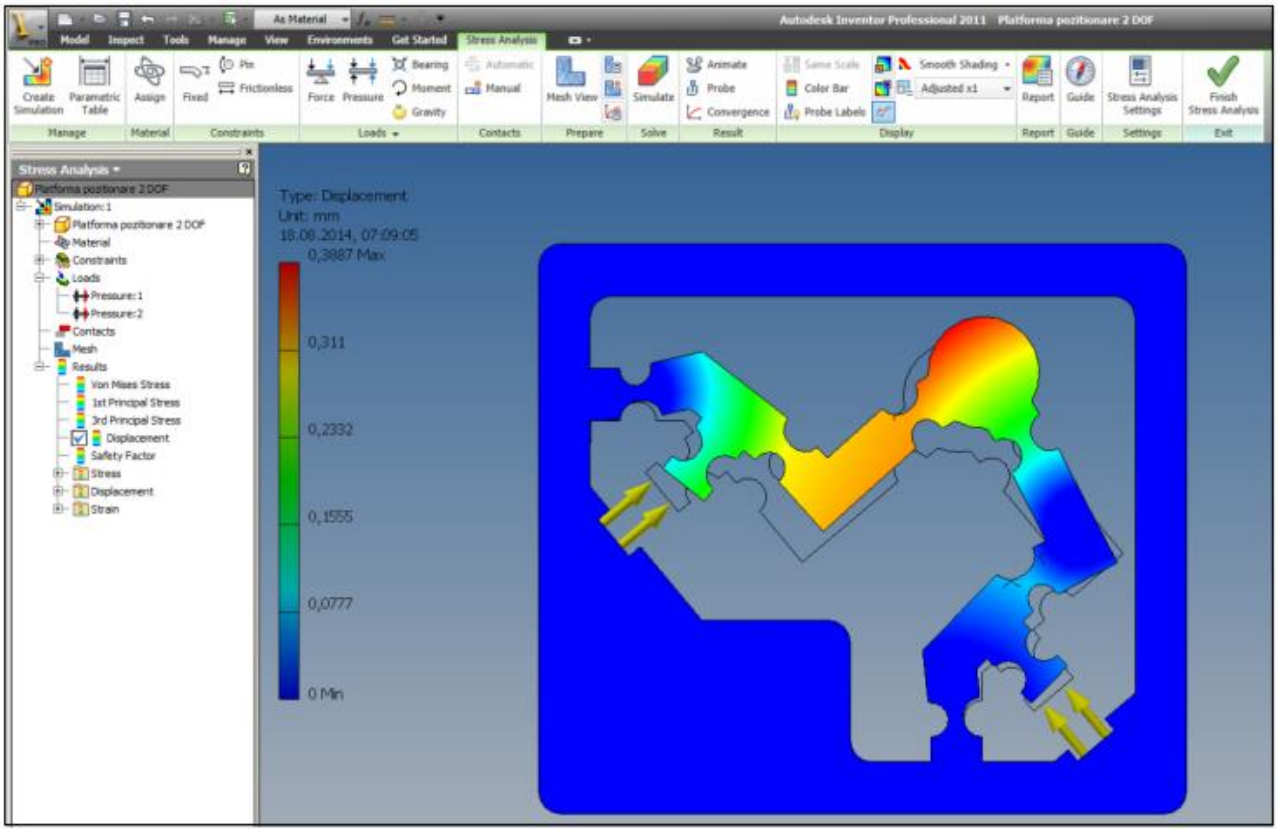

Figure 6. The determination of the mechanism displacement with the circular joints

In table 2 it can be seen the results obtained using the FEM method fot the final effector for the x, y axis and their composition.

Table 2

No. test	Actuator 1 (Left)	Actuator 2 (Right)	Force on actuator (N)	FEM Analisis Displacement (μm)		
				x	y	comp.
1.	x	-	0.07	1.2	0.4	1.3
2.	x	-	0.210	3.7	1.4	3.9
3.	x	-	0.350	6.1	2.4	6.6
4.	x	-	0.500	8.8	3.4	9.4
5.	x	-	0.700	12.3	4.8	13.2
6.	-	x	0.150	-0.6	0.8	1.2
7.	-	x	0.450	-1.7	2.7	3.2
8.	-	x	0.750	-2.9	4.5	5.4
9.	-	x	1.05	-4.1	6.3	7.6
10.	-	x	1.35	-5.4	8.2	9.8

The last mechanism studied, the one with joint of elliptical section can be seen in Figure 7.

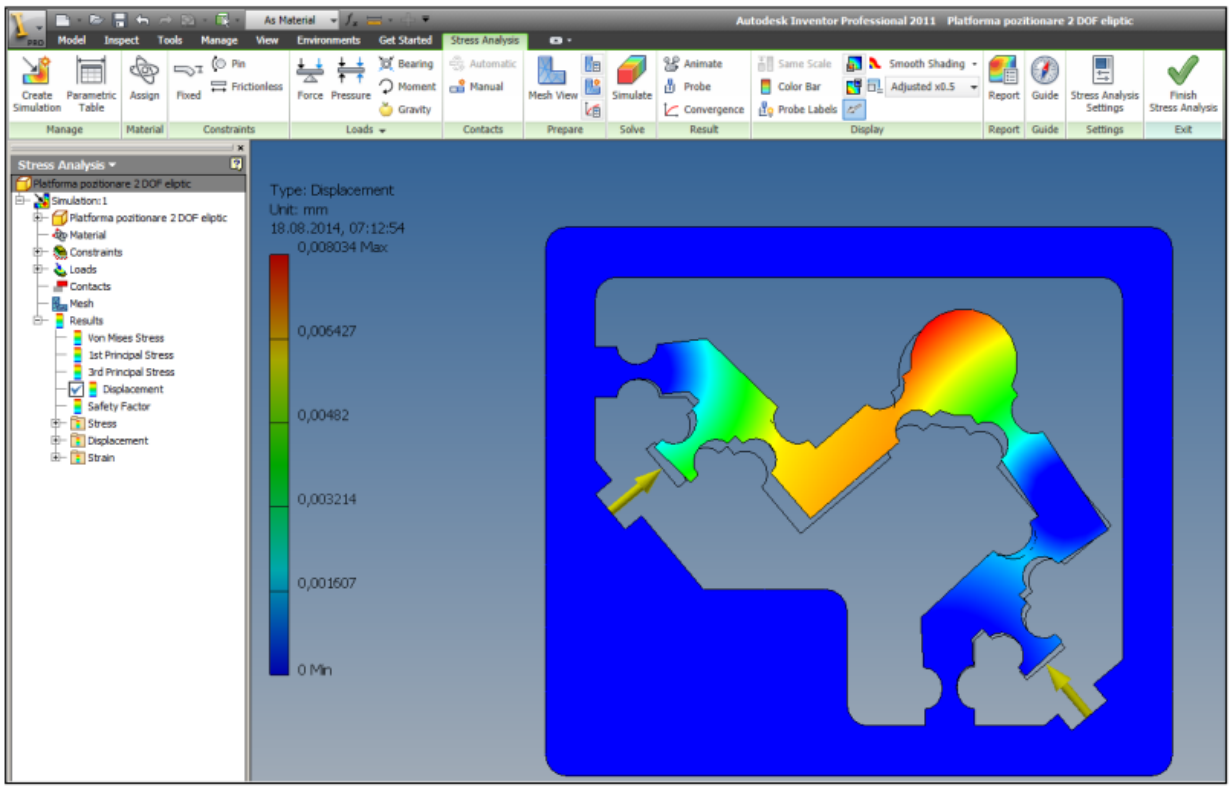

Figure 7. The determination of the mechanism displacement with the elliptical joints

In table 3 it can be seen the results obtained using the FEM method for the final effector on the x, y axis and their composition. The values from the x axis from the seccond actuator have negative values in all of the three cases because of the chosen coordinate system.

Table 3

No. test	Actuator 1 (Left)	Actuator 2 (Right)	Force on actuator (N)	FEM Analisis Displacement (μm)		
				x	y	comp.
1.	x	-	0.075	1.6	0.6	1.7
2.	x	-	0.225	4.6	1.7	4.9
3.	x	-	0.340	6.9	2.6	7.4
4.	x	-	0.476	9.7	3.7	10.4
5.	x	-	0.612	12.5	4.8	13.4
6.	-	x	0.130	-0.5	0.9	1.0
7.	-	x	0.390	-1.7	2.7	3.2
8.	-	x	0.650	-2.9	4.5	5.3
9.	-	x	0.910	-4.1	6.3	7.5
10.	-	x	1.150	-5.2	8.0	9.5

4. THE COMPARATIVE ANALYSIS FOR THE THREE MECHANISMS

For an easier and intuitive interpretation of the results there has been made a chart. The chart from figure 8 has the values from the first actuator in the compound system between the x and y axis.

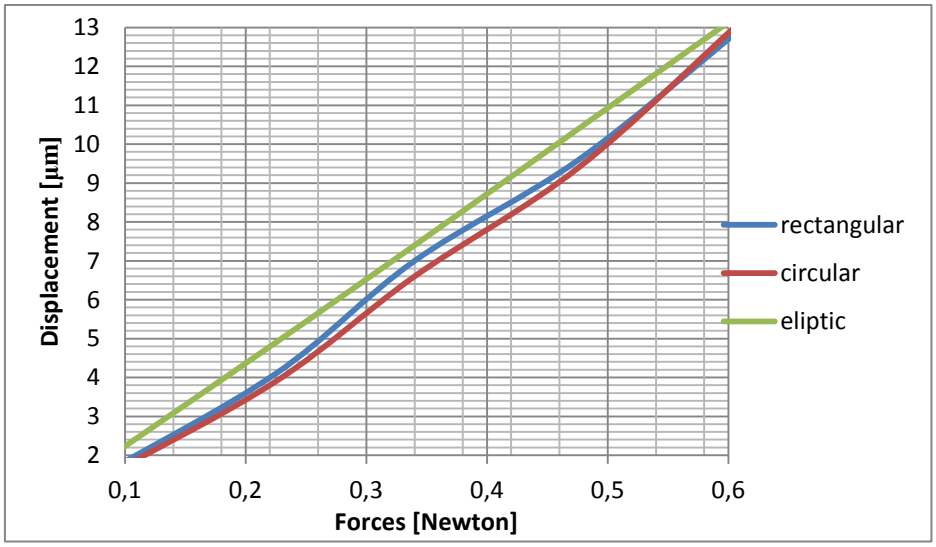

Figure 8. The comparative analysis between the rectangular, circular and elliptical joints

CONCLUSIONS AND FUTURE DIRECTIONS

The compliant mechanisms can solve the same problem as the jointed classic mechanisms, respectively: the taking of an element in a series of positions, the generation of a trajectory and the generation of a mathematical function.
The displacements allowed by these mechanisms are more restrictive and depend very much upon the constructive solution of the mechanism.
After the analysis of the three mechanisms studied in the work, it comes out the fact that the studied

mechanism using compliant joints with elliptical profile have a very good traceability imposing a constant in the requested movements.
In the future it is desired the realisation of an experimental stand for the analysis of these three compliant mechanisms with different joints.
A different step desired is the one of acting and control of these mechanisms for bringing an element in a series of positions, to generate a trajectory and to generate a mathematical function.

REFERENCES

[1] Hjalmar Ö., *Performance evaluation of a simplified FEM-tool for designers,* Master's Degree Thesis, ISRN: BTH-AMT-EX--2008/CI-04—SE, 2008.
[2] Lateș, D., Noveanu, S., Zah, M., *Analytical study on compliant joints with asymmetrical profiles*, 21th International Conference on Mechanical Engineering (OGET), ISSN 2068-1267, Arad 2013.
[3] Lates, D., *Cercetări teoretice și aplicative privind mecanismele compliante folosite în mecatronică, Teza de doctorat,* Cluj-Napoca, 2014.
[4] Lobonţiu, N., *Compliant mechanisms: design of flexure hinges* , CRC Press LLC: New York, 2002.
[5] Lobontiu, N., Ephrahim, G.,*Mechanics of Microelectromechanical Systems*, Kluwer Academic Publishers New York, Boston, Dordrecht, London, Moscow, 2005.
[6] Jairo, A., M.,István, K., *Overview in the Application of FEM in Mining and the Study of Case: Stress Analysis in Pulleys of Stacker-Reclaimers: FEM vs. Analytical*, Chapter 13, Finite Element Analysis – Applications in Mechanical Engineering, 2012.
[7] Nikolova,N.,S., Vasilev, V.,V., *Finite element analysis of the stress and strain distribution in a milling woodworking machine spindle*, Tome XII – Fascicule, ISSN: 1584-2673, 2014.
[8] Noveanu, S. *Contribuți iprivind studiul mecanismelor compliante specifice sistemelor mecatronice*, Teza de doctorat, 2009.
[9] http://ketiv.com/pdf/AMA2008/Understanding%20and%20Applying%20FEA.pdf
[10] http://www.autodesk.de/products/inventor/features/all/gallery-view
[11] http://www.autodesk.com/solutions/finite-element-analysis

CREATING HELICOID SURFACES IN INTELLIGENT FLEXIBLE MANUFACTURING SYSTEM-THE PROBLEM OF DRIVING

MÁNDY Zoltán

Faculty of Healthcare, University of Miskolc
E-mail: zoltan.mandy@uni-miskolc.hu

Abstract
During the classical manufacturing process of conical thread surfaces with lathe center displacement, the worm shaft is driven with the help of the driving pin through the lathe fork. As a result of the shifting of the worm shaft by half cone angle, the path curve of the driving pin will be an ellipse path instead of a circle on the perpendicular plane to axis. The peripheral speed of the spindle is constant, but due to the ellipse path, the radius is constantly changing as a function of time. That is why the angular velocity and the angular rotation are also changing, and these cause pitch fluctuation during the manufacturing process of conical worms. During the manufacturing process, we have examined pitch errors which are caused by angular velocity fluctuation and we have also determined the geometrical shaping of the driving pin by which errors of the pitch can be eliminated.

Keywords: *worm, pin, ellipse, process*

1. INTRODUCTION

The worm shaft is driven with the help of the driving pin through the lathe fork because of lathe center displacement [3][4]. As a result of the shifting of the worm shaft by half cone angle, the path curve of the driving pin will be an ellipse path instead of a circle on the perpendicular plane to axis [1]. The peripheral speed of the spindle is constant, but due to the ellipse path, the radius is constantly changing as a function of time. That is why the angular velocity and the angular rotation are also changing, and these cause pitch fluctuation during the manufacturing process of conical worms. Our objective was to determine the geometrical shaping of the driving pin in order not to have pitch fluctuation.

2. THE PATH OF THE CONTACT POINT OF THE LATHE DOG AND THE DRIVING PIN

During our examination, we started from the modeling of the driving of cylindrical driving pin . We supposed that there is a punctual connection between the driving pin and the lathe fork. That is how we could determine the path of the contact point between the lathe fork and the driving pin during one turning. Figure 1. shows that in the beginning of turning, on the axial intercept plane of the spindle the contact point between the driving pin [I.] and the lathe fork [III.] is point A′. The lathe fork [III.] is situated perpendicular to the worm axis [IV.], namely it encloses half cone angle δ1 with the head surface of the spindle [II.]. After turning the spindle with angle φp, the contact point is taken from point A′ to point P′ and during this movement it completes path sp. After turning of φp=180°, the contact point is taken from point A′ to point B′ and during this movement it completes the longest path Δs. It can be seen if the angular rotation φ is ranging between 0° and 180° then the path of the contact point is

increasing; in case of 180° the longest path Δs is completed; between 180° and 360° the path is decreasing and in case of 360° the contact point is taken back again to the initial distance x, i.e., the starting position (point A) [1].In Figure 1. you can observe the layout of driving.

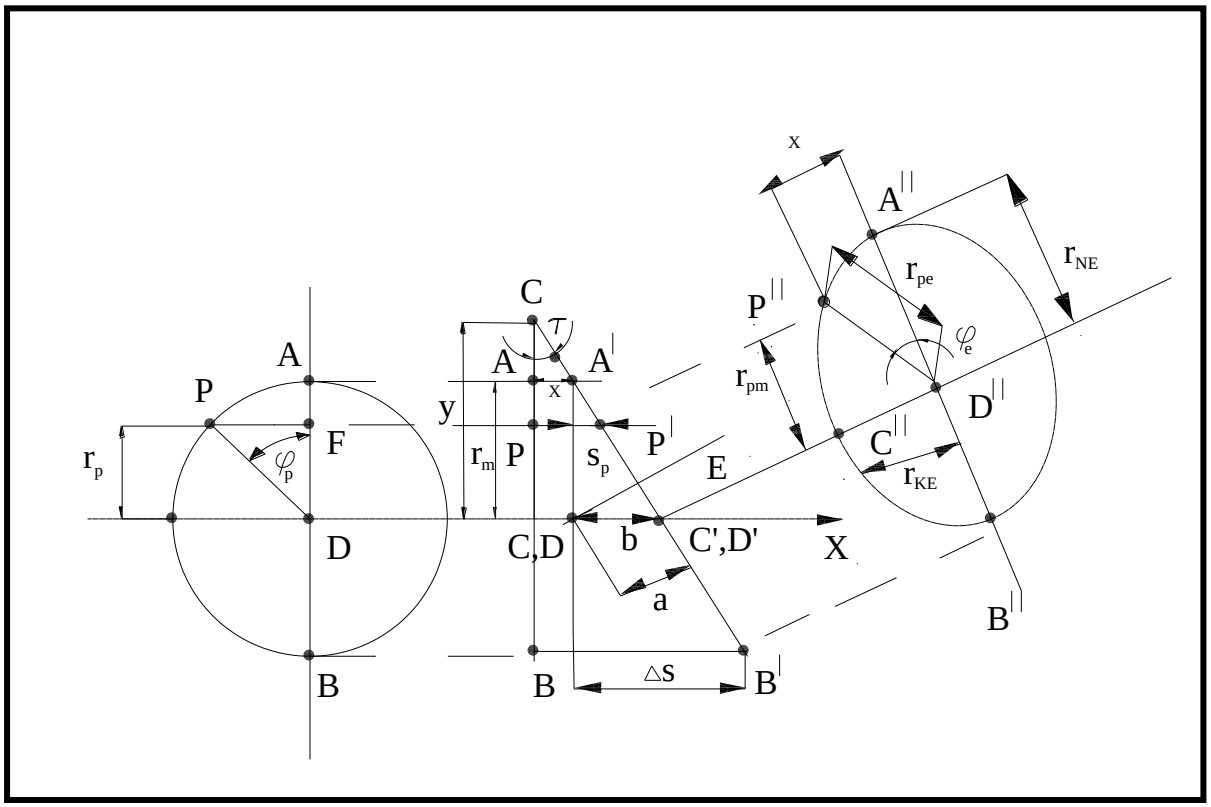

Figure 1 Analysis of Driving [1]

The following expressions are based to the next equations and the CDE rectangular triangle :

$$y = \frac{a}{\sin \tau} \tag{1}$$

Based on the CAA' rectangular triangle :

$$x = (y - r_m)tg\,\tau \tag{2}$$

Substituting (1) to (2)

$$x = (\frac{a}{\sin \tau} - r_m)tg\,\tau \tag{3}$$

$$\begin{aligned} x + \Delta S &= (y + r_m)tg\,\tau \\ \Delta S &= (y + r_m)tg\,\tau - x \end{aligned} \tag{4}$$

The situation of the contact point on an arbitrary angle position: φ_p

We have developed a universal correlation based on which the situation of a contact point for an arbitrary angle position φ_p could be defined.Based ont he PFD triangle:

$$r_p = r_m \cos\varphi_p \tag{5}$$

Based on the CPP' triangle:

$$S_p = (y - r_p)tg\,\tau - x \tag{6}$$

Substituting (6) to (7) situation of the contact point in case of an arbitrary angle position: φ_p

$$S_p = [y - r_m \cos\varphi_p]tg\,\tau - x \tag{7}$$

3. CALCULATION OF AN ELLIPTICAL RADIUS ON AN ARBITRARY POINT P

Because of stopping of worm shaft with half cone anglle the path curve of the driving pin will be an ellipptical path instead of circle in perpendicular plane for an axis. Since the half cone angle of conical worm is between 5 °-10° that's why the perpenicular for worm axis section major axis of elliptical is only small degree larger than the path circle radius of the spindle. The minor axis of the elliptical way is equal with the path circle radius of the spindle [1].

The major axis radius of ellipse is

$$r_{ne} = \frac{r_m}{\cos\tau} \tag{8}$$

The minor axis radius of ellipse is :

$$r_{ke} = r_m \tag{9}$$

So the equation of the ellipse is the following:

$$\frac{y^2}{r_{ne}^2} + \frac{x^2}{r_{ke}^2} = 1 \tag{10}$$

The radius r_{pm} is:

$$r_{pm} = \frac{r_p}{\cos\tau} \tag{11}$$

Solving the last 2 equations together the distance x_{ep} is:

$$x_{ep} = \sqrt{(1 - \frac{r_{pm}^2}{r_{ne}^2}) r_{ke}} \quad (12)$$

Based on the P"F"D" rectangular triangle the r_{pe} ellipse radius is:

$$r_{pe} = \sqrt{x_{ep}^2 + r_{pm}^2} \quad (13)$$

4. THE GEOMETRICAL ESTABLISHMENT OF THE DRIVING PIN FOR CONSTANT LEAD OF THREAD ASSURANCE

The number of revolutions is given (n_g) during the manufacturing process of conical worm. Based on the spindle angular velocity is:

$$\omega_g = 2\pi \cdot n_g \quad (14)$$

The spindle circumferential velocity along the r_m radial pitch is constant , namely :

$$v_m = \omega_g \cdot r_m \quad (15)$$

Due to the worm shaft stopping with half cone angle along the perpendicular for worm axis ellipse path curve the angular velocity is changed by constant spindle circumferential velocity:

$$\omega_p = \frac{v_m}{r_{pe}} = changeable \quad (16)$$

5. ABOUT THE COMPUTER PROGRAM

As the program knows the following pieces of information: the geometrical data of the worm, the driving pin diameter, the distance between the lathe fork and the worm shaft neck, the worm half cone angle, and the distance between the center line of the driving pin and the rotational axis of spindle.
Then it calculates and represents the angular velocity fluctuation ω_p as a function of spindle angular rotation φ_p.

CONCLUSIONS

Besides the manufacturing process, we have examined pitch errors which are caused by angular velocity fluctuation and we have also determined the geometrical shaping of the driving pin by which errors of the pitch can be eliminated.Then we designed a computer programme, because we want to represents the angular velocity fluctuation ω_p as a function of spindle angular rotation φ_p.

REFERENCES

[1] Dudás, I., Bodzás, S., Mándy, Z.: *Solving the pitch fluctuation problem during the manufacturing process of conical thread surfaces with lathe center displacement*, International Journal of Advanced Manufacturing Technology 69**:**(5-8) pp. 1025-1031. (2013)

[2] Dudás I, Bodzás S, Dudás I. Sz, Mándy Z.: *Konkáv menetprofilú spiroid csigahajtópár és eljárás annak köszörüléssel történő előállítására*, Szabadalmi iktatószám: P1200405, Szabadalmi bejelentés napja: 07.04., 2012

[3] Dudás I.: *Designing of worm gear drives in manufacturing system*. J Prod Process Syst 6(1):9–12, Miskolc University Press, 2012, HU ISSN 1215–0851

[4] Dudás I.: *The theory and practice of worm gear drives.* Penton Press, London, 2012, ISBN 1 8571 8027 5

[5] Hegyháti J.: *Untersuchugen zur Anwendung von Spiroidgetrieben*. Diss. A. TU. Dresden, 1988

[6] Dudás I., Bodzás S.: *Production geometry analysis, modeling and rapid prototyping production of manufacturing tool of spiroid face gear*. Adv Manuf Tech 66(1–4):271–281. DOI: 10.1007/s00170-012- 4323-9, Springer, ISSN 1433–3015 (Online), 2012.07.19. (Online), ISSN 0268–3768 (Print), (IF 1.103), 2013

[7] Dudás I., Bodzás S.: *Measuring technique and mathematical analysis of conical worms*. Adv Manuf Tech. DOI: 10.1007/s00170- 012-4483-7, Springer, ISSN 0268–3768, 2012.09.14., (IF 1.103), 2012

[8] Dudley D. W.: *Gear handbook. the design, manufacture, and application of gears.* McGraw-Hill, New York, 1962, ISBN 1 8571 8027 5

[9] Nelson W. D.: *Spiroid gearing*. Mach Des 33(4):136–144, (5):93–100, (6):165–171, 1961

[10] Litvin F. L., Fuentes A.: *Gear geometry and applied theory*. Cambridge University Press, Cambridge, 2004, ISBN 978 0 521 81517 8

INTERNATIONAL SCIENTIFIC CONFERENCE ON ADVANCES IN MECHANICAL ENGINEERING

19 November 2015, Debrecen, Hungary

SHAPE DESIGN OF AXIALLY SYMMETRIC RUBBER PART USING FINITE ELEMENT METHOD AND SUPPORT VECTOR MACHINES

[1]MANKOVITS Tamás PhD, [2]VÁMOSI Attila, [3]KOCSIS Imre PhD, [4]HURI Dávid, [5]KÁLLAI Imre, [6]SZABÓ Tamás PhD

[1,4]Department of Mechanical Engineering, Faculty of Engineering, University of Debrecen
E-mail: tamas.mankovits@eng.unideb.hu, huri.david@eng.unideb.hu
[2,3]Department of Basic Technical Studies, Faculty of Engineering, University of Debrecen
E-mail: vamosi.attila@eng.unideb.hu, kocsisi@eng.unideb.hu
[5]Institute of Polymer Product Engineering, Johannes Kepler University Linz
E-mail: imre.kallai@jku.at
[6]Institute of Machine Tools and Mechatronics, University of Miskolc
E-mail: szabo.tamas@uni-miskolc.hu

Abstract
Non-linear FEM calculations are indispensable when important technical information like operating performance of a rubber component is desired. Rubber parts may undergo large deformations under load, which in itself shows non-linear behaviour. The material characterization of an elastomeric component is also a demanding engineering task. The shape optimization problem of rubber parts led to the study of FEM based calculation processes. In this paper a novel solution for the shape optimization of compressed rubber parts is presented. A special purpose FEM code written in Fortran has been developed for the analysis of nearly incompressible axially symmetric rubber parts. A rubber shape is evaluated via the work difference and the area between the desired and the actual load-displacement curves. The objective of shape optimization is to find the geometry where the work difference is under a specified limit. The tool of optimization is the SVR method, which provides the regression function for the work difference. The minimization process of the work difference function leads to the optimum design parameters. The efficiency of the method is verified by a numerical example.

Keywords: *rubber, finite element method, support vector regression, shape optimization*

1. INTRODUCTION

Engineering rubber parts have to meet several kinds of requirements as a result of their function. One of these is that they must have a predefined load-displacement curve under load while the material characteristics remain the same. Achieving this aim is a problem of optimization.
The load-displacement curves of the investigated rubber parts of different shapes were determined with the help of a special purpose FEM code. Number of papers is devoted to the application of *h*-version FEM for the analysis of hyperelastic materials [1-6]. The *p*-version of finite elements is proved to be very efficient tool to analyze linear elastic problems [7], its application geometrically and physically nonlinear problems are relatively recent [8-10].
More and more papers are devoted to find the answer how to obtain robust and non-locking finite elements and the majority prefers the mixed formulation [3] and [11].
A finite element code is developed for the investigation of rubber parts, assuming a material that is nearly incompressible also in case of large deformation. The mixed method is based on a three-field functional where the displacement field is continuously approximated, and the change in volume

and the hydrostatic pressure are approximated discontinuously, independently of each other. The same order of approximation is selected for the hydrostatic pressure and the volumetric change. The displacement fields are approximated using the quadratic tensor product space. The program is suitable for the quasi-static calculation of axially symmetric rubber components.
The literature does not devote much room to the shape optimization of the rubber parts. The stiffness of rubber mounts in three directions on the basis of parameter examinations is optimized in [12]. Optimization based on sensitivity analysis using a special purpose finite element code is performed in [13] for material properties and shape, where stiffness was also taken into consideration. Determining the shape had the aim of minimizing the volume of the rubber part. For the purpose of minimizing the cross-sectional area and the maximum stress of the rubber mount and for that of maximizing the life cycle, shape optimization using an Ogden-type material model and commercial finite element software is applied in [14]. Several objective functions in a system where the optimization had several stages are handled. A back-propagation neural network (BPN) is used to find the connection between the input and output data and then a micro-genetic algorithm (MGA) is used for global optimization. A large number of finite element running results are used as learning points. The differential evolution (DE) algorithm produced excellent results for different applications in engineering. The optimization process is performed by Fortran routines coupled with finite element analysis code Abaqus in [15]. A formulation of the non-parametric shape optimization problem of a rubber bushing in order to fit the static load-displacement curve with the desired one was presented in [16].
The support vector regression (SVR) proposed by [17] is a widely used application of support vector machines (SVM) for regression problems, e.g. in optimization models. A great number of applications can be found in the fields of materials science, chemistry, economics and data procession, where connections are sought between a numbers of input data (e.g. some mechanical or chemical property). Although there are results in the field of engineering problems based on SVR models [18], this method is not yet particularly widespread for engineering optimization. The application of SVR in non-linear models has the advantage that the transformation function between input space and the so-called feature space (where a linear regression problem is to be solved) can be hidden [19], and machine learning procedures can be applied to find an appropriate regression function.

2. METHODS

The procedure is based on the finite element method and the support vector regression (SVR) model. A finite element code developed by the authors and based on a three-field functional is used for the rapid and appropriately accurate calculation of the characteristics of rubber parts. The geometry and the load-displacement curve of the investigated rubber part calculated by the FEM code can be seen in *Figure 1* and *Table 1*. A rubber shape is evaluated by the work difference and the area between the desired and the actual load-displacement curves.

Table 1 Data for the investigated rubber part

Geometry		**Numerical material properties**	
Height (H)	120mm	Material constant (μ_{10})	0.8MPa
Outer diameter (D)	120mm	Material constant (μ_{01})	0.2MPa
Hole diameter (d)	20mm	Bulk modulus (κ)	1000MPa
Distance (c_d)	-5mm		
Distance (c_u)	5mm		

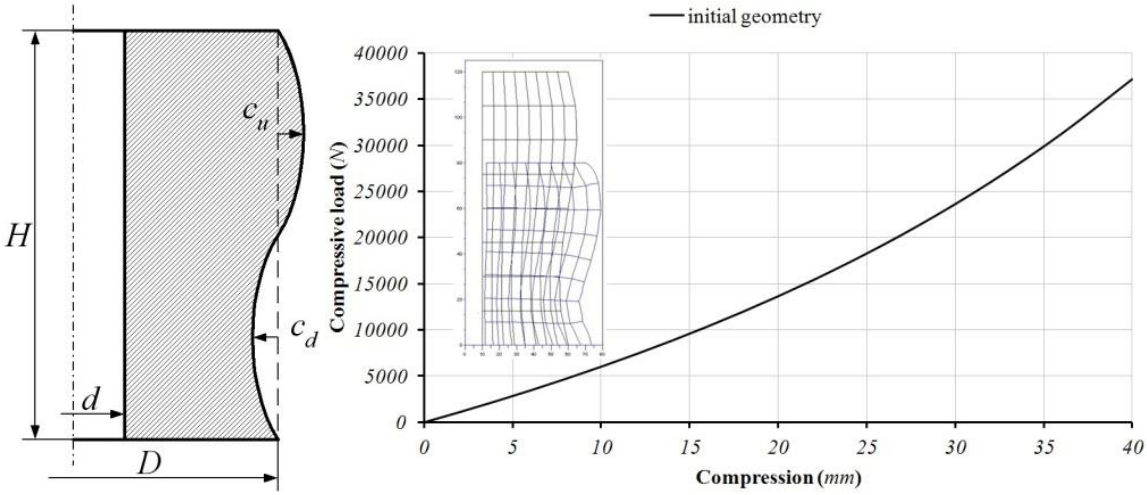

Figure 1 The geometry and the load-displacement curve of the rubber part

The objective of shape optimization was to find the geometry where the work difference is under a specified limit. The tool of optimization was the SVR method, which provides the regression function for the work difference. The minimization process of the work difference function leads to the optimum design parameters. The work difference is the area (filled with grey) between the desired load-displacement curve and the curve obtained by finite element computation for a specific rubber shape, see in *Figure 2*.

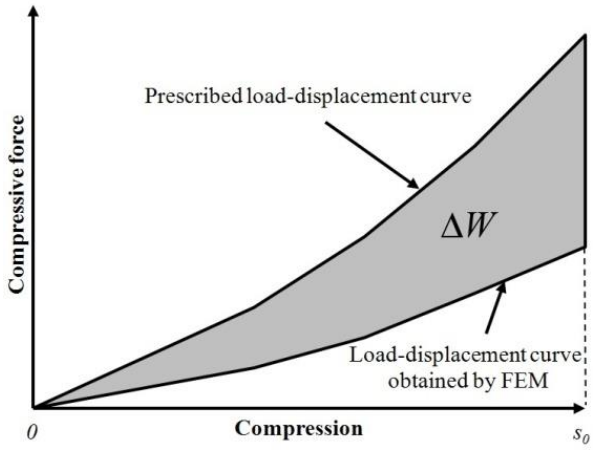

Figure 2 The derivation of the work difference

The aim is to minimize function ΔW for determining the optimum design parameter vector $\boldsymbol{d}^{opt}$, that is,

$$\Delta W(\boldsymbol{d}^{opt}) = \min_{\boldsymbol{d}\in\Omega} \Delta W(\boldsymbol{d}). \tag{1}$$

where Ω is the optimization range given by inequality conditions coming from technology limitations, $\boldsymbol{d}$ is the design parameter vector and $\boldsymbol{d}^{opt}$ is the optimum design parameter vector. The SVR model related to the theory of learning machines and kernel methods plays central role in the investigations. The SVR model is used to find the regression function, the calculations are carried out with the program package of *R* open source code programming environment using SVR. Values of the regression function provided by the software are available for arbitrary design parameter vectors in Ω. The place of the minimum of function ΔW, that is the value of the optimum design parameter vector, can be determined numerically.

3. RESULTS

The initial load-displacement curve obtained by the FEM and the prescribed load-displacement curve can be seen in *Figure 3*, which has to be reached with the change of three geometry parameters of the rubber part, see in *Figure 1*.

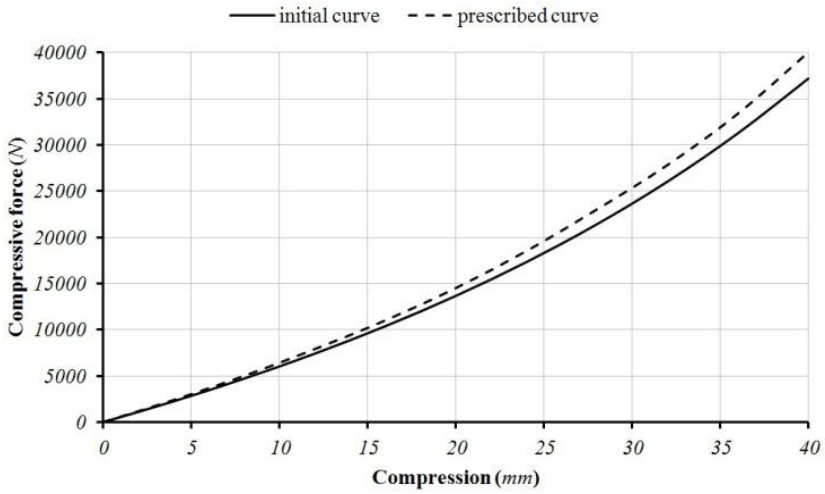

Figure 3 The optimization task

The outer skirt of the rubber part investigated is described by means of cubic spline in five control points. For design parameters the $d_1 = d$ hole diameter, the $d_2 = c_d$ and $d_3 = c_u$ control point positions are chosen. In the investigation the design parameters in *mm* are defined according to the following conditions:

$$\boldsymbol{d} = (d_1, d_2, d_3) \qquad \text{where} \begin{cases} d_1 \in [16{,}24] \\ d_2 \in \{-5, -4, \dots, 5\} \\ d_3 \in \{-5, -4, \dots, 5\} \end{cases} \quad \text{and } d_1 \text{ is even number.} \qquad (2)$$

Under the specified accuracy, the number of possible solutions is $P = 605$. The number of learning points is $N = 27$.

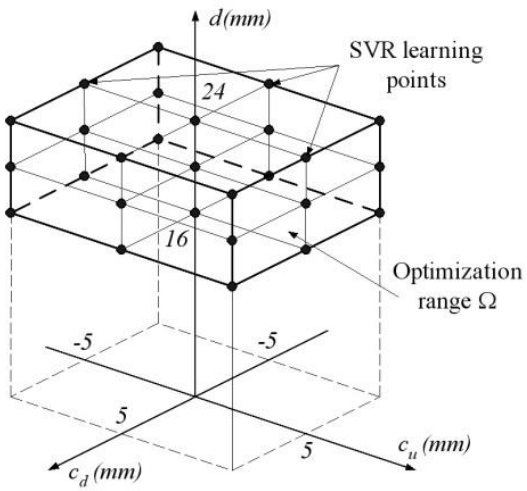

Figure 4 The optimization range and learning points

In determining the learning points the objective was that they should properly cover the optimization range. The optimization range and the learning points can be seen in *Figure 4*. The optimum values of hyperparameters in the SVR program are determined numerically.
On the basis of the calculation, the minimum work difference out of the possible solutions is $\Delta W_{SVR}(\boldsymbol{d}^{opt}) = 0.2735Nm$, for which the optimum design parameters are $d^{opt} = 16mm$, $c_d^{opt} = 3mm$ and $c_u^{opt} = 2mm$. The curve obtained for the control FEM calculation run for the optimum design variables and the prescribed load-displacement curve and the optimal geometry are shown in *Figure 5*.

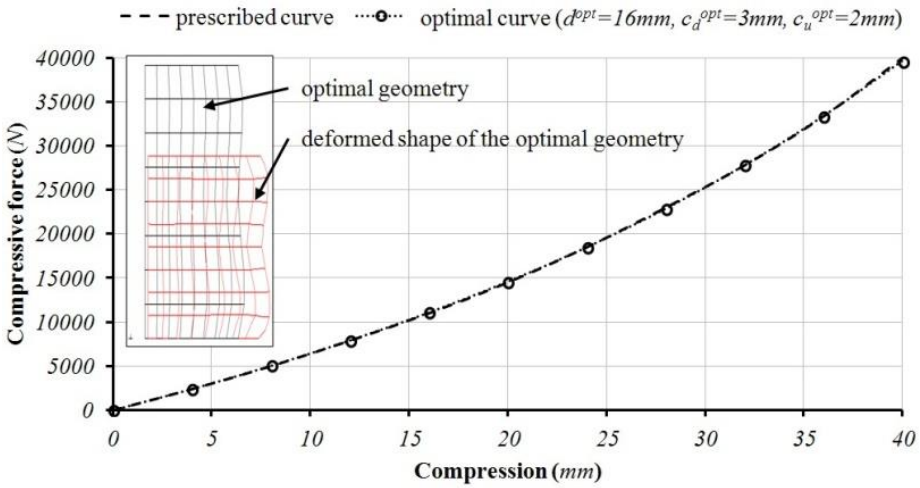

Figure 5 The optimal rubber geometry and the optimal load-displacement curve

CONCLUSIONS

A three dimensional shape design of a rubber part is presented. The characteristics of the investigated rubber part were determined with the help of the finite element method using special purpose FEM code. In the investigations, the SVR was used by means of open-source software to perform the optimization task. Combining the above two methods into one system, a shape optimization problem was solved to prove the efficiency of the presented procedure for axially symmetric rubber parts.

ACKNOWLEDGEMENT

The described work was carried out as part of a project supported by the National Research, Development and Innovation Office – NKFIH, K115701.

REFERENCES

[1] Malkus, D.S.: *Finite Element with Penalties in Nonlinear Elasticity*. International Journal for Numerical Methods in Engineering, 16, 121-136., 1980.
[2] Swanson, S., Christensen, L., Ensing, M.: *Large Deformation Finite Element Calculations for Slightly Compressible Hyperelastic Materials*. Computers & Structures, 21(1-2), 81-88., 1985.
[3] Zienkiewicz, O.C, Qu, S., Taylor, R.L., Nakazawa, S.: *The Patch Test for Mixed Formulations*. International Journal for Numerical Methods in Engineering, 23, 1873-1883., 1986.

[4] Sussman, T., Bathe, K.J.: *A Finite Element Formulation for Nonlinear Incompressible Elastic and Inelastic Analysis*. Computers & Structures, 26(1-2), 357-409., 1987.
[5] Simo, J.C., Taylor, R.L.: *Quasi-incompressible Finite Elasticity in Principal Stretches*. Computational Methods in Applied Mechanics and Engineering, 85, 273-310., 1991.
[6] Gadala, M.S.: *Alternative Methods for the Solution of Hyperelastic Problems with Incompressibility*. Computers & Structures, 42(1), 1-10., 1992.
[7] Szabó, B.A., Babuska, I., Chayapathy, B.K.: *Stress Computation for Nearly Incompressible Materials by the p-version of the Finite Element Method*. International Journal for Numerical Methods in Engineering, 28, 2175-2190., 1989.
[8] Düster, A.: *High Order Finite Elements for Three-dimensional, Thin-walled Nonlinear Continua*. Shaker Verlag GmbH., 2002.
[9] Hartmann, S., Neff, P.: *Polyconvexity of Generalized Polynomial-type Hyperelastic Strain Energy Functions for Near-incompressibility*. International Journal of Solids and Structures, 40(11), 2767-2791., 2003.
[10] Mankovits, T., Szabó, T.: *Finite Element Analysis of Rubber Bumper Used in Air-springs*. Procedia Engineering, 48, 388-395., 2012.
[11] Bonet, J., Wood, R.D.: *Nonlinear Continuum Mechanics for Finite Element Analysis*. Cambridge University Press, 1997.
[12] Kim, J.J., Kim, H.Y., *Shape design of an engine mount by a method of parameter optimization*. Computers & Structures, 65(5), 725-731, 1997.
[13] Choi, K.K., Duan, W.: *Design sensitivity analysis and shape optimization of structural components with hyperelastic material*. Computer Methods in Applied Mechanics and Engineering, 187, 219-243, 2000.
[14] Lee, J.S., S.C. Kim, S.C.: *Optimal design of engine mount rubber considering stiffness and fatigue strength*. Journal of Automobile Engineering, 221(7), 823-835, 2007.
[15] Vu, V.T.: *Minimum weight design for toroidal pressure vessels using differential evolution and particle swarm optimization*. Structural and Multidisciplinary Optimization, 42(3), 351-359, 2010.
[16] Kaya, N.: *Shape optimization of rubber bushing using differential evolution algorithm*. The Scientific World Journal, ID 379196, 1-9., 2014.
[17] Drucker, H., Bruges, C.J.C., Kaufman, L., Smola, A.J., Vapnik, V.: *Support vector regression machines*. Advances in Neural Information Processing System, 9, 155-161., 1997.
[18] Andrés, E., Salcedo-Sanz, S., Monge, F., Pérez-Bellido, A.M. (2012). *Aerodynamic design through evolutionary programming and support vector regression algorithm*. Expert Systems with Applications, (39)12, 10700-10708., 2012.
[19] Haykin, S.: *Neural networks and learning machines*. Pearson Prentice Hall, Upper Saddle River, 2009.

INTERNATIONAL SCIENTIFIC CONFERENCE ON ADVANCES IN MECHANICAL ENGINEERING
19 November 2015, Debrecen, Hungary

FINITE ELEMENT ANALYSIS OF PRESSURE VESSELS

[1]MARINKÓ Ádám, [2]NAGY András, PhD, [3]DUDINSZKY Balázs

[1]Faculty of Mechanical Engineering, Budapest University of Technology and Economics
E-mail: marinko.adam@gmail.com
[2,3]Department of Building Service Engineering and Process Engineering, Budapest University of Technology and Economics
E-mail: nagy.andras@mail.bme.hu, dudinszky@mail.bme.hu

Abstract
The study is about an internal gas pressure loaded, a conical bottom and a torispherical head bounded pressure vessel strength analysis. First, based on the initial geometrical data, structural material (carbon steel) and loads, in accordance with the Ad Merkblatt standard, the required wall-thickness was calculated for each part of the vessel.
During further analysis the vessel actual wall thickness defined in regard to the previous calculation.
For the finite element analysis we used Ansys, first a two-dimensional reference model was created, then two three-dimensional models were developed. The finite element calculations were defined in the structural materials elastic deformation range.
The study investigate the differences in the results of the stress concentration points in these two kinds of model, then outlines the possible direction to refine the model, which is discussed in a subsequent paper.

Keywords: *finite element analysis, FEA, FEM, pressure vessel.*

1. INTRODUCTION

For a long time engineering solved the mathematical problems analytically.
Buildings, equipment and machines strength and stability calculations used simplified models, or simply used the standards.
In the second half of the 20th century the appearance of computer technology, and later its spread made possible that the numerical models could challenge the analytical methods, due to the calculation has become faster, easily programmed, and previously non-calculable problems has become solvable.
An example of this in mechanical engineering science is the finite element method applied in strength calculations.
In today's engineering practice, although not essential, but great competitive advantage to use finite element method in design and devices strength test.
It should be noted that knowing how to use the program does not release the engineer from understand the scientific knowledge, relations, which the program is based on, because estimate the real values badly leads to accept an erroneous solution.
The application of the finite element method has been released in the modelling of pressure vessels. The stressed state of these equipment become more accurately known, thus we could optimize the wall thickness and geometry of the structure, and could reduce the investment cost.

2. METHODS

The equipment used for the storage of inert gases, operates at room temperature, and modelled as an elastic strain body, the remaining plastic deformation is not counted. The raw material is P235 GH labelled carbon steel, for its physical properties and operational conditions see *Table 1*. The equipment include a 1000 mm diameter cylindrical mantle, bounded by a conical bottom and a torispherical head (*Figure 1*). On the torispherical head a DN200 diameter nozzle is located.

Table 1 Design parameters

Quantity	Description	Value	Unit
σ_{eH}	Yield strength	180	MPa
σ_M	Tensile strength	360	MPa
p_{des}	Design pressure	5	bar
$\sigma_{max\ des}$	Allowable stress at design pressure	120	MPa
p_{test}	Test pressure	8,53	bar
$\sigma_{max\ test}$	Allowable stress at test pressure	163	MPa
E	Young modulus	212	GPa
ν	Poisson ratio	0,3	1

Before the finite element simulations, based on the scientific literature the specified geometry was analysed, and modified the non-standard dimensions, then strength calculations were carried out according to AD Merkblatt standards. Based on that, the required thickness of the vessel is 6 mm.
The calculations from the standard does not give information about the stress distribution, for more accurate understanding of the equipment's behaviour the finite element method provides the most cost-effective solution.
FEA simulations were carried out using Ansys software at the vessel's operating conditions in each modelling and meshing methods.
First, a two-dimensional, rotationally symmetric model has served as a reference for the future (*Figure 2*, left side). For this model Plane 182 element (4-node Axissymmetric element) was used. The element size was 1 mm, so 6 element were located along the wall thickness.
Then a three-dimensional modelling is followed (*Figure 2*, right side). The body geometry is generated by a 90° rotation around the axis, so the simulation was run down on a quarter segment. For the meshing Solid 185 element (8-node rectangular element, nodes located at the peaks) was used. The element size was 2 mm, 3 element along the wall thickness, so the meshing was rarer in a cross-section than the two-dimensional, but because the rotation there were more nodes, and too high element number was not permitted due to computing capacity.
During the simulations, on the cylindrical part pure membrane stress state was formed, so it gave the opportunity to cut the vessel in two parts, then replace foregone participate with the membrane stress. So in the third approach in the modelling and simulation was that the conical bottom and a torispherical head managed separately (*Figure 3*), with the same meshing as in the three-dimensional, full-body model.

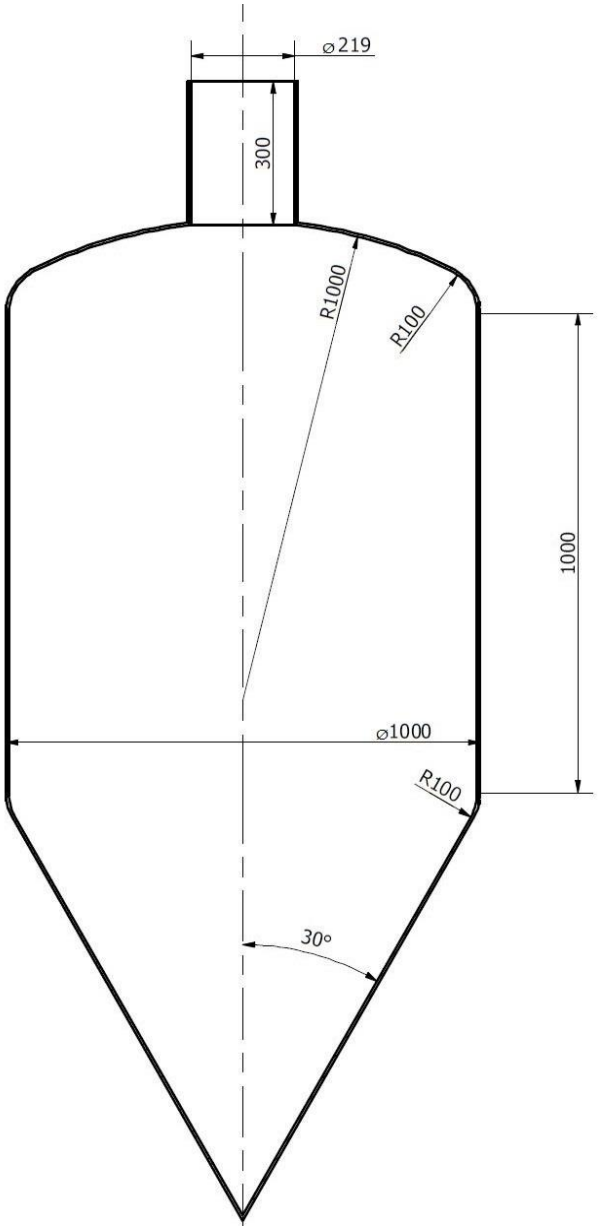

Figure 1 Dimensions of the vessel

3. RESULTS

The simulations were run under operating conditions, the deformed shape and stress distribution were formed. The program calculated the Mohr-Coulomb principle stress in the nodes, and these were plotted along the centre line of the wall (*Figure 4*, *Figure 5*).
There is 15-20% difference between the highest principles stress values of the models.
The highest principle stress were at the nozzle connection, and there is another focus of stress concentration at the smaller radius sphere. But further investigations shown, that the inner curve on the torispherical head the principle stress approach Yield strength (*Figure 6*).

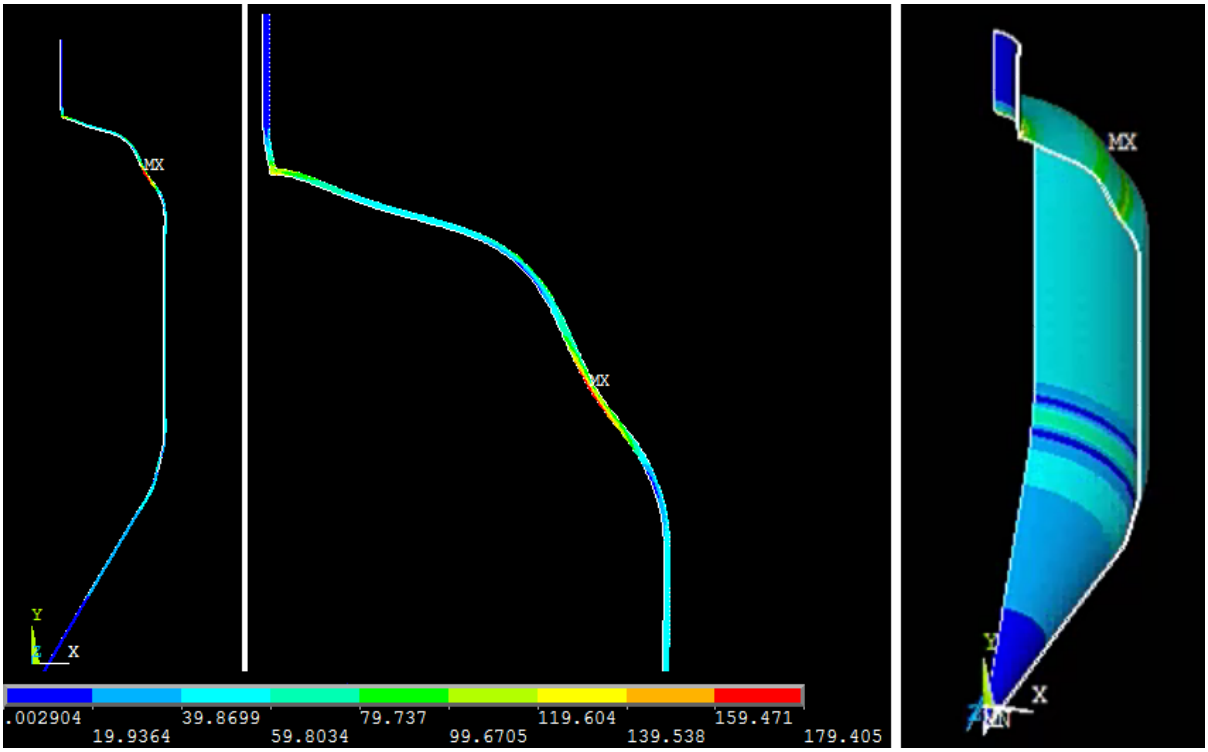

Figure 2 Stress distribution on deformed shape

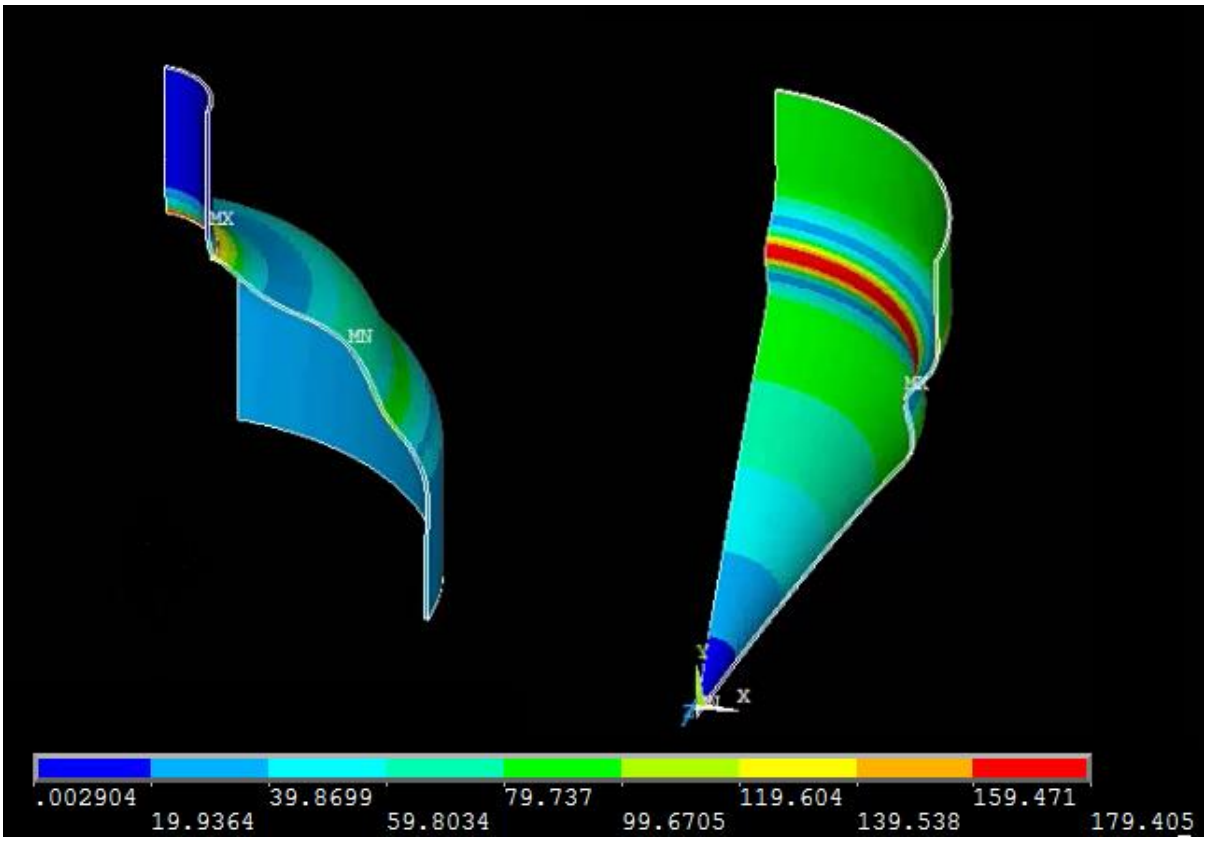

Figure 3 Stress distribution on deformed shape

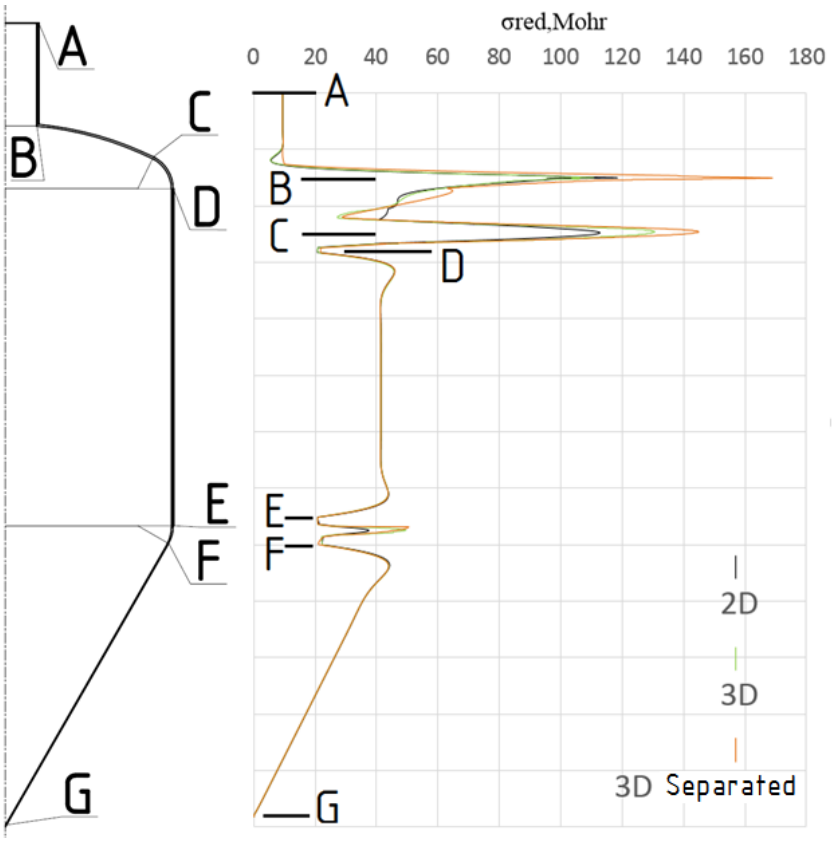

Figure 4 Stress distribution along the centreline of the wall

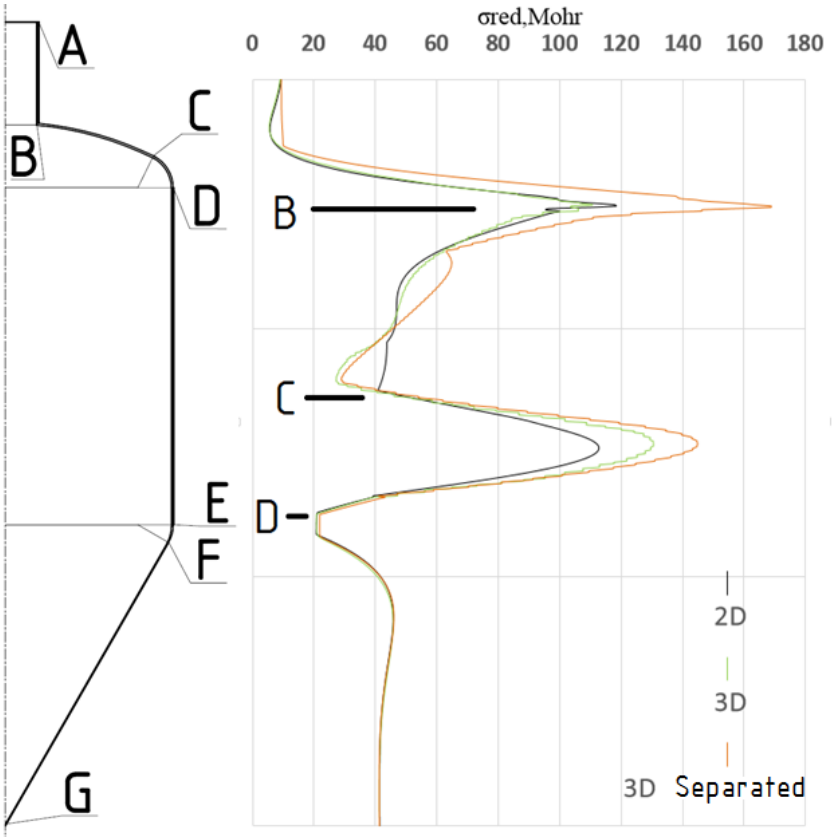

Figure 5 Stress distribution along the centreline of the wall. Torispherical head enlarged.

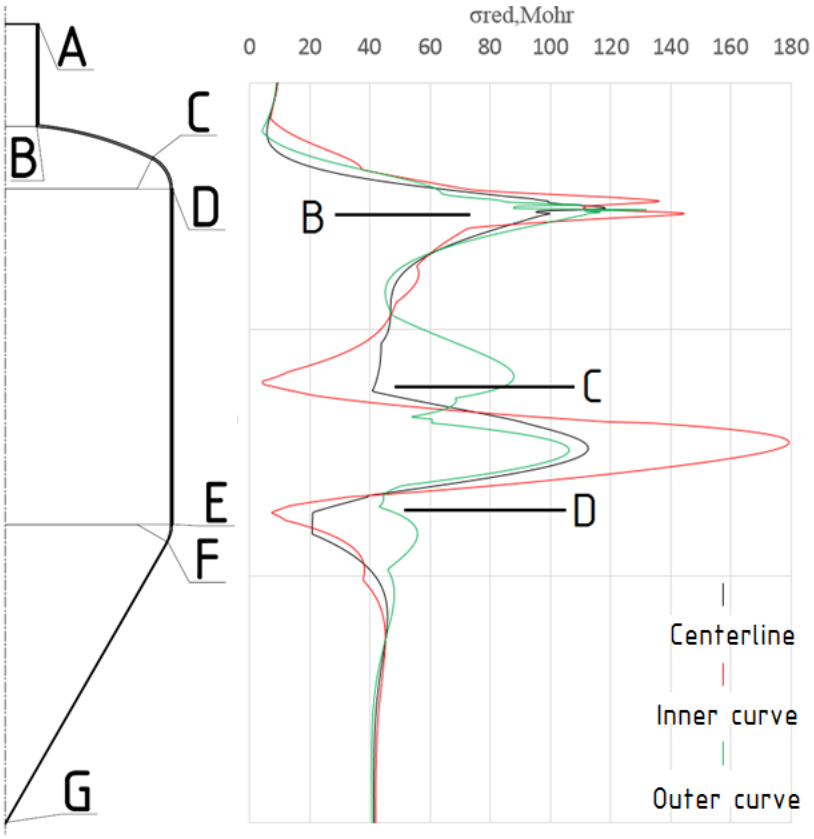

Figure 6 Stress distribution along the centreline, inner and outer curve of the wall. Torispherical head enlarged

CONCLUSIONS

The standardized wall thickness calculations does not give us information about the real stress distribution of the vessel, so we created a utilizable one we could use in following studies. The stress distribution had quantitative mismatch in the different FEA methods. The most accurate was the two-dimensional, densely meshed reference model. The difference between the calculated stress data at the 2D and 3D methods is 15-20%, but mention must be made the deformed shape and the stress distribution had the same character in all cases. The reason of the difference is in the different element size, therefor in the different mesh size.
The value of the yield strength never exceeded each of the simulations, while at the torispherical head the value of the allowable stress at operating pressure in all cases exceeded.
In further research the material model will be turned into elastic-plastic model. Furthermore a weld neck flange will be added to the cylindrical mantle, after the inner forces calculation of the flange a finite element simulation will be created.

REFERENCES

[1] Pálfi Z.: *Vegyipari készülékek szerkesztése atlasz*, Műszaki Könyvkiadó, Budapest, 1973
[2] *AD Merkblatt B0 – B3*: 1995
[3] Varga L.: *Nyomástartó edények tervezése*, Tankönyvkiadó, Budapest, 1984

INTERNATIONAL SCIENTIFIC CONFERENCE ON ADVANCES IN MECHANICAL ENGINEERING
10 October 2014, Debrecen, Hungary

LASER SURFACE REMELTING TO IMPROVE THE WEAR RESISTANCE OF THERMAL SPRAYED NICRBSI COATINGS

[1]MOLNÁR András, [2] FAZEKAS Lajos PhD, [3]CSABAI Zsolt PhD, [4]RÁTHY Istvánné PhD

[1]Institute of Materials Sciences and Technology, University of Miskolc
E-mail: a.molnar2007@gmail.com
[2,4]Department of Mechanical Engineering, Faculty of Engineering, University of Debrecen
E-mail: fazekas@eng.unideb.hu, rathyne@eng.unideb.hu
[3]Csabai Pharma AG Svitzerland, Zug
E-mail: dr.csabai@csabai.de

Abstract
Thermal spray processes, especially high velocity oxygen fuel (HVOF), are widely used coating techniques in many gas, oil industrial applications and to protect automobil worm parts materials from various degradation processes such as wear, erosion, high temperature and corrosive atmosphere. In addition, inhomogeneous structures of the HVOF coatings limit their effectiveness to be used as physical barriers to inhibit corrosive species from getting into contact with the substrate to be protected. As a result, improvement against corrosion by such coatings is limited in most cases. In order to further improve the corrosion resistance of the coating properties, laser surface modification could be considered as a potential technique to eliminate or reduce the defects of the coatings. Laser surface modification via re-melting, offers many advantages including precisely controlled treatment dimensions, particularly in depth, and minimum heat-affected zones, resulting in no thermal effects on substrate materials.

Keywords: *HVOF, NiCrBSi-based coating, laser remelting*

1. INTRODUCTION

Ni-based coatings are used in applications where corrosion and wear resistance at moderate and elevated temperatures are required [1 - 5] NiCrBSi alloy is one of the alloys with betterperformances [6 - 7]. The addition of Si and B increase the self-fluxing capabilities of the Ni alloy, improving its ability to produce coatings by melting process. B addition reduces the melting point due to the presence of a eutectic phase at 3.6% wt. The broad solidification interval of the Ni alloys with high-boron content makes easier to get coatings by thermal spray process.
The quality of the thermal sprayed coatings manufactured by thermal deposition techniques depends on several parameters such as the sprayed particle size, the deposition temperature, the combustion gases, the feed speed, the angle and rate of deposition, the spray distance, the temperature of the substrate, the applied gas pressures during the process and the spraying methods. All these parameters should be carefully selected in order to obtain the best properties for each application.
Among the techniques employed to melt and spray material, flame spray and plasma spray processes are widely used. The coatings produced by flame spray are characterized by a high porosity and a poor adhesion to substrate. For that reason, this technique is commonly combined with a subsequent melting process. Laser cladding is a spray technique usually employed to produce coatings for valuable components and products. It is characterized by producing coatings with a very low porosity and, consequently, better wear and corrosion resistance are expected [8 - 11].

After the spraying process, the coating was melted at 1025 °C by either using a flame or a laser. The melting process by flame consists of applying an oxyacetylene flame on the coating until the melting temperature is reached [12 - 21].

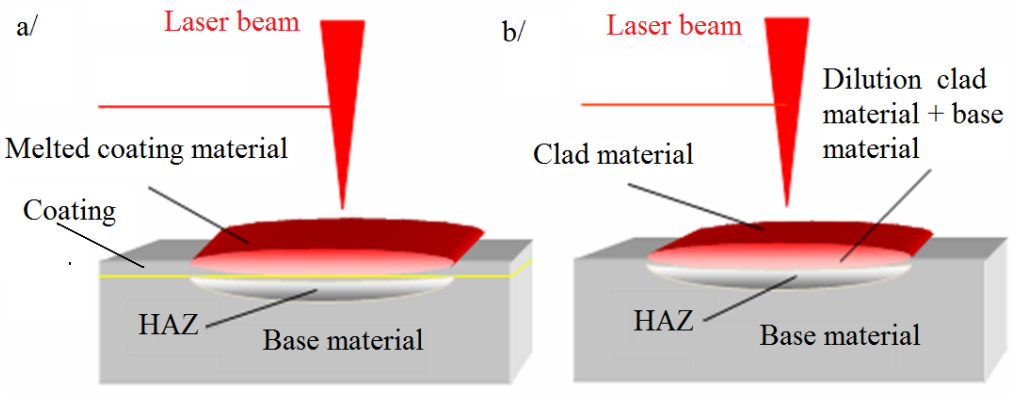

Figure 1 Laser surface treatment techniques; (a) laser surface remelting, (b) laser cladding

It is a manual process, and then the final quality of the coatings depends on the ability and experience of the operator. The melting process by laser consists of applying a CO_2 laser working with 1900 W of power on the coating.

Laser surface remelting

In this type of processing, the laser beam is used to melt a small region of the substrate surface. This processing does not change chemical compositions within the melted layer, but changes its microstructure, in terms of a refined and possibly metastable microstructure in small localised areas of base material (Figure 2 a/). The features of this process are: flexibility resulting from possibilities of computerisation (software control) of the process and automation, and it has small thermal penetration and therefore minimum distortion. By this procedure fine homogeneous structure can be obtained due to rapid cooling rates, where the unaffected substrate acts as a heat sink. When the beam traverses past, the solidification process starts from the solid/melt interface towards the surface.

Laser cladding

This method involves melting and adding another material as in the alloying process. However, dilution in this process is kept to minimum. This technique creates metallurgical bonding of the clad layer with the substrate to improve the surface properties of a material which will be subjected to corrosion, erosion or wear (Figure 2 b/).

2. THE EXPERIMENTAL PROCEDURE

A NiCrBSi UTP UB - 2760 alloy with an average grain size of 125 µm and a melting point of 976 -1063 °C was used as the coating material. The surface state before the flame spray process was typical for machining, with a rust- and impurity-free average surface roughness *R*a = 1.1 µm. The chemical composition of all the used materials is described in *Table 1-2*.

2.1 Feedstock materials

One NiCrBSi super-alloy powder was used as coating material. The powder was composed of spherical particles with an average size of 66 μm. The substrate material was Ck 45 steel in the form of bar, with a L = 300 mm and diameter of 50 mm in *Table 1*.

Table 1. Chemical composition and hardness of substrate steel

Grade of steel	Composition , [wt. %]			Hardness [HV 1]	
	C	Mn	Si	Normalized	Hardened
C 45*	0,45	0,60	0,30	200 - 235	480 - 515

*Wn. 1.1191 DIN Ck 45

NiCrBSi powders from Böhler – UTP referenced as grade UB 5-2760, was chosen as feedstock material. The composition of the sprayed powders is listed in *Table 2*.

Table 2 Chemical composition and particle size of used self-fluxing NiCrBSi spray powders

Trade mark	Composition, [wt %]						Particle size [μm]	Hardness of coating [HRC]	Melting range [C°]
	Ni	Cr	Si	B	C	Fe			
UB5-2760*	Balance	15,0	4,4	3,2	0,75	3,5	-125 - +45	60	964 - 1063

GmbH. Bad Krozingen, Deutschland

2. 2. The flame-spray process

The surface of the bars were prepared by corundum blasting using angular Al_2O_3 1% particle with nominal grain size of 0.5 mm before applying the flame-spray depositing process in order to eliminate grease and oxide contamination, and to improve the adherence between the coating and the substrate.

Table 3 HVOF flame spray parameters for the NiCrBSi powders

Thermal spray process	Acetylene flow rate [l/min]	Propane flow rate [l/min]	Oxygen flow rate [l/min]	Powder carrier gas (air) flow rate [l/min]	Spray distance [mm]	Spray velocity [m/s]	Scanning step [mm]
HVOF	-	62	240	15	180	450	6

The flame-spray process was completed with a UNY-SPRAY-JET UTP and a UTP TOP GUN AIR HVOF guns at a pressure of 2.5 bar for the oxygen gas and of 1 bar for the acetylene (Table 3). Powder consumption was 9.0 kg/h and the optimal spraying distance was 150-180 mm.

2.3 The laser remelting process

After spraying, the flame-spray coatings were laser remelted. Incomplete melting along the full thickness of the coating means a lack of metallurgical bonding between substrate and coating, and is a frequent outcome of the process. An alternative technique used for post-treatment coating consists of using a laser beam to melt the flame-sprayed layer; in our experiment we used the two-stage method. The BAYATI 5 kW CO_2 laser equipment with a nominal power of 1900 W was used to this end in our testing and a Kugler LK - 190 laser focusing head at a focal distance of 125 mm was applied for thermal treatment. Equipment optics was protected by a 2 bar pressure cross current of air.

Table 3 CO_2 laser operating parameters

Frequency (f) [Hz]	Pulse duration(t_p) [μs]	Scanning speed [mm/s]	Defocusing (z) [mm]	Spot diameter (d) [mm]
1500	20	2	+ 100	3

The laser equipment was used in continuous mode with argon as protective gas. The different process parameters and their influence on the layers obtained were studied under the above conditions. The most satisfactory results were achieved with the following parameters: power density on the surface of the piece of 38 W/mm^2, beam scanning speed of 150 mm/min and a laser beam diameter of 3 mm. In addition, in order to reduce cracking risk, the test specimens were preheated in a furnace and their cooling rate after the laser treatment was slowed by placing them in perlite.

3. MICROSTRUCTURE AND LAYER HARDNESS

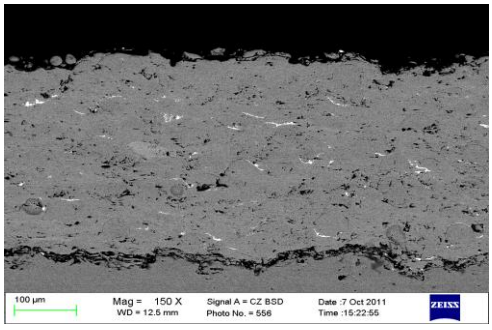

Figure 2 HVOF thermal sprayed layer (N = 150)

Scanning electron microscope techniques with energy dispersive spectroscopy ZEISS EVO MA 10 instrument (SEM–EDS) were used to metallographic investigation and analyse the coatings microstructures and micrhardness (Figure 4 – 5). Specimens for micro-structural analysis were firstly ground and polished to a mirror finish and then etched with solution of 1HCl:10HNO_3:10H_2O. Figure 3 shows the structure obtained after laser remelting. It can be clearly seen that the matrix phase is a solid solution of Ni with some Cr and Fe providing a dendrite

structure; there is an interdendrite lamellar eutectic phase made up mainly of Ni and small amounts of Si.

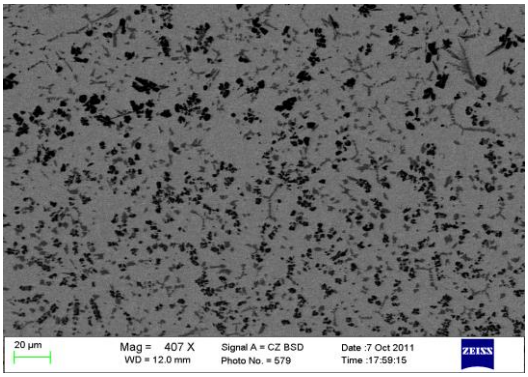

Figure 3 Micro-structure of a HVOF flame sprayed NiCrBSi coating fused by laser (M=407x).

Micro-hardness tests were carried out according to the ASTM E-384 standard with Mitutoyo MVK-H1 micro-hardness tester.

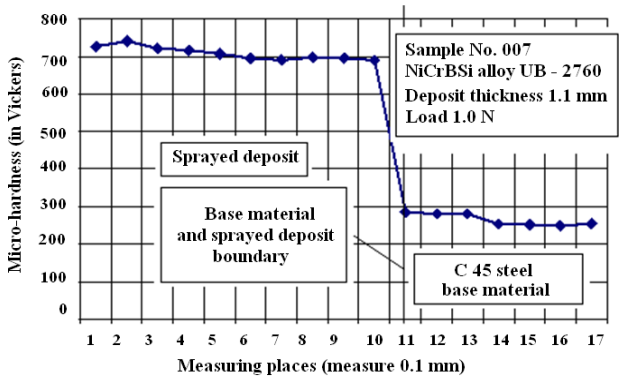

Figure 4 Micro-hardness testing results of the UB5-2760 NiCrBSi coatings as a function of the distance from the surface.

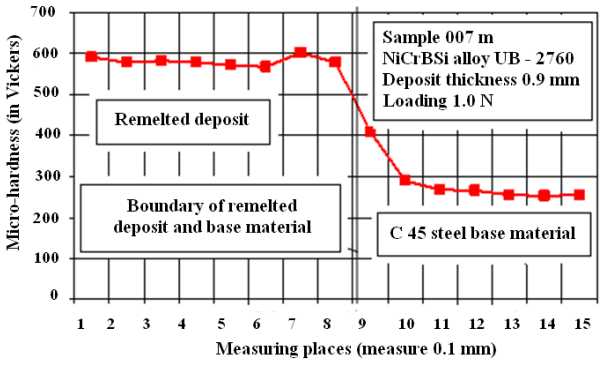

Figure 5 Micro-hardness testing results of the UB5-2760 NiCrBSi laser remelted coatings as a function of the distance from the surface

The surface is dotted with very hard precipitates, mainly of Cr (approximately 80 % by mass). This confirms the tendency of these alloys to form carbides and borides, thus supporting the results for similar alloys obtained by other researchers, who have identified these precipitates as chromium carbides and borides (mainly Cr_7C_3 and CrB) in a Ni solid solution with a dendrites morphology.

3. 3. SEM - EDXMA analysis

The UB5 - UB5 2560p - 2760p branded NiCrBSi dust-strewn and tested a laser beam remelted samples EDXMA SEM electron microscope method. The analysis EDXMA FS-sprayed and remelted samples with similar chemical composition. Figures 6 and shown in full section of the layer with a laser beam remelted layers chemical composition evolution. The contents of the analysis EDXMA conspicuous layers of high-Cr, which refers to the presence of hard phases.

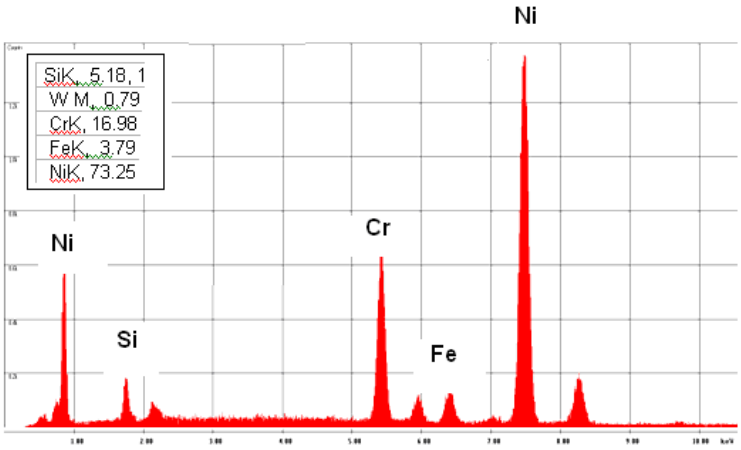

Figure 6. The USB-2760 HVOF & aser beam remelted coating EDXMA Analysis

Wear tests

Tests were carried out in a wear testing machine with a pin on disc configuration under dry sliding conditions without eliminating the debris formed [1]. Specimen and counter body were cleaned using methanol to avoid the presence of humidity and other non-desirable films such as grease. Most requirements of the ASTM standard G99-95 were followed (ASTM G99-95, 1995).

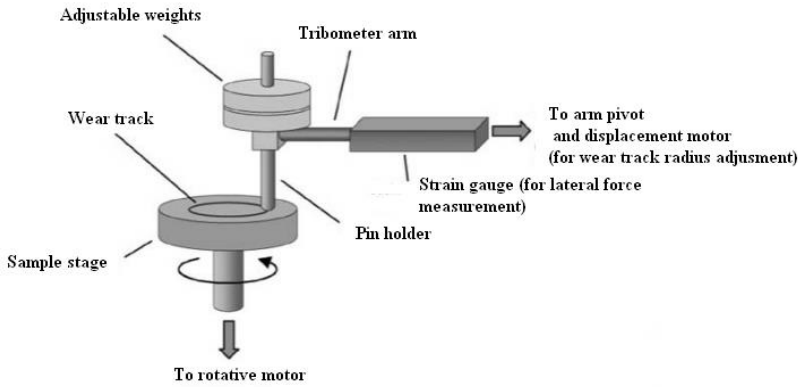

Figure 7. Wear test princip by ASTM G99-95, 1955

Cylindrical pins made of alumina (aluminium oxid) with diameter 3 mm. The cylinders were positioned in such a way that the nominal contact area was maintained constant during the tests in spite of the wear process (Figure 7).
The disc, made of the coating under study, rotates horizontally at sliding speed of 1m/s. A dead weight loading system was used to perform the tests at nominal normal pressures of 16 MPa.
The coefficient of friction was obtained by means of a torque transducer. The total sliding distance was 20.000 m.
After the wear tests, the worn volume were calculated measuring the transversal area of the wear groove (A), by using SEM. The worn volume is calculated using the following equation:

$$V = 2\pi RA \quad (1)$$

where *R* is the distance between the centers of the disc and the pin.
According to Archard law (Archard, 1953), the worn volume, *V*, is proportional to the sliding distance, *L* and the applied normal load, *F*:

$$V = kFL \quad (2)$$

where the proportionality constant *k*, is called specific wear rate and it is usually quoted in units of mm^3/Nm.
It represents the volume of material removed by wear (in mm^3) per unit of sliding distance (in m) and per unit of normal load (N).
The measure of *k* is helpful for comparing wear rates of the coatings (Table 1.)

Table 4. Wear rates of the NiCrBSi coating

Technology	***k* [x 10 $^{-5}$ mm^3/Nm]**
HVOF FS	3.39
HVOF FS + laser remelting	4.44
Laser cladding	1.51

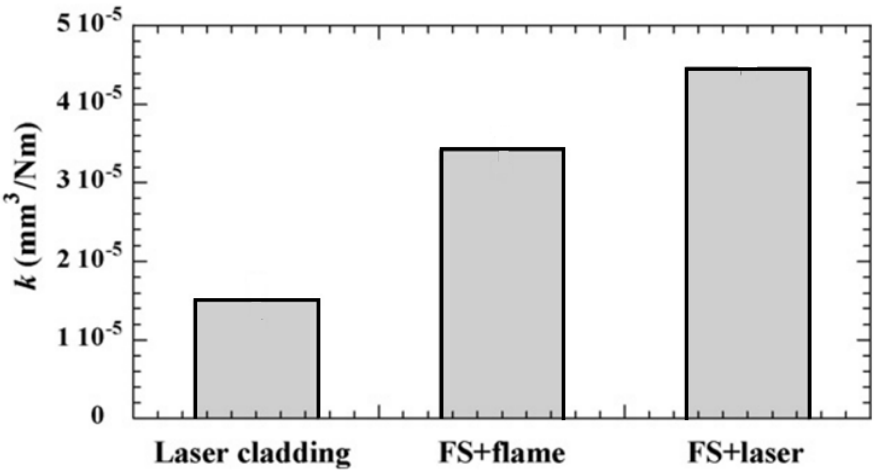

Figure 8. Wear coefficients *k* for the different coating technology

CONCLUSIONS

In this work, thermal sprayed NiCrBSi coatings have been tested: UB5 – 2760 HVOF flame sprayed with a subsequent remelting treatment of laser (HVOF FS + laser). Their micro-hardness and microstructure, properties were studied.

- *Micro-hardness* was determined by depth sensing indentation. A fine uniform distribution of equated precipitates increase the hardness, as it can be observed in laser remelted coatings. The non-homogeneous distribution of precipitates decreases the hardness values in FS + laser coatings.
- All coatings show a similar microstructure composed mainly of a Ni solid solution matrix with dendrites structure and common phases precipitated on it with different distribution and size. Laser remelted coatings show a uniform distribution of small and rounded precipitates, which results in a harder material.
- Results show that in situ laser remelting induces the growth of a dendrite microstructure that strongly decreases the HVOF FS-sprayed coating porosity.
- Wear behaviour Laser Cladding coatings show higher wear resisitance than HVOF FS and, especially HVOF FS + laser.

REFERENCES

[1] Gómez-del Río T., Garrido M. A., Fernández J. E., Cadenas M., Rodríguez J. 2 0 0 8. *Influence of the deposition techniques on the mechanical properties and microstructure of NiCrBSi coatings.* Journal of materials processing technology 2 0 4 304–312

[2] Cordia, M., Delogu, P., Nenci, F., 1987. *Microstructural aspects of wear-resistant stellite and colmonoy coatings by laser processing.* Wear 119 (2), 137–152.

[3] Ming, Q., Lim, L.C., Chen, Z.D., 1998. *Laser cladding of nickel-based hardfacing alloys.* Surf. Coat. Technol. 106, 174–182.

[4] Li, Q., Zhang, D., Lei, T., Chen, C., Chen, W., 2001. *Comparison of laser-clad and furnace-melted Ni-based alloy microstructures.* Surf. Coat. Technol. 137, 122–135.

[5] Kim, H.J., Hwang, S.Y., Lee, C.H., Juvanon, P., 2003. *Assessment of wear performance of flame sprayed and fused Ni-based coatings.* Surf. Coat. Technol. 172, 262–269.

[6] Xin, H., Hu, C., Baker, T.N., 2000. *Microstructural assessment of laser nitrided Ti–6Al–4V alloy.* J. Mater. Sci. 35 (13), 3373–3382.

[7] Miguel, J.M., Guilemany, J.M., Vizcaino, S., 2003. *Tribological study of NiCrBSi coating obtained by different processes.* Tribol. Int. 36, 181–187.

[8] Serres N. Hlawka F., S. Costil Langlade C. Machi F. *Microstructures and environmental Assessment of metallic NiCrBSi coatings manufactured via hybrid plasma spray process.* Surface and Coatings Technology 205 (3010) 1039 – 1046.

[9] Otsubo, F., Era, H., Kishitake, K., 2000. *Structure and phases in nickel-base self-fluxing alloy coating containing high chromium and boron.* J. Therm. Spray Technol. 9, 107–113.

[10] Navas, C., Colac¸o, R., de Damborenea, J., Vilar, R., 2006. *Abrasive wear behaviour of laser clad and flame sprayed-melted NiCrBSi coatings.* Surf. Coat. Technol. 200, 6854–6862.

[11] Leyland, A., Matthews, A., 2000. *On the significance of the H/E ratio in wear control: a nanocomposite coating approach to optimised tribological behaviour.* Wear 246, 1–11.

[12] Molian, P.A., Rajasekbara, H.S., 1987. *Laser melt injection of BN powders on tool steels. Part I. Microhardness and structure.* Wear 114 (1), 19–27.

[13] Atamert, S., Bhadeshia, H., 1989. *Comparison of microstructures and abrasive wear*

properties of stellite hardfacing alloys deposited by arc welding and laser cladding. Metall. Trans. A 20, 1037.

[14] Monson, P., Steen, W.M., 1990. *Comparison of laser hardfacing with conventional processes.* Surf. Eng. 6 (3), 185–193.

[15] Oberlander, B.C., Lugscheider, E., 1992. *Comparison of properties of coatings produced by laser cladding and conventional methods.* Mater. Sci. Technol. 8, 657–665.

[16] L. Pawlowski, *Thick Laser Coatings: A Review*, J. Therm. Spray Technol., 1999, 8(2), p 279-295

[17] J. Mateos, J.M. Cuetos, R. Vijande, and E. Fernandez, *Tribological Properties of Plasma Sprayed and Laser Remelted 75/25 Cr3C2/NiCr Coatings*, Tribol. Int., 2001, 34(5), p 345-351

[18] A. Lanin, I. Fedik, *Thermal Stress Resistance of Materials*, Springer, 2008

[19] S. Sasaki, *Tribological Properties of Coating Films Synthesised by Laser Assisted Plasma Spraying*, Surf. Eng., 1997, 13(3), p 238-242

[20] G. Antou, G. Montavon, F. Hlawka, A. Cornet, and C. Coddet, *Microstructures of Partially Stabilized Zirconia Manufactured via Hybrid Plasma Spray Process*, Ceram. Int., 2005, 31(4), p 611-619

[21] Z. Z. Bergant and J. Grum: *Quality Improvement of Flame Sprayed, Heat treated and remelted NiCrBSi Coatings,* Journal of Thermal Spray Technology (2009) Volume 18. September Pages 380-391.

INTERNATIONAL SCIENTIFIC CONFERENCE ON ADVANCES IN MECHANICAL ENGINEERING
19 November 2015, Debrecen, Hungary

CUSTOMER SATISFACTION OR HOW WE CAN KEEP SATISFIED CUSTOMER

[1]MORAUSZKI Kinga, [2]LAJOS Attila, Ph.D., [3]MENYHÁRT József

[1]PhD School in Business and Management, Szent István University
E-mail: morauszki.kinga@gtk.szie.hu
[2]Faculty of Economics and Social Sciences, Szent István University
E-mail: lajos.attila@gtk.szie.hu
[3]Department of Mechanical Engineering, Faculty of Engineering, University of Debrecen
E-mail: jozsef.menyhart@eng.unideb.hu

Abstract
This study briefly presents how we can keep our customers as suppliers in today's world. This article gives a short review with the help of specialized literature that was written nationally and overseas. The client is the most important partner independent of the type of industry all the time, and this will also remain in the future. The long-term success of a business can be achieved only in that case if the clients are satisfied and this is only possible if we take harmonised efforts in favour of building-up good client-relationship and its provision. One of the biggest challenges in the 21st century is to keep the already gained clients. This is one of the most difficult tasks sometimes.

Keywords: *customer satisfaction, KANO-Model*

1. INTRODUCTION

It is no longer enough if our customers are satisfied with our products or services. The markets are consolidating and more and more people are using the internet to compare prices and products. As a result, customer relationships are becoming of increasing importance in the entire process. As people's consumption habits are becoming more and more demanding, they are expecting more and higher quality services from companies. In the course of the increasing market competition, it is required to put more effort into obtaining new customers and keeping the existing ones. However, many companies are still unaware of how much they lose if they do not manage clients properly. We can say that we live in a time when the clients are a valuable asset, and we must treat them with utmost care. Of course, this effort is reflected in the processes.

2. CUSTOMER REQUIREMENTS

As a company's existence depends on its customers, it is in the suppliers' interest to keep customers or – in other words – the partners, and to enlarge the circle of them. In light of this fact, stagnation means a kind of negative change, so if the supplier companies are able to keep customers, or they are able to get new customers, it will result in some expansion by all means. After the advent of mass production, the handling of customer opinions was one of the tasks of the merchants. However, direct interaction with customers had stopped and the customers were not able to work with the sellers and there was no feedback about the customers' opinion. The system was not completely perfect, the level where customer feedback could have been analysed was missing [3]. Satisfaction does not only depend on the quality, characteristics and performance of the service, but among other things on consumer expectations, as well [18]. In today's world, we find that the

volume of the supply is in excess of the measure of the effective demand, so the companies which attempt to meet similar customer demands are facing a stiffer competition from their rivals. The companies want to ensure meeting the special customer requirements as much as possible to improve their competitiveness against their competitors in the market. Most of the experience shows that there are companies that do not know enough about their clients.

The problem is that the companies do not often have enough information about clients. But familiarity with the needs of our customers – which is given by the ISO standard as well – is a key factor in the retention of the purchasing power (our customers) and if it is possible you have to keep a record of them as organizational units or products. If we give it another thought – taking an example – that in the same production line more than 10 kinds of products can be made, and these products are transported to several customers, the company should maintain contacts with 20-30 customers and of course with every customer at the same high level. After a while – you must realize – it is impossible. Not every company knows the exact number of their clients, many of them are not aware of the value of each supplier. There are suppliers who – being purchasers themselves - classify their customers according to their products or services, while other companies group their customers according to their locations. This facilitates the handling (of customer relations). The lack of information, treatment and internal communication problems often lead to loss of customers. The customers do not become disloyal to a company because one employee of them made a mistake, but rather for what happened after that.

The customer likes to be attended to. Most mistakes are made in the course of complaints because we are impatient and disrespectful to the customer. It is not a good attitude if you want to leave the problem outside, as it is the customer's inalienable right to make a complaint, moreover, they generally turn to us, because we have made a mistake, and not because they want to behave in a disagreeable manner - if indeed a complaint can get to competent persons. If the client wants to complain by phone, it often takes time to find competent people to talk to about the existing problem with the product or service.

It is advisable to immediately get in touch with the buyer if we have received the problem via snail mail, or by e-mail nowadays. So, even if it is a big problem, we can reassure the customer, because they can see that we are dealing with them. The dissatisfied customer expects us to provide guarantee that a similar incident cannot happen in the future with him, and of course the error must be rectified. Some kind of compensation must be offered voluntarily for the damage and the inconvenience suffered by the customer, because the defective product or service is not worth as much as a perfect one [2]. It is important that the contact person should be flexible, have good conflict resolution skills, and try to exercise patience, even with the toughest customer. Claims are often rejected openly in many places, this attitude certainly leads to losing customers. But effective customer management can greatly contribute to keeping the fluctuating consumer, which can significantly improve the company's profitability.

Most companies lose a certain percentage of customers year after year. Customers can be lost for reasons beyond our control, but as we cannot change them, it is enough if we know the trends and focus on those cases instead when we can do something to prevent the loss of customers. The better we know our clients, our customers, the better chances we have to make our customers satisfied and keep them [20].

If the customer loss has happened for reasons beyond our control, it is worth considering to find out what is the reason for the customer’s disloyalty to us in order to become better at preventing similar cases. Not to mention that it is much better for the client to find a reliable company, brand, or product which they favour and do not need to search further. The client, the consumer must be provided with a suitable product at the right place at the right time, in the right quantity and quality.

It is important to keep in mind what kind of reaction we get from customers after shipping the ordered products or services. The task of the supplier has not been completed here. We have to measure the satisfaction of our customers to know which points in our processes need improvement to achieve our ultimate ambition, which is to keep the client. Unfortunately, we have to face customer complaints in negative cases. We are not supposed to forget the fact that it is more difficult to keep customers than to get new ones. Examining the topic in terms of cost-effectiveness, it costs less money to keep them according to surveys. Existing customers should be paid much more attention to. In order to maintain and reduce churn of customers, it is important to know how satisfied our customers are with a given product or service.

According to an English proverb "Customers do not complain. They just leave..." - Customers do not complain. They simply wander away. That is why it is important to be informed proactively of the level of customer satisfaction and before the customer wanders away light has to be thrown on the customer dissatisfaction and we have to find a solution to this problem [20].

According to STAUSS (1999) what is meant by customer satisfaction is the result of the comparison of service quality (actual state) and required performance (desired state). By actual state we mean the performance level when something is detected within the framework of making use of the service by the customer. We need to distinguish between the objective and the perceived performance [8]. If a customer is dissatisfied, the inspection must find out what causes this discontent and need to "establish" satisfaction with the right actions (eg. changing products, free servicing, etc). In this way the company can stop the buyer from contacting other suppliers [14]. The customer satisfaction depends primarily on the evaluation criteria. The supplier must always be aware of what his customers' requirements are and what significance these requirements have [15].

3. CUSTOMER SATISFACTION AND MEASUREMENT

We are not supposed to forget that the result of our company depends on the satisfaction of our customers. The dissatisfied customer can leave us. Satisfying the needs of our customers is not necessarily accompanied by customer satisfaction: e.g. if because of a lack of the product required by the customer, they are offered an alternative product. If it is accepted by the customer, it does not mean in all cases that the customer is satisfied. If as suppliers we are not able to meet the customer needs, the number of orders may decrease. If it becomes permanent, the costs must be drastically reduced, which among other things may lead to downsizing. If we have reached the level of being able to fulfill our customers' requirements, we must strive to meet the special needs and requirements. That means we must look for what is the extra service that turns the satisfied customer into a “thrilled” customer.

Studies from abroad show that the likelihood of a repeated purchase made by the satisfied customer is the rate of buyer loyalty. The success of the supplier companies is ensured by the clients who would like to make use of the products and services in the long term. The customer satisfaction strengthens loyalty attached to the supplier, which can increase the company's long-term sales security [21]. According to LEVY and SHARMA (1995), the company's profitability needs factors which are demonstrated in *Figure 1*.

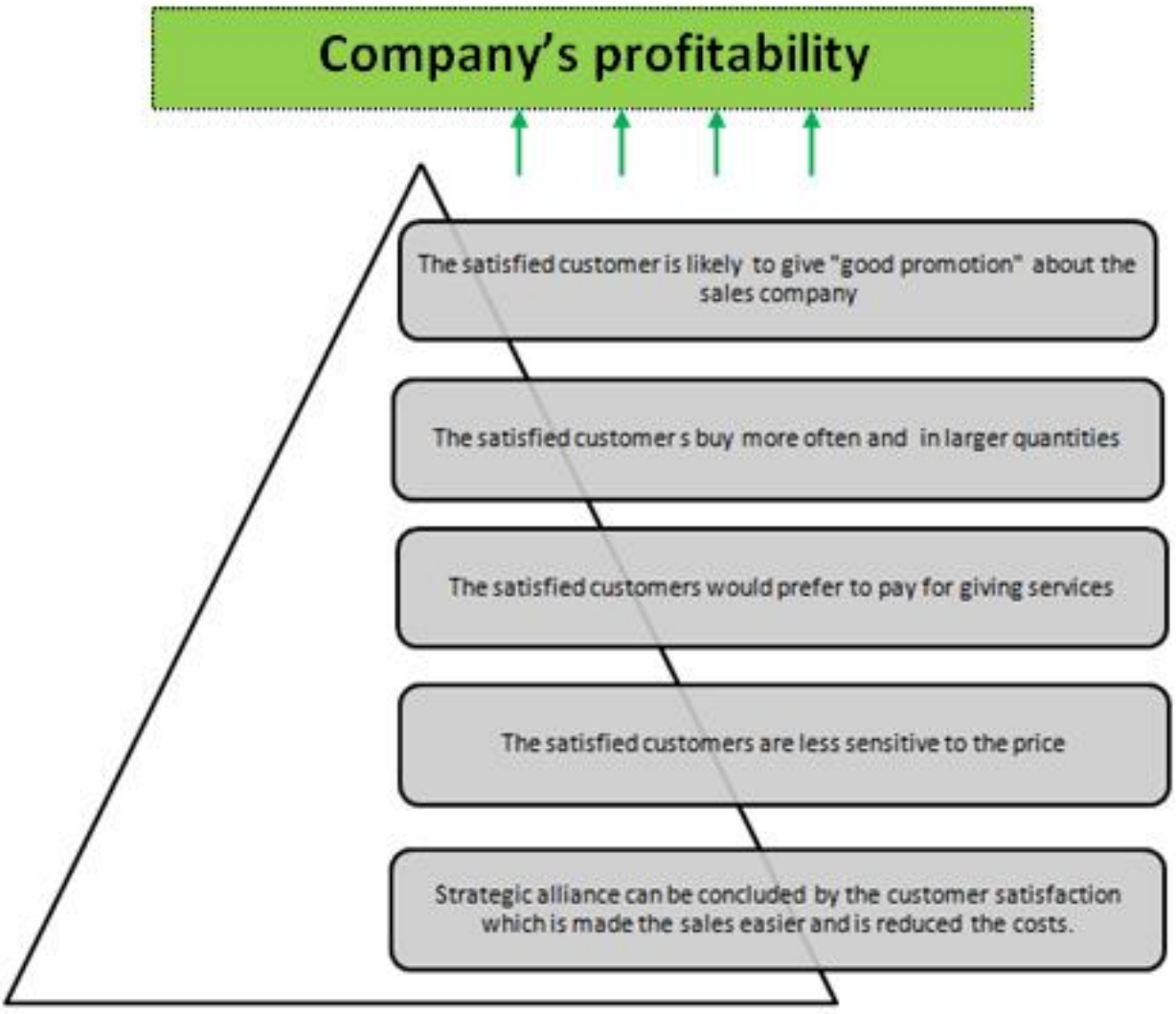

Figure 1 Factors necessary for a company's profitability
Quelle: Edited by authors (2014)

It can be generally said that most companies make a mistake when they fail to make a final interview with the departing customers to find out what was the reason for their departure. It is worth investing money and work into the constant improvement of the quality of the product and service and in order to increase customer satisfaction (*Figure 2*).
You need a strategy in accordance with the flow chart, which provides the basis for designing the steps of satisfaction measurement. If you have got the basic principle, the questionnaire can be prepared. After asking the target group, the incoming data is processed and then conclusions are drawn, possible action plans are prepared and executed and their documentation is done.
The degree of the satisfaction of the customers' needs is reflected in the Kano model, which puts the qualitative parameters in different categories (*Figure 3*). The chart's horizontal axis shows the level of the physical satisfaction of a certain quality attribute. On the vertical axis the satisfaction with the given quality attribute can be seen [13]. The starting point for the Kano model is that the connection between the performance level of the customer requirement and their satisfaction depends on the type (requirement category) of the requirements.

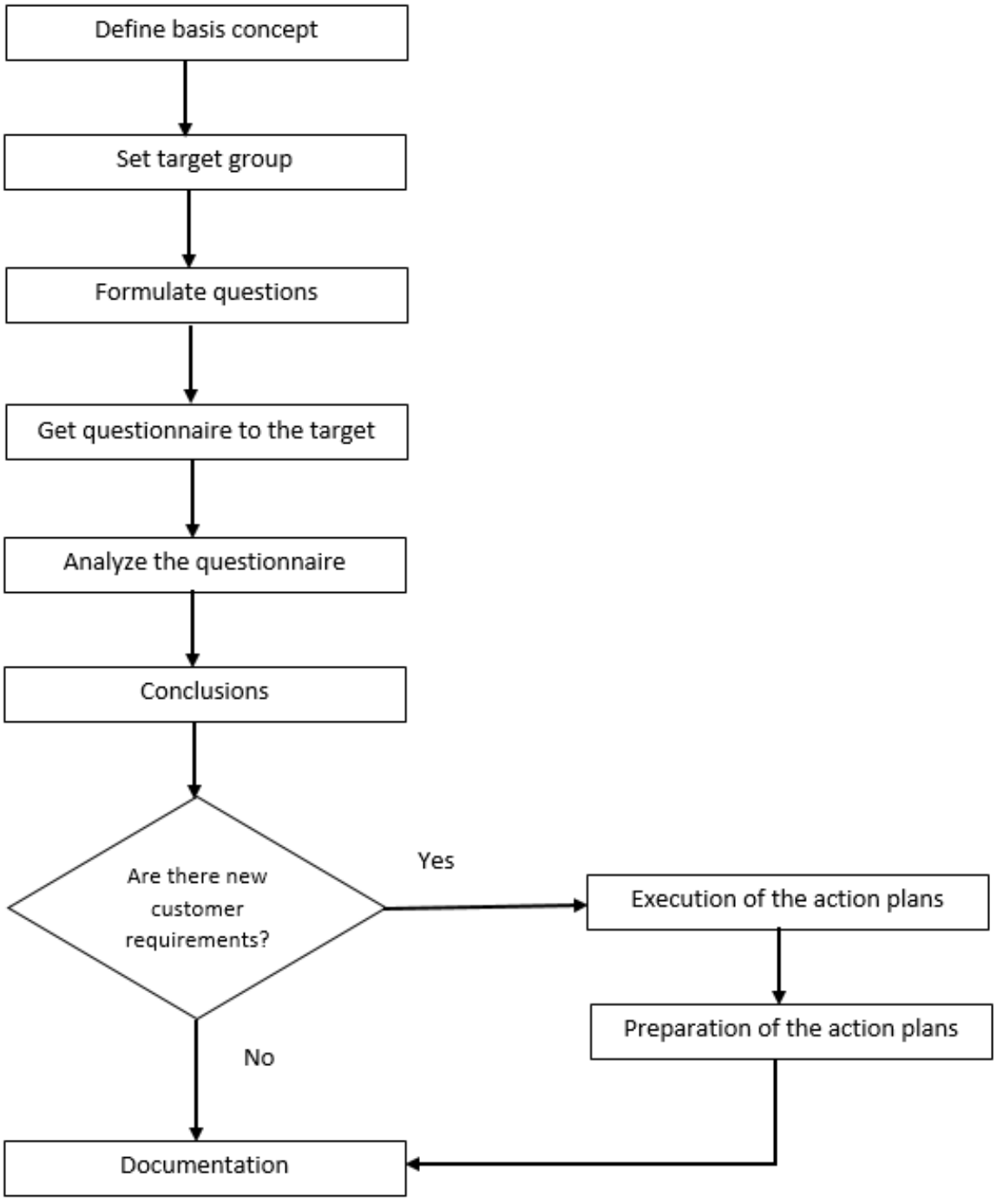

Figure 2 Customer satisfaction measurement process
Quelle: Edited by authors (2014)

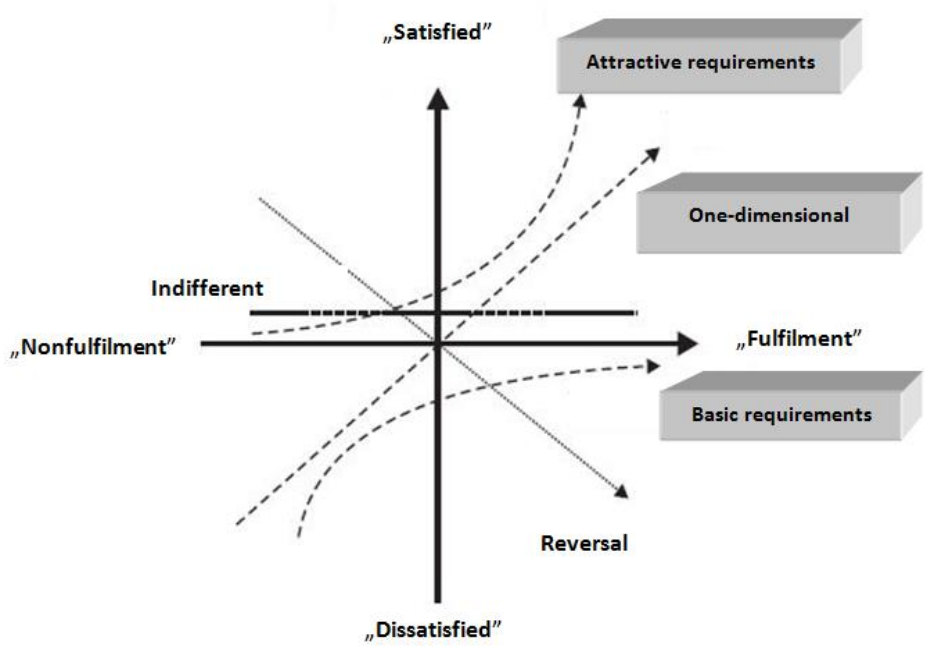

Figure 3 Quality sample based on two-dimensional conception of quality
Quelle: KANO et al., (1984)

A number of advantages are listed by specialized literature, which according to the Kano model are connected to the classification of the different requirements, for example, if the supplier receives information about which requirements have the biggest effect on the customer satisfaction. For example, there is no point in using sources in order to increase the performance degree of the basic requirements if the current status is appropriate for the customer. The Kano model makes it easier to answer the question because there is information about which changes in the performance profile have the strongest influence on customer satisfaction.
KANO (1984) is of the opinion that there are some features which are not defined clearly by the buyer, and are not stressed, as they are said to be natural [7]. These expectations and demands are called *basic requirements*. The customer will not be more satisfied if these "basic needs" are fulfilled, because this is the minimum. However, there are expectations which the customer only thinks of and they do not hope that these expectations will be fulfilled. These would be the *unspoken needs*. The third big group of expectations includes the requirements – which are between the two extremes – which customers and clients place great emphasis on and the customers insist on the fulfilment of these requirements from their suppliers at the highest possible level (*Table 1*).

Table 1 KANO's requirement categories

REQUIREMENT CATEGORIES		
Basic requirements (Must-be)	***One-dimensional***	***Attractive requirements***
- implicit - unspoken - it is self-evident - evident	- spoken - specific - measurable	- not required - unspoken

Quelle: Edited by authors (2015)

In connection with the basic requirements, there are some properties, factors which, if fulfilled, can normally only prevent dissatisfaction, which means we have just achieved the "not dissatisfied" state [16]. As a result, customer satisfaction cannot be clearly improved if the performance level – in the case of a basic requirement – is always raised above the level which is required by the customer. On the other hand, "not reaching" the performance level defined by the customer leads to extreme dissatisfaction and complaints, and it can quite often result in customer defection [11]. For the supplier companies these basic requirements are binding. If we take the basic requirements as a basis, the competitive advantage may be targeted only in the short term in comparison with our rivals. If a supplier company has managed to improve a performance characteristic which is defined as a basic requirement by their customer, their actions will lead to an increase in customer satisfaction in the short term. As we talk about a basic requirement, the improvement is relatively rapid.

The "One-dimensional properties zone" is the place where we can find the needs and requirements which are expressed by the customer, where satisfaction is proportionally related to the performance degree, which means that if this performance degree increases, the satisfaction will increase as well and vice versa. Only those products and services have a chance on the markets, which reach a high standard of the necessary requirements. Consequently, performance characteristics play a prominent role in the supplier's communication policy. This requirement category distinguishes the company from its competitors in many areas.

The requirements found in the "Attractive requirements" zone (or unspoken needs) have a great influence on customer satisfaction. If a supplier manages to "boost" his performance with these factors, it clearly leads to customer satisfaction. Otherwise, the customer will not be dissatisfied if that supplier company can meet all requirements – in the other two categories – on the power level which was specified by the customer.

In recent years, a lot of attention has been paid to the Kano model [14] [9]. One explanation for the model's current significance is that fulfilling the different customer needs at a high level does not necessarily have to result in higher customer satisfaction, because the quality of services and customer satisfaction are influenced by the requirement type [4].

Customer needs have been changing constantly from day to day, but there are expectations that are stable, e.g.:

- Customers require personalized treatment
- There is a need for a contact person who they can discuss everything with, be it logistical issues, and even quality complaints;
- Customers are primarily seeking solutions to their problems, and they do not simply want to buy a product or service;
- Some customers assess our activities on the basis of the total cost, which means they will accept a higher price, if they get impeccable, high-quality service for their money;
- The client wants to have a guarantee, which means they do not want to take risks, and want to be sure that the product or service meets their expectations [21].

In the specialized literature there is no single method to measure customer satisfaction, which would be perfect, but it is not the expectation to obtain positive results after the satisfaction survey has been conducted. Above all, the goal is to get to know the customer expectations in the course of the survey, which - we know - are changing, and so we as suppliers can keep up with the constant changes. The customer satisfaction survey is a kind of tool that helps us to be competitive suppliers in the market. In order to get to know our customers' expectations, we have several options:

- By means of customer visits;
- In customer meetings;
- On customer audits;
- On exhibitions, conferences;
- Through customer satisfaction surveys (questionnaire).

If a supplier must face a delivery problem, they need to solve this problem with "special trip". Of course, the quality, safety and work safety instructions should always be kept in mind, as infringement of them may lead to legal sanctions, while the supplier may put the customer at a disadvantage if we do not keep the rules. On the one hand, consumers have become more exacting and expect higher quality services from the corporations. On the other hand, in the increasing competition in the market companies have to put more effort into obtaining new customers and keeping the old ones. These changes make individual companies think over their customer management concepts. Their efforts aim to differentiate themselves from their competitors, to increase their customer satisfaction, to increase customer profitability and the company's profitability. There are rare cases when the customer's expectations closely coincide with the supplier's offer. The explanation is simple. These customer requirements are not clearly displayed. In this case the next step is to look for a compromise.
Customer satisfaction is measured with surveys most of the time. Questionnaires can be built up in different ways, and targeted at specific groups. We can only draw valid and useful conclusions from the results of a questionnaire if we can convert data received from the customer into numerals using the Likert scale (rating 1-6). As mentioned, the questionnaire can be built up in different ways. One example of them is illustrated in the following table (*Table 2*) [12].

Table 2 Example of questions of the customer satisfaction measurement

Global questions	Global issues per question groups	Segment-specific questions	Loyalty measuring questions
Comprehensive questions, which are aimed at the general satisfaction of the company	Related to the individual areas	Related to the subgroups of the individual areas	Deal with general questions where the consumer's loyalty can be analysed

Quelle: Edited by authors (2014)

The group of respondents can be different but it should be considered how the answers from each group can be aggregated and summarized. We can ask questions from our current and outgoing customers or the customers of our competitors as well. However, we are mainly interested in the information regarding our current customers. It should not be neglected who has completed these questionnaires. It is important to find the right person(s) to fill in these questionnaires. It is advisable to group the questions so that we can define corrective actions for the problem areas effectively and then swing into action. In the course of the surveys we will possibly get not only positive and negative answers, not only such questions may be answered as what is good or bad for the customer, but it can also be clarified why he considers the product or service good or bad. These can be further broken down into segments, areas. The given answers can be depicted with diagrams even more vividly. These surveys are usually conducted annually, and the resulting data can be represented on a timeline as well. A timeline is a series of observations made at certain time points,

usually at equal intervals. The time series analysis is a mathematical description of the ingredients. These may be important for the future, a forecast can be provided.

Achieving customer satisfaction is an essential aspect in a company's life when it comes to corporate success. The following positive elements can be achieved:

- the ability to prevent the customer churn, waiving from new orders
- profitability can be improved
- number of orders can be increased
- customer loyalty

CONCLUSIONS

As companies become more critical with regard to the expectations, they expect more and higher-quality products and services as well. However, many companies do not take it into account that they may lose customers if they and their expectations are not dealt with properly. The process of the customer satisfaction measurement is not a totally unknown area to businesses here in Hungary [1]. Quality does not mean only that we satisfy the expectations which the customer companies create for us as supplier, which means that we do not only have to meet the technical parameters in the drawing, but there are also many other factors that we should bear in mind, such as delivery on time, quantity, etc.

Businesses often operate on the principle that if things go wrong, customers, buyers will definitely hear about it. Numerous studies have documented the delusion that we need to rely on customer complaints. The problem is that 50% of customers who have faced problems have never complained to anyone. The majority of the second half (45%) complains only to the subordinates who do not forward it to the management or misinterpret the customer feedback. A total of 5% of the clients go as far as the management to make their voices heard [6]. So the complaints cannot be an effective tool of monitoring customer satisfaction. The customer satisfaction survey is a kind of tool that helps us to be competitive suppliers in the market, because this way we can get a more detailed picture of the customer requirements.

REFERENCES

[1] Akar, L. et al.: *A vevői és dolgozói elégedettség mérésének módszerei,* GKI Gazdaságkutató Rt. Marketing Centrum Országos Piackutató Intézet, Budapest, 1999, 7p.

[2] Arany, F.: *A jól működő CRM-rendszer versenyelőny, Letöltés: 2014.07.22. On-line: http://www.goldinvest.hu/images/stories/cikkek/Computerword.jpg 4/2013.március 27.*

[3] Aswad, D.: *Az értékinnováció kiterjesztése a belső és külső ügyfél-elégedettségen alapuló lojalitásra,* Doktori disszertáció, Miskolci Egyetem, 2012, Miskolc

[4] Bailom, F., Hinterhuber, H., Matzler, K., Sauerwien, E.: *Das Kano-Modell der Kundenzufriedenheit,* Marketing – Zeitschrift für Forschung und Praxis, Heft 2, 1996, pp. 117-126.

[5] Berger, C., Blauth, R., Boger, D., Bolster, Ch.: *Kano's method for understanding customer-defined quality;* in: The Journal of the Japanese Society for Quality Control, 1993, pp. 3-35.

[6] Goodman, J., Ward, D.: *The importance of customer satisfaction,* Direct Marketing 56(8), December, 1993, 23-4.

[7] Hofmeister, T. Á., Simon, J., Sajtos, L.: *Fogyasztói elégedettség,* Alinea Kiadó, Budapest, 2003, p. 115.

[8] Homburg, C.: *Kundenzufriedenheit. Konzepte – Methoden – Erfahrungen,* Gabler, Wiesbaden, 2001, p. 21.
[9] Kaapke, A., Hudetz, K.: *Der Einsatz des Kano-Modells zur Ermittlung von Indikatoren der Kundenzufriedenheit - dargestellt am Beispiel der Anforderungen von Senioren an Reisebüros, in: Müller-Hagedorn,* L. (Hrsg.): Kundenbindung im Handel, 2. Auflage, Deutscher Fach-Verlag, Frankfurt am Main, 2001, pp. 123 -146.
[10] Kano, N., Seraku, N., Takahashi, F., Tsuji, S.: *Attractive Quality and Must-be Quality,* Hinshitsu (Quality.) Volume 14. No. 2., 1984, pp. 147-156.
[11] Karpe, N., Scharf, A.: *Ermittlung relevanter Determinanten der Kundenzufriedenheit mittels Kano-Modell,* in: Scharf, A. (Hrsg.): Nordhäuser Hochschultexte, Schriftenreihe Betriebswirtschaft, Fachhochschule, Heft 1 2006, Nordhausen, 2006, pp. 5-11.
[12] Koczor, Z., Göndör, V.: *Az elégedettségmérés lehetséges gyakorlati módja,* Szakmai Cikkek, 2002 /6, 2007, pp. 9-17.
[13] *Löfgren, M., Witell, L.:* Letöltés: 2015.03.14. , 2011
[14] On-line: http:// image.dashofer.humuszakiforum/vevoi_elegedettseg_ii_1.jpg
[15] Sauerwien, E.: *Das Kano-Modell der Kundenzufriedenheit,* Gabler, Wiesbaden, 2000, pp. 15-29.
[16] Schuckel, M., Sobbelstein, T.: *Ausgewählte Methoden zur Kategorisierung von Kundenanforderungen auf der Basis der Penalty-Reward-Contrast-Analyse; in: Müller-Hagedorn,* L. (Hrsg.): Kundenbindung im Handel, 2. Auflage, Deutscher Fach-Verlag, Frankfurt am Main, 2001, pp. 147-176.
[17] Schwarze, J.: *Kundenorientiertes Qualitätsmanagement in der Automobilindustrie,* Deutscher Universitäts-Verlag GmbH, Gabler Edition Wissenschaft, Wiesbaden, 2003, pp. 128-130.
[18] Sharma, A., Grewal, D., Levy, M.: *The customer satisfaction / logistics interface,* Journal of Business Logistics 16, 1995, p. 1.
[19] Sprengel, R. A., Mackenzie, S. B., Olshavsky, R. W.: *„A Re-examination of the Determinants of Consumer Satisfaction."* Journal of Marketing, 1996
[20] Stauss, B.: *Kundenzufriedenheit; in: Marketing – Zeitschrift für Forschung und Praxis, Heft 1, 1999, pp. 5-24.*
[21] Tóth-Bajnáczi, Á: *Miért van szükség CRM-rendszerre? A CRM szerepe, 2009, Letöltés: 2010.04.12. On-line: http://www.hatekonysag.hu/crm_customer_relationship_management.php*
[22] Zsoldos, B.: *A vevői elégedettség és mérése a Dunapack Rt. Hullámtermékgyárban, Szakmai Cikkek, 2002/7, 2002, pp. 20-24.*

INTERNATIONAL SCIENTIFIC CONFERENCE ON ADVANCES IN MECHANICAL ENGINEERING
19November 2015, Debrecen, Hungary

MODELLING OF AN UNUSUALLY LOADED HELICAL TORSION SPRING

[1]NÉMETH Géza, [2]PÉTER József PhD, [3]NÉMETH Nándor

[1,2]Institute of Machine and Product Design, University of Miskolc
E-mail: machng@uni-miskolc.hu, machpj@uni-miskolc.hu
[3]Graphisoft SE
E-mail: nem.nandor@gmail.com

Abstract
Elastic machine elements are frequently used to store or absorb energy, lock a joint against loosening or to adjust an accurate and permanent load. The areas of their application expand and now they can substitute originally rigid elements too. The advance of their usage is the reduction of consumed material, the adaptation to the external loads, the less energy consumption and the higher life rating. The analysed spring is a helical one and due to its special loads, it is approached from the topic of flexible drives. Besides the questions modelling, the calculation of deflections and load carrying capacity of a special purpose helical torsion spring, the authors summarize the mechanism of its operation, demonstrating its functions like annular wheel, clamping device, torque limiting clutch and freewheel in an epicyclic traction drive.

Keywords: *helical torsion spring, belt drive, epicyclic traction drive, integration of functions.*

1. INTRODUCTION

Helical springs can be found in nature. The helix is part of the animate and inanimate nature, can both be found in micro and macrocosm, as the most general kinematic movement, the screw motion. If one looks at visible parts of the plants, experiencing that a part of the climbers grow along helical path, and the other part develop curling tendrils. The tendril is created to establish a bond between sprout aspiring to the light and an adjacent parts of plants or other shapes, in addition this binding should be flexible. The force emerging in the binding (helical spring is always the function of the external loading (dead weight, precipitation and wind load).
The helical springs that create such a flexible connection between two parts or assembly, can be found also in the man-made machines. Do think of a household refrigerating machine, in which the unit of an electric motor and a piston-compressor is in a closed room, and connected to three points of the surrounding container. One end of the spring creates the bond "growing into" a threaded hole and the flexible connection is assured by the free coils capable to swinging motion. The connection is rigid between the spring and the threaded hole, as between the tendril and the generally cylindrical outer surface on which the tendril grows by screw-like motion.
Frequently used machine elements are the wire thread inserts which are driven into plastic or light metal alloy parts and function as helical torsion spring during insertion. While inserting them into a tapped hole the first coil should be gripped by a tang and smoothly rotated because their outer diameter is slightly larger than the nominal size of the nut thread receiving them. The external torque that serves as to overcome the thread friction, acts to the first coil of the wire and reduces the outer diameter of the wire creating a clearance between the tapped hole and the wire.

2. FREE-RUNNING CLUTCH

A right-hand wound helical torsion spring can be inserted into a cylindrical hole having slightly less diameter than the spring when we insist on the right direction of rotation. Inversely, when installing a right-hand wound spring with right direction of rotation on an external cylinder having lightly greater diameter than the inner diameter of spring, the external torque should be applied to the last coil instead of the first one. The installed helical spring is tightened on the outer surface due to an opposite external torque and the line pressure formed between them will increase proportionally. Some force closing freewheels operates on this principle.
This applies also to the flexible shafts which consist of multiple (oppositely wound) layer of helical torsion springs, and are designed only one-way torque transmission in order the outer layer to be stretched on the subsequent layer of spring.
The usual direction of rotation of torsion springs is such that their diameter is reduced under load, because it will be the favorable case of their use when their production technology is the usual winding.
Freewheel clutch operating with force closing principle is also achieved when two hub holes are connected by an inserted helical spring with its outside diameter where the hole diameter is slightly smaller. In this solution, we have to be more prudent, as contrary to the usual solution where the ribbon-like spring is tightened on the outer cylinder, and is in tension, here there is a compression in the band, so stability must be checked and, if necessary, the thickness of the strip should be increased.
If helical springs are fit by interference both in the bores and on the outer cylindrical surfaces, then the springs depending on the direction of ascent, the following relationships may be formed between the hubs, and those of the their shafts. In case of the same wound sense, depending on the direction of rotation, the one or the other spring transmits the torque, and therefore the free-running capability disappears, and remains only a simple flexible connection. In case of opposite direction of wound the free-running mode of operation remains in addition to the flexible connection. Both springs take part in power transmission in driving service and at opposite sense of rotation both springs are in freewheel service.

3. BELT DRIVE

Let's consider those problems of the helical torsion springs where only some smaller, equal and symmetrically arranged parts of the outer cylindrical surface are kept and the helical spring is in contact in smaller contact arcs. The bending rigidity of the coil (belt) should be increased, but less torque is able to be transferred by the clutch. The peripheral force can be transmitted is not only the function of the diameter, material and cross-section of the belt, the initial tension and the coefficient of friction, but also the function of the angle of wrap. The transmissible torque is reduced by the wrap angle reduction if this unfavourable change is not balanced by increasing the pretension. Increasing pretension offers some opportunity to increase the thickness of the strip.
Assume that the thickness of spring strip, h is quite large when the number of contact areas pro coils, N = 2,3,4, ... in order to avoid the excessive deformation of the radial arc length. The transmissible circumferential force is

$$\begin{aligned} F_t &= F_1 - F_2, \\ F_t &\le F_2\left(e^{\mu\theta} - 1\right), \\ F_t &\le F_1\left(1 - e^{-\mu\theta}\right) \end{aligned} \qquad (1)$$

where the summated arc of contact, θ and the coefficient of friction, μ are in the known equations. To transmit a given amount of peripheral force, a pull of

$$F_1 \geq \frac{F_t}{1 - e^{-\mu\theta}} \tag{2}$$

should be assured in the tight bench of the belt. To transmit the torque of $T = C_2 T_n$, considering also the lead angle, α

$$F_1 \geq \frac{T/(r_s \cos\alpha)}{1 - e^{-\mu\theta}}, \tag{3}$$

where $r_s = r - h/2$. The tension in the belt is not only the function of the external torque, T but also the lead angle, α, the angle of wrap, θ and the contact radius, r_s.
Let's change the cylindrical pieces of contact surfaces by planet gears having radius of r_2. The arc of wrap is enlarged so as the spring coil should tightened on the planet gears as a ribbon having small bending rigidity. The angle of wrap pro coils became 2π independently of the number of planet wheels, like when a helical spring is installed tightly on a solid cylinder. In addition, the number of coils of the spring is increased compared to the unloaded state.

4. EPICYCLIC TRACTION DRIVE

There is a belt loaded by F_2 at the free end and F_1 acts at the other end. There is a linearly changing internal force at the intermediate sections. Imagining a common type of planetary drive with one inner and one outer meshing, besides the usual condition of adjacency, an auxiliary criterion should be established. Both the contact of planet wheels and the contact of sun and elliptical annular „wheel" should be avoided. When the drive is loaded by the nominal torque, the free stages of coils became straits between the planet wheels. In case of the number of planet wheels, N radius of sun wheel, $r_1$and that of planet wheel, r_2 the supplemented condition of adjacency is

$$\frac{1 - \cos(\pi/N)}{1 + \cos(\pi/N)} < \frac{r_2}{r_1} < \frac{sin(\pi/N)}{1 - sin(\pi/N)}. \tag{4}$$

The common part of the practical range of $0{,}2 < r_2/r_1 < 5$ and the (4) both determine the current domain of the drives.
The number of coils is varied while the simply unloaded spring become a polygon shape one, due to the increasing external load. The rate of increment of number of coils, starting with that of the unloaded spring, Z_b, is

$$\frac{Z_b'}{Z_b} = \frac{2 + h/r_3}{\frac{\left(\frac{\sin(\pi/N)}{(\pi/N)} + 1\right) i_{1k} - 2}{i_{1k} - 1} + h/r_3}, \tag{5}$$

where the kinematic ratio of the drive, i_{1k} the unloaded radius of the annular wheel, r_3, the number of planet wheels, N ,the thickness of the spring coil, h are known, and the increased number of

coils Z_b' is the result.

One end of the ribbon should be fixed, the other is free. The radial and frictionless reciprocating motion of the fixed end is the prerequisite of the high efficiency. This range of motion, when the drive is loaded by nominal torque, is

$$r_3 \geq \rho \geq \frac{r_3}{2}\left[1-\cos\left(\frac{\pi}{N}\right)\right]\frac{i_{1k}}{i_{1k}-1}. \tag{6}$$

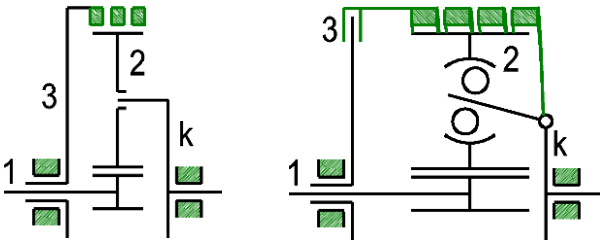

Figure 1 Helical torsion spring substituting the annular wheel in an epicyclic drive

5. MODELLING OF THE HELICAL TORSION SPRING

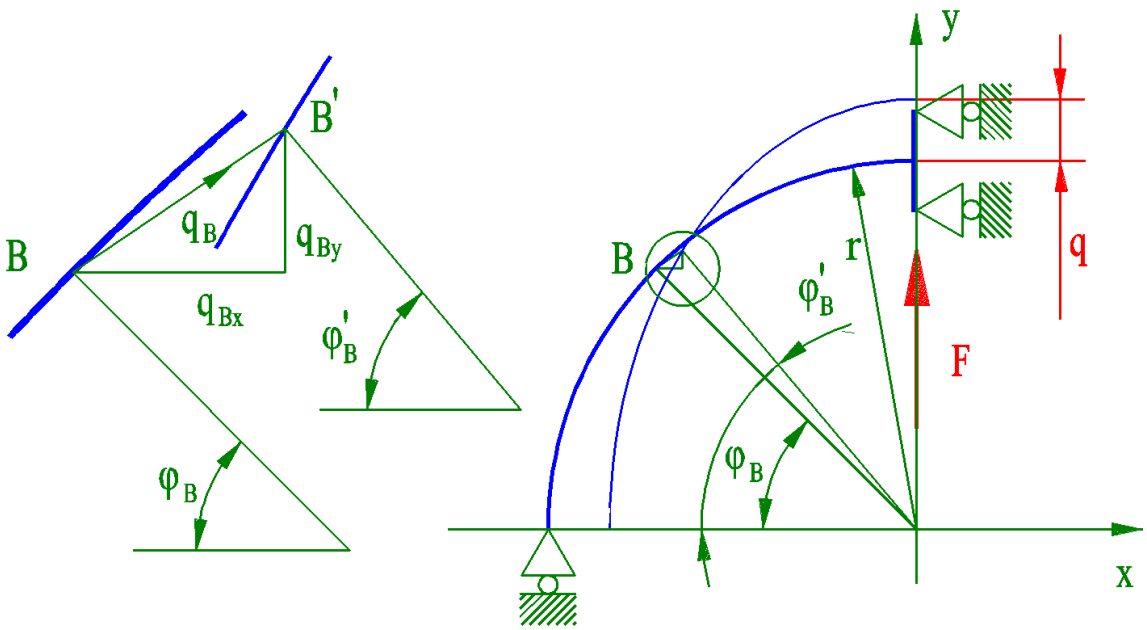

Figure 2 Deflection of the annular wheel

Let us imagine a closed cylindrical bar with a uniform cross-section. The distance between the centre of the ring (that is the origin of the coordinate system, too) and the neutral axis of its cross-section when loading it radially by a vertical force F, is $r_3 + h/2$, along the axis y, and that of at unloaded condition is equal to its mean radius , $r = r_3 + h/2 - q$. The radial deflection of the ring, q is generated by the radial force

$$F = \frac{IE}{r^3\left(\frac{3}{4}\pi - 2\right)} q \tag{7}$$

where the area moment of inertia, I, the Young module of the material of spring, E and the mean radius of the ring, r is known. The point B of the ring at an arbitrary polar coordinate of angle φ_B will move from the unloaded circle to an elliptical curve $y = y(x)$. Due to the symmetries a domain of angle π/N of the ring is sufficient to be analysed. Let us consider the problem of $N = 2$. The coordinates of the unloaded circle are r and φ_B or $x = -r\cos\varphi_B$ and y= $r\sin\varphi_B$. After loading it by F the coordinates of the elliptical curve are

$$x' = -r\cos\varphi_B + q_{Bx} \text{ and } y' = r\sin\varphi_B + q_{By}$$
$$\text{or} \quad \varphi_B' = \frac{r\sin\varphi_B + q_{By}}{r\cos\varphi_B - q_{Bx}} \text{ and } r' = \sqrt{\left(r\sin\varphi_B + q_{By}\right)^2 + (r\cos\varphi_B - q_{Bx})^2}\,. \tag{8}$$

Both the Cartesian coordinates of the deformed ring and the deflections of q_{Bx} and q_{By} of point B are expressible by the coordinate φ_B.
When $x(\varphi_B)$ and $y(\varphi_B)$ designate the new coordinates of x' and y' , from $x = x(\varphi_B)$ the $\varphi_B = \varphi_B(x)$ can be obtained. Substituting it in the $y = y(\varphi_B)$, the $y = y(x)$ is obtained, which describes the new shape after deflection. The $q_{Bx}(\varphi_B)$ and $q_{By}(\varphi_B)$ deflections are obtained easily by any theorem based on the strain energy. In such a way the functions of

$$q_{Bx}(\varphi_B) = \frac{Fr^3}{IE}\left\{\left[\frac{\pi}{2} - 1 - \varphi_B + \sin(\varphi_B)\right]\cdot[1+\cos(\varphi_B)] - \frac{1}{2}\left(\frac{\pi}{2} - \varphi_B\right)\right\},$$
$$q_{By}(\varphi_B) = \frac{Fr^3}{IE}\left\{\left[1 + \varphi_B - \frac{\pi}{2} - \frac{3}{4}\sin(\varphi_B)\right]\sin(\varphi_B) + \left[1 - \frac{1}{4}\cos(\varphi_B)\right]\cos(\varphi_B) - \frac{1}{4}\right\} \tag{9}$$

are obtained. The inner, contacting points of the deformed annular wheel (helical spring) is obtained approximately from

$$x = -\left[r'(\varphi_B) - \frac{h}{2}\right]\cos(\varphi_B')$$
$$y = \left[r'(\varphi_B) - \frac{h}{2}\right]\sin(\varphi_B') \tag{10}$$

equations. This ring will mesh with the solid planet wheel of radius, r_2 and the centre of $(0; r_3 - r_2)$.
The intersection of the elliptical curve and the circle of planet wheel, the arc of contact of the annular wheel and planet wheel can be estimated.
Analysing the surroundings of a single contact area, the value of $e^{\mu\theta}$ is obtained. The following, subsequent steps of calculations lead to the proper design of the helical torsion spring. Starting with a small radial deflection, q, the radial force, F is obtained. This normal force is acting in a single contact of the spring and one of the planet wheels at the vicinity of the free end of the spring. A maximum friction force, μF is got and this is the less force, F_2 of a belt drive. The greater value of force, $F_1 \leq F_2 e^{\mu\theta}$, and from estimating the arc of contact, the peripheral force that is able to transmit a part of the external load is $F_t = F_1 - F_2$. Starting from the free end of the spring towards

the fixed end, the forces of F_2 and F_1 are increasing, but the ratio of them, that is supposed to be constant.

In case of conical design of helical spring, where the smaller diameter is at the free end, the transmission of the load is guided first (when the rate of load is only a fraction of the nominal one) to the contact areas located at the vicinity of the free end. The other areas enter the transmission only with increasing external loads. The effect of increasing load is a greater deflection of spring, increasing radial forces at the contacts, greater arcs of contact at the middle coils and at last in the coils at the vicinity of the fixed end. In such a way, the clamping force that push the traction wheels to each other will be proportional to the external load. This proportionality is appeared also in the deflection of the annular wheel (torsion spring) and the loads of the other elements, increasing the efficiency and the life rating of the epicyclic traction drive.

CONCLUSIONS

Starting from the analysis of the patterns of the nature and following by the technical solutions of some machine elements containing elastic parts like some threaded fasteners, free-running clutches, elastic shafts and also belt drives, the authors tried to grip some essential issues of the operation and the loading of helical torsion springs. A stationary element, the annular wheel of an epicyclic traction drive was changed by a helical torsion spring. The similarity of this annular wheel when its bending stiffness is less than as usual, and the belt or rope drives were detected. The authors also recognised and presented the operability and viability of a traction drive containing a helical torsion spring where the single spring has got the function of meshing annular wheel, torque limitation and freewheel, and integrates also a clamping device.

ACKNOWLEDGEMENT

„The research work presented in this paper/study/etc. based on the results achieved within the TÁMOP-4.2.1.B-10/2/KONV-2010-0001 project and carried out as part of the TÁMOP-4.1.1.C-12/1/KONV-2012-0002 project in the framework of the New Széchenyi Plan. The realization of this project is supported by the European Union, and co-financed by the European Social Fund.”

REFERENCES

[1] Németh G., Németh N., Péter J.: *Dörzsbolygómű hajlékony elemeinek szilárdsági számítása,* In: Bodzás Sándor (szerk.), Műszaki Tudomány az Észak - Kelet Magyarországi Régióban 2015 Konferencia előadásai, Debreceni Akadémiai Bizottság Műszaki Szakbizottsága, ISBN 978-963-7064-32-6, 2015. pp.213-219.

[2] Németh G., Péter J., Németh N.: *A new type of epicyclic traction drive,* Advances in Mechanical Engineering, 1:(1) pp. 137-142. (2013),1st International Scientific Conference on Advances in Mechanical Engineering. Debrecen, Magyarország: 2013.10.10 -2013.10.11. (ISBN 978-963-473-623-3).

[3] Németh G., Péter J., Döbröczöni Á.: Németh N.: *Helical Torsion Spring Improvement for Epicyclic Traction Drive* in GÉP, LXIII (12): 85-88., 2012

[4] Németh G., Péter J., Döbröczöni Á.: *Helical Springs in Epicyclic Traction Drives* in DESIGN OF MACHINES AND STRUCTURES, 2(2): 81-92., 2012

[5] Németh G., Péter J., Döbröczöni Á.: *Ensuring the Clamping Force in Epicyclic Traction Drive by a New Sun Wheel Design* in DESIGN OF MACHINES AND STRUCTURES 2(2): 93-100., 2012

INTERNATIONAL SCIENTIFIC CONFERENCE ON ADVANCES IN MECHANICAL ENGINEERING

19 November 2015, Debrecen, Hungary

THE BIJECTIVITY OF MONGE PROJECTIONS IN THE PRODUCTION PROCESS OF THE ARCHED WORM GEAR

ÓVÁRINÉ BALAJTI Zsuzsanna PhD

Department of Descriptive Geometry, University of Miskolc
E-mail: balajtizs@uni-miskolc.hu

Abstract
The development of computer-aided image analysis opened a very wide possibility for the utilisation of CCD cameras and the application of image analysis and evaluation software. During picture evaluation carried out by machines the problem is that we have to reproduce the curves from two perpendicular pictures. This problem awaits a solution in several parts of engineering research work [8]. We have defined the method to reconstruct spatial curves from two perpendicular pictures [1, 3, 10]. Two photos have been taken with CCD cameras from the perpendicular direction of the cutting edge that give us two perpendicular pictures to get the Monge projection, from which the cutting edge or its interpolated spatial curve can be reconstructed. The reconstruction can be guaranteed by properly – suitable for the requirements – placing the cameras in the worm gearing box. The condition of the reconstruction is that the interpolation curve fitted to the cutting edge of the worm should not have a tangent in profile position. The present paper describes the formulation of these requirements with mathematical devices.

Keywords: *cutting edge, hob, wear, CCD cameras, Monge-cuboid.*

1. INTRODUCTION

The most important research field of the group of researchers at the Department of Production Engineering at Miskolc University is the arched worm gear drive pairs [3, 5, 6, 7]. The cylindrical helicoidal surface is generated by a circle with radius ρ_{ax} in axial section.

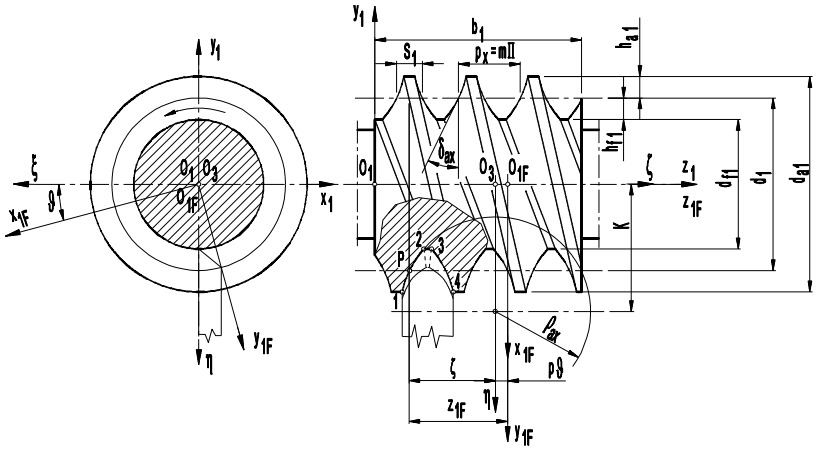

Figure 1 The cylindrical worm with circle profile in axial section [5]

The right-hand side surface of the worm in the rotating coordinate system $K_{F1}(x_{F1}, y_{F1}, z_{F1})$ can be written in the following form

$$\left.\begin{aligned} x_{1F} &= -\eta \cdot \sin\vartheta \\ y_{1F} &= \eta \cdot \cos\vartheta \cdot \\ z_{1F} &= p \cdot \vartheta - \sqrt{\rho_{ax}^2 - (K-\eta)^2} \\ t_{1F} &= t_{sz} = 1 \end{aligned}\right\}, \tag{1}$$

where η and ϑ are parameters of the helicoidal surface, p is the screw parameter of the helix on the worm, ρ_{ax} is the radius of the tooth profile in axial section, K is the distance between the centre of profile circle and worm ace.

The cutting edge V of the hob created from the worm can be obtained as an intersection of the backward grinded side surface R and the face surface H, while it must fit the replacing worm surface.

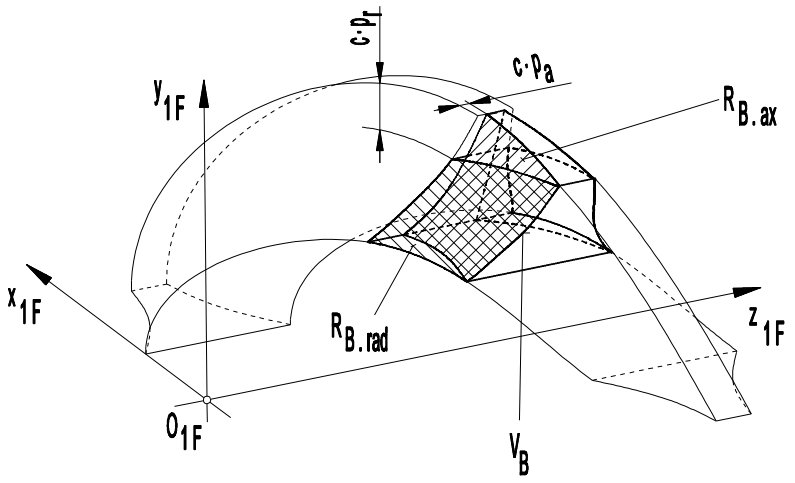

Figure 2 The cutting edge of the tooth surfaces of the hob in the rotation coordinate system [5]

The equation of the face surface is

$$\left.\begin{aligned} x_h &= -\eta \cdot \sin(\vartheta + \varphi_{oh}); \\ y_h &= +\eta \cdot \cos(\vartheta + \varphi_{oh}); \\ z_h &= -p_h \cdot \sin(\vartheta + \varphi_{oh}); \end{aligned}\right\} \tag{2}$$

The cutting edge V can be obtained as an intersection of the three surfaces:

- the relief side surface R, and/or Rb;
- the face surface H;
- the tooth surface of the substituting worm J and/or B.

The equation of the cutting edge in the examined case is the following:

$$\left.\begin{aligned} x_v &= -\eta \cdot \sin \frac{\sqrt{\rho_{ax}^2 - (K-\eta)^2} - z_{ax}}{p + p_h} \\ y_v &= \eta \cdot \cos \frac{\sqrt{\rho_{ax}^2 - (K-\eta)^2} - z_{ax}}{p + p_h} \\ z_v &= -p_h \cdot \frac{\sqrt{\rho_{ax}^2 - (K-\eta)^2} - z_{ax}}{p + p_h} \end{aligned}\right\} \quad (3)$$

We have done an analysis method of the wearing of the cutting edge of the hob in case of arched worm in our research work.
The wearing of the cutting edge of the hob is checked by CCD cameras in the production process to achieve precision manufacturing.

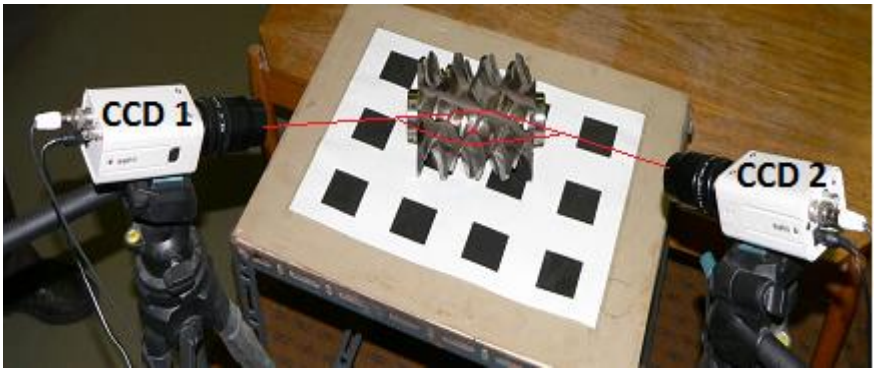

Figure 3 The measuring of the cutting edge with correctly placed CCD cameras

2. THE METHOD OF CORRECTLY PLACED CCD CAMERAS

There is a possibility for in-process cutting edge monitoring dimension inspection. During picture evaluation by machines the reconstruction of the cutting edge from two pictures without other information is not guaranteed. Correctly placed CCD cameras can solve this problem [3]. Our method describes the possibility to achieve such positions of CCD cameras, in which the reconstruction of the spatial curve can be carried out only with two pictures are fitted to the cutting edge of the hob. We consider the two pictures done by perpendicularly placed CCD cameras, as a Monge-projection of the cutting edge of the hob.
The representation of a point in Monge projection unambiguous provided the well-known conventions are fulfilled [9]. For example the representation of a circle of general position and the profile line is not bijective [9, 10]. Two perpendicular projections are not different in practice, if they can be translated to each other [4, 5, 6, 7].
We consider those Monge projections identical, which can be translated to one another. Projection lines and image planes go through the origin point in a fixed Descartes coordinate system. The Monge projections are determined by their projection lines [10]. The number of Monge projections to a given curve can be described by using three free real parameters that we have defined (Figure 4). The first direction angel is α and β is the second direction angel of the first projection line v_1,

and γ is the third direction angel of the second projection line of v_2. The triplet of all numbers (α, β, γ), which gives the Monge projection, creates the Monge cuboid.

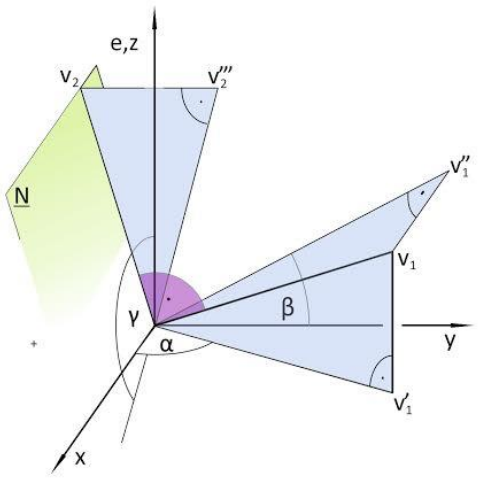

Figure 4 The first direction angel α and the second direction angel β of the first projection line v_1 and the third direction angel γ of the second projection line v_2 [10]

The inner points of the Monge cuboid satisfy the following condition

$$0<\alpha<\pi,\ 0<\beta<\pi/2,\ \pi/2<\beta<\pi,\ 0<\gamma<\pi. \tag{4}$$

The border points on the Monge cuboid satisfy the following conditions

- $0<\alpha<\pi,\ \beta=\pi,\ 0<\gamma<=\pi,$
- $0<\alpha<\pi,\ 0<\beta<\pi/2,\ \pi/2<\beta<=\pi,\ \gamma=\pi,$
- $\alpha=\pi,\ \beta=\pi/2,\ 0<\gamma<\pi/2,\ \pi/2<\gamma<\pi,$
- $\alpha=0,\ \beta=\pi/2,\ \gamma=\pi/2$
- $\alpha=\pi,\ \beta=0,\ \gamma=\pi.$ (5)

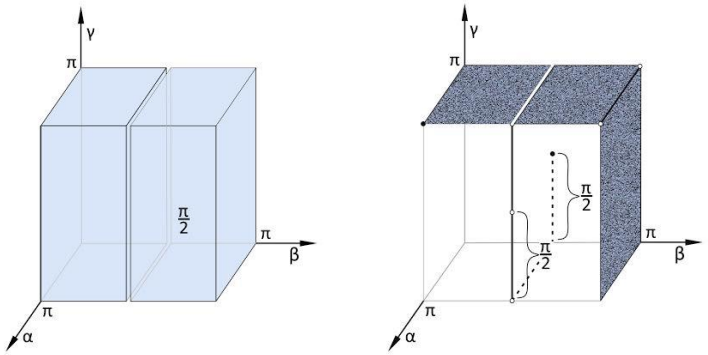

Figure 5 The inner points and border points of the Monge cuboid [10]

This method does not discuss all Monge projections, but discusses all two perpendicular projections, which is relevant in engineering work. The examination of the bijectivity with respect to a given curve gives us the same result if the first and second images are changed.

If the Monge projection of the curve of the cutting edge of the hob does not have a tangent in the situation of the profile line, then any part of the curve can be reconstructed from two pictures without any further information. All these situations provide us with correctly placed CCD cameras.

3. THE METHOD OF THE CUTTING EDGE ANALYSIS

Using cubic interpolation Bezier curve fitted to the cutting edge of the hob is recommended to do the examination in our research work [8]. Fitting the cubic Bezier curve to proportionally selected four points on the cutting edge gives us a correctly approaching spatial curve.

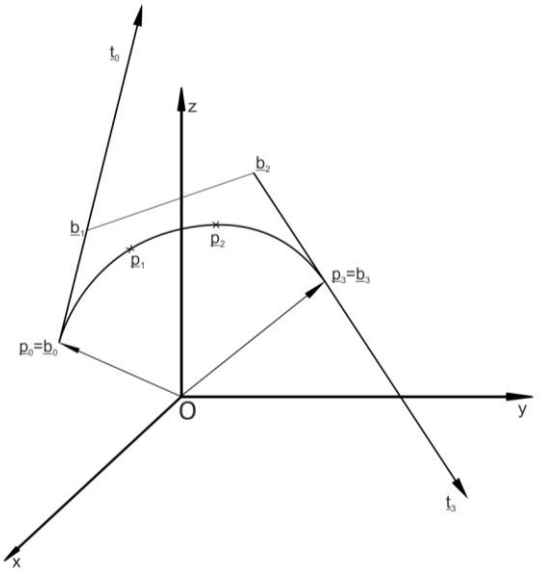

Figure 6 The connection of the Hermite arc and the Bezier curve

The Bezier curve is interpolated to the given points $\underline{p}_0$, $\underline{p}_1$, $\underline{p}_2$, $\underline{p}_3$ using parameters u_0, u_1, u_2, u_3, where $u_i \neq u_j$, if the $i \neq j$, and $u_0 = 0$, $u_3 = 1$.
We are looking for control points $\underline{b}_0$, $\underline{b}_1$, $\underline{b}_2$, $\underline{b}_3$, that determine the Bezier curve fitting to points $\underline{p}_0$, $\underline{p}_1$, $\underline{p}_2$, $\underline{p}_3$, so

$$\underline{b}(u_i)=\underline{p}_i \quad (i=0,\ldots,3). \tag{6}$$

The equation of the Bezier curve is determined in the following formula

$$\underline{b}(u)=\sum_{j=0}^{n} B_j^n(u)\,\underline{b}_j\,, \tag{7}$$

where $B_j^n(u)=\binom{n}{j}u^j(1-u)^{n-j}$ are Bernstein polynomial.

As it was mentioned earlier, the Bezier curve fitting to given points can be described in the following equation in case (i=0,...,3)

$$\underline{b}(u_i)=\sum_{j=0}^{n} B_j^n(u_i)\,\underline{b}_j\,. \tag{8}$$

Using the $\underline{b}(u_i)=\underline{p}_i$ (i=0,…,3) equation we can get the following linear inhomogeneous equation system

$$\begin{bmatrix} \underline{p}_0 \\ \underline{p}_1 \\ \underline{p}_2 \\ \underline{p}_3 \end{bmatrix} = \begin{bmatrix} B_0^3(u_0) & B_1^3(u_0) & B_2^3(u_0) & B_3^3(u_0) \\ B_0^3(u_1) & B_1^3(u_1) & B_2^3(u_1) & B_3^3(u_1) \\ B_0^3(u_2) & B_1^3(u_2) & B_2^3(u_2) & B_3^3(u_2) \\ B_0^3(u_3) & B_1^3(u_3) & B_2^3(u_3) & B_3^3(u_3) \end{bmatrix} \cdot \begin{bmatrix} \underline{b}_0 \\ \underline{b}_1 \\ \underline{b}_2 \\ \underline{b}_3 \end{bmatrix}. \quad (9)$$

The $u_i \neq u_j$ condition provides us with the result of the unambiguous solution to $\underline{b}_i$. So we receive the $\underline{b}_i$ control points of the interpolation Bezier curve fitting to point $\underline{p}_0$, $\underline{p}_1$, $\underline{p}_2$, $\underline{p}_3$.

The connection between the Bezier curve and the Hermite arc can be written in the following formula

$$\begin{aligned} \underline{p}_0 &= \underline{b}_0, \\ \underline{t}_0 &= 3\cdot\underline{b}_1 - 3\cdot\underline{b}_0, \\ \underline{p}_3 &= \underline{b}_3, \\ \underline{t}_3 &= 3\cdot\underline{b}_3 - 3\cdot\underline{b}_2. \end{aligned} \quad (10)$$

when the Hermite arc are given with points $\underline{p}_0$, $\underline{p}_3$ and then tangents $\underline{t}_0$, $\underline{t}_3$, where $u\in[0,1]$.
The Hermite arc can be written in parametric form, as

$$\underline{r}(u)=\underline{a}_3\cdot u^3+\underline{a}_2\cdot u^2+\underline{a}_1\cdot u+\underline{a}_0, \quad (11)$$

Tangent vectors can be described in the following form

$$\underline{r}_e(u) = \underline{e}_1\cdot u^2 + \underline{e}_2\cdot u + \underline{e}_3 \quad (12)$$

If we shift tangent vectors to the origin point O, we get the cone of tangents. If profile planes of Monge projections fit in the origin point, they have two, one or zero generator lines of the cone of tangents. If the profile plane of a Monge projection do not contain a tangent vector of the cone of tangents, the description of any part of the curve is bijective.

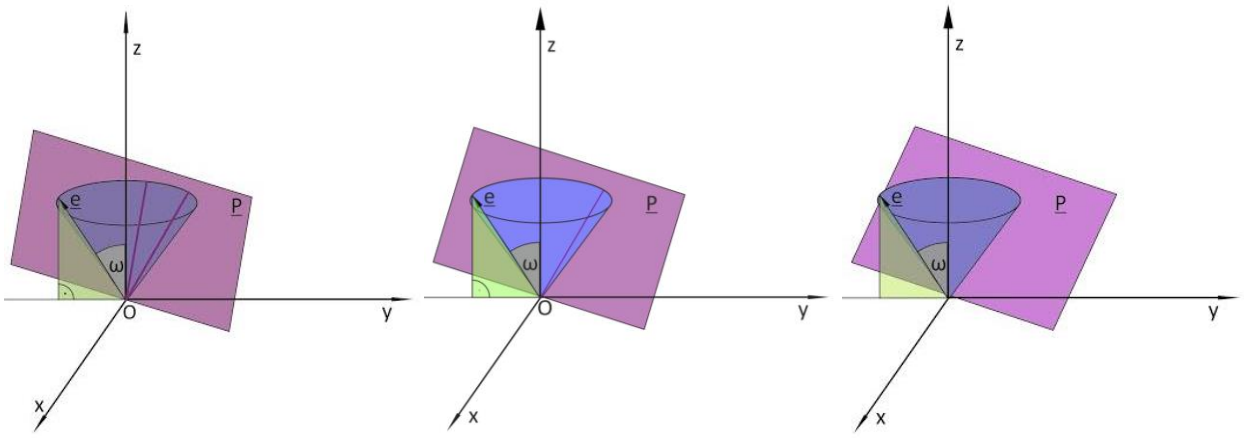

Figure 7 The profile plane contains one or two tangent vectors and does not contain a tangent vector of the Hermite arc

If the profile plane of the Monge-projection of the spatial curve does not contain a tangent vector of the curve, the description of any part of the curve is bijective [1, 10].
Normals $\underline{n}$ (n_x, n_y, n_z) of these planes are perpendicular to the tangents that satisfy the following equation:

$$\underline{n} \cdot \underline{r}_e(u) = 0, \tag{13}$$

We are looking for normal vectors $\underline{n}$ (n_x, n_y, n_z) of profile planes of Monge projections, to which the equation of the second degree considering u in case the given e_{ij} does not have any solutions. In this case the profile planes do not have tangent vectors of the given curve, so the description of the curve is bijective.
The condition can be written in a simplified way in the following form

$$c_1 \cdot n_x^2 + c_2 \cdot n_y^2 + c_3 \cdot n_z^2 + c_{12} \cdot n_x \cdot n_y + c_{13} \cdot n_x \cdot n_z + c_{23} \cdot n_y \cdot n_z < 0 \tag{14}$$

where

$$\begin{aligned} c_1 &= e_{2x}^2 - 4 \cdot e_{1x} \cdot e_{3x}, \\ c_2 &= e_{2y}^2 - 4 \cdot e_{1y} \cdot e_{3y}, \\ c_3 &= e_{2z}^2 - 4 \cdot e_{1z} \cdot e_{3z}, \\ c_{12} &= 2 \cdot e_{2x} \cdot e_{2y} - 4 \cdot e_{1x} \cdot e_{3y} - 4 \cdot e_{1y} \cdot e_{3x}, \\ c_{13} &= 2 \cdot e_{2x} \cdot e_{2z} - 4 \cdot e_{1x} \cdot e_{3z} - 4 \cdot e_{1x} \cdot e_{3z}, \\ c_{23} &= 2 \cdot e_{2y} \cdot e_{2z} - 4 \cdot e_{1y} \cdot e_{3z} - 4 \cdot e_{1z} \cdot e_{3y}. \end{aligned} \tag{15}$$

Bijective Monge projections are determined by points from the border of the Monge cuboid, which points satisfy the following condition:

If $\alpha=\pi$, $\beta=0$, $\gamma=\pi$, or $\alpha=0$, $\beta=\pi/2$, $\gamma=\pi/2$, or $\alpha=\pi$, $\beta=\pi/2$, $0<\gamma<\pi/2$, $\pi/2<\gamma<\pi$, the

$$c_2 < 0 \tag{16}$$

condition give us bijective Monge projections of the given curve.
If $0<\alpha<\pi$, $\beta=\pi$, $\gamma=\pi/2$, the

$$c_3 < 0 \tag{17}$$

condition give us bijective Monge projections of the given curve.
If $0<\alpha<\pi$, $\beta=\pi$, $\gamma=\pi$, the

$$c_1 \cdot \sin^2\alpha + c_2 \cdot \cos^2\alpha - c_{12} \cdot \sin\alpha \cdot \cos\alpha < 0 \tag{18}$$

condition give us bijective Monge projections of the given curve.
If $0<\alpha<\pi$, $\beta=\pi$, $0<\gamma<\pi/2$, $\pi/2<\gamma<\pi$, the

$$c_1 \cdot \sin^4\alpha/tg^2\gamma + c_2 \cdot \cos^2\alpha \cdot \sin^2\alpha/tg^2\gamma + c_3 - c_{12} \cdot \cos\alpha \cdot \sin^3\alpha/tg^2\gamma + c_{13} \cdot \sin^2\alpha/tg\gamma - c_{23} \cdot \cos\alpha \cdot \sin\alpha/tg\gamma < 0 \tag{19}$$

condition give us bijective Monge projections of the given curve.

If $\alpha=\pi/2$, $0<\beta<\pi/2$, $\pi/2<\beta<\pi$, $\gamma=\pi$, the

$$c_1 < 0 \tag{20}$$

condition give us bijective Monge projections of the given curve.
If $0<\alpha<\pi/2$, $\pi/2<\alpha<\pi$, $0<\beta<\pi/2$, $\pi/2<\beta<\pi$, $\gamma=\pi$ the

$$c_1 + c_2\cdot(tg\gamma - ctg\beta\cdot ctg\alpha)^2/(ctg\beta+ctg\alpha\cdot tg\gamma+tg\beta)^2 + c_3\cdot ctg^2\alpha/(-tg\beta-ctg\beta)^2 + c_{12}\cdot(tg\gamma-ctg\beta\cdot ctg\alpha)/(ctg\beta+ctg\alpha\cdot tg\gamma+tg\beta) + c_{13}\cdot ctg\alpha/(-tg\beta-ctg\beta) + c_{23}\cdot ctg\alpha\cdot(tg\gamma - ctg\beta\cdot ctg\alpha)/(ctg\beta + ctg\alpha\cdot tg\gamma + tg\beta)\cdot(-tg\beta - ctg\beta) < 0 \tag{21}$$

condition give us bijective Monge projections of the given curve.
If $\alpha=\pi/2$, $0<\beta<\pi/2$, $\pi/2<\beta<\pi$, $\gamma=\pi/2$ esetén $\underline{n}(0, -\sin\beta, \cos\beta)$, the

$$c_2\cdot\sin^2\beta + c_3\cdot\cos^2\beta - c_{23}\cdot\sin\beta\cdot\cos\beta < 0 \tag{22}$$

condition give us bijective Monge projections of the given curve.
If $\alpha=\pi/2$, $0<\beta<\pi/2$, $\pi/2<\beta<\pi$, $0<\gamma<\pi/2$ $\pi/2<\gamma<\pi$

$$c_1 + c_2\cdot tg^2\gamma/(tg\beta+ctg\beta)^2 + c_3\cdot tg^2\gamma\cdot ctg^2\beta/(-tg\beta-ctg\beta)^2 + c_{12}\cdot tg\gamma/(tg\beta+ctg\beta) + c_{13}\cdot tg\gamma\cdot ctg\beta/(-tg\beta-ctg\beta) + c_{23}\cdot tg^2\gamma\cdot ctg\beta/(tg\beta+ctg\beta)\cdot(-tg\beta-ctg\beta) < 0 \tag{23}$$

condition give us bijective Monge projections of the given curve.
If $0<\alpha<\pi/2$, $\pi/2<\alpha<\pi$, $0<\beta<\pi/2$,$\pi/2<\beta<\pi$, $\gamma=\pi/2$ the

$$c_1\cdot(tg\alpha\cdot ctg\gamma + tg\beta + tg\alpha\cdot tg^2\beta\cdot ctg\gamma)^2/(-ctg\alpha - tg\beta\cdot ctg\gamma - tg\alpha)^2 + c_2\cdot(tg\alpha\cdot tg\beta - ctg\gamma)^2/(-ctg\alpha - tg\beta\cdot ctg\gamma - tg\alpha)^2 + c_3 + c_{12}\cdot(tg\alpha\cdot ctg\gamma + tg\beta + tg\alpha\cdot tg^2\beta\cdot ctg\gamma)\cdot(tg\alpha\cdot tg\beta - ctg\gamma)/(-ctg\alpha - tg\beta\cdot ctg\gamma - tg\alpha)^2 + c_{13}\cdot(tg\alpha\cdot ctg\gamma + tg\beta + tg\alpha\cdot tg^2\beta\cdot ctg\gamma)/(-ctg\alpha - tg\beta\cdot ctg\gamma - tg\alpha) + c_{23}\cdot(tg\alpha\cdot tg\beta - ctg\gamma)/(-ctg\alpha - tg\beta\cdot ctg\gamma - tg\alpha) < 0. \tag{24}$$

condition give us bijective Monge projections of the given curve.

CONCLUSIONS

The aim of the paper was to reconstruct the cutting edge of the hob without any further information is achieved.
The theorem of the insurance of the bijectivity between the spatial curve and its two perpendicular images was shown in this article. Furthermore, the correct positions of the cameras to reconstruct the interpolated curve fitting to the cutting edge of the hob were calculated. The right positions of the CCD cameras can check the wearing in the production process without other information in the gear box.

REFERENCES

[1] Balajti, Zs.: *Examination of the bijectivity of the Monge projection*, (in Hungarian) dr. univ. dissertation, First draft, 1995. Miskolc. 84 p.
[2] Balajti, Zs., Bányai, K.: *A possibility method for the solve of 3D evaluation with 2 CCD cameras,* Miskolc, Production Process and Systems, A Publication of the University of

Miskolc, Miskolc University Press, 2004, HU ISSN 1215-0851 : 237-242.

[3] Bodzás, S., Dudás, I.: *Mathematical model for investigation of face gear tooth surface manufactured by new cutting edges of spiroid hob having arched profile in axial section*, Machine Design, Volume 6, Numbers 1, Novi Sad, Szerbia, 2014, ISSN 1821-1259: 1 - 4.

[4] Drahos, I.: *The Two-view Drawing in the Epoch of Computational Geometry*, Proceedings ICEGDG Vienna 1998, vol.l.: 117-121.

[5] Dudás, I.: *The Theory & Practice of Worm Gear Drives*, Kogan Page US, Sterling, USA, 2004, ISBN 1 9039 96619 9, p. 320

[6] Dudás I., Balajti, Zs., Bányai K.: *Accurate Production of Helicoid Surfaces*, III. International Congress of Precision Machining Vienna-Austria, 2005, pp. 27-32.

[7] Dudás, I., Bodzás, S., Balajti, Zs.: *Geometric analysis and computer aided design of cylindrical worm gear drive having arched profile*, International Journal of Innovative Research in Engineering & Management (IJIREM), ISSN: 2350-0557, Volume-2, Issue-5, 2015, pp. 10-14.

[8] T026566 sz. OTKA (2002) *Development of CCD cameras systems to the area of machin industry*, Miskolc, (Research Leader: Prof. Dr. Dr. h. c. Dudás I. DSc.)

[9] Petrich, G.: *Ábrázoló geometria (in Hungarina) Descriptive Geometry*, Budapest, 1973, p. 413.

[10] Óváriné Balajti, Zs.: *A Monge ábrázolás bijektivitásának elméleti elemzése és alkalmazása a mérnöki gyakorlatban (in Hungarian) Theoretical examination of Monge projection and application in engineering practice*, Miskolc, Gazdász-Elasztik Kft. kiadása, 2015, ISBN: 978-963-358-097-4, p. 101

INTERNATIONAL SCIENTIFIC CONFERENCE ON ADVANCES IN MECHANICAL ENGINEERING

19 November 2015, Debrecen, Hungary

PLANNING OF EXPERIMENTS IN ORDER TO DETERMINE THE RELATIONSHIP BETWEEN THE HEAT TREATMENT AND DURABILITY OF CULTIVATOR TINES

PÁLINKÁS Sándor PhD, GINDERT-KELE Ágnes PhD, GAJDÁN Bence

Department of Mechanical Engineering, Faculty Engineering, University of Debrecen
E-mail: palinkassandor@eng.unideb.hu, battane@eng.unideb.hu, gajdanb@gmail.com

Abstract
The efficiency of agricultural activity is significantly influenced by the condition of power machines used in the agricultural production. Among others, the formation and maintenance of suitable soil-conditions play a very important role in obtaining the desired harvest yield. The implement tools of tillers are exposed to an extraordinary high load and a significant wear, therefore it is necessary to investigate the relationship between their heat treatment and durability. The individual production process of a cultivator tine mounted on an agricultural cultivator is described in our present paper. The purpose of our research work is to change the old, worn cultivator tines to tines having a longer durability; different heat-treatment technologies have been developed in order to realize our aim. The products made by us will be used in the agricultural production in the future therefore, the type of heat treatment technology to be used during the production can be determined. As a cultivator is equipped with a lot of cultivator tines, the expenses can be decreased significantly by the use of cultivator tines made by a well-chosen heat-treatment technology and a higher yield/agricultural area can be obtained during the cultivation.

Keywords: *agricultural, forging, cultivator tines, heat treatment, durability.*

1. INTRODUCTION

The samples were made in Márton Gajdán's forge-shop who is a forgeman in Hajdúböszörmény and has been working in this field for 40 years. The hand forging is a plastic deformation technology which demands a significant practical knowledge and this tradition is handed down from father to son. In the first period of his career, the forgeman dealt mainly with horseshoeing later coaches, forged iron fences, ballustrades and furniture-accessories were made by him. As Hajdúböszörmény is an agricultural town, the agricultural forging e.g. the renewal of cultivators, the making and sharpening of cultivator tines have always belonged to his sphere of activity.
The cultivator tines were made by using the free-forming hand forging technology. The drop-forging is more economic in case of high number of samples but it was necessary to make only a few samples for our experiments therefore these samples were made by hand forging.

2. DESCRIPTION OF THE FUNCTION OF CULTIVATOR TINES

The specimen to be made is a cultivator tine alias a duck-foot which is mounted on a cultivator. The cultivators (Fig. 1) are tillers which are suitable for doing a lot of different tasks. The implement tools of cultivator can be very different. The soil can be broken up and mixed by them moreover they can act as a weeding machine as well therefore they play a very important role in the preservation of the soil structure and in the process of the care of the crop moreover in the process of plant protection. The cultivator tines having a duck-foot shape can also be used on the cultivators operating in the plough lands and on the cultivators performing the within-the-row cultivation.

Figure 1 Agricultural cultivator [4]

The plough-land cultivators can also be used for the dressing of surface of ploughed land, for preparing the seedbed and for stubble-ploughing on a friable soil. The effect of weed control is good in case if the cultivator tines with a duck-foot shape arranged in many rows are placed by an overlapping of 40-60 mm. As a result of their operation, the soil can be broken up uniformly without dust- and clod-formation. The dressing depth is usually 8-12 cm. The weed control and soil loosening can be done in the between-the-rows of row crops of higher row distance by means of the within-the-rows cultivators. By this, it becomes possible to use less weed killer as merely the vicinity of plant rows has to be treated by using chemical agents. The cutting of the roots of starting up furrow-weeds can also be ensured by the shallow tilling (20-40 mm).
The cultivator tines are similar to the duck-foot, they are mounted by their tip ahead; the roots of weeds are cut by the cutting edge. As the back edge of tine is placed at a higher position as compared to the cutting edge, it elevates and breaks the soil. As a consequence, the parts of roots being under the surface tilt on the surface. The duck foot tines deliver the soil laterally during their operation.

3. DEVELOPMENT OF THE FREE-FORMING FORGING TECHNOLOGY OF CULTIVATOR TINES

A worn cultivator tine can be seen in Fig. 2; a hard, abrasion-proof layer was developed on it by a surface-layer welding on the edges in order to increase the durability. At the beginning of our research work, we did not want to use the surface-layer welding instead the effect of the different heat treatment processes on the durability of tines were investigated by using 5 samples.
As the worn cultivator tine was not suitable for determining the original size, a new cultivator tine was purchased by us. The experimental tines were manufactured by the forgeman by taking into consideration the new tine-pattern (Fig. 3).

Figure 2 Worn cultivator tine

Figure 3 Pattern

3.1. The selection of material

The basic material is a hot-rolled sheet of a grade of C60. The heat-treatability is a very important aspect when selecting the material.

3.2. Flattening of the existing pattern (Fig. 4)

The flattening is necessary in order to determine the exact size and shape of the initial sample. Later this flattened sample is contoured on the material to be cut. The flattening is made in hot conditions. Cracks can develop in the sample in case if the sample is not heated up enough.

Figure 4 The process of aligning

3.3. Cutting

The templet the size of which is equal to the aligned pattern is put on the sheet to be cut and is contoured by using a scribe then the line obtained during contouring is dotted by using a punch in order that the line of cutting can well be seen even in case if the workpiece is hot. A hole corresponding to the radius of pattern is made by means of a worm auger of a size of 13 before cutting. Owing to the radius of this hole, a rounded part is obtained; it was necessary to create this part because we can cut only cornerwise by using the chisel-hammer. The cutting takes place on the anvil by means of the chisel-hammer. In this case we need an assistant who beats the cutting device kept by the forgeman by means of a sledge-hammer. It is a time-consuming process as the material has to be warmed up many times in order that it can be cut to the desired shape and size (Fig. 5).

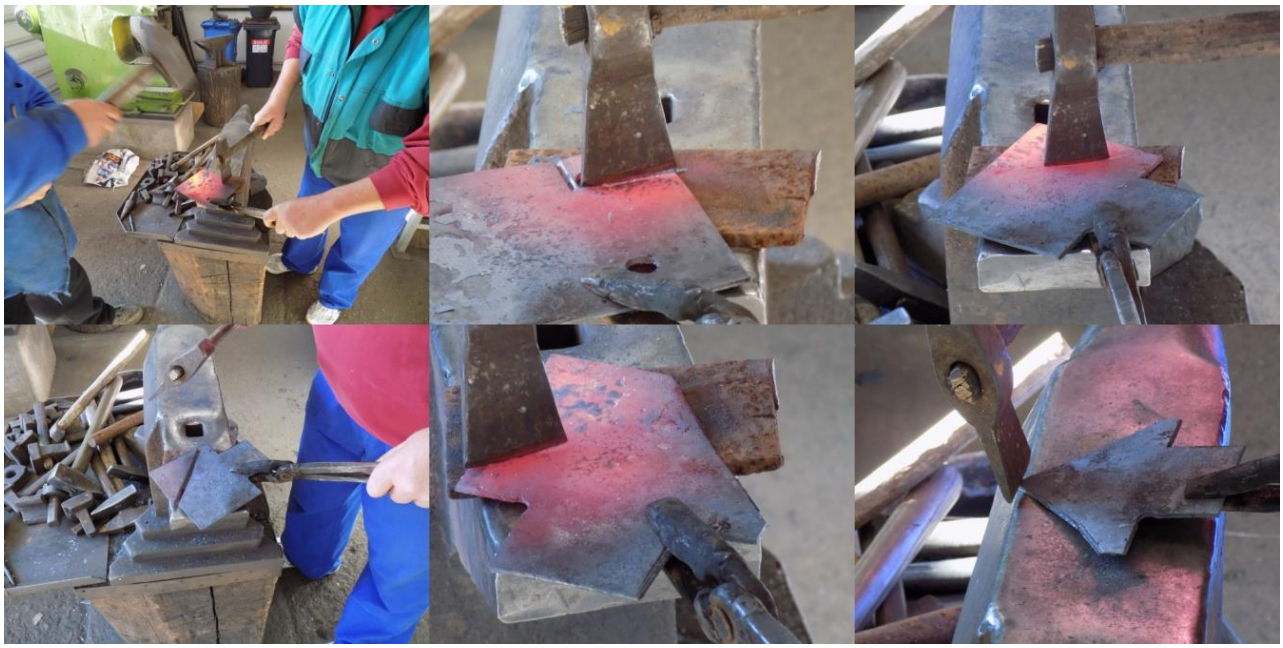

Figure 5 The process of cutting

3.4. Flash-removal

The sharp parts remaining on the cut workpiece during cutting can be removed by using a rasp or a hand grinder.

3.5. Punching, pricking of a square

The punching is made on a hot sample by means of a handled puncher. The punching can be made from one or two sides. A two-side punching was used by us during manufacturing. The puncher has got a cone-shape in order that it can be lifted more easily. First the puncher is hammered into one side of the workpiece at the indicated point. In this case, a black, colder part develops on the other side of hammering. We have to perform the hammering quickly on the other side in order to avoid the rising of temperature of this black part because in this case the exact place where the puncher shall be put cannot be seen. In case of an exact punching, the puncher pushes out the flash and the hole is made. Then it is necessary to warm up the workpiece again and a plunger the diameter of which corresponds to the desired diameter of hole is pierced through the existing hole. Afterwards the square plunger is pierced through.

3.6. Bending in hot conditions by means of a special service tool

The punched workpiece cut in size is bended into a semicircle shape at the place of clamping at the suitable temperature by means of a special service tool. Then the desired shape of tine is formed by the same warming. In the course of bending, a tensile stress develops in the external bar and a compression stress develops in the internal bar and the neutral bar is stress-free. In accordance with the mechanical stresses, the external layers of bended part become elongated and the internal parts shorten so the shape of bended section becomes strain as well: e.g. the cross-section of circle becomes a skew ellipse and the square becomes a trapeze. The change developing in the bended cross section shall be eliminated by flatting and smoothing after bending.

3.7. Sharpening/straining

The edges of the cultivator tine are formed by straining. After warming up, the workpiece is elongated by uniform knocks on the anvil by means of the thinner part of hammer. So a thinner part, the edge of tine develops. Then it can sharpen by using a rasp or a hand grinder if necessary.

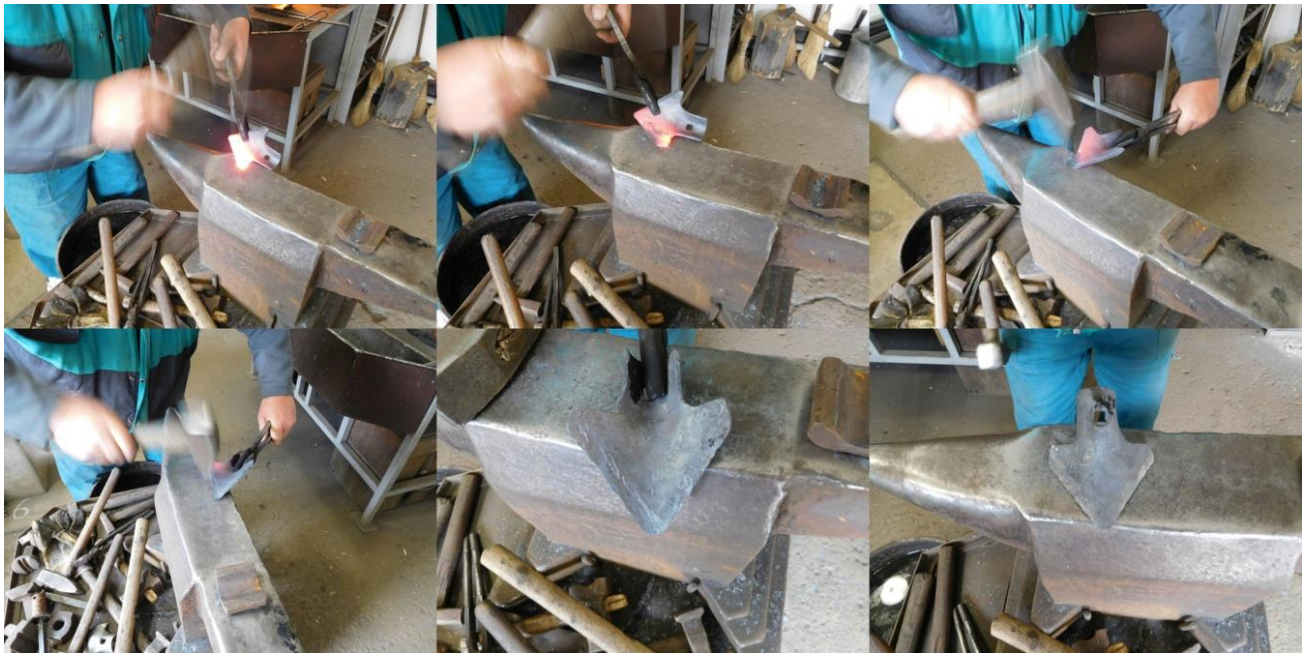

Figure 6. The formation of edges by drawing out

4. HEAT TREATMENT

In the course of developing the heat treatment technology, two types of heat treatment processes were used namely the hardening and annealing processes.
The hardening process consists of the austenitizing procedure followed by chilling with the purpose of increasing the hardness, abrasion resistance and strength. The temperature and duration of austenitizing process as well as the cooling velocity depend on the steel grade. The hardening temperature-range of unalloyed steels is A3+50 °C (hypoeutectoid steels) or A1+50 °C (hypereutectoid steels). The hardened martensitic structure is rigid. This rigidity can be decreased by annealing. The strength of hardened material decreases and its toughness increases by increasing the annealing temperature. The duration of annealing has got a similar effect as well. In case of

hard, abrasion-proof parts, our purpose is to maintain the martensitic structure. In this case, the workpiece is heated to a temperature at which the structure does not change but the own stresses disappear (180-200 °C). This process is called annealing at a low temperature.

Table 1: The planned heat treatment

No. of sample	*Planned heat treatment*
1.	The sample cools on free air
2.	Hardening of edges
3.	Hardening and annealing of edges (tempering)
4.	Hardening of the entire surface
5.	Hardening and annealing of the entire surface (tempering)

CONCLUSIONS

The purpose of our research work has been realized; the free-forming forging technology of cultivator tines of duck-foot shape has been planned then patterns have been made for experimental purposes in order to promote the research work done by the Department of Mechanical Engineering of Faculty of Engineering of University of Debrecen. The cultivator tines having a duck-foot shape were heat treated by different methods in order to determine the relationship between their duration and heat treatment. One of our aims in the future is to produce a hard, abrasion-proof layer on the edges of cultivator tines of duck-foot shape by means of deposition welding and to investigate its effect on their duration. Owing to the fact that the quality of soil is excellent in Hungary, the agriculture plays a determining role in the economic life of our country therefore the aforementioned research work aiming at increasing the productivity is of an extraordinary great importance.

REFERENCES

[1] Kiss, E.: *Képlékeny alakítás*, Tankönyvkiadó, Budapest, 1991.
[2] Forging Design Handbook. American Society for Metals, Ohio, 1972.
[3] Szabó, L.: *Szabadalakító kovácsolás*, Miskolc, 2001, http://www.uni-miskolc.hu/~wwwfemsz/szabkov.htm
[4] http://static.mascus.com/image/product/large/ff06fb96/other-caldiz-sorkozmuvelo-kult,409ac3f8.jpg

CONSIDERATION AND RESEARCH ON DIFFERENT TYPES OF PLASMA JET TECHNOLOGY

PINTYE* Gábor, *ACHIMAŞ Gheorghe PhD, PATAI Gavril

Department of Manufacturing Engineering, Technical University of Cluj-Napoca
E-mail: pintyegabor@yahoo.com, gheorghe.achimas@tcm.utcluj.ro, gabor_patai@yahoo.com

Abstract
Plasma processing technology was first used in World War II in the US aviation factories. In the early 60s, the engineers made a new discovery, increase the jet speed by narrowing the plasma nozzle. Due to the rapid development of science engineering, the plasma technology is used today in various fields: automobile manufacturing, aerospace, automotive industry, medicine, biology, etc. In processing of plasma jet, there are two patterns: at low pressure and at atmospheric pressure. Research carried out at atmospheric pressure have their advantages: size bodies is not limited, surfaces can be modified without altering the volume properties, low temperature can avoid destroying the materials. Surface modification of plasma materials refers to changing the properties of the surface, creating surfaces with unique properties and characteristics thus improving the mechanical properties. Modification of surfaces ,,texture'' permit infiltration of adhesive thus improving mechanical resistance.

Keywords: *Plasma arc, plasma jet, superficial surface, roughness, penetration, mechanical strength.*

1. INTRODUCTION

Plasma technology is based on a simple physical principle, this phenomenon was first discovered by Irving Langmuir in 1928.
The material is presented as one of the four types of state: solid, liquid, gas or plasma. Material changes its state when applied to a power source (temperature): the solid becomes liquid, and the liquid becomes gas. If more energy is applied to a gas, it ionizes and it goes into a state of energy-rich plasma, thus, the fourth state of material [2].
It is called the state of plasma, the state obtained under certain conditions of temperature and pressure and a degree of ionization of a gas, when it reaches in a quasi-stationary state made of a mixture of ions, electrons and photons, which representing the state of the plasma.
Plasma technology is an unconventional technology comprising different processing methods: cutting and plasma arc trimming is the most common processing method and plasma welding, erosion processing plasma (drilling plasma, plasma grooving, filleting with plasma jet, rolling – assisted turning with plasma, assisted milling with plasma jet, assisted adjustment with plasma arc) and plasma metallization [5].
Research with plasma jet is dealing with the use and application of plasma jet in other method than cutting. Using the principle of operation but with a lower intensity we try to modify the surface properties, in other words not fully penetrate the material but stay at its surface.
So far it has been studied a metal sheet made of stainless steel to which an adhesive (paste-like) is applied, followed by the brazing operation.
This article presents the result of the test where a modified structural surface was obtained so the adhesive penetrates into the material studied.

Research has a vision to study another metal support covered with paint but that does not conduct electricity.

2. PLASMA GENERATOR

The plasma jet processing is the technological operation that seeks the total or partial separation of a portion of a material or in the case studied, the modification of surface ,,texture''. This operation is achieved by bombing with electrons. These electrons hit at high speed the workpiece and split molecules *(Figure 1).*

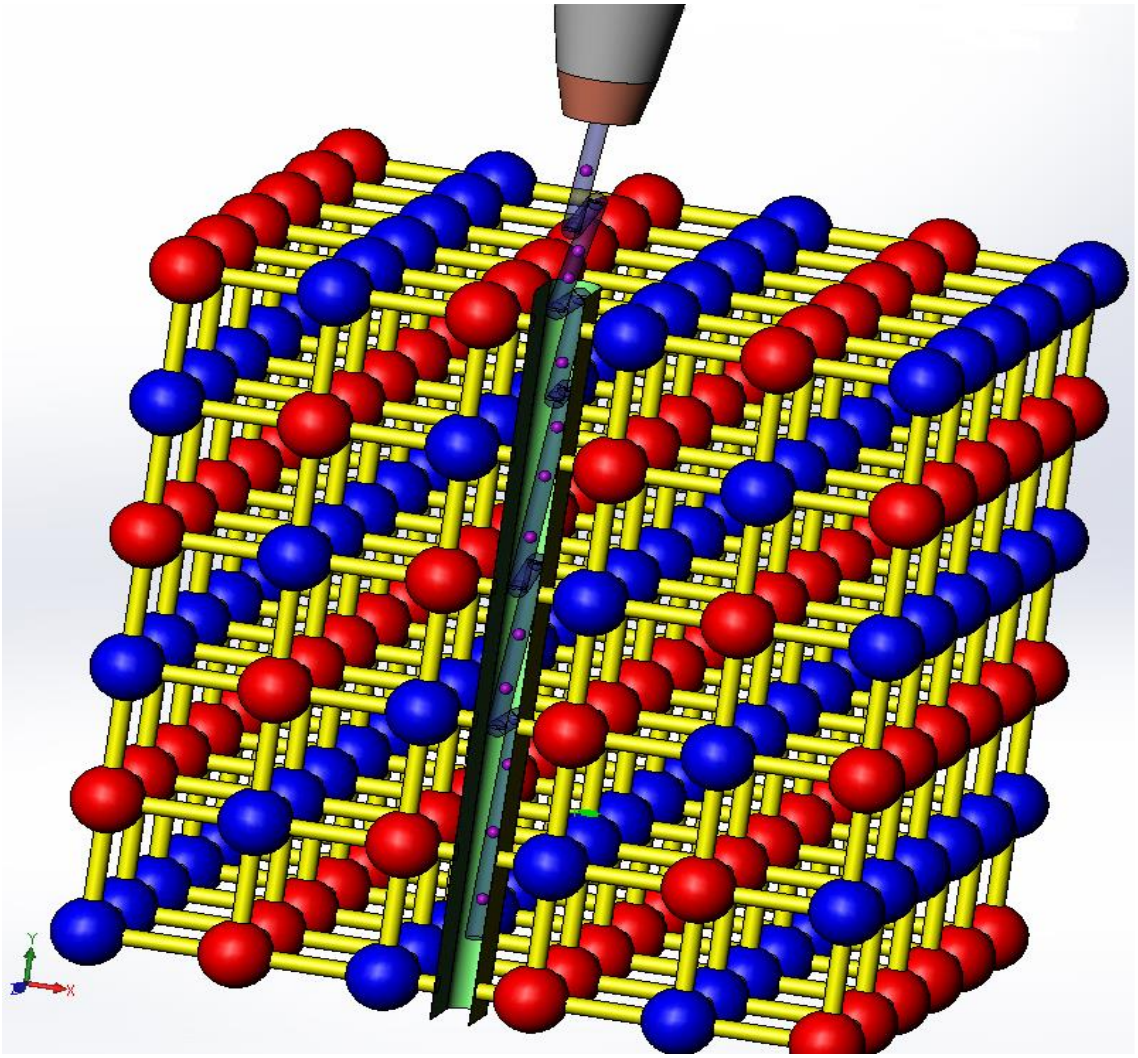

Figure 1 Electrons splitting molecular bonds and passing through molecular structure of the workpiece

To achieve bombing, plasma generators are used where two running versions are distinguished: Plasma arc, the arc burns between the cathode electrode and anode piece passing through nozzle *(Figure 2):*

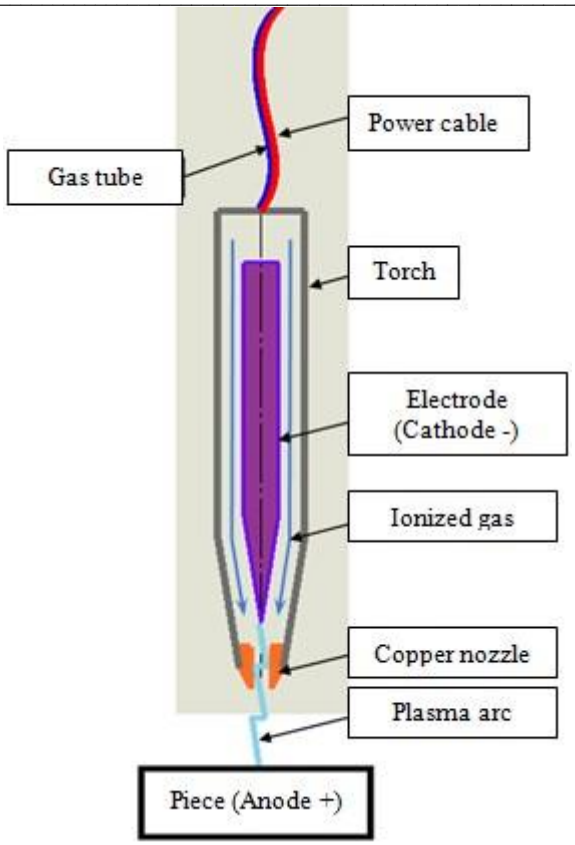

Figure 2 Plasma arc torch

The most well known technological operation with plasma arc is: cutting, trimming and welding.
In vehicle manufacturing, plasma of temperatures 5700 . . . 29700˚C (6000 . . . 30000˚K) is used, obtained following electrical discharges in gas environment through arc. *(Figure 3).* Used working gases can be: argon, hydrogen, nitrogen, helium, krypton or mixtures thereof. Plasma is developed by plasma generators, where the electric arc column is forced under a gas jet to pass through a limited space to fit a nozzle [4].
Devices used for plasma cutting can be portable, of small size *(Figure 4),* or mehanical with CNC for cutting different profiles using the CAD software *(Figure 5).*

Figure 3 Plasma arc

Figure 4 Cutting using a portable device

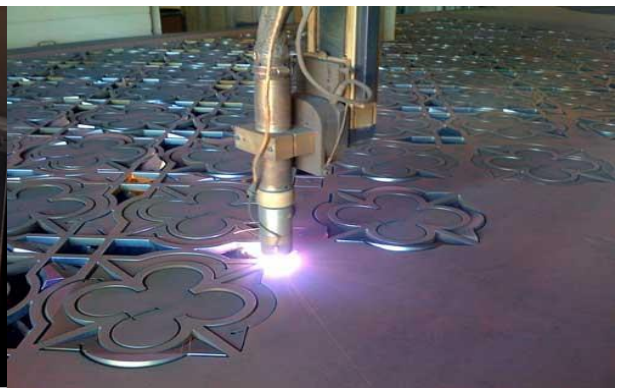

Figure 5 Cutting using a mechanical device

With plasma jet when the arc burns between the cathode electrode and anode nozzle, plasma is blown by the gas pressure as jet *(Figure 6)* [4]:

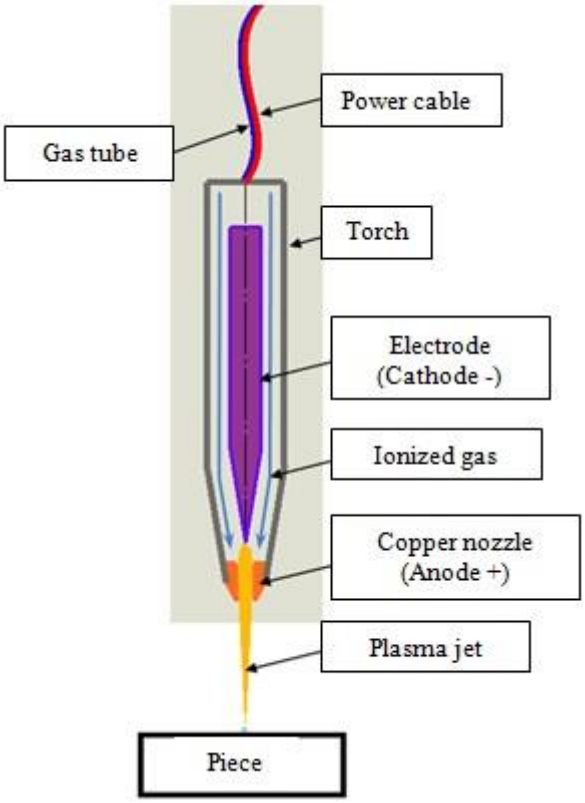

Figure 6 Plasma jet torch

Recently, new techniques for surface modification were exploited, a new alternative for processing materials surface is the plasma jet treatment. Modification of the material surface using the plasma jet refers to changing the surface properties, thus obtaining unique surfaces. *(Figure 7).* Through this method, mechanical properties can be improved.

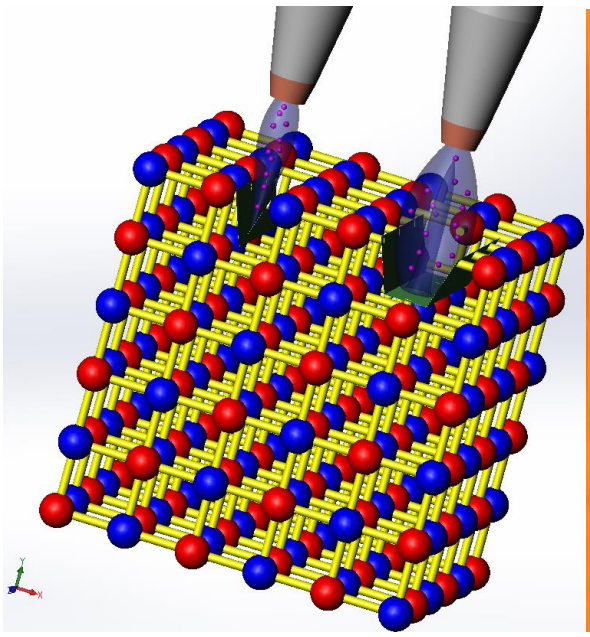

Figure 7 Electrons splitting molecular networks at superficial surface using nozzles with different fits

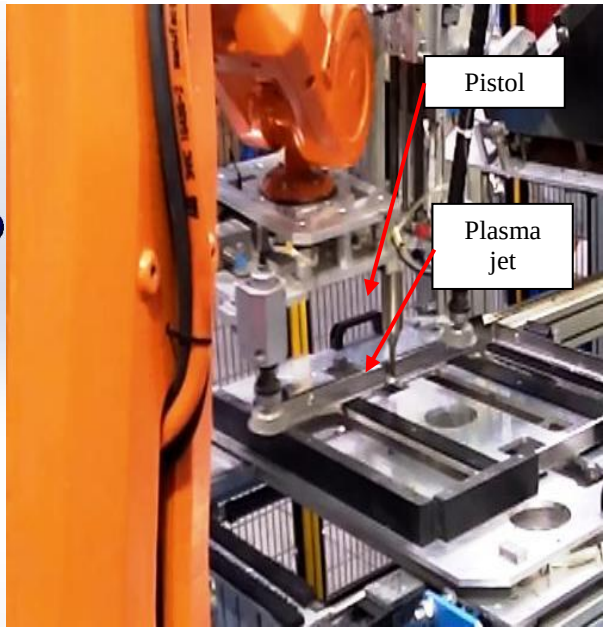

Figure 8 Apply plasma jet using an industrial robot

Due to the high speed of electron bombardment when applying the plasma jet a hissing sound that can achieve a noise level of 70 dB can be heard *(Figure 8),* depending on type of nozzle.

3. PRESENTATION OF GENERATORS PARAMETERS

At plasma technology operations there are two types of generators, for comparing their parameters we present two generators which are basic units of their category.
Powermax30 XP generator is a portable device of small size [6].
Powermax30 XP device *(Figure 9)* is designed to cut quickly and easily, while providing a high capacity for cutting thich metal and a detailed cutting on thin metal [7].

Figure 9 Powermax 30 XP device

Figure 10 FG 5001 device

FG 5001 generator is more complex as it is equipped with a transformer and a controller.
FG 5001 device *(Figure 10.)* is designed to repair or prepare areas depending on the technological operation that follows [8].
FG 5001 device has a greater advantage than Powermax30 XP allowing processing or surface treatment of materials that do not conduct electricity, for example: plastics, polymer foils, ceramics, painted surfaces, fabrics and fibers, paper, wood, etc.

Table 1

	Powermax30 XP	FG 5001
Power supply	120 - 240 V	100 - 260 V
Power generator	5,5 kW	1 kW
Supply safety	15 - 30 A	16 A
Output voltage	125 V	1 kV
Output frequency	50 - 60 Hz	15 - 25 kHz
Gas source	Air or N_2	Air
Work pressure	5 - 6 bars	Atmospheric
Work temperature	min. 1500℃	0 - 40℃
Dimensions	360x170x300	600x510x310

Analysing the parameters operating value *(Table 1)* we notice the following:
Powermax30 XP:
Disadvantage:

- a more powerful generator should be used for cutting and trimming ensuring total removal of workpiece;
- moreover, a stronger fuse is needed for current intensity;
- to fully remove the processed material it is necessary to ensure the working pressures from a compressed air network or special tubes;
- high work temperature;
- use protection equipment;
- protect work area, ignition hazard.

Advantage:

- due to its small size, it prides a high level of mobility;
- it is a simple construction with a pleasant design;
- fast and easy use;
- it is very cost effective in serial production use or households.

FG 5001device:
Disadvantage:

- due to its size and high complexity cannot be portable;
- provide a transformer to obtain high frequency;
- high cost due to its complexity.

Advantage:

- allows surface processing and treatment without altering its volume properties;
- no sparking;
- atmospheric pressure;
- ambient temperature.

4. STUDIED SURFACE FOLLOWING THE APPLICATION OF PLASMA JET

Areas were studied with a scanning electron microscope at the UT-CN Department of Materials Science and Technology.
Studied metalic support *(Figure 11)*, as a result of the plasma jet is made of stainless steel - 304-2B ASTM, (X5CrNi18-10), numeric symbol 1.430 [3].
Chemical composition:

C_{max} - 0,07%;
Si_{max} - 1 %;
Mn_{max} - 2 %;
Cr - 17-19 %;
Ni - 8-11 %;
P_{max} - 0,045 %;
S_{max} - 0,015 %.

Mechanical features:
Tensile strength: R_m=520 *MPa*.
Flow strength, flow limit: $R_{p\,0,2}$=205 *MPa*.
Elongation: *A*=40 %.

Figure 11 Studied metalic support

Steel 304-2B ASTM, (X5CrNi18-10), is the type of chromium nickel austenitic stainless steel most commonly used. Its most important property is: ductility (elongation) and tenacity, cold processing and light marking. The content of at least 7% Ni makes its structure to become fully austenitic, which provides ,,non-magnetic'' properties and a very good weldability. It is widely used in the manufacture of household appliances, industrial pipes and tanks, industrial buildings.
2B (DIN 17441) – is the most common finished surface to ensure corrosion resistance and flatness, roughness of R_a= 0,10 - 0,30 µm and max.reflectance 40 %.

Figure 12 Initial surface, enlarged by 500

Figure 13 Initial surface, enlarged by 1000

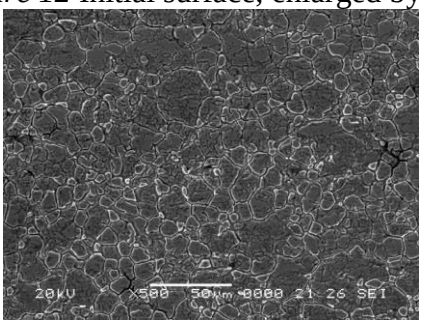

Figure 14 Treated surface, enlarged by 500

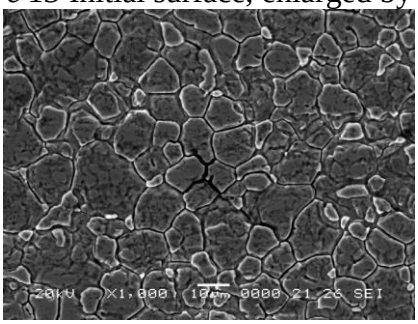

Figure 15 Treated surface, enlarged by 1000

After applying the plasma jet on the studied surface (*Figure 14-15*), we obtain some ,,craters". These craters have resulted from electron bombarding and are very useful when adhesive has to be applied, paint or other on their surface.
According to theory of mechanical connection [1] bonding between adhesive and bearing surface(or any coating, paint) is made by adhesive infiltration into the pores, asperities (roughness) of bearing surface.

CONCLUSIONS

The most common and best known plasma technology operation is cutting and trimming. We know two types of plasma generators, which also offers other kinds of processing (processing or surface treatment).
In the field of car manufacture, we tend to get finer surfaces, more smooth and less roughness. This is an upside down case, where we, distroy'' the surface but it helps us improve the mechanical properties. These damages are of microns size and helps glue or paint infiltration ensuring a better grip.
Following plasma surface treatment, areas with unique characteristics and surface properties are obtained.
Therefore, the plasma treatment is more often used in the industrial sector: automotive industry, electronic devices industry, textile industry, etc
In the medical field and biology, plasma processing allows activation of surfaces to prepare them for growth /or cell attachment or protein binding. At the same time, plasma may be used for surface sterilization of medical devices and components.

REFERENCES

[1] Balázs, Gy.: *Ragasztástechnika.* Műszaki Könykiadó. Budapest, 1982.
[2] Bâlc, N.: *Tehnologii neconvenționale.* Editura Dacia. Cluj-Napoca, 2001.
[3] Cândea, V.: *Clasificarea și simbolizarea aliajelor feroase și neferoase.* Editura U.T.PRESS. Cluj-Napoca, 2010.
[4] Făgărășan, C.: *Studii și cercetări privind utilizarea instalațiilor cu jet de plasmă la debitarea diverselor tipuri de materiale.* Teză de doctorat. UT- Cluj-Napoca, 2009.
[5] Grama, L.: ,*Principalele tehnologii neconvenționale utilizate în construcția de mașini.* - Curs, Editura Tehnică, București, 2003.
[6] http://www.plasmaserv.ro/produse/aparate-de-taiere-cu-plasma.html
[7] http://www.plasmaserv.ro/produse/aparate-de-taiere-cu-plasma/powermax-30xp.html
[8] http://www.plasmatreat.com/plasma-system-components/plasma-generators/plasma-generator-fg5001.html
[9] Solid Works, 2013.

INTERNATIONAL SCIENTIFIC CONFERENCE ON ADVANCES IN MECHANICAL ENGINEERING
19 November 2015, Debrecen, Hungary

LITERATURE REVIEW OF THE VOLUMETRIC HEAT TRANSFER COEFFICIENTS ON ROTARY DRUM DRYERS

POÓS Tibor PhD, SZABÓ Viktor

Department of Building Services and Process Engineering, Budapest University of Technology and Economics
E-mail: poos@mail.bme.hu, szabo.viktor@mail.bme.hu

Abstract
In industrial drying processes heat is usually transferred from air or flue gas to the wet material, and moisture diffuses to the drying gas simultaneously. Transfer coefficients between drying gas and material are needed to be known in order to scale up drying processes. These physical properties are generally determined by measurements. The literature defines these parameters as volumetric transfer coefficients, eliminating uncertainties in the determination of the heat transfer surface. Transfer coefficients are input data for solving differential equations which describe the drying process.

Keywords: *drying, rotary drum dryer, volumetric heat transfer coefficient, mathematical model*

1. INTRODUCTION

In the course of drying, the drying gas transfers heat to the drying material in most cases, as a consequence of which the temperature of the drying gas can be considerably reduced. Evaporation of moisture in the drying material into the drying gas significantly increases the moisture content of the drying gas. Therefore neither the temperature nor the moisture content of the drying gas can be deemed as constant ($T_G \neq$const. and Y≠const.) Under such circumstances, the motive force reduction by temperature and moisture cannot be disregarded. As opposed to a case modelled by constant gas state variables, motive force reduction leads to increasing the drying time, the contacting surface required for drying, or the length of the dryer.
In case of a continuous dryer with changing gas state variables, the input and output temperature and moisture of the drying gas considerably differ from each other. The drying process is also characterized by four main phases in case of drying in the presence of changing gas state variables.
In many cases, the geometric or evaporating surface of drying materials can only be specified clumsily and inaccurately. For the most part, a characteristic dimension of the dryer equipment – e.g. its length or height – is required to be known instead of the contacting surface size. The measure to characterize the surface of the drying material can depend on both the geometry of the dryer and the method of contact and material transport. This is the so-called specific contacting surface between the gas and the material, also used for characterizing sets:

$$a_{G-P} = \frac{dA_{G-P}}{dV_D} = \frac{dA_{G-P}}{A_D dz}, \tag{1}$$

where A_{G-P} is the contacting surface between gas and particles, V_D represents the volume of the drum dryer, A_D is the cross-section of the dryer and z is the differential length of the dryer.
In case of convection heat transfer, dryer length can be determined without presenting the development in detail [1]:

$$Z = \int_{z=0}^{z=Z} dz = \frac{-\dot{m}_G c_G}{\alpha_{G-P} a_{G-P} A_D} \int_{T_G=T_{G,in}}^{T_G=T_{G,out}} \frac{dT_G}{(T_G - T_F)}, \quad (2)$$

where α_{G-P} represents the heat transfer coefficient between gas and particles, c_G is the isobaric specific heat of the gas, T_F is the temperature of the material surface, T_G is the temperature of the gas, Z is the total length of the dryer, $\dot{m}_G$ is the mass flow of the gas.
The method of transfer units can be widely applied in cases where the contacting surface of heat transfer and / or materal transfer cannot or can hardly be described by a regular geometric surface. In Equation (2), the product $\alpha_{G-P} a_{G-P}$ is the volumetric transfer coefficient. This value depends on the form of contact between drying gas and drying material at any given type of dryer and can be generally determined by experiment. The volumetric heat transfer coefficient represents heat flux transferred on a unit volume of the drum as a result of a unit of temperature difference.
Models can be applied for describing a given process. The mathematical model is a type of quantitative model which can consist of algebraic, differential or integral equations. The principal advantage of mathematical models is that they can be used for describing the process steps of the operation concerned without experiments to be performed. The mathematical models of chemical industry processes, including drying, are based on the basic laws of physics and chemistry, such as the continuity equation, the conservation of mass, energy and momentum, transfer processes, the transport of mass, energy and momentum, balance equations, phase and chemical balance, kinetic and static equations. Due to the complexity of solving equations separately or in a system, a model is either a rough mapping of the entire process or a detailed description of an element of the process. Model development involves assumptions, determining the accuracy, validity and complexity of model use. Solving a numerical model involves the knowledge of material characteristics and transport coefficients as well. These parameters are usually the complex function of temperature and moisture content of he dried material and have to be determined experimentally [2].

2. METHODS

Volumetric heat transfer coefficients are required to be known for the simulation-based examination, and operational as well as construction design of drum dryers. Heat transfer in drum dryers takes place between gas and material, wall and material, and gas and wall. Based on literature studies [3-6], heat transfer to dominate drying is effected between gas and material, therefore our tests were also performed in this respect. The value of the volumetric heat transfer coefficient can be determined empirically for the most part, which correlation can be applied under various conditions.
Miller et al. [7] were among the first to publish a correlation for determining the volumetric heat transfer coefficient for rotary drum dryers. They examined the impact of the following variables on the volumetric heat transfer coefficient in convection drying:

- number of mixing elements;
- logarithmic mean temperature difference;
- mass flux of drying air;
- mixer size;
- duration of stay.

Experiments were performed in a counter-current rotary dryer of *0.2 m* diameter and *1.22 m* length, equipped with *6* or *12* mixing elements. Each measurement was performed at a constant *4.3 1/min* rotational speed, but the slope of the drum was altered between *30 mm/m* and *60 mm/m*.

It was established that heat transfer is not affected by the slope of gradient and the rotational speed influencing the duration of stay. Miller et al. established the following correlations for calculating volumetric heat transfer coefficients in case of *6* mixing elements:

$$\alpha a_{G-P} = 19{,}4\left(N_f - 1\right)\frac{\dot{m}_G{}^{0{,}46}}{d_D{}^{1{,}92}}, \tag{4}$$

and in case of *12* mixing elements:

$$\alpha a_{G-P} = 14{,}1\left(N_f - 1\right)\frac{\dot{m}_G{}^{0{,}46}}{d_D{}^{2{,}2}}, \tag{5}$$

where N_f represents the number of mixing elements, and d_D is the internal diameter of the dryer.
Friedman and Marshall [8] performed a total of *134* unidirectional and counter-current measurements on four different types of sand in a drun dryer. The average granule size of the material varied between *150* and *2300 μm*, drum rotational speed between *3.35* and *18.5 1/min*, drum slope between *0* and *46 mm/m*, the number of mixing elements between *0* and *8*, the volumetric flow of air between *195* and *7320 kg/m^{2}h*, feed rate between *35* and *304 kg/h*, and the load rate between *0.8-12.4%*. In the course of measurements they examined the impact of gas mass flux, load rate, rotational speed, and mixing element number on the volumetric heat transfer coefficient. The impact of the mass flux of the material on the volumetric heat transfer coefficient was examined on two sand types subject to four different volumetric flows of the drying gas in a counter-current drum dryer with *8* mixing elements.
The authors examined the impact of load rate at constant slope of gradient and rotational speed. By testing at various volumetric flows of the gas, they concluded that the rate of load also affects the volumetric heat transfer coefficient.
Friedman and Marshall performed further measurements to examine the impact of rotational speed on the volumetric heat transfer coefficient, on the basis of which they concluded that the effect of rotational speed is negligible. In examining the impact of the munber of mixing elements on the volumetric heat transfer coefficient, they found that without mixing the material takes up heat from the drum wall by convection along the surface of the bed, and by conduction at the bottom of the drum. In case of two mixing elements, there is a considerable increase in the volumetric heat transfer coefficient between gas and material as the mixing material significantly increases the contacting surface. By increasing the number of mixers from *4* to *8*, it was found that the contacting surface increases less, consequently there is no major increase in the volumetric heat transfer coefficient, either.
Friedman and Marshall concluded that the volumetric heat transfer coefficient depends on drying gas velocity, as well as on the speed and duration of stay of the material. In their work, they published the following expression to determine the volumetric heat transfer coefficient, which equation is to be applied by Alvarez and Shene [9] in a subsequent work:

$$\alpha a_{G-P} = 31{,}5\left(N_f - 1\right)\frac{\dot{m}_G{}^{0{,}46}}{d_D{}^{1{,}92}}. \tag{6}$$

McCormick [10] used and further developed the measurement results of Miller et. al [7], Friedman and Marshall [8], and Saeman and Mitchell [11]:

$$\alpha a_{G-P} = 278 \frac{\dot{m}_G{}^{0,67}}{d_D{}^{2,34}} \ . \tag{7}$$

Myklestad [12] dried granular pumice of *2.5 mm* diameter in a counter-current rotary drum dryer. Pumice was characterized by X_{in}*=0.3÷0.36 kg/kg* initial moisture content and $\dot{m}_{dP}$*= 6÷10 kg/h* mass flux. Air mass flux varied between *119* and *192 kg/h*, its inlet temperature was *30, 40* and *50 °C,* respectively.
Based on the measurements, the correlation stated for the volumetric heat transfer coefficient is as follows:

$$\alpha a_{G-P} = 513{,}5 \frac{\dot{m}_G{}^{0,8}}{d_D{}^{1,6}} \ . \tag{8}$$

Douglas et al. [13] applied a mathematical model based on a different heat and material balance for the dynamic control of a rotary drum dryer used for crushed sugar. The volumetric heat transfer coefficient functional relationship applied in their model also took into consideration the load rate of the material with reference to the drum:

$$\alpha a_{G-P} = 221{,}5 l^{0,5} \frac{\dot{m}_G{}^{0,6}}{d_D{}^{0,32}}, \tag{9}$$

where *l* is the load of drum.

3. RESULTS

Equations of the volumetric heat transfer coefficient collected from the literature considerably differ from each other. At many instances, the ranges of definition of the equations are not or only incompletely diclosed by the authors. Therefore their conditions of application are also unclear. The diagrams in *Figure 1* show the differences between Equations (4-9). As the ranges of definition of the equations are incomplete, they were applied subject to the most frequent machinery and operating parameters to be found in industry and laboratory conditions.

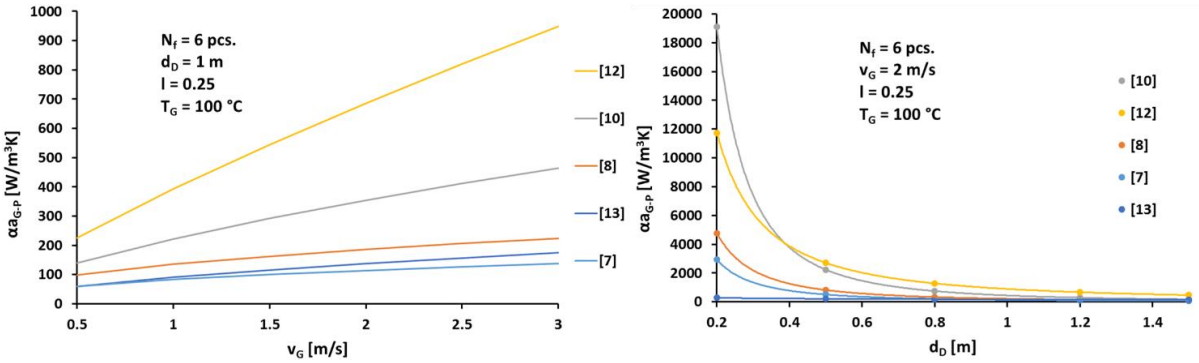

Figure 1 Volumetric heat transfer coefficient versus velocity of drying gas and diameter of drum

Equations in the literature differ considerably from each other. There are operating conditions where the value of the volumetric heat transfer coefficient shows a difference of more than 100% depending on which equation is applied. The rate of difference significantly deviates from the maximum 40% error range customary in heat transfer. In order to narrow down the error range, the applicability and range of definition of the equations should be definitely known, which requires further research.

CONCLUSIONS

Having reviewed the special literature on the subject, it can be established that heat transfer coefficients can only be applied for drying subject to a number of conditions, therefore so-called volumetric heat transfer coefficients are expedient to be used. Volumetric heat transfer coefficients are required to be known for the simulation-based examination, and operational as well as construction design of drum dryers. As regards rotary drum dryers, the volumetric heat transfer coefficients found in the literature are suitable for dimensioning dryers only within a narrow range. The principal advantage of mathematical models is that they can be used for describing the process steps of the operation concerned as well as for examining the impact of certain operational and equipment parameters on the process of drying without experiments to be performed. A mathematical model can describe drying parameters such as varies in the moisture content and temperature of the material as well as of the drying gas along the length of the drum.

ACKNOWLEDGEMENT

Special thanks for Dr. Mária Örvös for her helps in this work. This paper was supported by Richter Gedeon Talentum Foundation (H-1103 Budapest, Gyömrői str. 19-21, Hungary), and by Hungarian Scientific Research Found (OTKA-116326).

REFERENCES

[1] Örvös, M.: *Diffusion processes and equipment, 1st part: Drying*, Edu. guide, Budapest, 2006.
[2] Szentgyörgyi, S., Tömösy, L., Molnár, O.: *Convection Heat Transfer Coefficients at Convective Drying of Porous Materials*, Drying Technology, 18(6): 1287-1304., 2000.
[3] Nastaj, J. F.: *Numerical model of vacuum drying of suspensions on continuous drum dryer at two-region conductive-convective heating*, Int. Comm. Heat Mass Transfer, 27(7): 925-936., 2000.
[4] Shene, C., Bravo, S.: *Mathematical modelling of indirect contact rotary dryers*, Drying Technology, 16(8): 1567-1583., 1998.
[5] Deng, W. Y., Yan, J. H., Li, X. D., Wang, F., Lu, S. Y., Chi, Y., Cen, K. F.: *Measurement and simulation of the contact drying of sewage sludge in a Nara-type paddle dryer*, Chemical Engineering Science, 64: 5117-5124., 2009.
[6] Kassai, M., Gaoming, G., Simonson, C. J.: *Dehumidification performance investigation of liquid-to-air membrane energy exchanger system*, Thermal Science: 129-143., 2014.
[7] Miller, C. O., Smith, B. A., Schuette, W. H.: *Factors influencing the operation of rotary dryers*, American Institute of Chemical Engineers, 38: 841-864., 1942.
[8] Friedman, S. J., Marshall, W. R.: *Studies in rotary drying, Part II – Heat and Mass transfer*, Chemical Engineering Progress, 45(9): 573-588., 1949.
[9] Alvarez, P. I., Shene, C.: *Experimental determination of volumetric heat transfer coefficient in a rotary dryer*, Drying Technology, 12(7): 1605-1627., 1994.
[10] McCormich, P. Y.: *Gas velocity effects on heat transfer in direct heat rotary dryers*, Chemical Engineering Progress, 58(6): 57-61., 1962.
[11] Saeman, W. C., Mitchell, T. R.: *Analysis of rotary dryer and cooler performance*, Chemical Engineering Progress, 50(9): 467-475., 1954.
[12] Myklestad, O.: *Heat and mass transfer in rotary dryers*, Chemical Engineering Progress Symposium Series, 41(59): 129-137., 1963.
[13] Douglas, P. L., Kwade, A., Lee, P. L., Mallick, S. K., Whaley, M. G.: *Modelling, simulation & control of rotary sugar dryers*, Drying ’92, 1928-1939., 1992.

INTERNATIONAL SCIENTIFIC CONFERENCE ON ADVANCES IN MECHANICAL ENGINEERING

19 November 2015, Debrecen, Hungary

THE STUDY OF MECHANICAL PRESSES DRIVES USING COLD PLASTIC DEFORMATION

POP-SZOVÁTI Anton-Gheorghe, GYENGE Csaba DSc

Faculty of Manufacturing Enginering, Tehnical University of Cluj-Napoca
E-mail: anton_pops@yahoo.com, csaba.gyenge@tcm.utcluj.ro

Abstract
It is well known that in the industrial manufacture of general household products, cold plastic deformation plays an important role. Thus, the Electrolux *Satu Mare (RO), over 80% of the components of household products, is carried out by plastic deformation through cold pressing. Our collective, addressed the issue of improving the systems for operating the machinery of plastic deformation through cold pressing of components used in the manufacture of small-sized and medium-sized parts. In the context of the work we set out to present our achievements so far in this area.*

Keywords: *plastic deformation, cold forming, optimization, drive.*

1. INTRODUCTION

The research aims to budge the current state of the companies in the area and popularize advanced processing techniques to sheet metal through cold pressing, because their activities take place in the area specialized companies in manufacturing sub-assemblies for household cooking machines at S.C. Electrolux-Romania in Satu Mare, S.C. Anvis Rom S.R.L.
The authors of this paper have contributed to improving the processes of plastic deformation through cold pressing through implementation of technical solutions for the replacement of the driving press systems or combined reuse of their current operating systems.
In the course of manufacturing processes there has been chosen a press corresponding with functional and technical features for the operation which the sheet metal or semi-finished product was subjected in the intermediate stages of processing.
To every operation of plastic deformation through cold pressing (stamping or embossing) corresponds to a optimally technological time.
The classical mechanical press is the technological time during descent and ascent of the ram during a double cycle race.
The speed of the executor organ (ram) during a double cycle race, to a classical mechanical press it does not change, being determined by the main engines strokes, reports of transmission gears and safety coefficient ratings that were imposed in the construction of the press.
To a press with an open frame (2500 kN) through direct involvement of the flywheel, with the main engine (22 kW, 1500 rot./min) with a wide belt transmission, it is done a number of 40 double strokes per minute, of the ram it will be studied the possibility of adopting a mechanical speed variator drive.

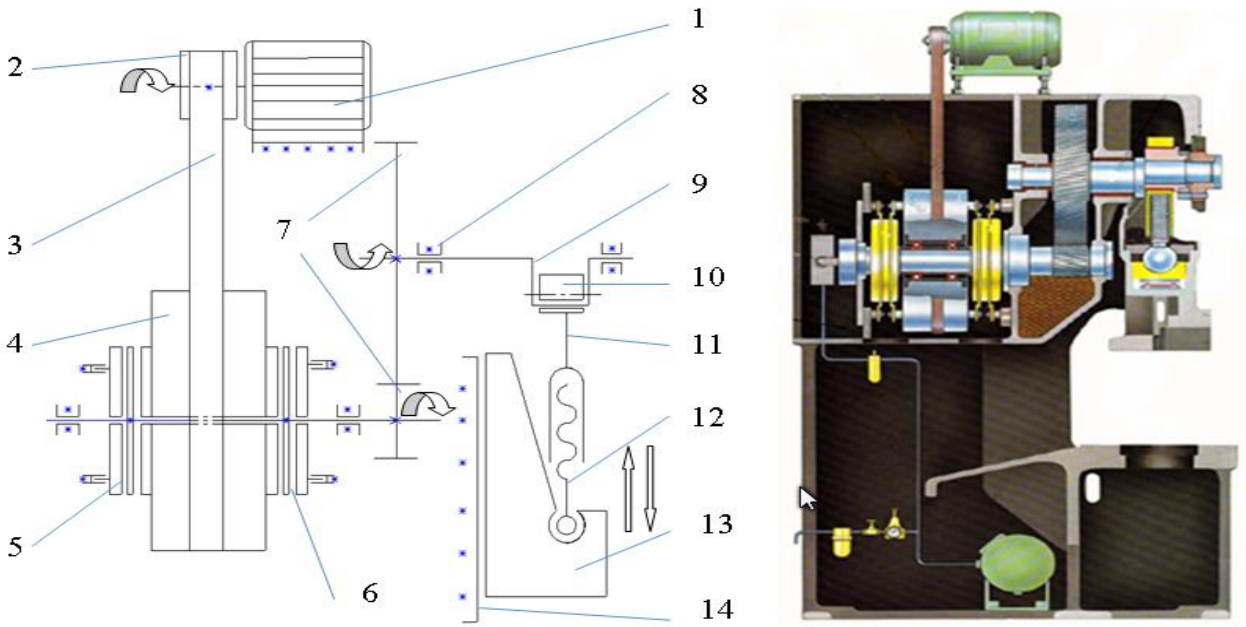

Figure 1 The kinematics scheme of a press with an open bed frame, with an electric engine drive; A press construction section
(1-main engine; 2- belt wheel; 3-wide belt; 4- flywheel; 5 and 6- the whole clutch-brake; 7- toothed wheels; 8- eccentric bushing; 9- eccentric shaft; 10- eccentric bushing; 11- connecting rod; 12- spherical-head screw; 13- ram; 14- guide)

To a press with a closed bed frame (2000 kN) will study the possibility of adopting a digital speed variator.
Control functions from this press were determined by the blending mode of the relays, contactors, limiters, etc. so that this control was called enabling heavy ties (classical cabling).
Such a system can be installed only after every movement of the system is known, the position and role of each component. In case of errors, it is necessary to rewiring the parts that does not work, any additional work require a reorganization of the entire system.

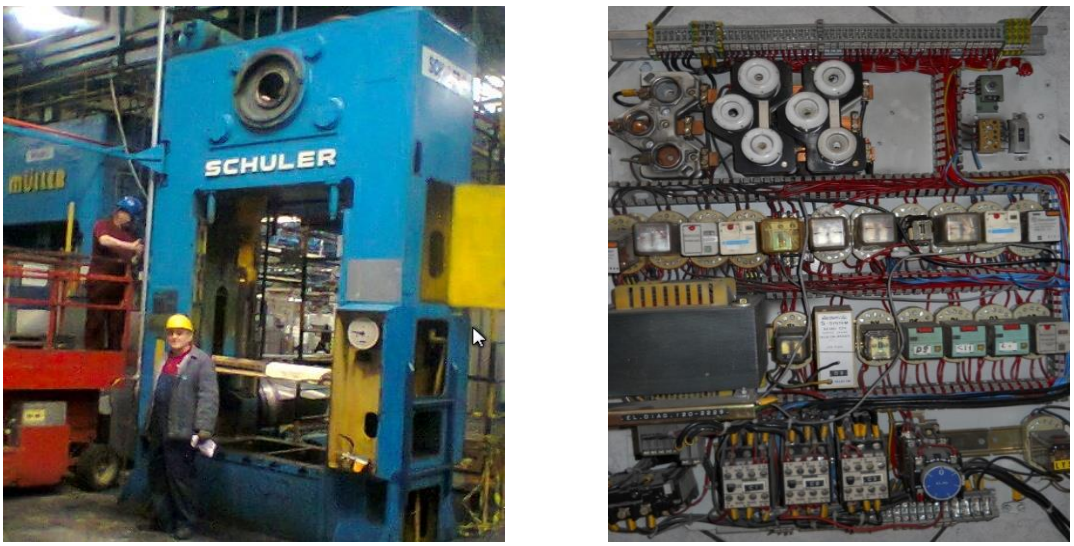

Figure 2 Press frame closed undergoing modernization; Analog electric panel.

2. OBJECTIVES

For more flexibility in the manufacturing of semi-finished products there where studied the possibility of embossing and stamping operations on the same release through implementation of technical solutions that make it possible to perform such operations on the same press.
In order to achieve this goal, formulated above, there have been established the following objectives: study of principles of plastic deformation through cold pressing, realization of the mechanical actuator model with a speed variator designed in 3D with Solid Works and equipping the presses with a speed variator device for this type.
The paper aims to illustrate the phases and activities necessary for the modernization of presses and guillotines with computer-assisted operation with frequency converter for adjusting the speed of the main electric engine.

3. METHODS OF ACHIEVING OBJECTIVES

3.1. Mechanical Model of speed variator

The possibility of decreasing the number of double races per minute of the press ram, optimizing technological parameters of stamping, safety in operation and adjustments, increase productivity and quality of the finished products obtained through cold pressing.
The ram's speed after mounting the speed variator must not be smaller than that of the manufacturer(40 double courses per minute), in order to not alter the stopping time of ram (0,2 s).
Adaptation of a speed variator, designed for this purpose, it gives the possibility to adjust the number of double races per minute from the executor organ (from the presses ram).
For this purpose it has been designed a mechanical speed variator with trapezoidal belt, without changing the distance between the shafts, achieved with computer aided design program 3D Solid Works.

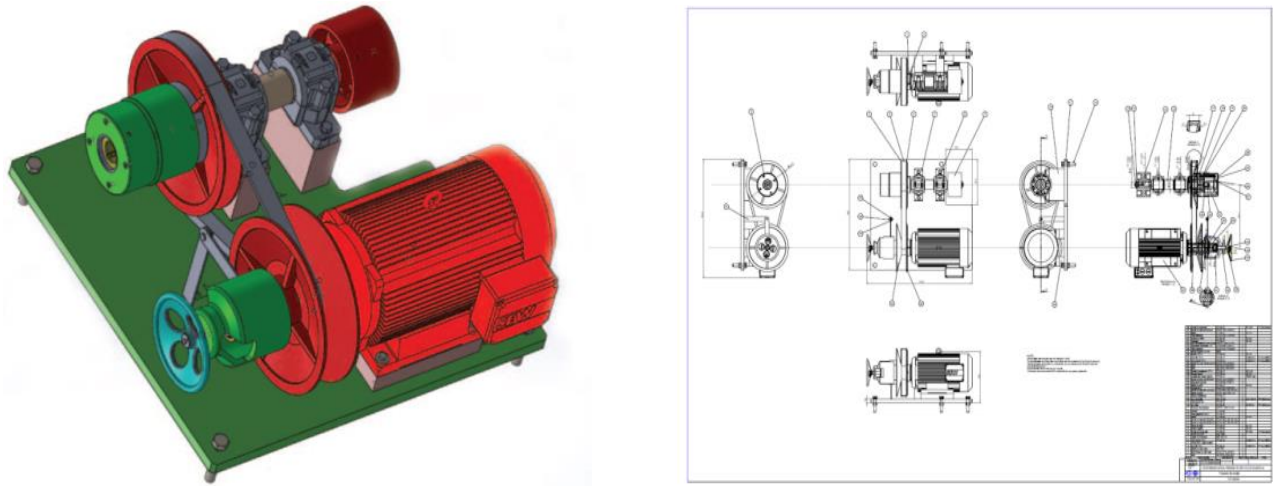

Figure 3. 3D model of the mechanical speed variator; Technical drawing

The speed variator is placed between the electric engine and the mechanical energy accumulator (flywheel), adjusts the number of double races per minute of the presses ram, contained between 20 and 40 double races per minute.

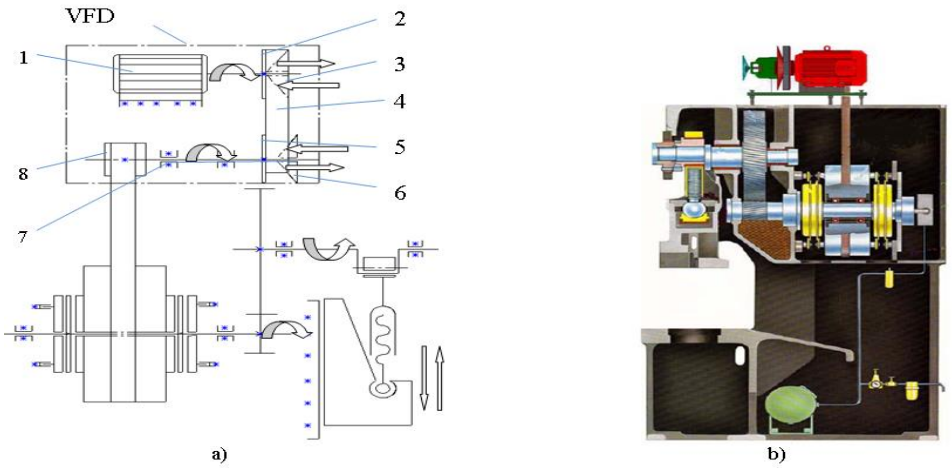

Figure 4 Kinematic diagram of a press with an open frame with speed variator; A press construction section.
(VFD (Variable Freegveny Drive);1- Main electrical engine; 2 and 5- fixed cones; 3 and 6-movable cones; 7- bearings with ball bearings; 8- belt wheel)

This speed variator has the advantage that you can get great gear at times low rev drive to the flywheel, provides a wide range of adjustment in the number of double races per minute for the ram

3.2. Electric Model

To adjust the running speed with a digital frequency converter it is needed an operating program, Siemens-Step 7, installed in the main memory of PLC, programmable from a removable PC. The program carries out the interference between PLC and a touch panel. It requires the replacement of wiring and electrical panel.
Now a PLC (Programmable Logic Controller) it is frequently used in command of some electrical components, hydraulic or pneumatic because is simpler to rewrite the PLC program and adding new connections than a complete rewiring.
PLC operation is determined by the program that is found in its memory.

Figure 5 Closed press frame*;* Electric panel with frequency converter

Programming is possible for optimizing the time required for the transfer movements of the semi-finished product during the double race per minute.

Compared to a mechanical press with classic movement, press operated with engine with frequency converters have the advantage through the myriad possibilities of operation through programming of software.
You can program in such a way that the deformation speed would be most optimal for material which is processed, to ensure the optimum time for transferring semi-finished product between cycles in the case of transfer presses.
This speed variator has the disadvantage that in the low speed the flywheel produces moments of low transmission resulting from the formula U/f = constant.
Where: U-voltage; f-frequency

CONCLUSIONS

Using a mechanical speed variator has the advantage that when the revs are lowered it increases the time of transmission of the electric motor. By adapting a speed variator will create an additional adjustment of the number of double races per minute of the ram between 20 and 40 double races/minute.
To adjust the running speed with a digital frequency converter it is needed an operating program for example, Siemens-Step 7, installed in the main memory of PLS, programmable from a removable PC. The program carries out the interference between PLC and a touch panel. It requires the replacement of wiring and electrical panel. The speed variator with digital frequency converter, has the disadvantage that decreases the time of transmission of the engine if the speed decreases, has a high price, the pieces are not reused, requires skilled staff for maintenance.
New generations of presses simplifies the classic actionating versions of presses with screws, with knees, eccentric or crank. Presses with servo drive engine is the concern of several manufacturers of presses. They work with a wide range of racing adjustment and even the ram's speed during a cycle. The press ram can execute movement of balance because the servo engine can change the direction of rotation during it's course and the brake works as a generator of electric current that it puts in capacitors to be used during the task.

REFERENCES

[1] Verlag Berlin Heidelberg: *Metal Forming Handbook*, Schuler, Springer, 1998.
[2] Taylan, A., Tekkaya, A.E.: *Sheet metal forming*, Processes and Application
[3] Tăpălagă, I. , Achimaş, Gh., Iancău, H.: *Cold pressing technology*, 1980.
[4] Pop-Szováti, A. Joldeş, N: *Specific achievements in the direction of the automated assembly through adhesion of household machines*, 2015.
[5] Pop-Szováti, A., Gyenge, Cs., Borzan, M.: *Dynamic analysis of vibration and noise metal forming presses*, 2014.

INTERNATIONAL SCIENTIFIC CONFERENCE ON ADVANCES IN MECHANICAL ENGINEERING
19 November 2015, Debrecen, Hungary

FORCE AND POSITION CONTROL OF PNEUMATIC DRIVES

SÁRKÖZI Eszter, FÖLDI László PhD, JÁNOSI László CSc

Institute for Mechanical Engineering Technology, Szent István University
E-mail: sarkozi.eszter@gek.szie.hu, foldi.laszlo@gek.szie.hu, janosi.laszlo@gek.szie.hu

Abstract
Despite of non-linear behavior, pneumatic drives are more widely used as an actuator in controlled systems. Typically the two main controlled variables of them are the position and the force. In this paper we worked out an algorithm with two embedded PID controllers in a cascade control system in order to control force or position of pneumatic cylinders within one application.

Keywords: *Pneumatic cylinder, Position control, Force control, Cascade control method*

1. INTRODUCTION

In order to achieve linear motion -among other drives- pneumatic actuators are widely used, because they have several advantages: they are fast, robust, simple to maintain and low in cost. The challenge to the use of pneumatic drives is that due to piston friction and the characteristics of compressed gas flow their behavior is non-linear. In the last decade such industrial controllers became available which have adequate computing capacity for real-time usage. With the use of them and with proper control method, the non-linear behaviour of pneumatic system is well managable so they can be applied in position or force controlled applications. There are several control methods used (e.g. PID variations, fuzzy logic, sliding mode, status controller), in this work cascade control with PID is examined.

2. METHODS

2.1. Control method

Nowadays the PID controller (proportional-integral-derivative controller) algorithm is the most widely used in industrial control systems. It is able to respond to the current control error, the past error and the future error. The past error is characterized by the integral of error, the future error by the derivative of the error. Accordingly, this algorithm modifies the error through three channels: via the proportional channel, the integral channel and the derivative channel. PID controller is popular because it is reliably able to fulfil the prescribed control requirements in most industrial applications despite of it's relatively simple structure. The algorithm calculates the control variable as a function of the difference of the process output and the setpoint. There are several designs of PID controllers due to the used channels (proportional, integral, derivative channels) in the controller, e.g. P, PD, PI, PID controllers.
The PID controller summarizes the effects of the three channels (proportional, integral, derivative). Accordingly the calculation of the control variable as a function of the error in continuous time domain is:

$$u(t) = K_P\left(e(t) + T_d\frac{de}{dt} + \frac{1}{T_i}\int_0^t e(\tau)d\tau\right), \quad K_P, T_i, T_d > 0 \tag{1}$$

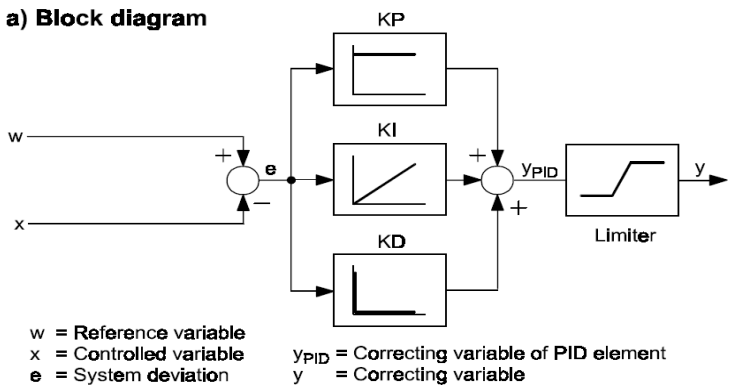

Figure 1 Block diagram of PID controller with limited output

In practice the designation of the proportional element is P or K_P. The integral effect can be defined with the use of the integral gain or the integral time constant. Similarly, the derivative effect can be defined with the use of derivative gain or derivative time constant. The form which is used in practice is:

$$y_{PID} = K_P \cdot e + K_I \cdot e \cdot t + K_D \cdot \frac{de}{dt}. \tag{2}$$

Cascade control is one of the most popular structures for process control as it is a special architecture for dealing with disturbances. The cascade control structure is such a method where the control loop contains an another control loop within itself. The outer control loop supplies the setpoint to the inner loop. The control tasks should be shared between the embedded control loops. However, the drawbacks of cascade control are obvious that primary controller and secondary controller should be tuned together, which influences each other (Geng, 2014).

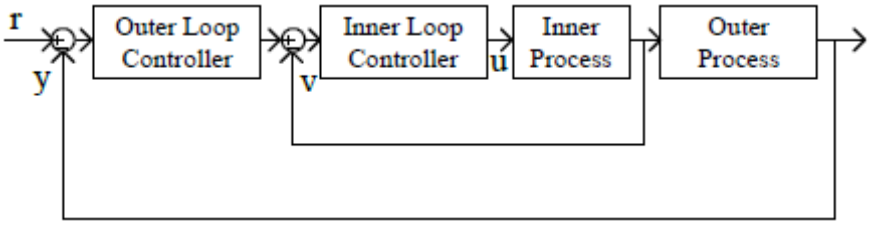

Figure 2 General block diagram of cascade control (Geng, 2014)

2.2 Apparatus

Figure 3 DGPL-25-450 Pneumatic cylinder with attached encoder and servo valve

As an actuator we applied a Festo DGPL-25-450-PPV-A-KF-B cylinder of 450mm stroke length, to which we attached a Festo MLO-POT-0450-TLF analogue displacement encoder, which has a 0,01 mm travel resolution (Fig. 3). In order to move the cylinder we applied two MPYE-5-1/8-LF-010-B 5/3 proportional valve. The controller was a modular NI CompactRIO™ (cRIO 9073) programmable automation controller, out of its modules we used the analogue-to-digital converter (NI 9201). We controlled the proportional solenoid valve with the help of the analog output module (NI 9472). The circuit diagram of the pneumatic positioning system is presented on figure 4.

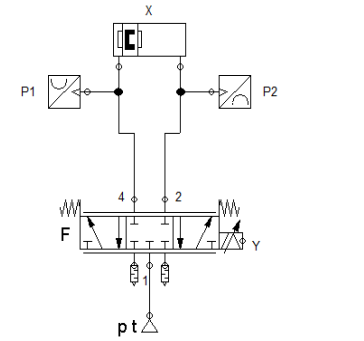

Designation	Description
F	Proportional 5/3-way directional valve
pt	Compressed air supply
x	Cylinder without piston rod
	Electrical connection 24V
	Electrical connection 0V
X	Displacement encoder
Y	Proportional valve solenoid, position controlled
P2	Analog pressure sensor
P1	Analog pressure sensor
P1	Analog pressure sensor
P2	Analog pressure sensor
NI cRIO 9037	Logic module

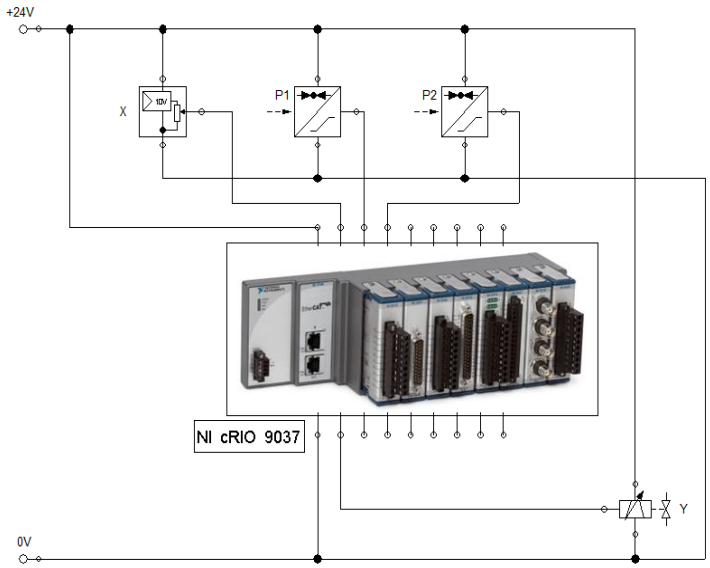

Figure 4 The pneumatic and electric circuit diagram

2.3 Control algorithm

In order to control force or position within one algorithm we used cascade contol method with two embedded PID contollers. The used control algorithm was developped in LabView softver. On the front panel (Figure 4) there is a switch to chose between position or force control. The setpoints of the control algorithms can be adjusted by two sliders. The applied gains of the PID algorithms can be defined as well. In case of positioning a force limit can be adjusted due to the cascade control structure.

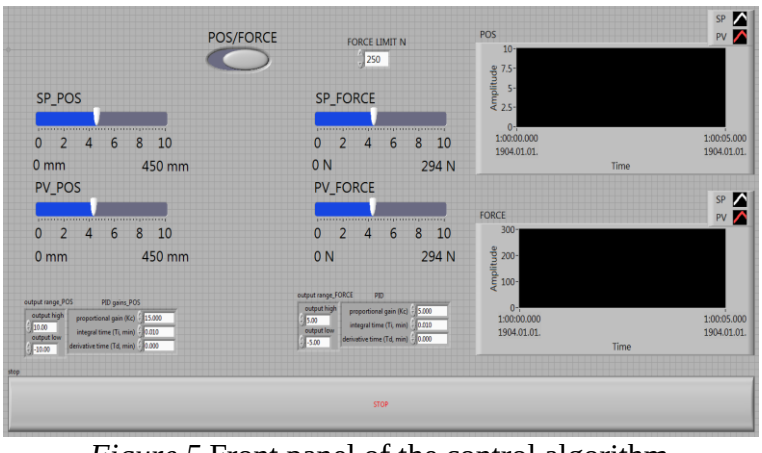

Figure 5 Front panel of the control algorithm

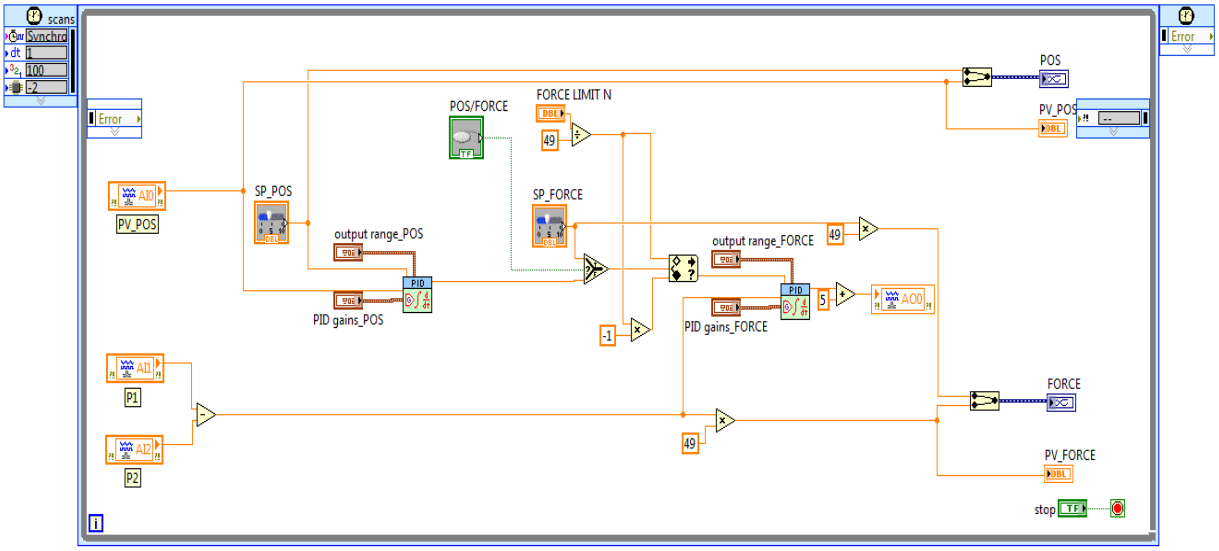

Figure 6 The applied cascade control structure with two PID controller

3. RESULTS

During the positioning we have determined the settling time for step responses from 98 mm to 350 mm, overshoots and steady-state error graphically based on measurement results. The moved load was m=2 kg. In case of force control the examined step response was form 50 to 198 N. The moved load was m=2 kg and there was a linearly rising outer force from 0 to 300 N depend on the stroke. In both cases the value of supply pressure was 6 bar.

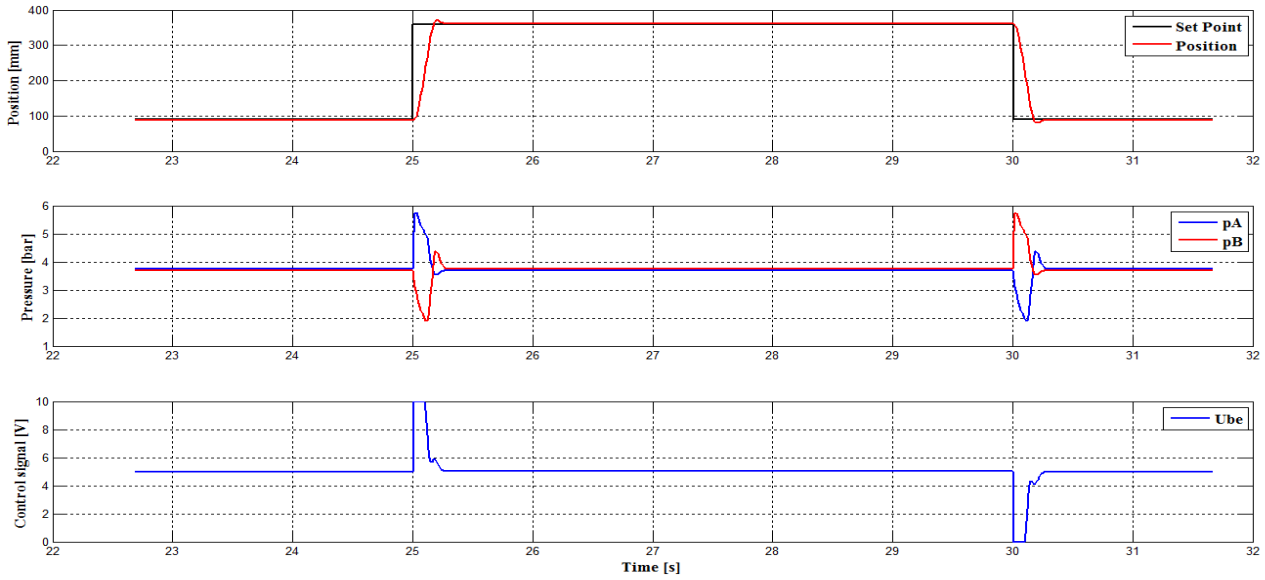

Figure 7 The result of the position control

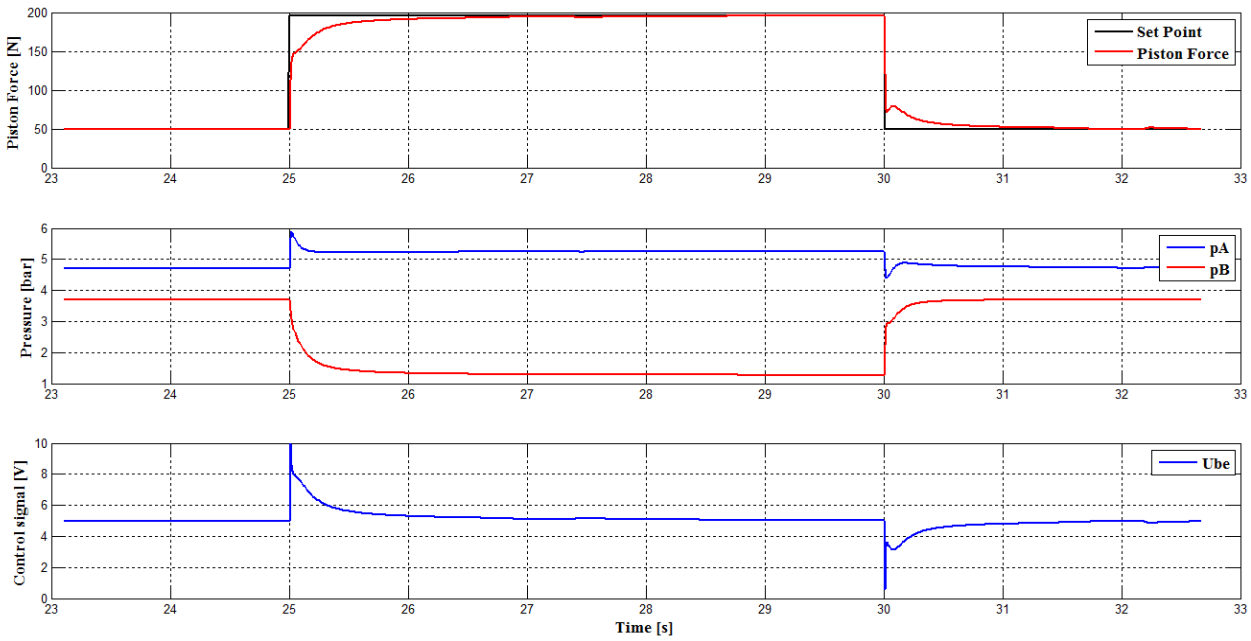

Figure 8 The result of the force control

CONCLUSIONS

We have worked out such a control algorithm which is suitable to control force or position of pneumatic cylinders within one application. This algorithm contains two embedded PID controllers in a cascade control system. Furthermore it ensures a force limitting option during the positioning. Based on the test results it is concluded that this algorithm is working point dependent, as it uses PID control method. Further deficiency of this algorithm that it does not take into consideration the effect of the static friction in the pneumatic cylinder. Further development is needed to work out such self tuning control method which can measure the static friction force and applies it during the control process. Another development direction should be using other working point independent control methods embedded into the cascade structure, for example status or sliding mode control.

REFERENCES

[1] Ahn, K., Yokota, S.: *Intelligent switching control of pneumatic actuator using on/off solenoid valves*, Mechatronics,15, 683–702., 2005.
[2] Barth, E.J., Zhang, J., Goldfarb, M.: *Control Design for Relative Stability in a PWM-Controlled Pneumatic System*, Journal of Dynamic Systems, Measurement, and Control, 125, p. 504-508., 2003.
[3] Geng, T. and Zhao, J.: *Adaptive Cascade Generalized Predictive Control*, International Journal of Intelligence Science, 4, 70-79., 2014.
[4] Gyeviki, J.: *Szervopneumatikus pozícionálás pontosságának növelése DSP alapú csúszómód szabályozással*, PhD Thesis, Debreceni Egyetem, Debrecen, 2007.
[5] Messina, A., Giannoccaro, N.I., Gentile, A.: *Experimenting and modelling the dynamics of pneumatic actuators controlled by the pulse width modulation (PWM) technique*, Mechatronics, 15, p. 859–881., 2005.
[6] Nguyen, T., Leavitt, J., Jabbari, F., Bobrow, J.E.: *Accurate Sliding-Mode Control of Pneumatic Systems Using Low-Cost Solenoid Valves*, IEEE/ASME Transactions on mechatronics, 12(2), p. 216-219., 2007.

[7] Parnichkun, M., Ngaecharoenkul, C.: *Kinematics control of a pneumatic system by hybrid fuzzy PID*, Mechatronics, 11, 1001-1023., 2001.
[8] Saleem, A., Taha, B., Tutunji T., Al-Qaisia, A.: *Identification and cascade control of servo-pneumatic system using Particle Swarm Optimization*, Simulation Modelling Practice and Theory 52, p. 164–179., 2015.
[9] Shih, M.C., Ma, M.A.: *Position control of a pneumatic cylinder using fuzzy PWM control method*, Mechatronics, 8, 241-253., 1998.
[10] Thomas, M.B., Maul, G.P., Jayawiyanto, E., Novel, A.: *Low-Cost Pneumatic Positioning System*, Journal of Manufacturing Systems, 24(4), 377-387., 2005.

MODELING OF A GEOTHERMAL WELL

SCHRÓTH Ádám

Budapest University of Technology and Economics
E-mail: schrothadam@gmail.com

Abstract
The geothermal aptitude of Hungary belongs to the frontline of Europe. In course of the hydrocarbon exploration many wells were drilled. Our country is one of the geologically best explored countries in the world, but some of the wells are abandoned. Currently the utilization of these wells is unsolved and the mope-up would take large sums of money. A feasible way to produce electricity would be if these wells were used as heat sources of an enhanced geothermal power generation system (EGS).
In this paper, I introduce the method of the hydrodynamic and thermal modeling of a 2200 meters deep depleted hydrocarbon well. With the simulation of the whole system more accurate results can be achieved with the complex investigation of the model of the well and the ORC system. Besides, the interaction of the underground and above-ground system can be also examined.
The bottom of the liner pipe is closed without perforation and the production tube is placed coaxially inside. The well functions as a double-tube heat exchanger. The working fluid goes down to the bottom while heats up, then turns back on the bottom into the producer tube and comes up to the surface in supercritical state.
In my paper, I'm modeling the well in the program called MATLAB and I fit an energy conversion system to it. I'm investigating several working fluids.
My proposed solution has two advantages. On the one hand, the abandoned wells can be utilized, on the other hand, a significant part of the investment cost can be avoided because the drilling of a new well is not necessary.
This method can contribute to fulfillment of the climate protection requirements for Hungary.

Keywords: *geothermal, abandoned hydrocarbon well, renewable energy, ORC*

1. INTRODUCTION

Geothermal energy is the heat inside Earth's reserves, which is fed by the decay heat of the radioactive elements in the earth's crust. Because of the extra-thin, 60-100 km lithosphere beneath the Pannonian Basin Hungary can be classified as a geothermal forefront of Europe. The average geothermal gradient in Hungary is around 50 °C / km. The geothermal gradient is higher in South-Hungary than in North. In spite of the favorable conditions, the measured fluid temperature on the surface rarely exceed 100 ° C [1].
The current economic environment enables cost efficient power generation only when the media temperatures are above 100 °C. Many researches are being undertaken to ensure the exploitation of the geothermal resources for electricity production on lower temperature levels.
Considering geothermal energy our country is very well explored, which means that drilling exploration are the most dense around the world (1 well / 5 km2). The number of the non-productive wells drilled by the hydrocarbon industry in 66 years is approximately 3000 [2].
The elimination of the abandoned wells represents a significant cost to the owners. However, if the well is located in an area with sufficiently high geothermal gradient, there should be a research

about the utilization for energetic purposes. After the reconstruction, the wells can function as EGS (Enhanced Geothermal System), also known as HDR (Hot Dry Rock) system.
By conventional EGS's at few kilometers depth rock fractures are used as a heat exchanger systems. The surface water is injected into this system to heat up. Then it streams up in the production well or wells.
In my case there was no fracture system in the rock, so the hydrocarbon well is the heat exchanger, and the heat transfer medium is not water, but other organic media: the well has to be hermetically closed in order to prevent fluid loss. The artificially developed geothermal systems use Rankine or Kalina Cycle solutions for recovering heat power.
The possibility of single and double loop ORC systems were investigated. In case of the single loop version, supercritical pressure was used to avoid the back streaming of working fluid caused by the density changing. The medium warmed up in the well expands directly on the turbine. Based on our calculations [3] the single loop system has a significantly higher efficiency than the double loop systems. Different working fluids were investigated.

2. METHODS

There were several uncertainties in the modelling. I neglected the change of the rock composition and underground water flows. The contact between the rock and the pipe is not perfect therefore the heat resistance higher than the ideal. There wasn't available data about it therefore I didn't take it into consideration. The heat is transferred vertically not only by convection but also by conduction. I neglected the effect of the conduction because the ratio to the convection was significantly smaller. At the calculation of the heat transfer coefficient between the inner side of the tube and the medium I used the Sleicher-Rouse equation [4]. The correlation was developed on liquid metals but in my case the Reynolds- and Prandtl-numbers fall into the range of validity. In the supercritical state second-order phase transition takes place while anomalies in the material properties could be detected. There is a peak in the specific heat which increases the intense of the heat transfer. This effect was also neglected. Radial temperature profiles are not counted because the flow rate is high. I assumed the perfect mix-up. Due to the high pressures the pressure change caused by the lifting force was neglected because the effect is with two orders of magnitude smaller. The production tube is assumed an adiabatic system therefore there is no heat exchange between the annular space and the production tube. There is no fluid loss. The system applies the law of continuity.
The thermal resistance due to the well design depends on the depth. The shaping of the well is like a telescope. There are fewer and fewer layers with the increase of the depth. The complete resistance model can be seen on the *Figure 1*.

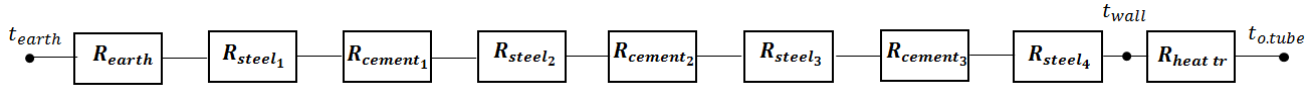

Figure 1 Thermal resistance between the rock and the fluid in the tube

My method is not continuous. I divided units of the same lengths the depth of the well. The temperature of the earth can be determined from the depth (H) and from the geothermal gradient (γ = 0055 ° C / m).

$$t_{earth} = f(H) \rightarrow t_{earth,n} = f(n \cdot \Delta H) = t_{surface} + \gamma \cdot H \quad (1)$$

The pressure and temperature is used to determine the material properties and state variables like density (ρ), kinematic viscosity (ν), thermal conductivity coefficient (λ), Prandtl-number (Pr),

enthalpy (h), isobaric specific heat (c) etc.

$$p_n, t_n \rightarrow \rho_n,\ v_n,\ \lambda_n,\ Pr_n,\ h_n,\ c_n \tag{2}$$

The pressure of the next unit increases with the hydrostatic pressure and decreases with the pressure loss caused by the friction *(Equation 3)*.

$$p_{n+1} = p_n + \rho_n \cdot g \cdot \Delta H - \Delta p' \tag{3}$$

The friction factor of the tube was calculated with the correlation of S. E. Haaland *(Equation 4)* [4]. It returns the result of the Colebrook-White correlation with accuracy ± 2% and the relation is explicit.

$$\frac{1}{\sqrt{\zeta_n}} \approx -1{,}8 \cdot \lg\left[\left(\frac{\frac{\varepsilon}{D}}{3{,}7}\right)^{1{,}11} + \frac{6{,}9}{Re_n}\right] \tag{4}$$

The pressure loss can be determined according to Equation 5

$$\Delta p' = \frac{\rho_n}{2} \cdot {v_n}^2 \cdot \frac{\Delta H}{D} \cdot \zeta_n \tag{5}$$

With the Prandtl-number and the Reynolds-number the Nusselt-number can be determined and from that the heat transfer coefficient can be calculated

$$Re_n,\ Pr_n \rightarrow Nu_n \rightarrow \alpha_n \tag{6}$$

The calculation of the Nusselt-number with the Sleicher-Rouse correlation *(Equation 7)*

$$Nu_n = 6{,}3 + 0{,}0167 \cdot {Re_n}^{0{,}85} \cdot {Pr_n}^{0{,}93} \tag{7}$$

The transmitted heat power can be determined as a quotient of the temperature difference and the thermal resistance *(Equation 8).*

$$\dot{Q} = \frac{\Delta t}{R_T} \tag{8}$$

The enthalpy of the next unit is the sum of the enthalpy of the previous unit and the specific transferred heat *(Equation 9).*

$$h_n = h_{n-1} + \frac{\dot{Q}}{\dot{m}} \tag{9}$$

The temperature of the unit can be determined by the temperature and pressure.

$$t_n = f(p_n, h_n) \tag{10}$$

The equations above can be written in one cycle.
For the meshing 1, 10 and 100 m units were investigated. With 1 m and 10 m units, there are no significant differences in the results. 100 m meshing represents a slight deviation. For this reason the 10 m meshing was used during the calculation.

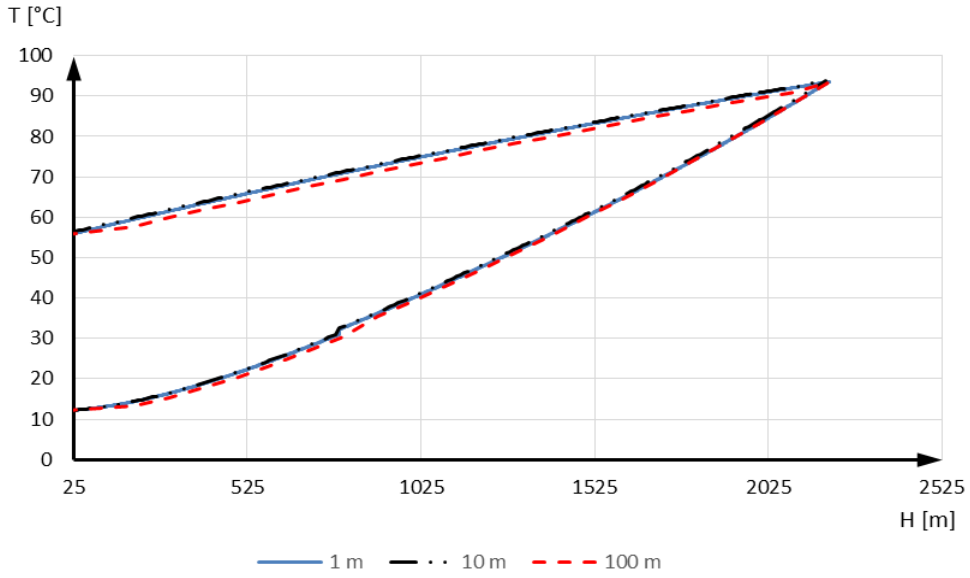

Figure 2 Examination of the meshing with CO_2

3. RESULTS

The extractable heat power is smaller than expected. It could be increased with the increase of the mass flow *(Figure 3)*, but this occurs during the decrease of the wellhead temperature therefore has got a negative influence on the efficiency and the operability of the energy conversion system. Another option is the increase of the enthalpy which can be achieved with the increase of the production tube diameter or the increase of the injection pressure. Due to the increasing pressure the well head pressure increases too. It has got also a negative influence on the efficiency.

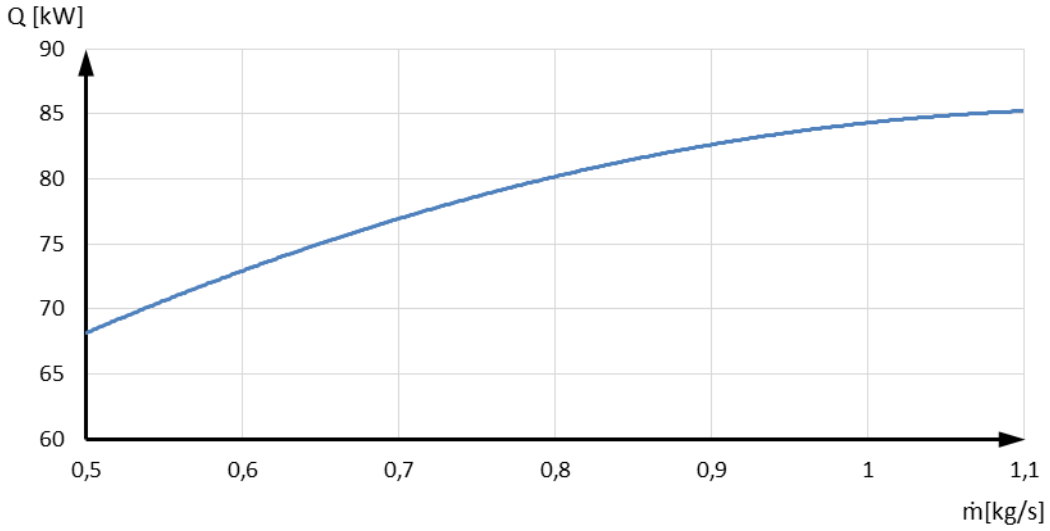

Figure 3 Extractable heat power as a function of the mass flow (CO_2) (t_{cond}=12 °C)

The temperature distribution with carbon-dioxide can be seen on the *Figure 4*. The well head temperatures are smaller than expected.

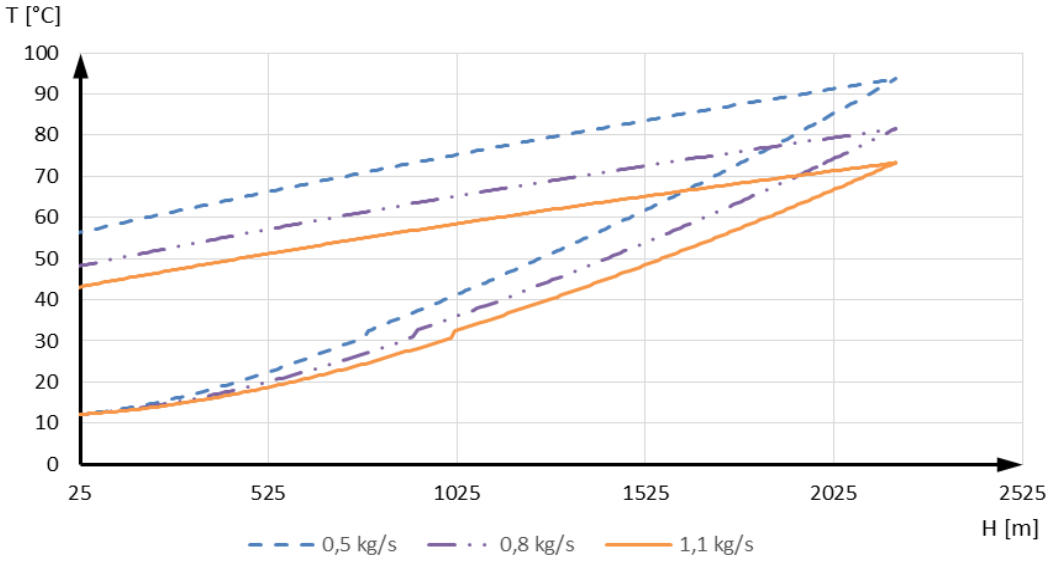

Figure 4 Temperature distribution along the well with CO_2

The temperature distribution with R125 can be seen on the *Figure 5*. The well head temperatures are higher than in case of carbon-dioxide but still smaller than expected. If the mass flow is 1 kg/s the wellhead temperature doesn't achieve the critical temperature.

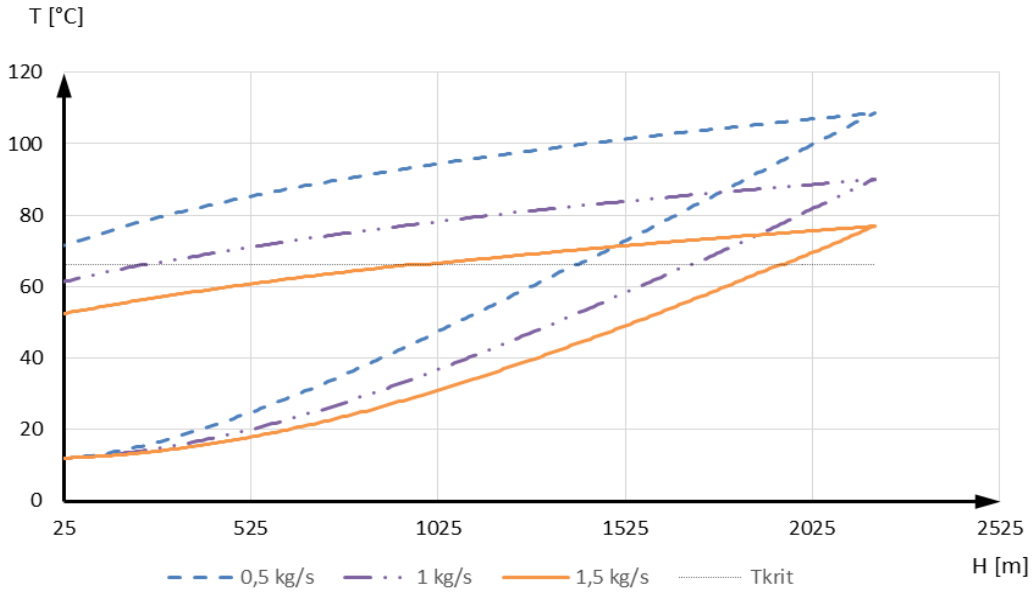

Figure 5 Temperature distribution along the well with R125

The well head temperatures in case of propane are also smaller than expected. The critical temperature could not be achieved even at 0.5 kg/s mass flow.

CONCLUSIONS

The heat power of the well and the wellhead temperature are also smaller than expected. The propane earlier had [1] many advantage like high efficiency and power but now due to the lower temperatures it can't be used as working fluid. With carbon-dioxide the cycle is operational but the efficiency remains very low. The R125 is a good choice for working fluid which is also operational. At 72 °C wellhead temperature the efficiency is 7.15%. At this temperature the mass flow is 0.5 kg/s and the power of the cycle is 41.6 kW.

References

[1] Mádlné Szőnyi, J.: *A geotermikus energia*, Grafon Kiadó, 2006.
[2] Groniewsky A.: *Geotermális lehetőségek Magyarországon,* Magyar Energetika, 2005/3.
[3] Mayer, M.J., Nyerges V., Schróth Á.: *Geotermikus erőmű illesztése kimerült szénhidrogén kutakhoz*, Tudományos Diákköri Konferencia, BME, 2014.
[4] Çengel, Y.A.: *Heat Transfer: A Practical Approach*, McGraw-Hill, 2002.
[5] Mayer, M.J., Nyerges V., Schróth Á.: *Investigation of geothermal power generation on abandoned hydrocarbon wells*, 5th International Youth Conference on Energy, IEEE Explore, 28.05.2015.

WEAR OF COPPER AND GRAPHITE TOOL ELECTRODES IN THE DIE-SINKING EDM

STRAKA Ľuboslav PhD, HAŠOVÁ Slavomíra

Department of Manufacturing Processes Operation, Technical University of Kosice
E-mail: luboslav.straka@tuke.sk, slavomira.hasova@tuke.sk

Abstract
Electrical Discharge Machining (EDM) uses thermal energy in material removal, in which is the electrical energy transformed, generated between the tool electrode and workpiece. The material removal occurs through the rapid periodic repetitive electrical discharges in the presence of dielectric fluid. By the action of electrical discharges occurs to decline not only particles of a metal workpiece material, but also to decline in a certain proportion of metal particles in tool electrode. The paper deals with the research the size of the electrode wear of tools made from copper and graphite used in die-sinking EDM.

Keywords: *Electrical Discharge Machining (EDM), Die-sinking EDM, Relative Electrode Wear (REW), tool electrode, technological parameters (TP).*

1. INTRODUCTION

For the workpieces produced by die-sinking EDM technology is often narrowed the concept of quality only for achieving a certain desired values of machined surface roughness, for example *Ra*, *Rz*, *Rq*, i. e. a compliance with its values in a certain tolerance range [1, 10]. In doing so in many cases nearly is not considered the fact that the influence of the thermal effect in some changes directly beneath the machined surface, which cause errors of geometric shape [12, 14]. One of the reasons, which results in a geometric inaccuracy of machined surface [4], is a tool electrode wear (TEW).

2. THE TOOL ELECTRODE WEAR IN DIE-SINKING EDM

The TEW [13] in die-sinking EDM is an undesirable effect. Despite the fact that modern die-sinker EDM machines can significantly eliminate the wear rate with the optimal settings of technological parameters (TP), but they cannot completely prevent the electrode wear [6, 11]. In assessing the TEW are considered the values of material loss of key locations such as sharp corners, edges, projections, etc. [7]. The following Fig. 1 shows simple places of tool electrodes for die-sinking EDM, which are susceptible to increased wear.

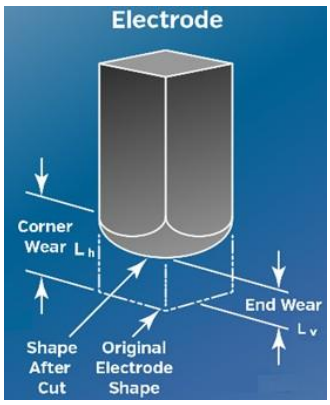

Figure *1* Simple places of tool electrodes which are susceptible to increased wear

The REW is expressed in percentage and it is given by the ratio of the volume loss electrode V_E to the volume loss of removed material V_m according to the relationship:

$$m_V = \frac{V_E}{V_m} \cdot 100\% \tag{1}$$

An important parameter in assessing the extent of TEW, used in die-sinking EDM is the Material Removal Rate (MRR) [3]. The physical properties of the material of tool electrodes, such as melting point, thermal and electrical conductivity, magnetic properties, homogeneity and the like, significantly influence this parameter [2, 5, 8]. MRR in die-sinking EDM is generally defined as the amount of removed material (usually in mm^3) per unit of time (usually in minutes).
It can be determined mathematically by the relationship [3]:

$$MRR = S.H.t \left[mm^3 \cdot \min^{-1} \right] \tag{2}$$

Where: S – is the area of the electrode [mm^2], H – the depth [mm], t – time [min].

MRR is primarily influenced by the thermal conductivity and the melting point of the material the tool electrode and the workpiece. For example, copper has good thermal conductivity, which means the low MRR, on the other site, graphite has a high melting point, what expresses in the lower intensity of TEW. Therefore, the machining of metal materials by die-sinking EDM are often used combinations of copper and graphite electrodes. The following Table 1 summarizes the basic physical properties of selected materials used for tool electrodes in die-sinking EDM.

Table 1 Basic physical properties of two materials used for the die-sinking EDM tool electrodes

Electrode material	Melting point [°C]	Thermal conductivity [$W.m^{-1}.K^{-1}$]	Electrical conductivity [$S.m^{-1}.10^6$]	Strength in tension [MPa]	Elastic module [$MPa . 10^3$]
Copper *Cu58*	1083	390	59.6	220	130
Graphite *R8500*	3000	165	0.1	34	5.9

Another parameter that significantly affects the MRR and thus the TEW is the melting point. How may be observed from Table 1, copper has a high thermal conductivity 390 $W.m^{-1}.K^{-1}$, but low melting point 1083 °C. Along this line, the graphite significantly achieves more favourable results, which has a melting temperature of approximately 3000 °C. Its significant disadvantage is low

strength in tension, only 34 MPa. Itself MRR has subsequently considerable influence on the machined surface roughness [9, 15]. Fig. 2 describes dependence of the machined surface roughness on MRR.

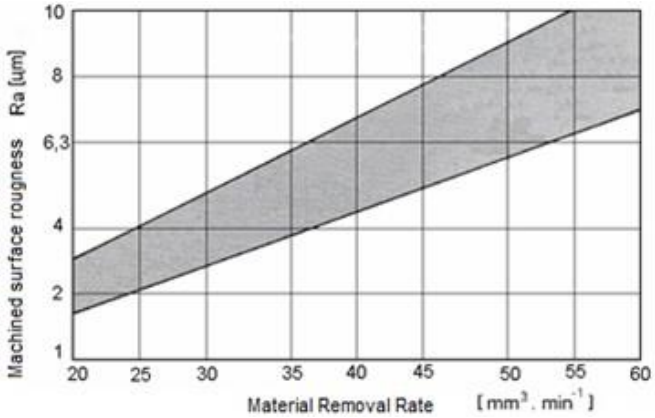

Figure 2 Dependence parameters surface roughness Ra on MRR in die-sinking EDM [3]

3. MATERIAL AND METHODS

The experiments were conducted in the company 1. PN in Prešov on die-sinker EDM machines by company Agie Charmilles, in the concrete on Agietron 100, Agietron 100C and Agietron IMPACT 3, which are shown in Fig. 3.

Figure 3 AGIE die-sinker EDM machines applied in the experiment

In the experiment were used shaped tool electrodes made from copper Cu58 and graphite R8500. The basic shapes of the Cu58 and graphite R8500 tool electrodes used in experiment are shown in the following Fig. 4.

shape No.1 shape No.2

Figure 4 Basic shapes of Cu58 and R8500 tool electrodes used in experiment

Shape No.1 – tool electrode having a square cross section with dimensions of 15×15 mm and a working length of 60 mm. On the one site of the shape of the electrode is made a special groove with a width 4 mm, which serves to orientation the position of the hole that is necessary to sink.

Shape No.2 – tool electrode with metric thread M12 × 1.5 and the functional length of 60 mm. In the axis of the electrode is drilled hole ϕ 4 mm that serves for the internal washing out of impurities from the work space. On the one site of the thread is designed the area to allow effective exhaust waste products from the place of erosion. The proposed shape of electrode is used to manufacture threading M12 ×1.5 with an overall length up to 25 mm.

Material of tool electrodes:
Copper – for manufacturing the simple tool electrodes of shape No.1 and No.2 was used copper with designation DIN E-Cu58, EN Cu-ETP with a purity of 99.9%.
Graphite – for manufacturing the simple graphite electrodes of shape No.1 and No.2 was used graphite labelled R8500. In both cases, it was used universal material for the production of tool electrodes for die-sinking EDM.

Fig. 5 shows an example of an experimental sample made from tool steel EN 90MnCrV8 using the shape tool electrodes Cu58 and R8500, shape No.1 and No. 2 with the application of die-sinker EDM machine Agietron by Agie Charmilles.

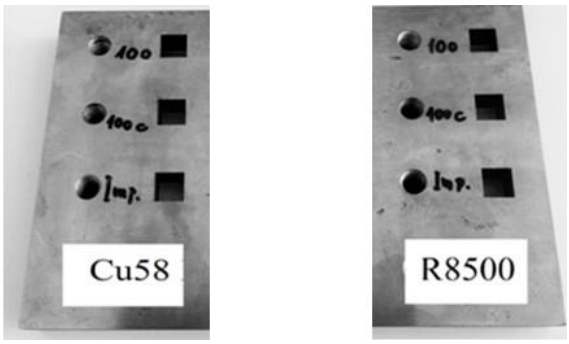

Figure 5 Experimental sample made from tool steel EN 90MnCrV8 using tool electrodes with shape No.1, 2

The following table 2 shows a basic setting of TP, which were used in the experiment, with the application of the copper electrode Cu 58 and R8500 of shape No.1, 2 on die-sinker EDM machine Agietron.

Table 2 Setting of TP with using Cu 58 and R8500 tool electrodes of shape No. 1, 2

Die-sinker EDM machine	Agietron IMPACT 3		Agietron 100 C		Agietron 100	
Dielectric fluid	IonoPlus IME-MH					
Electrode shape	No. 1	No. 2	No. 1	No. 2	No. 1	No. 2
Generator [A]	72		60		60	
Electrode material	Cu58					
Surface roughness Ra [μm]	1.8	5	1.8	5	1.8	5
Peak current [A]	17	10	22	11	18	12
Pulse duration [μs]	1.4	1.2	2	2	2	2
MRR [$mm^3.min^{-1}$]	1200	1800	700	500	700	500
Electrode material	R8500					
Peak current [A]	21	10	22	11	18	12
Pulse duration [μs]	1.2	1.2	1.5	2	1.5	2
MRR [$mm^3.min^{-1}$]	1800	1800	600	200	600	200

The other TP, including the parameters related to the dielectric fluid, were set with a view to ensuring the stability and efficiency of EDM process.

4. RESULTS OF THE EXPERIMENT MEASUREMENT

Evaluated parameter in experiment was the REW m_v of two shapes of tool electrodes made from copper Cu58 and graphite R8500, which are normally used in die-sinking EDM. Individual values m_v of relative size of copper Cu58 and graphite R8500 shaped tool electrodes wear, type No. 1, 2 used in experiment in each cycles, are given in following Table 3.

Table 3 The REW values m_v of copper Cu58 and graphite R 8500 tool electrodes of type No.1, 2

Cycle No.	Copper Cu58 tool electrode							Graphite R 8500 tool electrode						
	The REW measurement values m_v [%]													
	No.1	No.2	No.3	No.4	No.5	No.6	Average [%]	No.1	No.2	No.3	No.4	No.5	No.6	Average [%]
1.	1.5	1.7	1.5	1.6	1.7	1.6	1.6	1.2	1.3	1.1	1.1	1.3	1.2	1.2
2.	1.8	1.9	1.8	1.9	2	2	1.9	1.3	1.4	1.4	1.5	1.4	1.4	1.4
3.	2.1	2.1	2	2.2	2.2	2	2.1	1.6	1.7	1.6	1.7	1.6	1.7	1.65
4.	2.4	2.3	2.2	2.2	2.4	2.3	2.3	1.7	1.7	1.8	1.8	1.9	1.9	1.8
5.	2.5	2.5	2.6	2.4	2.5	2.5	2.5	1.9	1.8	1.9	2	1.8	2	1.9
6.	2.6	2.7	2.5	2.5	2.6	2.7	2.6	1.9	1.9	1.9	2.1	2.1	2.1	2
7.	2.7	2.8	2.6	2.6	2.7	2.8	2.7	2	2	2.1	2.1	2	2.1	2.05
8.	2.8	2.8	2.9	2.9	2.7	2.7	2.8	2	2.2	2.2	2.1	2	2.1	2.1
9.	2.8	2.8	2.9	2.8	2.9	2.9	2.85	2.2	2	2.1	2.1	2.1	2.1	2.1
10.	2.9	2.9	2.9	3	2.8	2.9	2.9	2.2	2.1	2.2	2.1	2.2	2.1	2.15

Illustrative comparison of individual results of experimental measurements of the REW m_v of Cu58 a R8500 electrode material of type No. 1, 2 which were used in die-sinking EDM shows the next Fig 8.

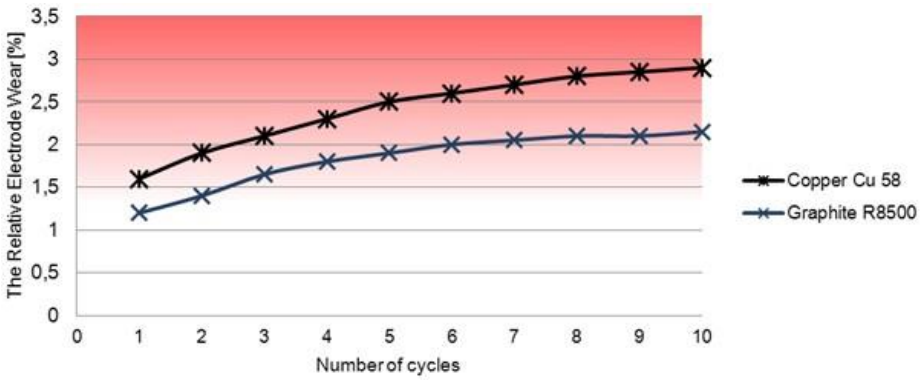

Figure 6 The REW m_v in each cycles of EDM process

The above of graphic dependence it can be observed the increased level of REW m_v of tool electrodes from Cu58 a R8500 the both types, that with increasing number of cycles the die-sinking EDM process is slightly increasing. In comparing the REW of tools made of copper and graphite we can see at higher intensities electrode wear made from copper that our initial estimates were confirmed.

CONCLUSIONS

The rate of REW used in die-sinking EDM is an important factor in choosing a suitable tool electrode material. Inappropriate physical and chemical properties of materials, used for the manufacture of tool electrodes, can cause their excessive wear, and thus impair the final accuracy and quality roughness of machined surface. By optimizing process parameters in die-sinking EDM can however eliminated the wear size of tool electrodes. Simultaneously by eliminating the wear rate of the electrode is demonstrably improved the quality of the machined surface, what has a significant impact on the efficiency of the production process itself. Aim of this article was an assessment of REW of Cu58 and R8500 tool electrodes made from materials usually used in die–sinking EDM. From the measured data it can be observed slight variations in tool electrodes wear made of copper and graphite, in which the shape of electrodes had only a minor impact on their REW.

REFERENCES

[1] Fabian, S., Straka, Ľ.: *Operation of production systems*, Edition of scientific literature, FVT TU in Košice with seat in Prešov, 252 p., 2008.
[2] Kreheľ, R., Straka, Ľ., Krenický, T.: *Diagnostics of production systems operation based on thermal processes evaluation*, Applied Mechanics and Materials, No.308, p.121-126., 2013.
[3] Maňková, I.: *Progressive Technologies*, Technical University of Kosice, Faculty of Mechanical Engineering, 2000.
[4] Neslušan, M. et al.: *Experimental methods in splinter machining*, ŽU Žilina, pp.343., 2007.
[5] Panda, A., Prislupčák, M., Pandová, I.: *Progressive technology diagnostic and factors affecting to machinability*, Applied Mechanics and Materials, vol. 616, p.183-191., 2014.
[6] Panda, A., Duplák, J.: *Comparison of theory and practice in analytical expression of cutting tools durability for potential use at manufacturing of bearings*, Applied Mechanics and Materials, vol. 616, p. 300-307., 2014.
[7] Ružbarský, J., Paško, J., Gašpár, Š.: *Techniques of Die Casting*. Lüdenscheid, RAM-Verlag, 199 p., 2014.
[8] Ružbarský, J.: *Dynamics of core taking out at die casting*, Applied Mechanics and Materials, vol. 616, special issue, p. 244-251., 2014.
[9] Straka, Ľ.: *Analysis of Wire-Cut Electrical Discharge Machined Surface*, LAP Lambert Academic Publishing, Germany, 98 p., 2014.
[10] Straka, Ľ., Čorný, I., Kreheľ, R.: *Evaluation of capability of measuring device on the basis of diagnostics*, Applied Mechanics and Materials, vol. 308, p. 69-74, 2013.
[11] Stephen, P., Radzevich, P. S., Kreheľ, R.: *Application priority mathematical model of operating parameters in advanced manufacturing technology*, The International Journal of Advanced Manufacturing Technology, vol. 56, no. 2, p. 835-840., 2011.
[12] Straka, Ľ., Čorný, I.: *Heat Treating of Chrome Tool Steel before Electroerosion Cutting With Brass Electrode*, Acta Metallurgica Slovaca, roč. 15, č. 3, p. 180 – 186., 2009.
[13] Straka, Ľ., Simkulet, V.: *Wire Tool Electrode Wear in the Electrical Discharge Pro*cess, Scientific papers: Operation and Diagnostics of Machines and Production Systems Operational States, RAM – Verlang, Germany, p. 35 – 41., 2010.
[14] Straka, Ľ., Čorný, I., Mižáková, J.: *Analysis of heat-affected zone depth of sample surface at electrical discharge machining with brass wire electrode*, Strojarstvo: Journal for Theory and Application in Mechanical Engineering, vol. 51, no. 6, p. 633-640., 2009.
[15] Žitňanský, J., Žarnovský, J., Ružbarský, J.: *Analysis of physical effects in cutting machining*, Advanced Materials Research, vol. 801, p. 51-59., 2013.

INTERNATIONAL SCIENTIFIC CONFERENCE ON ADVANCES IN MECHANICAL ENGINEERING

19 November 2015, Debrecen, Hungary

DETERMINATION OF VOLUMETRIC HEAT TRANSFER COEFFICIENT IN FLUIDIZED BED DRYER ON FULL PERIODS

SZABÓ Viktor, VARJU Evelin, POÓS Tibor PhD

Department of Building Services and Process Engineering, Budapest University of Technology and Economics
E-mail: szabo.viktor@mail.bme.hu, varjuevelin93@gmail.com, poos@mail.bme.hu

Abstract
For the scale up model of the fluidized bed dryer the heat transfer coefficient between the surface of material and the drying gas is needed. To determine the heat transfer coefficient, the heat transfer surface of the material should be exactly known. This includes a number of uncertainties due the irregular surface of the particles and the size standard deviation. The volumetric heat transfer coefficient functions can determined with measurements where the parameters of the drying gas and the particles are needed. We analyzed the drying operation on the constant and falling drying rate period by the developing a more accurate measurement method. We created the volumetric heat transfer coefficient on the full range of drying period. Using the measurements results a mathematical model can be determined to describe the fluidized bed drying.

Keywords: *Drying, Fluidized bed, Volumetric heat transfer coefficient, Heat- and mass transfer*

1. INTRODUCTION

If air flows through a bed of solid particles in upward direction with the velocity which greater than the settling velocity of the particles, the solid particles will expanding and large instabilities with bubbling and channeling of gas are observed. At this state, solid bed looks like a boiling liquid, the particles blend and bump to each other, therefore this phenomenon called as fluidized state [1, 2].
Fluidized bed drying is the optimal method for drying of wet solids. The intensive heat- and mass exchange of the fluidized bed product makes this method particularly effective and time-saving [3]. During the movement of the particles intensive simultaneous heat– and mass transfer occurs, where from the material the moisture diffuses in vapour phase to the drying gas. Among the diffusional operations drying is one of the most power demanding process, therefore to reduce the invested energy is needed. In favour of reduction of invested energy is important to know the heat– and mass transfer procedure during drying, to determine and to use the exact mathematical model describing the phenomenon.
It is important to know the heat and mass transfer process during the drying and to apply sufficiently accurate thermal models describing the process to determine device parameters. For scaling up the dryer the heat transfer coefficients between the particles and the drying gas are required, which can be determined by measurements.
The widely used approaches for modelling the fluidized bed dryers are:

- Mathematical models with heat- and mass balance equations involving transfer coefficients;
- Empirical correlations involving the parameters of drying;
- Models which assumed the bed to be made of several phases with heat and mass transfer between them [4].

2. METHODS

The measuring equipment – a pilot plant fluidized bed dryer – which is located at the Department of Building Services and Process Engineering. Figure 1 shows the instrumental flow diagram of the fluidized bed dryer apparatus.

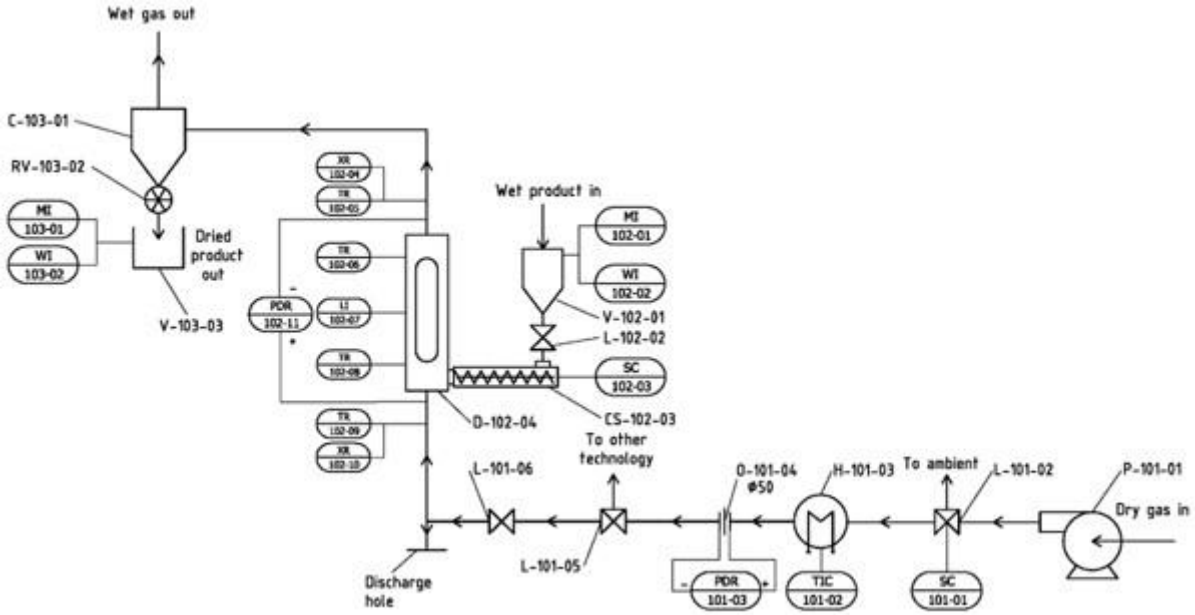

Figure 1 The instrumental flow diagram of the fluidized bed dryer

The measurement begins by turning on the fan (P-101-01), the flow rate can be modified by the knife gate valve (L-101-02), and be measured by the orifice flow meter (O-101-04) from the pressure difference (PDR-101-03). The drying gas temperature can be modified by the adjuster (TIC-101-02) of the electric heater (H-101-03). Before drying the apparatus shall be run empty until the stationary state is reached – stabilized values measured by the thermometers. Before measuring the wet material moisture content is determined by small sample experiment (WI-102-02), then the weight of the particles (MI-102-01) is measured. Through measurements in the vertical positioned dryer (D-102-04) the inlet temperature (TR-102-09) and absolute humidity (XR-102-10), the outlet temperature (TR102-05) and the absolute humidity (XR-102-04) of the drying gas, the differential pressure of the fluidized bed (PDR-101-11) and the surface temperature of the particles (TR-102-06) are measured. The height of the static bed (LI-102-07) is measured by a measuring scale with stopping the air flow in an arbitrary moment. The measured data are imported to Microsoft Excel for analysis. After reaching the stationary state the wet particles are fed to the fluidized bed dryer from a vessel signed V-102-01 by a conveyer screw (CS-102-03). At the end of the drying, when the final moisture content of particles is reached, the particles are carried out from the tube to the cyclone (C-103-01), where the particles are separated from the gas. The wet air leaves the apparatus to the ambient. The dried particles are collected in a vessel (V-103-03) through a rotary valve (RV-103-02). At the end of the drying, the weight of the dried particles (MI-103-01) is measured, then the final moisture content (WI-103-02) is determined by small sample experiment.
The volumetric heat transfer coefficient can be determined by experimental measurements. The volumetric heat transfer coefficient includes the spcific contact surface and the heat transfer coefficient between the drying gas and the particles. [5] Determination of the volumetric heat transfer coefficient from the measured data at fluidized drying is described below.

The total heat flow:

$$\dot{Q} = \dot{Q}_{heat-up} + \dot{Q}_{evap} \tag{1}$$

The volumetric heat transfer coefficient can be determined from expanding convective heat flow, to the heat flow for heating up the particles ($\dot{Q}_{heat-up}$) and to the heat flow from evaporation ($\dot{Q}_{evap}$).

$$(\alpha a)_{j+1} = \frac{1}{\left(\bar{T}_{G\,j+1} - T_{P\,j+1}\right) \cdot A_D \cdot L}\left[m_{P\,j+1} \cdot c_{P\,j+1} \cdot \frac{T_{P_{j+2}} - T_{P_j}}{t_{j+2} - t_j} + \dot{m}_G \cdot (Y_1 - Y_0)_{j+1} \cdot r_{P\,j+1}\right] \tag{2}$$

Where αa is the volumetric heat transfer coefficient, T_G is the average gas temperature in dryer, A_D is the cross section of dryer, L is the static height of bed, $\dot{m}_G$is the mass flow of gas, Y_0 and Y_1 are the inlet and outlet absolute humidity of gas and r_P phase transition heat. The weight of the wet product can be determined in every sampling moment.

$$m_{P\,j+1} = m_{P\,j} - \dot{m}_G \cdot (Y_1 - Y_0)_{j+1} \cdot \Delta t \tag{3}$$

The specific heat of the wet product (c_P) is determined from literature data [6]. The surface temperature of the particles (T_P) is measured by infrared thermometer placed in the dryer. The measured values of the infrared thermometer are checked by PT100 resistance thermometer as a reference. Figure 2 shows the checking of infrared thermometer at drying of sorghum with stopping the fan during drying. The checking points are marked with red circles. Between the values of resistance thermometer and the values of the infrared thermometer the difference is around 3%, so the infrared thermometer measures the right surface temperature.

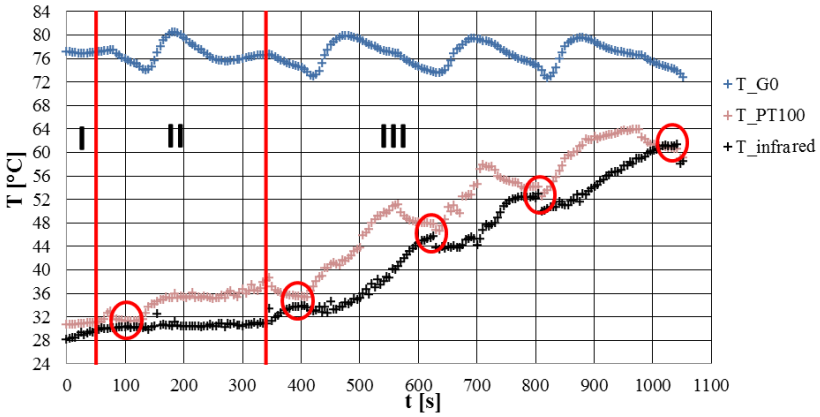

Figure 2 Surface temperatures of different thermometers in dryer at intermittent drying of sorghum in the function of time

3. RESULTS

The evaluation method is presented on drying of sorghum, where the particles were dried near to the equilibrium moisture content. During drying, the inlet temperature and velocity of gas are fixed. The wet product was dried with drying gas, which temperature was 70°C and the drying took nearly one hour. Drying curves are represented from measured data, which are similar to the theoretical drying curves. Figure 3 shows the inlet (Y_0) and outlet (Y_1) absolute humidity in the functions of

time. Figure 4 shows the inlet (T_{G0}) and outlet (T_{G1}) temperature of drying gas and the surface temperature of particles (T_P) in the function of time.

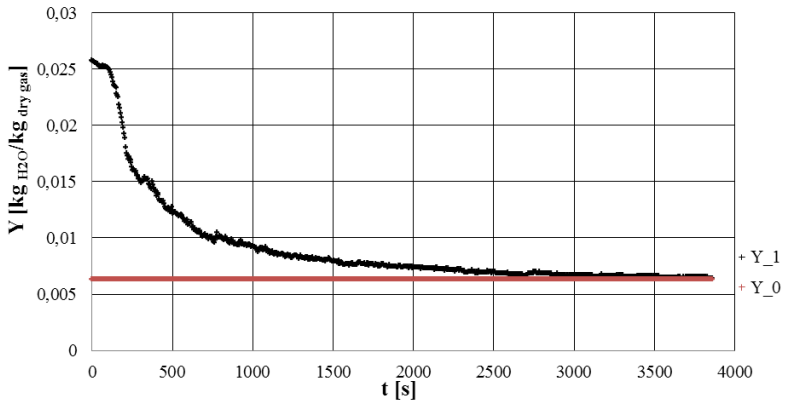

Figure 3 The inlet and outlet absolute humidity of drying gas in the function of time

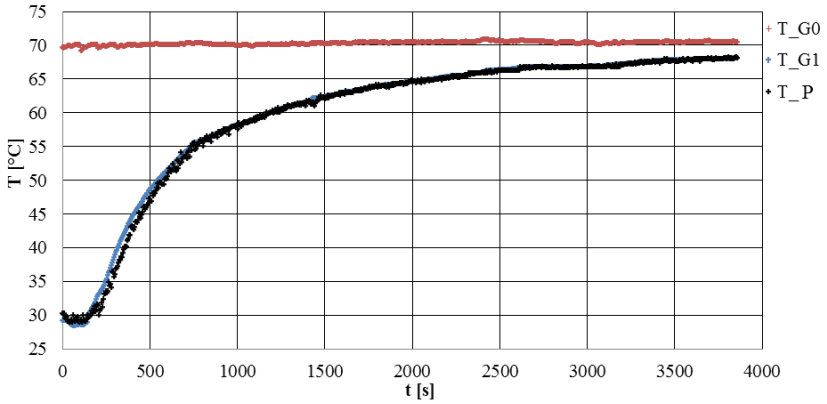

Figure 4 Temperatures in the function of time

On the constant drying rate period the surface temperature of the particles and the outlet absolute humidity of drying gas can be checked on Mollier-diagram (Figure 5). Starting from the features of the drying gas, on constant enthalpy line the surface temperature can be read on the 100% relative humidity line. On the constant drying rate period the measurement error are around 2%, which is negligible. So the infrared thermometer and the hygrometer measure the right values during drying.

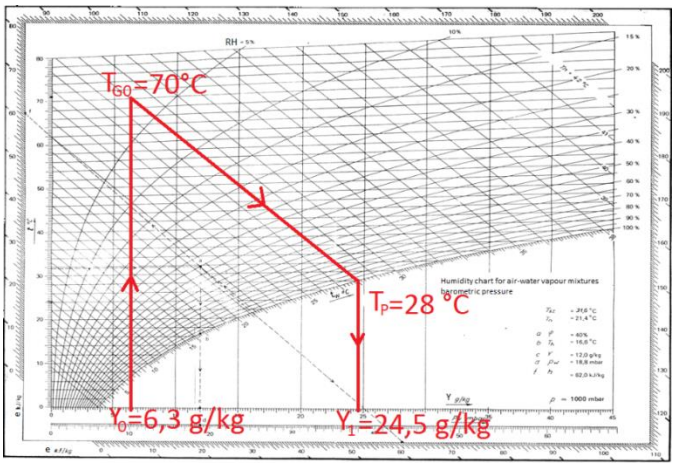

Figure 5 The checking of surface temperature on Mollier-diagram

During drying moisture content of the particles and weight of the wet product are decreasing (Figure 6, Figure 7). The variation of the moisture content and the weight of the wet product are similar to the theoretical drying curves.

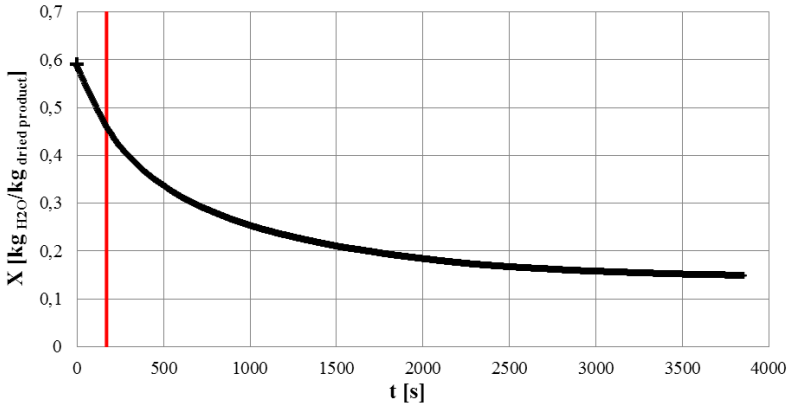

Figure 6 Moisture content of sorghum in the function of time

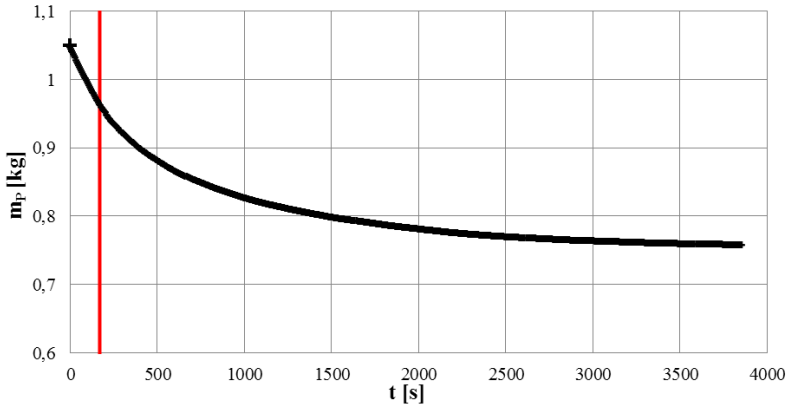

Figure 7 Weight of sorghum in the function of time

Inserting the measured values the equation (2) the volumetric heat transfer coefficient can be determine. Figure 8 shows results of the calculations, where the volumetric heat transfer coefficient constant on the constant drying rate period, and decreasing on the falling rate period.

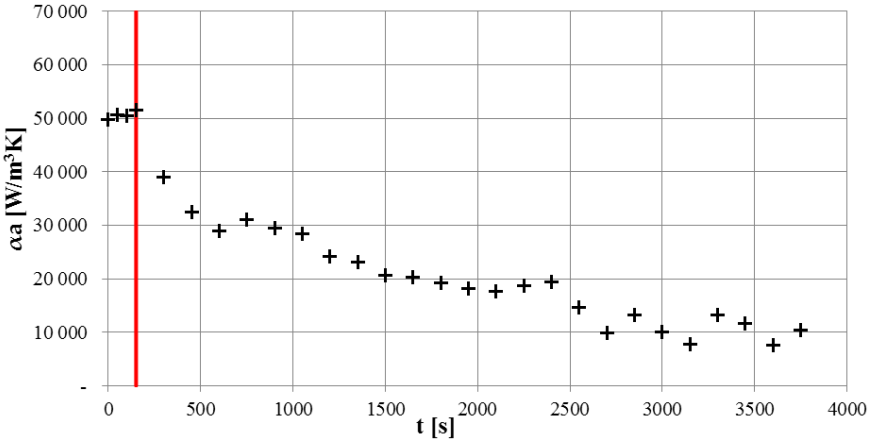

Figure 8 Volumetric heat transfer coefficient at drying of sorghum in the function of time

Figure 9 shows the volumetric heat transfer coefficient in the function of moisture content. The volumetric heat transfer coefficient constant on the constant drying rate period, and decreasing on the falling rate period and tends to equilibrium moisture content.

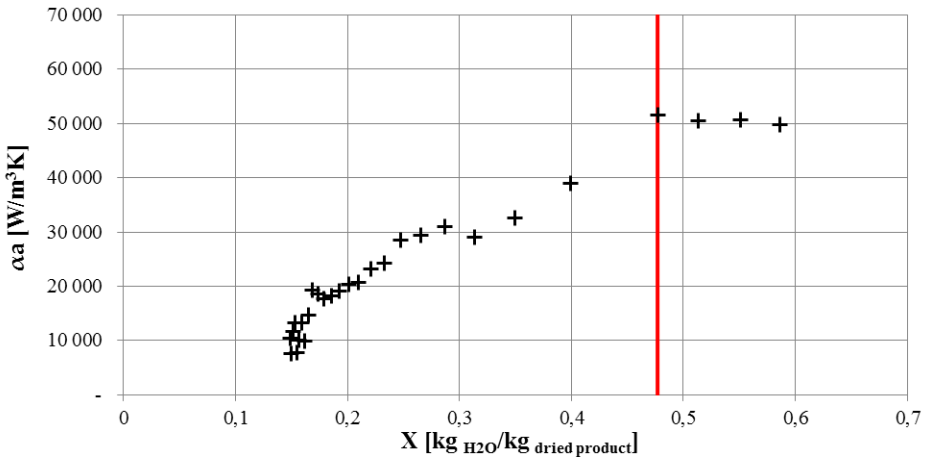

Figure 9 Volumetric heat transfer coefficient at drying of sorghum in the function of moisture content

CONCLUSIONS

The drying process can be studied on the constant and falling rate period by the described measurement method, which led to a more precise description of the fluidized bed drying. The heat transfer functions can be determined by the volumetric heat transfer coefficient, and using the heat transfer functions and the volumetric heat transfer coefficient can be created a mathematical model for description of the fluidized bed drying.

ACKNOWLEDGEMENT

Special thanks for Dr. Mária Örvös for her helps in this work. This paper was supported by Richter Gedeon Talentum Foundation (H-1103 Budapest, Gyömrői str. 19-21, Hungary), and by Hungarian Scientific Research Found (OTKA-116326).

REFERENCES

[1] Principle and working of fluidized bed dryer (17.11.2015) http://www.pharmaguideline.com/2014/08/principle-and-working-of-fluidized-bed-dryer-fbd.html
[2] Leva, M.: *Fluidizáció,* Műszaki Könyvkiadó, 1964.
[3] Kunii, D., Levenspiel, O.: *Fluidization Engineering*, 2nd edition, Butterworth-Heinemann, New York, 1991.
[4] Örvös, M., Szabó, V., Poós, T.: *Volumetric heat transfer coefficient for modelling the fluidized bed dryers*, 2015.
[5] Gangadhar, R.V., Pfost, H.B., Chung, D., Burroughs, R.: *Some properties of cereal grains, food legumes and oilseeds (hygroscopic, thermal, physical) affecting storage and drying*, Food & Feed Grain Institute Manhattan, Kansas, 1980.

INTERNATIONAL SCIENTIFIC CONFERENCE ON ADVANCES IN MECHANICAL ENGINEERING

19 November 2015, Debrecen, Hungary

VEHICLE DYNAMICS MODELLING OF AN ELECTRIC DRIVEN RACE CAR

[1]SZIKI Gusztáv Áron Ph.D, [2]HAJDU Sándor, [3]SZÁNTÓ Attila

[1]Department of Basic Technical Studies, Faculty of Engineering, University of Debrecen
E-mail: szikig@eng.unideb.hu
[2,3]Department of Mechanical Engineering, Faculty of Engineering, University of Debrecen
E-mail: hajdusandor@eng.unideb.hu, szanto930922@freemail.hu

Abstract
In the following we are presenting a vehicle dynamics simulation program developed in MATLAB environment. The program is capable of calculating the dynamics functions of a vehicle from its technical data. The program has been successfully applied for the optimization of the technical data of an electric driven race car that was designed and constructed at the Department of Mechanical Engineering of the University of Debrecen.

Keywords: *vehicle dynamics, simulation, MATLAB, optimization, electric drive*

1. THE MVM RACE

Nowadays environmental pollution is a serious and urgent global problem. Road transport in its present form is one of the most significant sources of environmental pollution. There are some new technologies [1] which can revolutionize vehicles reducing their pollutant emission. Inevitably, further research is necessary for the improvement of these technologies.
The MVM race [2] is a competition of alternative drive vehicles based on environmental friendly technologies. The constructors of the vehicles are young experts, mostly engineer students who are supported by firms or university departments. We took part in competitions in 2014 and 2015 with a race car, which was developed by the Department of Mechanical Engineering of the University of Debrecen, and we won the first and second places.

Figure 1 The start of the 2015 MVM race, with the race car of the Department of Mechanical Engineering at the first place

2. THE AIM OF THE SIMULATION PROGRAM

The optimization of the technical data of the race car is vital to be able to race effectively. (The optimization of the chain drive e.g. is of key importance.) For the above aim we developed a simulation program [3] to determine the optimal values of technical data with which we can reach the best performance (e.g. we can cover a given distance in the shortest possible time).

3. TECHNICAL DESCRIPTION OF THE RACE CAR

The race car is designed according to the basic rules of MVM student competition (prototype category), it is debuted in 2014. The frame structure of vehicle is a welded tubular space frame which is made up of aluminium tubes and hollow profiles. The front suspension of this car is a double wishbone suspension system while the rear suspension is provided by the independently suspended rear member. This member involves the complete drive-train with electric motor and chain drive, the motor control unit as well as the rear wheels. The frame structure is also consists accumulator holders at both sides of the pilot and a safety rollover hoop as well.

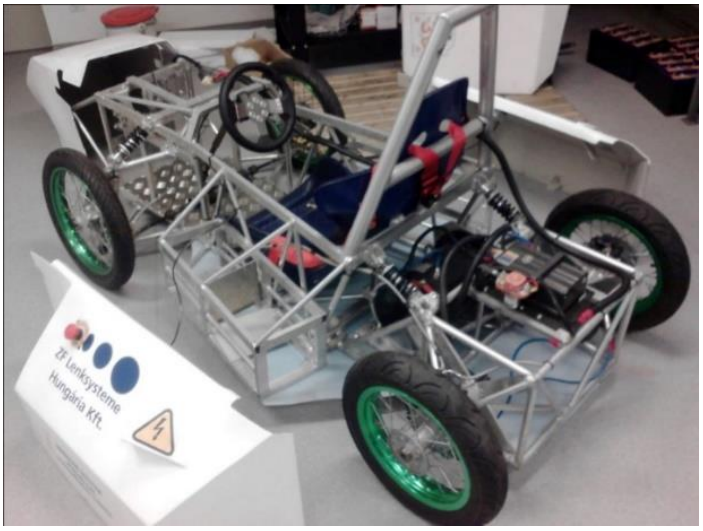

Figure 2 The race car without coverage and accumulators

The drive of vehicle is provided by a series wound DC motor with 4 kW power [4]. This motor is connected to the rear shaft of wheels via chain-drive. For the support of rear shafts bevel roller bearings are applied. For the proper deceleration of race car a divided brake system with four brake discs is used.

4. THE VEHICLE DYNAMICS MODEL

For the simulation program we elaborated a vehicle dynamics model in which the car is divided into four construction parts. These parts are the following:
1) The driven back wheels together with the connected rotating machine parts;
2) The freely rotating front wheels together with the connected rotating machine parts;
3) The body of the car together with the fixed parts of the electric motor;
4) The rotor of the electric motor.
To describe the motion of the above construction parts quantitatively, we wrote dynamics equations taking all the external and internal (between the different parts) forces and torques into account.

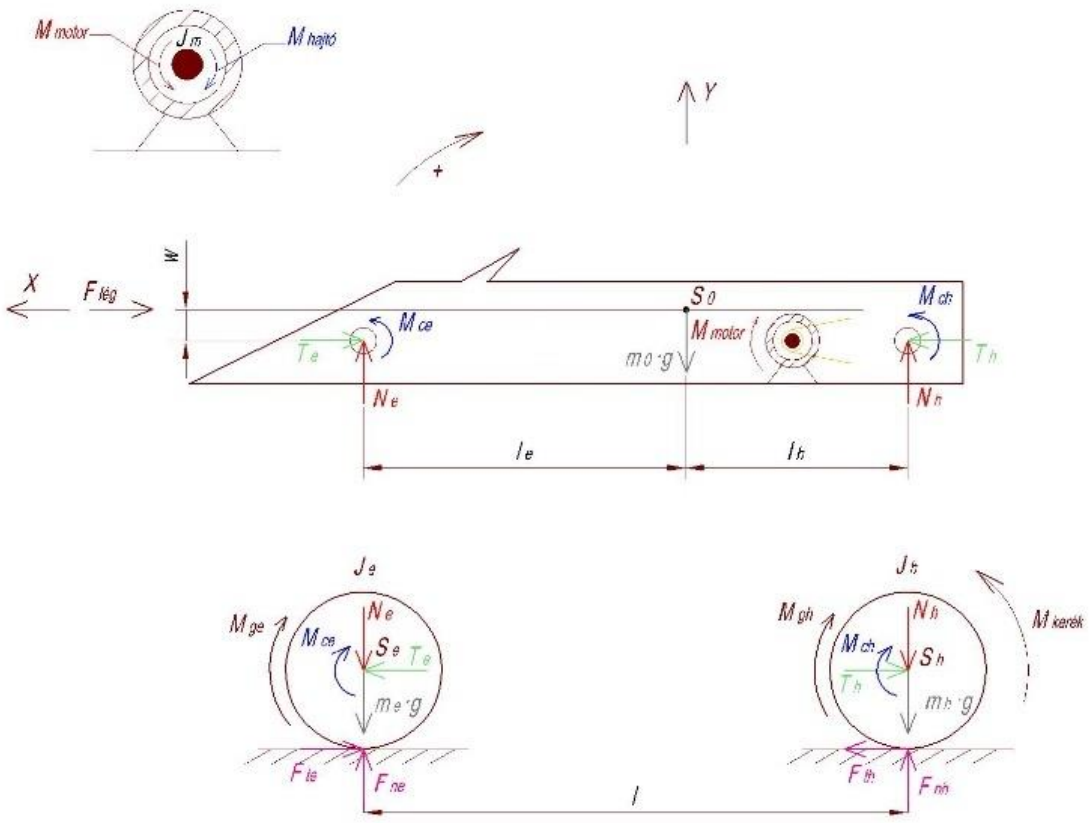

Figure 3 Forces and torques acting on the different construction parts of the race car

On the basis of *Figure 3* the dynamics equations of the motion of the different construction parts are the following:
Equations for the freely rotating front wheels together with the connected rotating machine parts:

I. $\sum_i F_{ix} = T_e - F_{te} = m_e \cdot a_s \rightarrow T_e = m_e \cdot a_s + F_{te}$

II. $\sum_i F_{iy} = F_{ne} - N_e - m_e \cdot g = 0$

III. $\sum_i M_{i(S_e)} = M_{ge} + M_{ce} - F_{te} \cdot R = J_e \cdot \varepsilon_e$

Equations for the driven back wheels together with the connected rotating machine parts:

IV. $\sum_i F_{ix} = F_{th} - T_h = m_h \cdot a_s \rightarrow T_h = -m_h \cdot a_s + F_{th}$

V. $\sum_i F_{iy} = F_{nh} - N_h - m_h \cdot g = 0$

VI. $\sum_i M_{i(S_h)} = M_{gh} + M_{ch} + F_{th} \cdot R - M_{kerék} = J_h \cdot \varepsilon_h$

Equations for the body of the car:

VII. $\sum_i \mathrm{F_{ix}} = T_h - \mathrm{T_e} - F_{lég} = \mathrm{m_0} \cdot \mathrm{a_s}$

VIII. $\sum_i \mathrm{F_{iy}} = \mathrm{N_e} + \mathrm{N_h} - \mathrm{m_0} \cdot \mathrm{g} = 0$

IX. $\sum_i \mathrm{M_{i(S_0)}} = \mathrm{M_{motor}} - (\mathrm{M_{ce}} + M_{ch}) + \mathrm{N_e} \cdot l_e - - \mathrm{N_h} \cdot l_h - T_e \cdot \mathrm{w} + T_h \cdot \mathrm{w} = 0$

Equation for the rotor of the electric motor (only for rotational motion):

X. $-M_{motor} + M_{hajtó} = J_m \cdot \varepsilon_{mot} = J_m \cdot i_{12} \cdot \varepsilon_h \left(\varepsilon_h = \varepsilon_{mot} \cdot \frac{1}{i_{12}}\right)$

Tyre slip: the slip of the back tyres was calculated by the following formula:

$$slip = \frac{\omega_h \cdot R - v_s}{v_s} \cdot 100\%$$

where ω_h is the angular speed of the wheel, R is wheel radius at the point of contact and v_s is vehicle speed.
Coefficient of friction: the coefficient of friction (the ratio of the tangential and normal force that the road exerts on the tyres) was calculated by the Pacejka "magic" formula [5, 6, 7]:

$$\frac{F_{th}}{F_{nh}} = \mu = c_1 \cdot \sin\left(c_2 \cdot \mathrm{atan}\left(c_3 \cdot slip - c_4 \cdot (c_3 \cdot slip - \mathrm{atan}(c_3 \cdot slip))\right)\right)$$

where c_1,c_2, c_3 and c_4 are constant parameters.

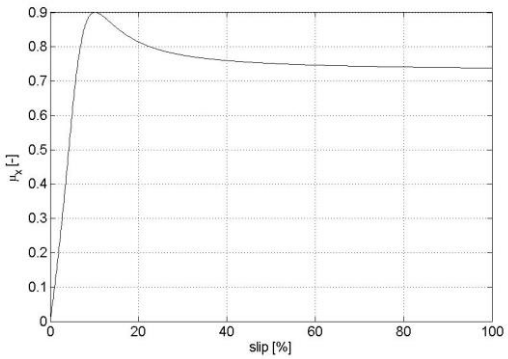

Figure 4 The graph of the Pacejka „magic" formula at values c_1*=0.9,* c_2*=1.4,* c_3*= 7.936,* c_4*= -10.*

Drag force (air resistance force): the magnitude of drag force is calculated by the following formula [7]:

$$F_{lég} = \frac{1}{2} \cdot C \cdot A \cdot \rho \cdot v_s^2$$

where C and A are the drag coefficient and cross section area of the vehicle, ρ is the mass density of air and v_s is the velocity of the vehicle relative to air.

Rolling resistance torques: the rolling resistance torques for the front and back wheels of the vehicle are calculated by the following formulas [8]:

$$M_{ge} = f_e \cdot F_{ne}, \quad M_{gh} = f_h \cdot F_{nh}$$

where f_e and f_h are the lever arms of rolling resistance, F_{ne} and F_{nh} are the normal forces exerted by the road on the front and back wheels respectively.
Bearing resistance torques: the bearing resistance torques for the front and back wheels of the vehicle are calculated by the following formulas:

$$M_{ce} = \sqrt{N_e^2 + T_e^2} \cdot \mu_{cs} \cdot \frac{d}{2}, \quad M_{ch} = \sqrt{N_h^2 + T_h^2} \cdot \mu_{cs} \cdot \frac{d}{2}$$

where, N_e, T_e and N_h, T_h are the loads on the front and back shafts in normal and tangential direction, μ_{cs} is the bearing resistance coefficient and d is the diameter of the bearing.

5. THE SIMULATION PROGRAM

On the basis of our dynamics model we created a simulation program in Matlab [9] environment. The program is capable of calculating the vehicle dynamics functions of the car from its technical data. The block diagram of the program is presented in *Figure 5*.

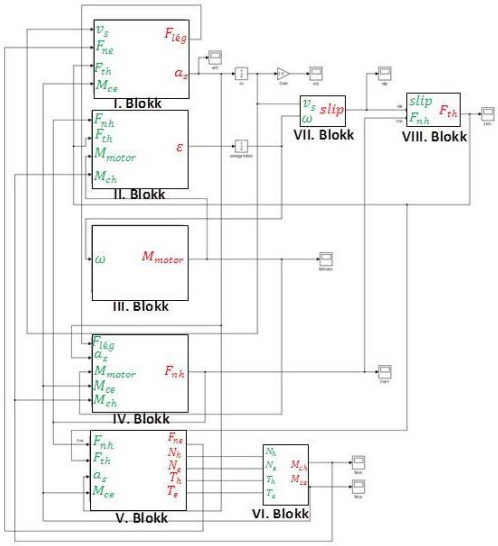

Figure 5 The block diagram of the simulation program

All of the blocks have a complicated internal substructure which is described in reference [3] in details.

6. EXPERIMENTAL DETERMINATION OF INPUT PARAMETERS FOR THE PROGRAM

For the determination of some input parameters of simulation program complex measurement procedures are required. Some of these parameters (e.g. characteristics of DC motor, masses and

moments of inertia of components, centre of gravity of car, etc.) are already determined during this research, while some other parameters (e.g. resistance to rolling, friction and drag coefficients, etc.) will be determined in the future. In the following section the experimental determination of DC motor characteristics is discussed.

6.1. Characteristics of DC motor

The experimental determination of DC motor characteristics is made in cooperation with an educational partner (Debreceni Képző Központ/DKK Debrecen, Budai Ézsaiás u. 8/A) in their electrical laboratory (E04). The actual measurement is presented in Figure 6.

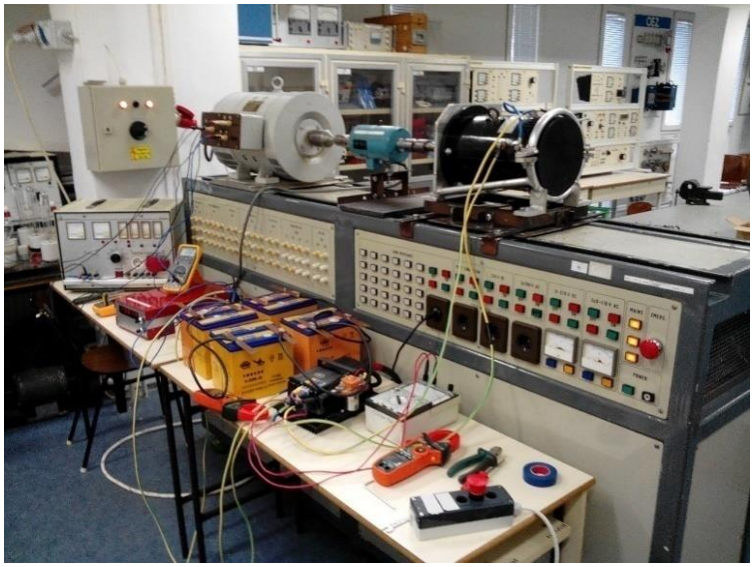

Figure 6 Measurement of DC motor characteristics

The schematic drawing of measurement setup is shown in Figure 7.

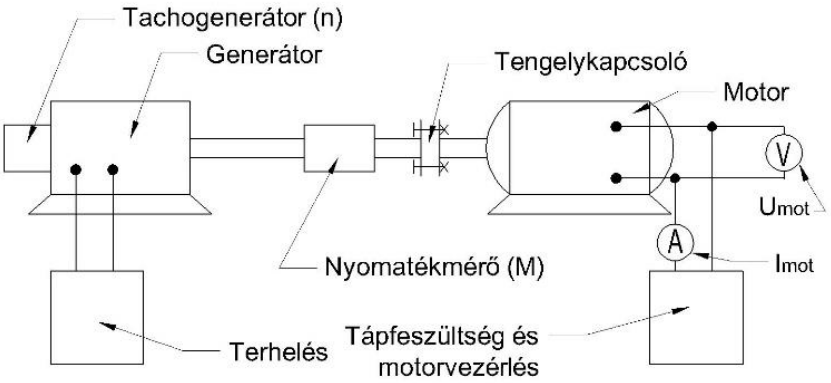

Figure 7 Schematic drawing of measurement setup

The measured DC motor is fed by four accumulators (with voltage 12V) connected in series via an electronic motor control unit. The final voltage of DC motor can be controlled by a “throttle” pedal. The introduced setup is exactly the same as the system applied in vehicle during race. The measurements of motor characteristics are performed with maximum position of control pedal (i.e. maximum “throttle”). The results of measurements are presented in *Table 1*.

Table 1 Results of the measurements

48 [V]	1	2	3	4	5	6	7	8	9	10	11
n [V]	3,9	8,3	10	13	16	20	26	32	37	42	54
n [1/min]	156	332	400	520	640	800	1040	1280	1480	1680	2160
M [Nm]	70	65	57	46	43	37	29	28	23	23	19
Imot [A]	410	390	341	307	280	258	216	202	177	180	136
Umot [V]	18	22	21	21	22	22,5	24,5	27,5	29	34	39
Ibe [A]	340	270	290	270	250	220	208	203	177	180	140
Ube [V]	49	49	49	49	49	49	49	49	49	49	49

The torque-speed curve of the investigated DC motor is shown in *Figure 8*.

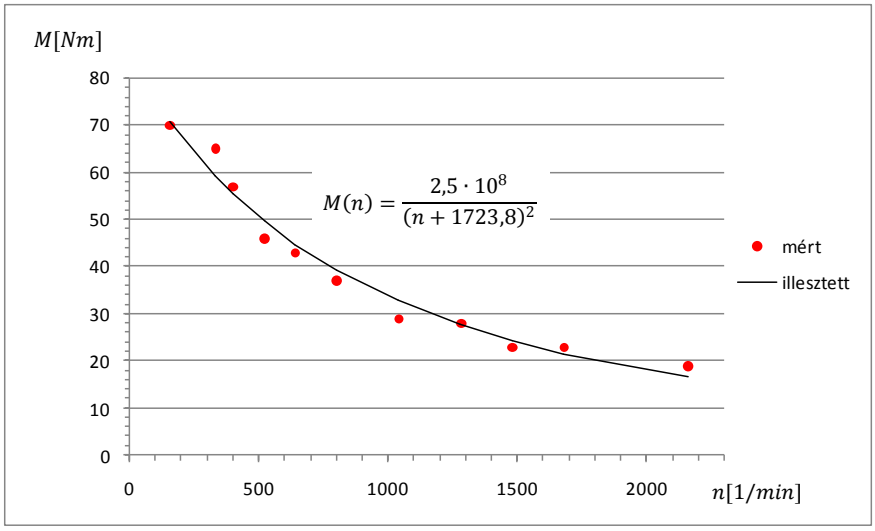

Figure 8 Torque-speed curve of DC motor

In *Figure 8* the measured data is denoted by red dots. In the simulation program the torque-speed characteristic is approximated by a regression curve which is made by the help of Maple13 [10]. The regression curve as well as its formula is also presented in *Figure 8*.

7. VEHICLE DYNAMICS FUNCTIONS GENERATED BY THE PROGRAM

The vehicle dynamics functions of the car which can be generated by the program are the following:

- The acceleration, velocity and covered distance as a function of running time
- The forces exerted by the road on the tyres in tangential and normal direction as a function of running time
- The loads on the front and back shafts in tangential and normal direction as a function of running time
- Rolling and bearing resistance moments as a function of running time
- Drag force as a function of running time
- Tyre slip as a function of running time

Figure 9 shows the tractive (tangential) force that the road exerts on the back wheels of the car as a function of running time at different gear ratios in the chain drive. Except for the gear ratio, all the other parameters have the same value in the presented three cases.

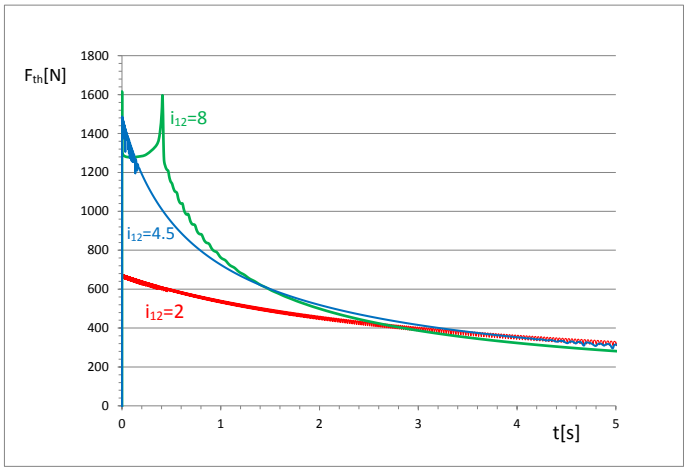

Figure 9 Tractive force acting on the periphery of the back wheels as a function of running time

Figure 10 shows the velocity-time functions of the car at the same gear ratios as those was presented in *Figure 9*.

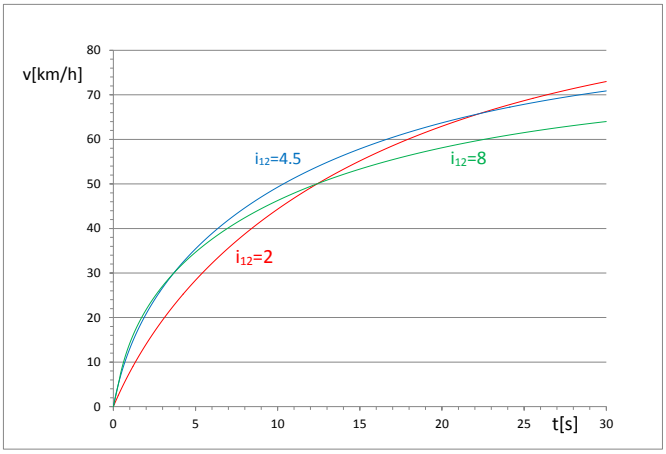

Figure 10 Velocity-time functions of the car at different gear ratios

Figure 11 presents the normal forces that the road exerts on the front and back wheels of the car as a function of running time.

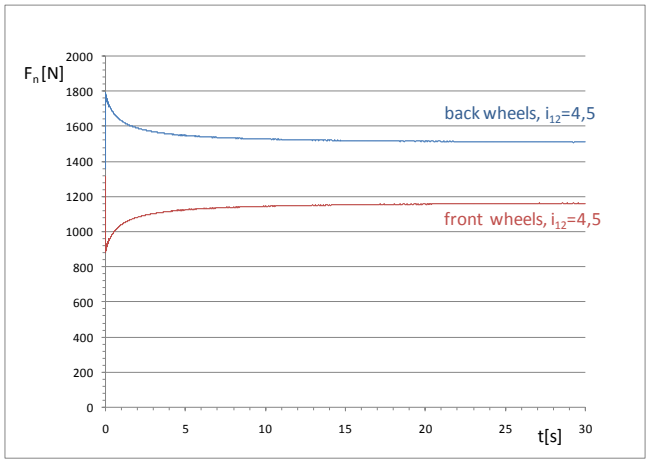

Figure 11 Normal forces that the road exerts on the front and back wheels of the car as a function of running time

8. APPLICATION OF THE PROGRAM FOR AN OPTIMIZATION PROBLEM

The main aim of the program is the determination of the optimal values of technical parameters at which the best vehicle dynamics characteristics can be obtained. Obviously for the different racing events different values are optimal. Different values are favourable e.g. for a long distance race on a circular track or for a shorter one (e.g 200m long) on a linear one. In the following we are going to deal with the latter case and perform the optimization for two technical parameters. One of the parameters is the distance between the centre of mass and back shaft of the vehicle in horizontal direction (l_h), the other one is the gear ratio in the chain drive (i_{12}). All the other parameter values are the same as the ones in the real race car. During the optimization process the values of the l_h and i_{12} parameters were varied in the [2;8] and [0;0,675][m] range respectively. The necessary time for covering the 200m distance was calculated and plotted as a function of the two parameters. The obtained graph is shown in *Figure 12*.

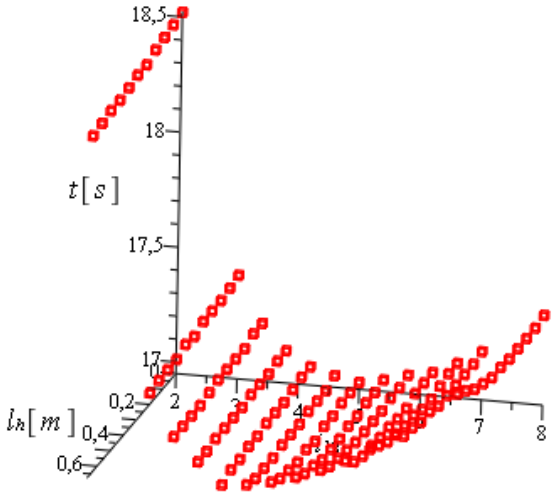

Figure 12 The necessary time for covering the 200 m distance as a function of the l_h and i_{12} parameters

From the results it can be seen that the minimum running time can be achieved applying the $l_h = 0.4[m]$ and $i_{12} = 5$ values.

CONCLUSIONS

The presented simulation program – at the recent stage of development – is capable of calculating the vehicle dynamics functions of a car – which is accelerating on a linear track – from its technical data. Besides the usual vehicle dynamics functions (acceleration-, velocity- and covered distance-time functions) the program is capable of calculating the normal and tangential (tractive) forces that the road exerts on the tyres and also the shaft loads in tangential and normal direction as a function of running time.
The program takes into account almost all the factors that have an effect on the motion of the car (e.g. the motor characteristics, bearing, rolling and air resistance, the moment of inertia of the rotating parts, the position of the centre of mass of the vehicle, the interaction between the road and the tyres as a function of tyre slip)

In the case of the electric driven race car – that was designed and constructed at the Department of Mechanical Engineering of the University of Debrecen – we have already measured some of the input technical data. These data are motor characteristic, moment of inertia of the rotating machine parts and position of the centre of gravity of the vehicle. We also intend to measure the remaining data in the future.

At the recent stage of development – regarding an accelerating car on a linear track – the program is capable of calculating the optimal values of technical data at which the best vehicle dynamics characteristics can be achieved. We demonstrated it with the solution of an optimization problem containing two independent variables. In the near future we are planning to improve our program for a vehicle which is moving on a curvilinear track and can have accelerating and decelerating motion periods.

REFERENCES

[1] Zöldi, M., Emőd, I., Tölgyesi, Z.: *Alternatív járműhajtások,* Maróti Könyvkereskedés és Könyvkiadó Kft. ISBN 9639005738, 2006.
[2] http://energiafutam.ahjv.hu/content/index/id/1/m/5
[3] Szántó, A.: *Elektromos hajtású tanszéki versenyautó járműdinamikai modellezése*, TDK dolgozat, konzulensek: Síki Gusztáv Áron, Hajdu Sándor, 2015.
[4] http://webaruhaz.permanent.hu/termek/elektromos_auto-1-motorok-135/dc48v_os__4kw_os_soros_villanymotor-187
[5] Pacejka, H.B., Igo Besselink, I.: *Tire and Vehicle Dynamics*, (Third edition) Published by Elseiver Ltd. ISBN 978-0-08-097016-5, 2012.
[6] Reimpell, J., Betzler, J.W., Bári, G., Hankovszki, Z., Kádár, L., Lévai, Z., Nagyszokojai, I.: *Gépjármű futóművek I.*, ISBN 978-963-279-606-2, 2012.
[7] Heissing, B., Ersoy, M.: *Chassic Handbook*, ISBN 978-3-8348-0994-0, 2011.
[8] Ilosvai, L.: *Járműdinamika*, 2013.
[9] Matlab (2014b), TheMathWorks, Inc, Natick, Massachusetts, United States.
[10] Maple 13.0, Copyright © Maplesoft, a division of Waterloo Maple Inc. 1981-2009.

INTERNATIONAL SCIENTIFIC CONFERENCE ON ADVANCES IN MECHANICAL ENGINEERING
19 November 2015, Debrecen, Hungary

IMPLEMENTATION AND OPERATION FEATURES OF ECVT

[1]TIBA Zsolt PhD, [2]FEKETE-SZŰCS Dániel

[1]Department of Mechanical Engineering, Faculty of Engineering, University of Debrecen
E-mail: tiba@eng.unideb.hu
[2]AFT Soft Ltd.
E-mail: fszdani@unideb.hu

Abstract
The designation CVT and ECVT are common term and refer to the operation principle of the transmission, namely it changes the kinetic ratio continuously. This type of devices is continuously variable transmission. Designation ECVT refers to the way of controlling its ratio by means of variable RPM of an electric motor. The application field of ECVT is versatile. The object of this paper is to compare the two operation principles and to analyse the electronic control implemented by an electric motor. The control of ratio needs power provided by the prime mover. The measure of removed power and its utilization possibility in the drive influences the operation of the vehicle or any other devices

Keywords: *planetary gear, harmonic drive, continuously variable transmission.*

1. INTRODUCTION

1.1. CVT based on V-belt drive

A transmission without discrete stages may be implemented by different constructions. The most common applied CVT can be seen in Fig. 1 representing the drivetrain of a scooter.

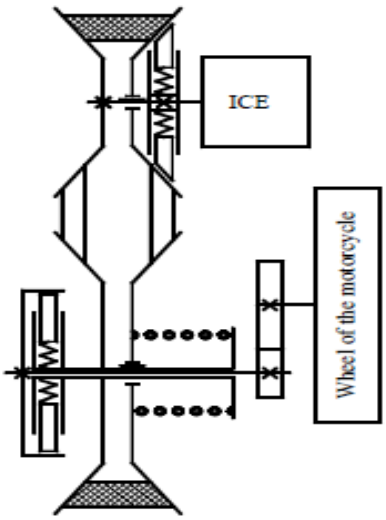

Figure 1 CTV with a centrifugal coupling

Its operation principle is based on the V-belt drive having constant centre distance and continuously variable ratio. The two pulleys have split construction with an adjustable distance between the pulley disc halves. The V-belt runs on the datum diameters of the pulleys determined by the

distance between the pulley disc halves and transmit the peripheral force. The precondition of the operation is the appropriate synchronization of the axial displacement of the disc haves. The axial displacement of the driver disc half is implemented by the flyweights, which proportional to the rotational speed exert centrifugal force enforcing the movable disc half toward the fixed one modifying the datum diameter of the pulley. Since the centre distance and the belt datum length will not change, the momentary position of the movable disc half of the driven pulley has to be in accordance with the datum diameter of the driver disc. This may be implemented simply with a half disc enforced by a cylindrical spring in axial direction.
The CVT transmits the power to the driven wheel through another centrifugal coupling. The flying shoes of the centrifugal coupling rotating at the rpm of the driven pulley of the CVT are forced to the inner surface of a drum which is assembled on the output shaft by a splined joint. This output shaft drives the rear wheel of the scooter through a geared transmission.
The control of this type of CVT operating with 2-3% slip, removes negligible power from the prime mover represented by the kinetic energy of the flyweights. In engine brake mode this energy is into the environment in the form of heat energy. When increasing the RPM again, the kinetic energy of the flyweights is provided by the prime mover.

1.2. ECVT based on 3 degree of freedom system gears

The operation principle of ECVT is based on the freedom system of different type of gear drives e.g. planetary gear and harmonic drive. If one of the shafts of a 3 degree of freedom gear is the output (driven) shaft, the other two shafts left are input (driver) shafts. By modifying the speed of one of the input shafts the speed of the output shaft hence the ratio of the transmission may be controlled continuously.
Following three ECVT-s are introduced and analysed.

1.2.1. ECVT implemented with harmonic drive

Fig. 2 shows the active steering-gear of AUDI, providing variable ratio between the steering wheel and the wheels.

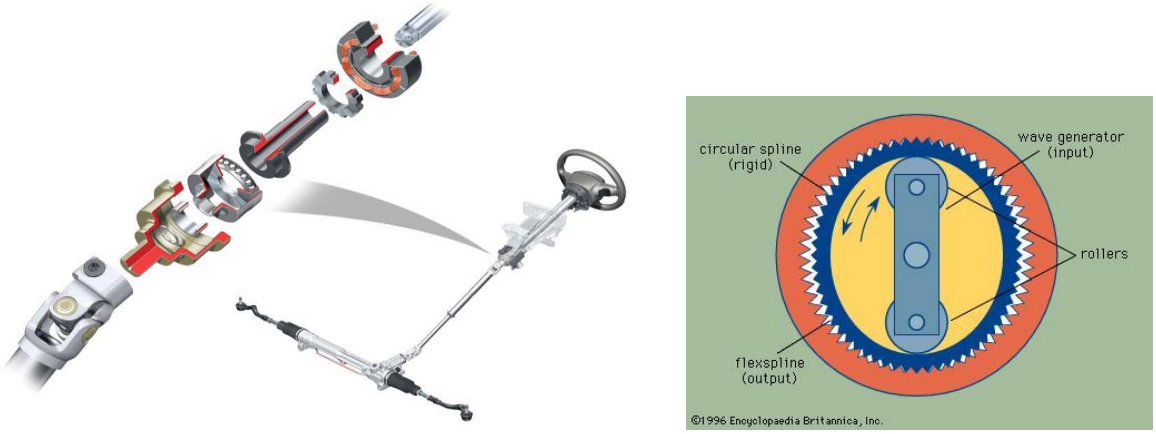

Figure 2 AUDI steering unit with harmonic drive [1]

The circular spline has internal teeth that mesh with external teeth on the flexspline. The flexspline has fewer teeth and consequently a smaller effective diameter than the circular spline. The wave generator is a link with two rollers that rotates within the flexspline, causing it to mesh with the circular spline progressively at diametrically opposite points. The ratio of the drive [2]:

$$i = \frac{z_{circular\ \ spline}}{z_{circular\ \ spline} - z_{flexspline}} \tag{1}$$

The circular spline, driving the pinion of the rack and pinion gear, is the output of the harmonic drive. The other two elements serve as input of the harmonic drive. The flexspline is driven by the steering wheel, while the wave generator is driven by an electric motor having variable RPM in clockwise and counter-clockwise.

1.2.2. ECVT implemented with K+K type planetary gear

Fig. 3 shows the active steering-gear of BMW, providing variable ratio between the steering wheel and the wheels. One of the sun gears, driving the pinion of the rack and pinion gear, is the output of the planetary gear. The other two elements serve as input. The another sun gear is driven by the steering wheel, while the arm of the planetary gears is driven by an electric motor having variable RPM in clockwise and counter-clockwise. The RPM equation of the K+K type planetary gear [2]:

$$n_1 - \frac{r_2}{r_1} + \frac{r_3}{r_2'} n_3 = \left(1 - \frac{r_2}{r_1} + \frac{r_3}{r_2'}\right) n_k \tag{2}$$

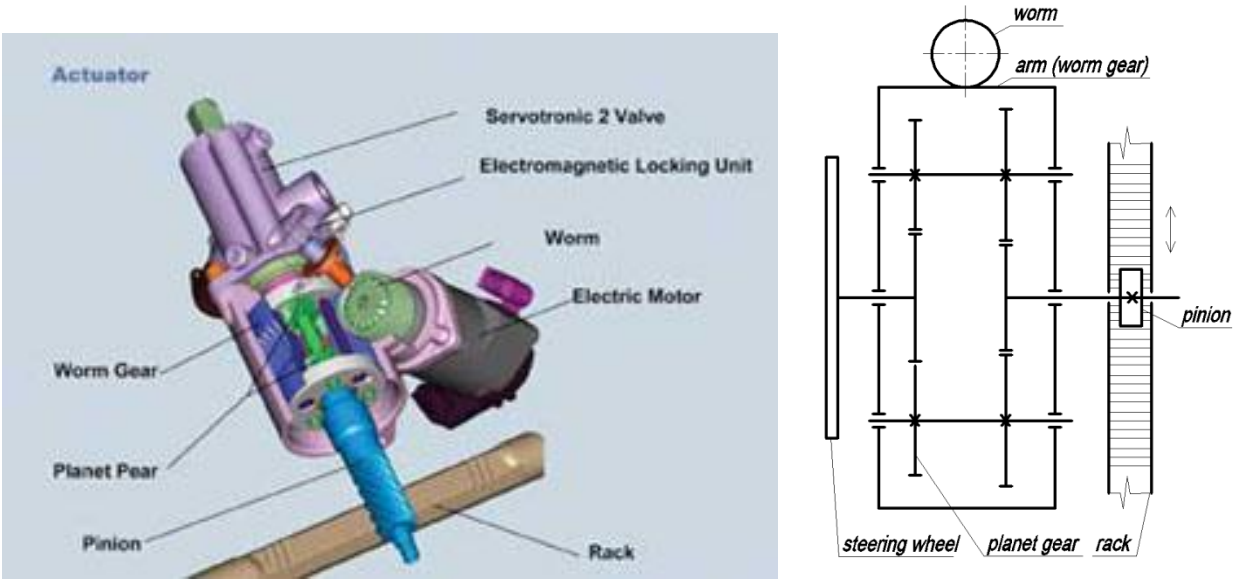

Figure 3 BMW steering gear unit with planetary gear [3]

The control of ECVT implemented with harmonic drive and K+K type planetary gear removes power from the prime mover however the power of the steering unit contains the power of both of the input shafts, hence it is utilised in the drive.

1.2.3. ECVT implemented with KB type planetary gear

ECVT implemented with KB type planetary gear applied in Toyota Auris HSD 1.8 hybrid car. The Fig. 4 shows the simplified scheme of Toyota Auris HSD 1.8 drivetrain in which the e-CVT transmits the whole power of the ICE to the driven wheels. In this chapter we determine the power demand of the ECVT control in proportion to the ICE power.

The transmission contains a three degree of freedom system KB type planetary gear which active elements connect to MG1, MG2 and ICE. In the Toyota Full Hybrid system the momentary kinematic ratio of the ECVT is adjusted by controlling the sun gear's RPM with the MG1 generator.

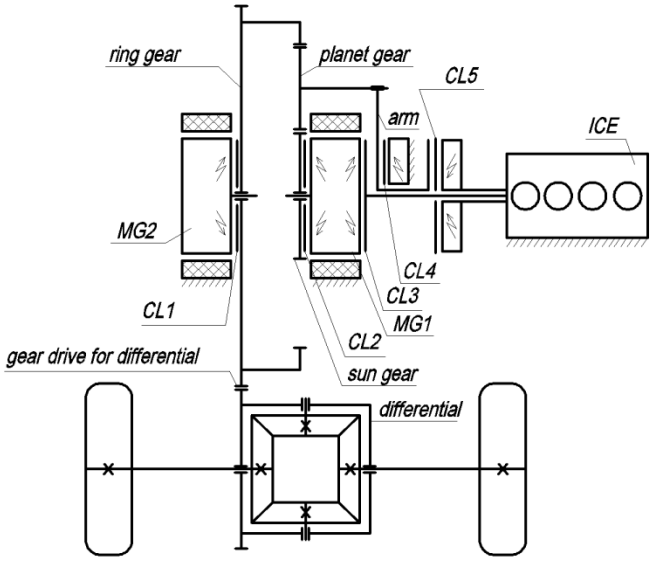

Figure 4 Simplified scheme of the Auris HSD drivetrain

The units of the system:
HV (high voltage) battery [4]
Liquid-cooled, 201 V nominal voltage NI-Mh battery has 6.5 Ah nominal capacity. It is charged via the inverter by the MG1 and MG2 electric motors in generator mode and it supplies the MG1 and MG2 electric motors. The battery can store approximately 1.9 kJ energy provides 2-3 km mobility with pure electrical drive at a low speed. The battery storage capacity is sufficient only for some regenerative braking and it is really not appropriate for assisting the ICE by supplying the MG2.
Data of the drivetrain [5]:
ICE
Nominal power: 73 kW (99 LE), 5200 1/min**;**
Nominal torque: 142 Nm, 4400 1/min
Maximal RPM: 5800 1/min
Displacement: 1798 cm^3 (Atkinson-Miller) suction petrol engine
RPM equation of the transmission [2]:

$$n_1 + \frac{r_3}{r_1} n_3 = \left(1 + \frac{r_3}{r_1}\right) n_k \tag{3}$$

Electric motors/generators:
MG1
RPM range: 0-11000 1/min
MG2
Power: 60 kW; maximal torque: 207 Nm; RPM range: 0-5000 1/min
Vehicle
Overall power: 100 kW (136 LE) (according to the owner's manual)
max. speed: 180 km/h

Analyzing the data of overall power and maximal speed, there is a contradiction between them since the car with 136 LE power should have the max. speed above 210 km/h. To the given 180 km/h max. speed approximately 75-80 LE power corresponds. It is in conformity with the owner's feedback namely the 136 LE power is only for a few minutes at disposal and after that the performance of the ICE drops expendable for drive. We will discover that MG1 generator is responsible for the low performance since it takes off power from the ICE in order to control the ratio.

Operation of the ECVT:
A KB type planetary gear has three active elements: ring gear, sun gear and arm. All of the clutches applied are electromagnetic operated and controlled by the ECU (electronic control unit). The ICE is connected to the arm via a single disc friction clutch fixing one degree of freedom. In addition to, the arm connects to the frame via a multi disc clutch as well. The MG2 connects to the ring gear via a multi disc clutch thus to the driven wheels as well fixing one degree of freedom. It follows from this that if the ICE drives the planetary gear in this set-up, only the sun gear representing the only degree of freedom allowed would revolve, forasmuch as that its resistance is substantially less than one represented by the car drive. This is why the kinematic ratio of the ECTV can be modified by the control of the MG1's RPM connecting to sun gear via a multi disc clutch. Apart from reversing, the MG1 operates as a generator to brake the sun gear. In reverse gear the MG1 operates as an electric motor and rotates in the opposite direction. In addition to the basic task of the MG1, it is connected to the ICE via a multi discs clutch in order to start the ICE.
According to the measure of the gas potentiometer and the travelling resistances, the ECU determines the RPM of the ICE and the MG1 required, by this means the momentary kinematic ratio of ECTV. Fig. 5 represents the operation stages of hybrid vehicles. The power requirement of the car is small when creeping in traffic jam or standing at signal lamp; it can be provided by the electric motor as well. In this case the use of the ICE at low RPM, performance and efficiency can be avoided. A common hybrid car with a pure electric drive may run the car at a speed of about 10-30 km/h for approximately 2-5 km distance.

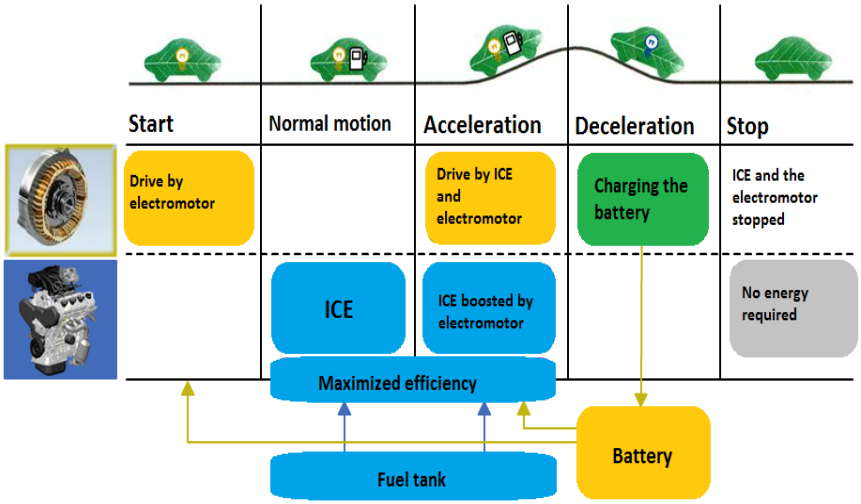

Figure 5 Operation stages of hybrid vehicles

In case of higher power demand or discharged battery, the ICE starts and drives the car as well as charges the battery if required. When accelerating the car very hard, the MG2 electric motor helps ICE drive the car provided that enough battery capacity is at disposal. In brake mode the ICE shuts

down and the kinetic energy of the vehicle would not transform into friction heat in the mechanical brakes but stored in the battery by driving the MG2 generator. All of these technical solutions result in decreasing fuel consumption; e.g. the combined fuel consumption of a common Toyota Auris 1.33 is approximately 5.9 l/100 km, and its emission is about 128 g of CO_2/100 km; whereas the urban fuel consumption of Toyota Auris HSD 1.8 (hybrid car) is about 3.8 l/100 km and its emission is about 88 g of CO_2/100 km. Although this data is only informative however it can be seen, that in special traffic circumstances significant fuel consumption decrease can be achieved.

Take-off (the ICE is out of order)

In pure electric mode MG2 drives the ring gear via the CL1 (all the other clutches are disengaged).

Acceleration

At intensive speed-up the ICE and the MG2 drive together. For this the ICE must be started effected by the MG1 via the CL3. After that CL3 disengages, CL2 and CL5 engage, by this means the ICE drives the arm and the kinematic ratio results from the MG1's RPM in generator mode (taking off power from the ICE).

The measuring results show that the MG2 utilize the energy stored in the battery very fast, accordingly at intensive speed-up it can assist the ICE only for a few seconds. The ECU controls the ECVT so that the ICE operates at high RPM and efficiency.

Steady operation

The car runs at an approximately steady speed driven by the ICE. The CL1 and CL3 are disengaged; the CL2 and CL5 are engaged. The task of MG1 is to control the e-CTV hence it operates in generator mode taking off power from the ICE. To avoid the battery overcharging, the MG2 is supplied by the battery accordingly the MG2 drives occasionally the ring gear via the engaged CL1.

Braking, downhill

The ICE stops, CL5 disengages and simultaneously CL4 engages. Clutches of MG1 and MG2 (CL1 and CL2) are engaged hence the wheels of the car drive back the MG1 and MG2 generators utilizing the kinetic energy of the moving vehicle.

Charging during drive

In case of run-down battery, one part of the ICE's power is provided for driving the MG2. Apart from CL3 and CL4 all of the clutches are engaged. When the battery is charged-up, the clutch of MG2 (CL1) disengages accordingly the power of ICE is devoted only for driving the car.

2. MEASURING

Measuring were conducted with the Toyota Motor Corporation Techstream application [6] can be connected to the ECU provides ON-LINE diagnostics for data acquisition and evaluation.

Fig. 6 shows measuring records of measurement carried out in NORMAL mode with average charged HV battery. The records show one minute measuring interval of (from top to down) ICE's RPM, MG2 torque, MG1's RPM, MG1 torque and the velocity of the car in the function of time. It can be seen, that during the measurement we stopped two times, the maximum speed was 107 km/h and the acceleration achieved pertained to 80% gas potentiometer. The fourth diagram from the top represents the MG1 torque. It shows that the MG1 is always in generator mode however there are protuberant peak values when the MG1 connects to the inverter.

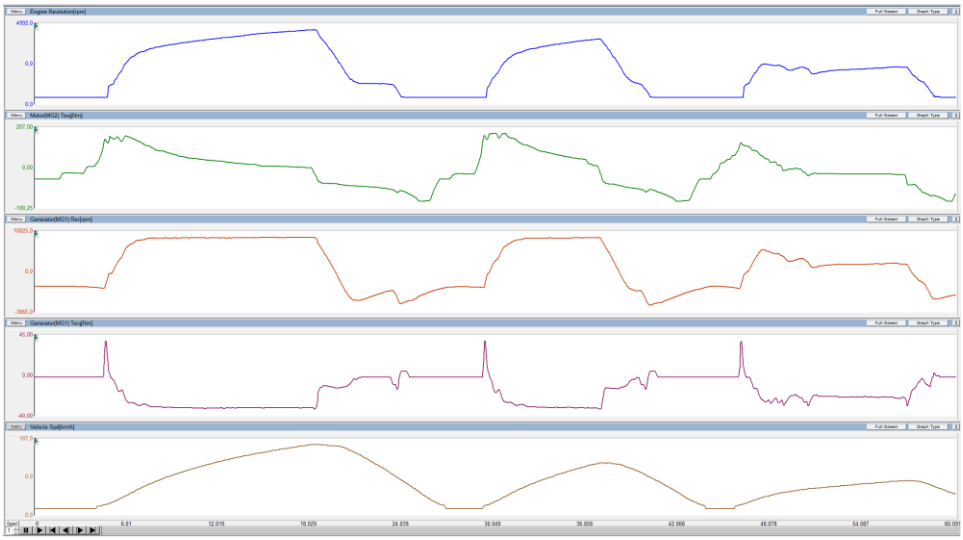

Figure 6 "drive performance" on the road [7]

The fifth diagram shows that car speed does not proportionally increase with the ICE's RPM, because the necessary tractive force can be provided by increasing RPM of MG1in order to adjust appropriate kinematic ratio. This way MG1 takes off more and more power from the ICE. It is very important to analyse the MG2 torque. At the beginning of speeding up, MG2 assist in driving the car, later on its torque drops to zero. The assists take approximately 5 s. After throttling-down, the MG2 switches into generator mode and the ICE stops.

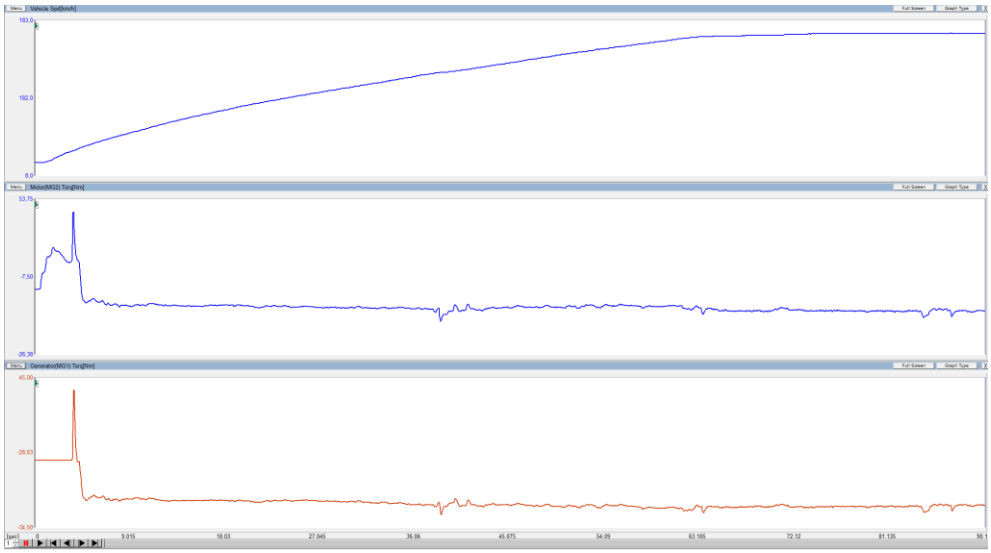

Figure 7 Test stand measuring "drive performance" [7]

Facts and figures of measurement:

- Significant part of the ICE power is devoted for driving the MG1 (approx. 40 kW from 73 kW), which is compensated for a limited time with the MG2 power (approx. 60 kW).
- MG2 can assist the ICE for approximately 5 s, since the battery runs down.
- Inference: in case of hard speeding up (continuous, sequential overtaking) the drive dynamic of the car is worse as if it was driven only by the ICE. In braking mode the recuperation effects, however the kinetic energy recovered is not sufficient for charging the HV battery.

Fig. 7 shows measuring record of maximal acceleration in NORMAL mode with a slightly run-down HV battery. The test took 90 seconds the car was speed-up to 183 km/h on test stand. This data is only informative since the resistances generated by the test stand can not be considered authoritative. The diagrams show from the top to the bottom the velocity of the car, torque of MG2 and MG1.

Facts and figures of measuring:

- MG1 torque has a transient peak value, which can not be good for power electronics.
- MG2 operates only 5 sec long as electric motor, after that in generator mode it takes off 3-7 Nm torque from the ICE.
- MG1 operates all the time as generator taking off 15-20 Nm torque from the ICE. It is approximately the half of the previous measuring result, which shows that the resistances on the test stand are not real.
- In spite of the driver intention to achieve maximum acceleration, from the 73 kW nominal ICE power only 56 kW is at disposal because of the power demand (17 kW) of the ECVT operation.
- The battery cannot be charged during the 90 sec of test operation.

According to the owner manual the power of the ICE is 73 kW. It appeared from the measuring that one part of the ICE power (17/73 = 23 %) is not used for powering the car. It means that actual available total power of the system (ICE and electric motor) is only 56 kW instead of the given 100 kW. Similar to the previous test, MG2 was able to assist the ICE only for 5 sec.

Measurements conducted in ECO and POWER modes were similar to the previous one in NORMAL mode, therefore do not set them forth.

CONCLUSIONS

The electronic control of the ECVT removes a lot of energy from the prime mover. Although this energy used for charging the battery is utilized by driving the car with MG2, however the mechanical energy was transformed four times (electrical energy - electric charge – electrical energy – mechanical energy) causing power loss because of the efficiency of energy transformations. Eventually 73 kW max. power ICE can provide only 56kW average power for driving the car. The electronic control requires 23% of the power to be transmitted.

REFERENCES

[1] http://mag.ebmpapst.com/en/industries/automotive/audi-a4-the-adaptive-steering_1321/
[2] Tochtermann-Bodenstein: *Gépelemek 2.*, Műszaki Könyvkiadó, Budapest, 1986., ISBN: 963 106407 7.
[3] http://www.ai-online.com/Adv/Previous/show_issue.php?id=277#sthash.iu0kpP3D.dpbs
[4] Nickel Metal Hybrid Handbook and Application Manual, data.energizer.com, Energizer Battery Manufacturing Inc. 2010.
[5] Toyota Owner's manual
[6] Techstream on-line help, Toyota Motor Corporation, V10.00.028, 2015.
[7] Imre Toth's Thesis 2015, University of Debrecen, Faculty of Engineering, Department of Mechanical Engineering

INTERNATIONAL SCIENTIFIC CONFERENCE ON ADVANCES IN MECHANICAL ENGINEERING
19 November 2015, Debrecen, Hungary

NEW DEVELOPMENTS IN AUTOMOTIVE MATERIALS

TISZA Miklós DSc

Institute of Materials Sciences and Technology, University of Miskolc
E-mail: tisza.miklos@uni-miskolc.hu

Abstract
In this paper, some recent developments in materials applied in sheet metal forming processes will be overviewed mainly from the viewpoint of automotive industry as one of the most important application fields. If we consider the main requirements in the automotive industry we can state that there are very contradictory demands on developments. Better performance with lower consumption and lower harmful emission, more safety and comfort are hardly available simultaneously with conventional materials and conventional manufacturing processes. These requirements are the main driving forces behind the material developments in sheet metal forming: application of high strength steels, low weight light alloys are the main target fields of developments summarized in this paper.

Keywords: *high strength steels, light alloys, advanced materials, sheet metal forming.*

1. INTRODUCTION

Sheet metal forming is one of the most important manufacturing processes particularly in the automotive industry. Since the automotive industry is the leading sector in many countries and the main driving force behind the sheet metal forming developments as well, development trends in sheet metal forming are strongly determined by the developments in the car manufacturing [1].
The competition in car manufacturing is extremely strong and the requirements are often very contradictory: for example from the customers' side more economical, more safe and higher comfort together with better performance. These requirements are further increased by legal requirements as lower harmful emission, more safety: some of these requirements are in accordance with the customers' demands, some imposes further requirements on car manufacturing. However, due to the global competition in car manufacturing, the automotive industry has to find the right answers for these challenges. It is obvious that to meet all these requirements is hardly possible with conventional materials and conventional manufacturing methods. This is the main reason that the development needs in the automotive industry are the main driving forces in material sciences and manufacturing processes, too.
The increased competition also leads to a very intense development activity to increase productivity and to reduce costs. Application of light-weight design principles is one of the most important trends to meet the above requirements. Obviously, the new design concepts require new materials, and vice versa, new materials often require new, innovative forming processes and new tooling concepts, as well. In this paper, the present state and some future outlook of these developments will be summarized concerning first of all the material developments.

2. MAIN FIELDS OF MATERIAL DEVELOPMENTS IN SHEET METAL FORMING

It is obvious that the reduction of the total mass of the cars is a possible way to meet several requirements listed in the former paragraph. This is the main reason of the application of light-

weight design principles. Reducing the weight leads to lower consumption and lower harmful emissions meeting on the one side the customers' demand for more economical cars and the legal requirements for lower harmful emissions, too. However, both the customers and the legal requirements require higher safety, simultaneously. These contradictory requirements can be met by using higher strength materials. However, it leads to another big contradiction: increasing the strength results in the decrease of the formability. It is a well-known fact in material science that for example the ultimate tensile strength and the total elongation has a hyperbolic relationship, i.e. lower strength with better formability and higher strength with lower formability. Therefore, it is of utmost importance to find a good compromise between strength and formability properties.
As we could see from the main requirements, the application of light-weight design principles is one of the main tendencies in the automotive industry. From the side of materials science, the application of this design principle can be met by applying materials with high specific strength (UTS/□) and high specific stiffness (E/□□). Considering these properties, application of high strength steels, light metals and their alloys (particularly aluminum and magnesium), as well as an increasing amount of various non-metallic materials (primarily various fiber reinforced plastics) can be meant as the main development trend.

2.1. Steel developments

Since in car manufacturing, the ratio of ferrous metals and alloys is still the dominant one, therefore, first the recent developments is steel materials will be overlooked. Enhanced stiffness together with weight reduction resulted in the development and wide-spread application of various grades of high strength steels. From the most significant developments achieved during the last 35-40, it can be seen that from the elaboration and first industrial application of various micro-alloyed steels in the mid-seventieth of the last century, there is a continuous pressure on steel development leading to the appearance of new advanced steel materials practically in each five year [2].
Nowadays, several micro-alloyed and phosphorous-alloyed steels both with and without bake-hardening are frequently used. An increasing use of interstitial-free (IF) steels, dual-phase (DP) and TRIP-steels, as well as the ultra-low and super ultra-low carbon steels can also be observed.
Another aspect of steel developments is shown in Figure 1. In this Figure, the tensile strength is drawn in the function of total elongation for the so-called conventional low- and high strength steels. It is also well-known that with the increase of strength properties a decrease of ductility parameters can be observed, however, it is worth mentioning that for these new high strength steels the increase of strength parameters is much more significant than the decrease of the ductility parameters [3].
As it was mentioned before, the product of the tensile strength and the total elongation follows a hyperbolic function, i.e.

$$R_m \times A_5 = C \tag{1}$$

where R_m is the ultimate tensile strength, A_5 is the total elongation and C is a constant value. As it can be seen from Figure 1, the conventional cold rolled steels (e.g. mild steel, the interstitial free-IF steel, the isotropic-IS steels, and even the High Strength Low Alloyed-HSLA steels, which may be regarded as one of the first representative of these new steel development trends) lies along the constant C = 10,000. Dual Phase (DP steels) and Complex Phase (CP steels) are located approximately at C = 15,000, whilst the advanced high strength steel (TRIP steels) have about twice higher value, i.e. C = 20,000 to 25,000 values. On the basis of Figure 1, it is also worth mentioning the new Hot Press Forming (HPF) steels. One of the most widely used from this group is the boron

micro-alloyed manganese steels (22MnB5) which is an excellent example to illustrate the complex material and technological developments to get good formability during forming and extra high strength in operation conditions.

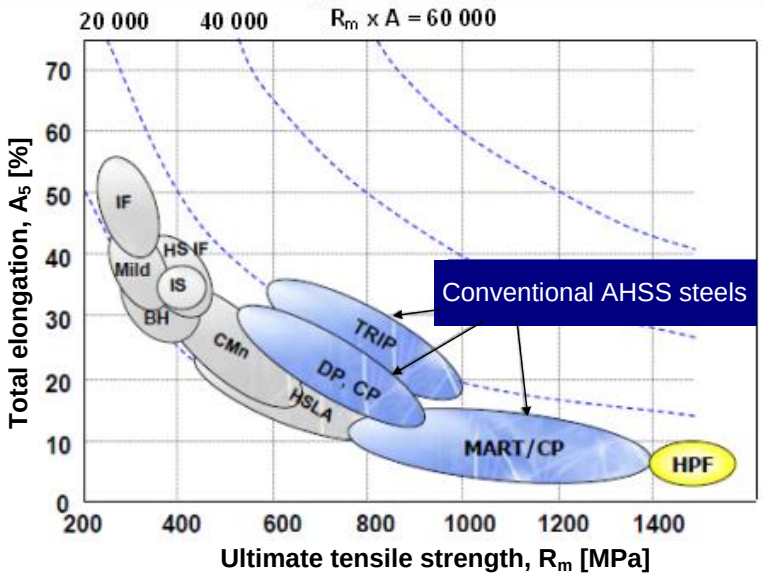

Figure 1 Tensile strength vs. total elongation for various steel grades [3]

Recently, completely new generations of high strength steels were developed. These are called as Extra Advanced High Strength Steels (X-AHSS) and Ultra Advanced High Strength Steels (U-AHSS). The product of the tensile strength and the total elongation for X-AHSS steels can be increased up to C = 40,000 whilst for U-AHSS steels this hyperbolic constant can achieve even up to C = 60,000 – 65,000 [4]. It means for example that at a given total elongation the tensile strength may be 3-4 times higher than the value for conventional high strength steels. In Figure 2, these X-AHSS and U-AHSS steels are shown.

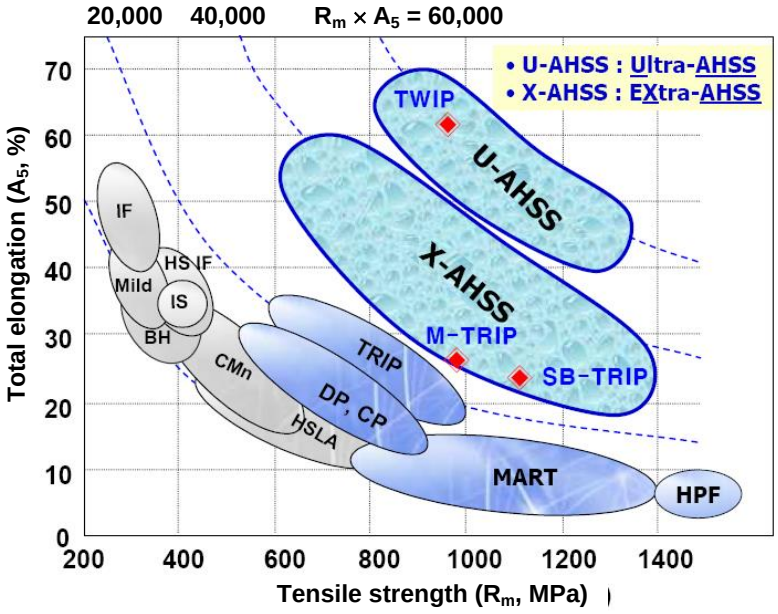

Figure 2 Tensile strength vs. total elongation for X-AHSS and U-AHSS steels [4]

The X-AHSS steels may be regarded as the further developed version of TRIP steels. These extra-advanced and ultra-advanced high strength steels were first developed and applied in automotive industry of the Far East automotive super powers, i.e. Japan and Korea. In the group of X-AHSS steels there are three main subgroups, namely: the FB-TRIP, SB-TRIP and the M-TRIP steels.

The FB-TRIP steels have ferrite-bainitic microstructure and they are excellent in those applications where good stretching-flanging and hole expansion properties are expected. The SB-TRIP steels have nano-sized lamellar type, carbide-free bainite matrix with low amount of rest-austenite. On the basis of this microstructure they are called as Super-Bainitic TRIP steels. They have extra high strength (R_m = 1600 MPa) together with good formability (the total elongation is about A_5 = 27-30 %). The third subgroup, i.e. the M-TRIP steels can be found in the upper third range of X-AHSS steels. They got their name also reflecting their microstructure: there are some rest-austenite phases among the small nano-sized, lamellar martensite matrix.
The U-AHSS steels can be found at the top edge of recent high strength steel developments. TWIN steels are one of the most excellent representatives of this group. The name Twinning Induced Plasticity reflects the main characteristics of deformation mechanism of this steel, i.e. a large number of twinning occur during plastic deformation. Due to the deformation twinning this steel has extra high hardening capability with a great value of hardening exponent since during twinning the microstructure becomes finer and finer. The grain boundaries arising from the twinning deformation result in extreme high strength increase. TWIN steels thus can be characterized besides the extreme high strength with very large uniform elongation due to the high value of strain hardening exponent: it may achieve n = 0,4 which leads to 50 % uniform elongation and more than 65 % total elongation. Thus, the $R_m \times A_5$ product can reach the constant value C = 65,000.

3. DEVELOPMENTS AND APPLICATION OF NON-FERROUS METALS

The application of non-ferrous (light metals) and non-metallic materials is one of the most evident solutions concerning the light weight design principles in the automotive industry. Among light metals the application of aluminum and magnesium alloys are in the forefront in car manufacturing. Due to their low density both light metals are very important concerning the reduction of consumption and CO_2 emission. This is the main reason that nearly all prime car manufacturers have already made or at least announced a model made of basically completely from light alloys. The Mercedes, the Audi and even the Porsche announced and already produced body-in-white concept using mainly aluminum alloys [5]. But the increasing application trend of light metal is not only limited for body panel elements. If we have a look on Figure 3, where the increasing amount of aluminum alloys in various car components are shown, we can state that during the last 30-35 years the amount of applied aluminum from a total of 32 kg in 1978 was increased to 130 kg for 2008. It means more than 400 % increase of the total mass applied. Even more significant changes can be observed if we consider the application of wrought and cast aluminum alloys. Whilst the ratio of wrought to cast alloys in 1978 was 90% to 10%, in 2008 this ratio was 55% to 45% and it is expected to be 50-50 % in 2012.
The tendency to use more and more light metals can be well illustrated by the so-called multi-material concept shown in Figure 4. In this multi-material design concept elaborated at Audi already more than 2/3 of body in white is made of various aluminum alloys (wrought sheets, profiles and castings) and only 31% is made of high strength steels.

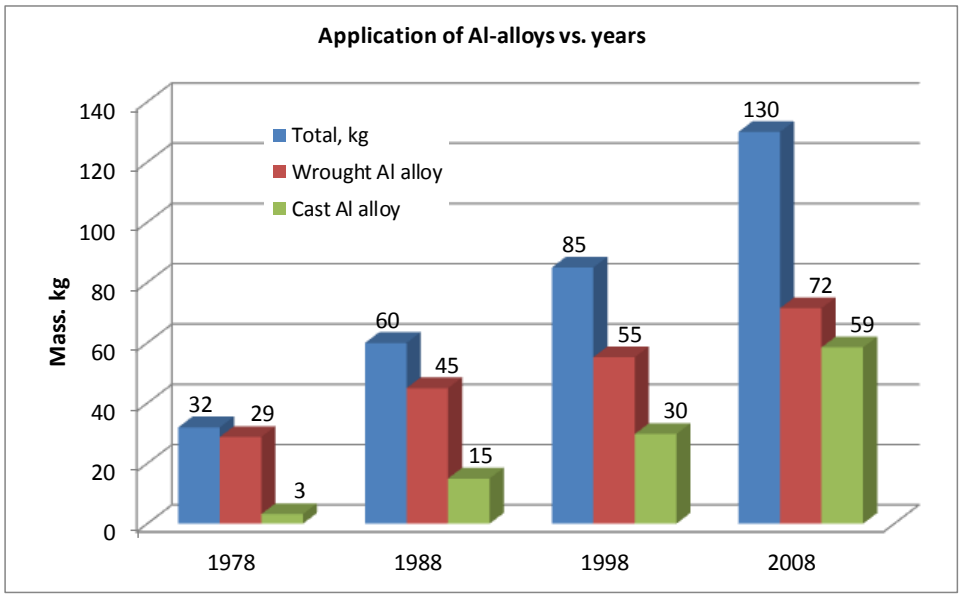

Figure 3 Application trends of aluminum wrought and cast alloys in car manufacturing [6]

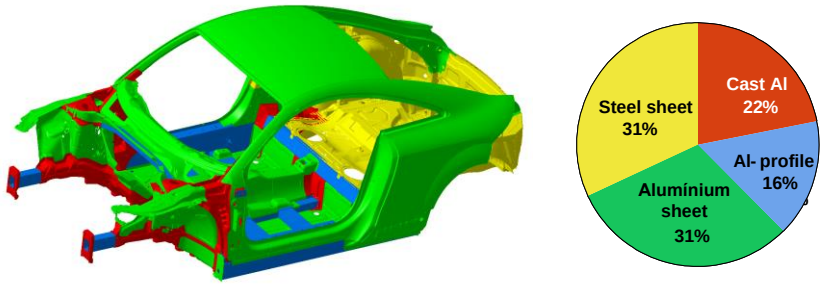

Figure 4. The multi-material car concept [5]

The application of another important light alloy, (i.e. Magnesium alloys) is also increasing continuously in the automobile industry though its volume still is much less compared to the aluminum alloys. The main reason that magnesium in normal conditions has very bad formability, therefore the applied magnesium parts are mainly castings. In the application of Mg-alloys, the VW Group has a leading role in Europe, however other big carmakers are also increasing the application of magnesium. An excellent example for the increasing application of magnesium alloys is shown in Figure 5.

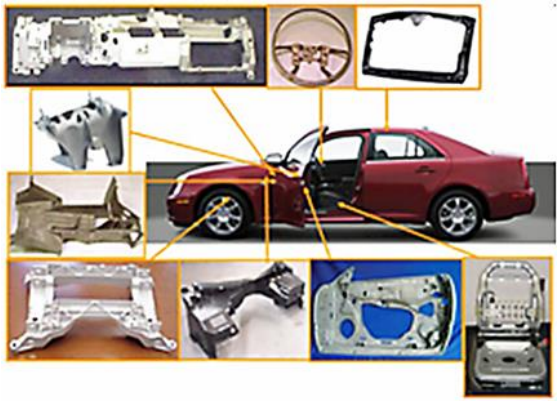

Figure 5. Mg alloy parts in a former edition of Volkswagen Passat [9]

CONCLUSIONS

In this paper the recent material developments for the sheet metal industry was overviewed particularly considering the requirements of automobile industry. Since till now, the steel materials have a dominant role in car manufacturing a significant part was devoted to the recent results in steel research leading to various grades of high strength steels. Due to the ever increasing needs both from customers' side and legal requirements light weight design principles are of utmost importance to meet these requirements. Therefore, the increasing application of light alloys – particularly aluminum and magnesium alloys – was shortly described, too.

REFERENCES

[1] Geiger, M.: *"Manufacturing science – Driving force for innovation"*, Adv. Technology of Plasticity, v.1., 2002.
[2] Wagener, H. W.: *New developments in sheet metal forming: sheet materials, tools and machinery*, Journ. Mat. Proc. Techn., 342-357., 1997.
[3] Opbroek, E. G. (World Auto Steel): *Advanced High Strength Steel (AHSS) – Application Guidelines*, June 2009. pp. 171. http://www.a-sp.org/
[4] Chung J. Y., Kwon, O.: *Development of High Performance Auto Steels*, ICTP 2008. Gyeongju-Korea, 7-11. September 2008. pp. 3-6.
[5] Waltl, H., Vette, W., Griesbach, B.: *Tool-making for future car bodies*, IDDRG'2007, 21-23. May 2007. Győr, Hungary, 31-44.
[6] Tisza, M.: *Recent development trends in sheet metal forming*, In. Journal of Microstructures and Materials Properties, 2013.vol.8.No.1-2.pp.125-140.
[7] Vöhringer, K.-D.: *"Metal forming – A key technology for automobile production"*, Adv. Techn. v. 1**.** **(**1999) 30-16
[8] The Auto/Steel Partnership Tailored Welded Blank Project Team: *Tailor welded blank: Applications and Manufacturing*, Southfield, Michigan, June 2001. pp. 1-91.
[9] B.L Mordike, T Ebert: *Magnesium: Properties — applications — potential*, Materials Science and Engineering: A Vol. 302. (2001) Issue 1, pp. 37-45.

INTERNATIONAL SCIENTIFIC CONFERENCE ON ADVANCES IN MECHANICAL ENGINEERING
19 November 2015, Debrecen, Hungary

GENERAL METHODS OF TOOTH MODIFICATIONS

TOMORI Zoltán

Institute of Machine and Product Design, University of Miskolc
E-mail: nordker94@t-online.hu

Abstract
Nowadays the literature of involute gear drives describe many different methods for the determination of the profile shift factor. These methods had been worked out for one pair of drives, but leaning on the main principles these can be generalized for simple planetary gears. We review the most significant methods for one pair of gears, then we advert to the methods for planetary gears.

Keywords: *Gear, profile shift factor, involute, planetary gear.*

1. INTRODUCTION

Nowadays the literature of involute gear drives describe many different methods for the determination of the profile shift factor. These methods had been worked out for one pair of drives, but leaning on the main principles these can be generalized for simple planetary gears. At first we review the most significant methods for one pair of gears, then we advert to the methods for planetary gears. The paper aims to review the different methods of the modification of tooth geometry.

2. METHODS

Literatures are known from the beginning of the XX. Century that deals with the methods of increasing the load capacity and lifetime of a gear. BÜCHNER K. [10] determined, that in the aspect of lifetime, the friction of the teeth is significant. He proves that for the amount of the friction the relative slip is typical, with taking notice on that the one tooth of the smaller gear contacts i times with the bigger gear. Consequently, the friction loss comes forward once on the bigger gear it appears i times on the smaller gear which is important for wearing. It means that for defining of the tooth correction we have to pay respect for the relative slip on the smaller gear multiplied by the gear ratio.
CSERHÁTI [12] defined the relative slip by drawing it on the points of the tooth profile. He stated that the biggest wear appears on the top of the bigger gear. He suggested to shorten the top of the bigger gear and to lengthen on the smaller gear.
According to VIDÉKI [39] the slip velocity is significant for the lifetime. He defined by the use of a general center distance between the gears, if $a_w > a$, the slip velocity reduces. It is practical to enlarge the center distance until the potential of the teething allow.
DIKER J. [13], SZENICZEI L. [32] and BOLOTOVSZKIJ I.A. [6] described the sizing for balanced relative slip by that the biggest values of relative slips on the two side of the line of action have to be equal. This means that calculated values in the contacting limit points are corrected, because the relative slip in the main point is zero and increasing hyperbolically. The offset values on the line of action divided by the main point are always on the contact points, either equal or not. Their values

can be efficiently lowered by increasing the profile angle. Moreover, at a given profile angle the two biggest slip can be equalized and minimized.

COLBOURNE J. R. [11] worked out a calculating method for inner gears, where the tooth thickness of the spurgear is increased to the previously calculated value by a correction factor, while the tooth thickness at the pitch circle of the inner gear is lowered by this factor. The correctional factor is determined to avoid the interferences with the geometry defined by the modified tooth thicknesses.

YU D.D. [42] draws attention to that data of the cutting tool have to be known during the design of an inner gear, because after a sharpening the outer diameter of the tool is cut back, the profile shift factor also decreases. If this change is disregarded at the definition of the geometric data of the inner toothed gear, interference can happen during operation or manufacturing.

BOTKA I.[7], [8], [9] patented the Ganz - Botka toothing system at 1954. He had shown that if the relative slip is equalized at the contact limit points, there is triple equalization. It means that beyond the relative slip, the momentary contact temperature increase and the two-factor Almen product (products of the Hertz stress and slip velocity) are also equalized and minimized. He stated that at lower contact angles the temperature increase of the tooth faces are the biggest at the contact limit points. By increasing the contact angle the heat gets its maximum at the contact limit points. In this case he aimed to equalize these heat pitches.

Based on these result Botka found that it is only recommended to use heat equalized teething when the gear drive has a tendency to seize. In other cases the equalization if relative slip is the effective method, moreover the root strength is higher. It is especially true for open drives and slow running, heavy loaded drives which are tend to wear faster. This invention can be found in the examinations of Erney Gy.[18] too. At high running speed it is also recommended to use this method instead of the heat equalization, if seizure is not likely to happen.

GAVRILENKO V. A. [19] suggested to define the profile shift factors by the equalized relative slip accelerations, because the relative slip method has a fundamental problem. Namely, at the main contact point the relative slip is zero, which would lead to the fact that there is no wear. However at the roots significant wear should have appeared. At the same time, the practice doesn't confirm this theory. Therefore, the places and extents of wear can be determined by the relative slip acceleration, that is the tangent of the angle between the line of action and the slip curves. In other words, the places of wear and pitting should be determined by the changing of the derivative of the relative slip along the line of action. The best results can be achieved by equalizing the relative slip accelerations at the contact limit points.

By the studies of NIEMANN G. [28] stated that the seizure safety factor is optimal when the slip velocities are equal at the contact limit points. It means that the addendum contact numbers are equal. So if these numbers are equal that means the slip velocities are also equal.

BLOK H. [4] found during his test about seizure of gears, that happens at high local temperatures. It comes from the difference of the temperature of the gear body and the local temperature increase at the contact spot. Seizure happens when the sum of the temperature of the gear body and the local temperature increase pass the so called seizure temperature of the lubricant. The seizure temperature can be determined experimentally. The local temperature increase can be determined by the differential equations created by the author, which can be used to define the contact temperatures of the contact points. In this way the optimal dimensions can be defined for the seizure safety knowing the critical temperature of the lubricant.

WINTER H. [41] created the universally applicable so called integrated temperature criteria method used to define the seizure toughness, based on the works of Blok and Niemann. The main principle of this is that the heat stress is defined by the sum of the temperature of the gear body and the local temperature increase which is considered to be permanent during the line of action. There is no seizure threat if the forming temperature is lower than the experimentally defined temperature which is based on the lubricant, the material of the gear and the loading conditions. According to

these calculations the optimal dimensions can be defined in the aspect of optimal seizure conditions, but it can hardly be used for the definition of profile shift factors.

TERAUCHI . Y. [33], [34] performed experiments on a gear test equipment with closed power flow. At the contact region they achieved the EHD (elasto-hydrodynamic) lubrication and then they seek the optimal parameters for the profile shift factor which gives the best results for the seizure safety. They stated that slightly positive values causes significant improvement. The defined the critical face temperature independently from the lubricant and the material of the gear, where the value of the seizure safety factor is the highest. They determined that the seizure safety can be estimated by the critical face temperature, thus they defined the profile shift factor which causes this critical temperature.

KOLONITS F. [22], [23] made a computer program for the Ganz-Botka teething to get the thermal equalization. He uses the newest, mainly Japanese literature which models the heat formation and distribution. He worked out a model similar to the Blok theory, but simpler than the Japanese model. This give adequate results for the industry.

Lí C. H. – CHIOU H. S. – CHANG Y. Y. – YEN C. C. [26] made a computational method where during the design of gears using FEM analysis. There they use the contact angle and the head clearance using as parameters get the optimal dimension for the longest lifetime minimizing the Hertz stress.

PEDERSEN N. L. – JORGENSEN M. F. [29] define the dimensions of a gear be FEM analysis so that the root has as much stiffness as possible. They show that in this way can be achieved the maximum load which means the longest lifespan at given conditions.

KINCZEL F. [21] examined the straight involute gears in his paper. His work deals with the pairing of the machining and computing methods in details. After the summary of profile shift factor defining methods the author concluded that the refinement of tooth profiles needs the refinement of the correctional methods. By bringing in the universal correctional principle it can be able to get a correct profile shift factor by using arbitrary friction coefficient and line pressure function. Moreover, it tells which kind of correctional factor should be used.

Starting from the general principle (using symmetric linear line pressure and permanent friction coefficient along the line of act) the examination of specific friction energies – in parity with the results of Kolonits – lead to Botka's theory. Furthermore he proved that, there is a contact angle, at which, using relative slip equation, the specific friction energies has a minimum. But this minimum is only the 60…30% of the compensated teething. This contact angle range is between 24° and 27°.

BAGLIONI S. – CIANETTI F. – LANDI L. [2] worked out a method by defining the slip velocities to improve the efficiency. The proved that by lowering the slip velocities, the noise, the wear and the performance degradation are also lowering. They made recommendations for choosing the profile shift factor to get the best efficiency.

IMREK H. – UNUVAR A. [20] verify the relationship between the tooth profile, the slip velocity along the line of act, the line pressure and the face temperature increase. They stated that the drive gear has to made with positive shift factor, while the driven gear with negative shift factor, to get the slip velocity equalized at the contact limit points. This ensures the smallest value also and minimum wear.

TERPLÁN Z. [36], [37] worked out a calculating and constructing method for the compensated teething of planetary gears. He proved that if we sizing for equalized relative slip and using ordinates at the contact limit points, the problem of fourfold equalization can be reduced threefold.

With his collaborators (Szota Gy. And Scholtz P.) Worked out a simpler method based on the VÖRÖS [40] method for the construction of the relative slips of a planetary gear. The calculation method is iterative which solves the problem of the threefold equalization numerically. It is advantageous to use this method to define the profile shift factors because it is simple and clear. He summarized the values of relative slips and shift factors in tables. [36], [37].

APRÓ F. [1] found out by examining the planetary gears with on degree of freedom, that by reducing the number of teeth of the planet gear general teething can be used when the energy-flow is the following: sun gear-arm, stopped ring gear. The main principle of the method was that holding the good contacts it is practical the improvement of outer-outer contact which can be achieved by reducing the number of teeth. He summarized in tables the reduction of the number of teeth of the planet gear depending on the sum of teeth on the sun and planet gears and the contact angle.
BOLOTOVSZKIJ I. A. [5] examined the teeth correctional factors planar and spatial limiting contours. These contours are created in the coordinate system of profile shift factors by using the different interference equations as limiting function which create there surfaces. These surfaces are used as limits for the interference free zone. If the sun gear and the planet gear contact is equalized for relative slip in the defined area, than the profile sift factor for the ring gear can be determined with an equation similar to the collinear assumption of the planetary gear.
In literature, beside the general solution of outer-outer contact, the following recommendation can be found for the profile shift factor of the ring gear:
According to BERGSTRÄSSER M. [3] the definition of the profile shift factor of the ring gear, after the definition of sun and planet gears as DIN 3992 [14], are the following:

$$x_3 \times m = B_{32} \times a_w + x_2 \times m,$$

Where x_3 *is* the profile shift factor of the ring gear, x_2 is the profile shift factor of the planetary gear, m is the module a_w is the general center distance and B32 parameter is the Kutzbach involute function:

$$B_{32} = \frac{inv\alpha_{wt32} - imv\alpha}{tan\alpha},$$

Where the α_{wt32} Contact angle of the outer-inner contact and α is the profile angle.
RICHTER W. [31] defines the profile shift factors outer-outer according to DIN, but uses the following equation for the ring gear:

$$x_3 = x_1 + 2x_2,$$

Where 3 means ring gear, 2 means planetary gear, 1 means sun gear.
KUDRJAVCEV V. N. [24] gave the same equation as Richter for the profile shift factor of the ring gear, but defines the profile shift factors of the outer-outer contact by the equalized relative slips method.
TOMORI [38] developed a method to determine the interference free area of the gear geometry of the gears of the simple planetary gear drives. The interference free zone parameters were determined according to POLDER [30], LITVIN [27] and DROBNI [15], [16], [17] theories.

CONCLUSIONS

We can see that the determination of the profile shift factor is as comprehensive as the widespread of the usage of gears.
We can settle also that there is no universal method for the determination of the profile shift factor, which only can ensure the best efficiency and longest lifespan for gears at the same time. Accordingly it is recommended to examine the literature carefully for the specific problem and find the best solution for the given conditions.

REFERENCES

[1] Apró F.:. Egyszabadságfokú fogaskerék-bolygóművek tervezésének néhány kérdése. Kézirat. Az NME Gépészmérnöki Karára benyújtott és elfogadott egyetemi doktori értekezés. Miskolc. 1967. 1-76
[2] Baglioni S. – Cianetti F. – Landi L. Influence of the addendum modification on spur gear efficiency. Mechanism and Machine Theory 49. (2012) 216-233
[3] Bergsträsser M.: Planetengetriebe mit auswechsebarer Übersetzung. Maschinenbautechnik. 10(1961)4. 209-211
[4] Blok H.: Les températures des surface dans des conditions de graissage sons pression extreme. Second World Petroleum Congress. Paris. June 1937.
[5] Bolotovszkij I.A. – Gurjev B.I. – Szmirnov V.E. – Senderej B.i.: Cilindricseszkije evolventnije zubcsatie peredacsi vnutrennova zacaplenyija. Masinosztrojenie. Moszkva. 1977.135-144
[6] Bolotovszkij I.A. – Bolotovszkaja T.P. – Bocsarov G.Sz. – Gurjev V.I. – Kurlov B.A. – Merkurjev I.A. – Szmirnov V.E.: Szprovocsnik po geometricseszkomu raszcsotu evolventnih zubcsatih i cservjacsnih peredacs. Masgiz. Moszkva. 1963. 24-40
[7] Botka I.: Egységes magyar homlokkerék fogazási rendszer. Mérnöki Továbbképző Intézet. Budapest. 1953.
[8] Botka I.: Fogaskerék-méretezés kiegyenlített kontakt-hőmérsékletre. GÉP XVI.évfolyam. 1964. 11. 425-430
[9] Botka I. – Erney Gy.: Fogaskerékpárok méretezése. Egyenes fogazat. Akadémiai Kiadó. Budapest. 1973. 14-23
[10] Büchner K.: Beitrag zur kenntnis der Abnutzungs- und Reibungsverhältnisse der Strinzahnräder. Zeitschrift des VDI. Nr.5. Februar 1902. 159-166.o., 278-284
[11] Colbourne J.R. The geometric deisgn of internel gear pairs. Gear Technology May/June 1990. 28-37.
[12] Cserháti J.: Gépelemek. Egyetemi jegyzet, amelyet készített Vidor J.Rezső, é.n. (valószínüleg 1910.) 53-56.
[13] Diker J.I.: Evolventnije zaceplenyije sz uprjamimi zubcami. Organyetall, 1935.
[14] DIN 3992
[15] Drobni J.: „Hajtóművek Gépszerkezettana II.” c. egyetemi előadásai az NME Gépészmérnöki Karán a Géptervező Szak Általános Gépészeti Ágazatos hallgatóinak 1980/81-es tanévben.
[16] Drobni J. – Szente J. – Gódor I.: Belső fogazatú fogaskerékpár csúszási sebességének kiegyenlítése. NME Közleményei III. sorozat. Gépészet 27. Miskolc. 1981.
[17] Drobni J.: Metszőkerék tervbezése belső fogazatú fogaskerékhez. Tervezési segédlet. Gé. 79-2067. NME. Miskolc. 1979. 10-29
[18] Erney Gy.: Fogaskerekek. Műszaki Könyvkiadó. Budapest. 1983. 5. fejezet
[19] Gavrilenko V.A.: Osznovi teoriji evolventnoj zubcsatoj peredacsi. Masinosztrojenie. Moszkva. 1966. 234-245
[20] Imrek H. – Unuvar A. Inverstigation of influence of load and velocity on scoring of addendum modified gear tooth profiles. Mechanism and Machine Theory 44.(2009)938-948.o.
[21] Kinczel F.: Egyenesfogú evolvensfogazatú hengeres kerékpárok fogazathatárai és fogazathelyesbítése. Kézirat. Az NME Gépészmérnöki Karára benyújtot és elfogadott műszaki egyetemi doktori értekezés. Miskolc. 1975. 1-79
[22] Kolonits F.: Hőfokvillám-kiegyenlítés egyenesfogú evolvenskerekeken. Műszaki Tudomány. 49. 1975. 353-370
[23] Kolonits F.: Fogaskerék-villámhőmérséklet II. A változó kapcsolódási viszonyok hatása. Műszaki Tudomány 52. 1976. 183-198

[24] Kudrjavcev V. N. – Kirdasev ju. N.: Planetarnije Peredacsi. Leningrad. Masinosztrojenie. Leningradszkoje otdelenyije. 1977. 1-137
[25] Lévai I. – Szarka Z.: D-függvény a fogaskerekek geometriai méretezéséhez. NME Gépelemek Tanszékének Közleményei 203.sz. Miskolc. 1969. 1-23
[26] Lí C.H. – Chiou H.S. – Hung C. – Chang Y.Y. – Yen C. C. Ingegration of finite element analysis and optimum design on gear systems. Finite Elements in Analysis and Design 38. (2002) 179-182
[27] Litvin F.L.: A fogaskerékkapcsolás elmélete. Műszaki Könyvkiadó. Budapest. 1972. 226-238
[28] Niemann G.: Maschinenelemente. Band II. Springer Verlag. Berlin (Göttingen) Heidelberg. 1965.
[29] Pedersen N.: - Jorgensen F. J. On gear tooth stiffness evaluation. Computers and Sturctures 135. (2014) 109-117
[30] Polder J.W.: Overcat interference in internalgears. International Symposion on Gearing and Power Transmissions. Tokyo. 1981.
[31] Richter W.: Auslegung von innenverzahnungen und Plametengetrieben Kostruktion 14.k. 12.sz. 1962. 489-497
[32] Szeniczei L.: Az általános fogazás. Királyi Magyar Egyetemi Nyomda. Budapest. 1941. 135-148
[33] Terauchi Y. – Nadano H.: Effect of tooth profile modification ont he scoring resistance of spur gear. Wear. vol 80. No.1. August 2. ud. 1982. 27-41
[34] Terauchi Y.: Scoring of spur gear teeth. Lubrication engineering. 40.k. 1.sz. 1984. 13-20
[35] Terplán Z. – Apró F. – Antal M. – Döbröczöni Á.: Fogaskerék-bolygóművek. Műszaki Könyvkiadó. Budapest. 1979. 17-19.o. 92-104
[36] Terplán Z.: Gépelemek II. Kézirat. Tankönyvkiadó. Budapest. 1981. 26-28
[37] Terplán Z.: A fogaskerék-bolygóművek méretezési kérdései. Kézirat. A TMB-hez benyújtott és elfogadott akadémiai doktori értekezés. 1965. 39-54
[38] Tomori Z.: Relatív csúszásra optimalizált kb típusú fogaskerék-bolygóművek számítógépes tervezése. Géptervezők VI. Országos Szemináriuma. Miskolc. 1985.
[39] Vidéki E.: Fogaskerekek. „Pátria" Irodalmi Vállalat és Nyomdai Rt. nyomása. Budapest. 1912. 1-94
[40] Vörös I.: Gépelemek III. Fogaskerekek. Tankönyvkiadó. Budapest. 1956. 101-121
[41] Winter H. – Richter M.: Verzahnungswirkungsgrad und Fresstragfähigkeit von Hypoid- und Schraubenradgetrieben. Antriebstechnik 15 Heft 4. 1976. 211-218
[42] Yu.D.D. On the interference of internal gearing. Gear Technology July/august 1989. 12-44

RELIABILITY GRAPH MODEL FOR SENSOR NETWORKS

VARGA Attila K., CZAP László PhD

Department of Automation and Infocommunication, Institute of Electrical Engineering, Faculty of Mechanical Engineering and Informatics, University of Miskolc
E-mail: varga.attila@uni-miskolc.hu, czap@uni-miskolc.hu

Abstract
The paper presents the idea of introducing a reliability graph model in connection with self-organising ad-hoc sensor networks. The sensor nodes are categorised on the basis of their communication activities. The activity value and the reliability factor introduced in the model make it possible to monitor the energy level of the sensor nodes, which leads to giving the reliability of the communication edges and of the complete sensor network. This contributes to increasing the predictability of the operation of the sensor network and to detecting the overloaded and underloaded nodes, which results in avoiding the development of isolated parts in the network and reducing the chances of the network becoming non-operational.

Keywords: *ad-hoc operation, self-organizing, sensor networks, reliability, graph*

1. INTRODUCTION

Wireless sensor networks have spread fast among civilian users and are currently playing more and more significant roles in a number of areas of everyday life. This is due to the rapid decrease in the price of sensors, their low energy consumption as well as to the sensors of small size but capable of performing increasingly complicated functions. This is particularly true of the fields in logistics, mechatronics and industrial communications. Industrial communications and the automation tasks which could not be solved previously by means of the automation built on communications or could only be solved at very high costs have become affordable reality today. As a result, the services offered by the devices provided with such systems have increased significantly, their size is decreasing, and they are increasing the added value of the products. In the examination of the effect of special industrial safety effects exerted on the safety of communications, the following objectives were set: a profound understanding of the operation of self-organising sensor networks, an exploration of the widespread localisation techniques used in practice and creating a model which can contribute to increasing efficiency in the energy consumption of sensor networks, thus increasing reliable and efficient operation without human intervention and reducing losses caused by unexpected malfunctions in operation (e.g. batteries going dead).

2. WIRELESS COMMUNICATION SYSTEMS

The development and use of industrial wireless communication systems has gathered speed since the 1990s. They share the common characteristic that they use the frequency bands not subject to authorisation with a relatively low transmission power. As a result, they are capable of communication at relatively short distances. The different types vary in their transmission speed to a very high extent. In wireless industrial communication the following requirements have to be met: real-time transmission (data exchange), data protection and noise filtering, access to high-reliability devices, meeting the industrial environmental requirements, meeting the data security and the technological security requirements. The advantages of the wireless solution are as follows:

- Costs: one of the significant advantages of the use of wireless communication technology as opposed to wired technology is saving the wiring expenses.
- Mobility: the greatest advantage of wireless communication is mobilisation, by which it is possible to solve technical problems which cannot be solved by wired data transmission at all or only with great difficulties.
- Rapid connection of plant and office networks.
- Simple possibility of system expansion.
- Cooperation of protocols: the protocols of wireless systems can cooperate much better and easier than those of wired systems.
- HMI connection: mobility ensures novel HMI possibilities.

At the same time in the use of wireless systems there arise a number of problems which are not or less characteristic of wired systems, e.g. noises in the space, interference, fading, screening and transfer medium.

3. AD-HOC OPERATION

In ad-hoc networks it is usually the device that is the first to intend to communicate that becomes the coordinator, after which the other devices can join the network after sending a request to join. Since no additional supervision is needed for constructing the network, these systems and networks can operate as ad-hoc or self-organising networks. If a mesh network is created, a message can be sent in several ways. Naturally, the objective is to select the most optimal route in transmitting the message. If a router does not work properly, e.g. the route of the message is hindered, the network will select an alternative route. This is called the self-healing ability of the mesh network.
Taking ZigBee as the basis, the search algorithm of the route is based on the principle of distance vectors. For this purpose every device suitable for searching for a route has what is called a routing table. This includes the distance to the destination and the address of the router next on the route to the destination. Device *(A)* initiates an exploration procedure with a request for route broadcast command, for which the destination device *(B)* sends back a route answer. Then data transmission can begin on the route set. The devices have several route algorithms. It may happen that a device cannot set a route, then the ZigBee coordinator, which has several hierarchic routes, takes over the search for the route. In some cases all the devices of the network send the data to an aggregator. This happens when several devices are looking for a particular device. In large systems it may happen that the aggregator does not contain the routes leading to all the participants. Let us imagine a network where the aggregator has only a few neighbours, and so the device wanted can be reached only after several jumps.

4. RELIABILITY GRAPH MODEL

The overwhelming majority of technologies used in wireless communication work in a rather unreliable way. Let us just think of mobile phones: almost everyone has experienced that the system rejects certain calls or that it cannot provide certain services due to small signal strength, and thus continuous reliable operation is not ensured. This can be attributed to the physical properties and behaviour of radio waves: they tend to produce interference; metal, a water body or a thick concrete wall can block them as well as several other factors such as the construction of the aerial, the extent of amplification or the weather conditions. At the same time the unreliable operation resulting from dead batteries and the concurrent network outages may also result in disruptions, overloaded nodes and undelivered messages.

Mathematically modelled, a sensor network can be regarded as a graph. Let E and V be disjoint sets, and let the ϕ mapping of set E into $V \times V$ (product arithmetical of V taken by itself) be given, then $G = (E,\phi,V)$ is called a directed graph. By the inordinate product of set V taken by itself we mean the set the elements of which are inordinate pairs of the form (v_i, v_j) , that is the inordinate pairs (v_i, v_j) and the ordinate pairs (v_j, v_i) are considered to be identical. V is a finite set of vertices and E is a finite set of edges. The vertices of the graph ($V=\{v_1,...,v_n\}$) denote the sensor nodes and its edges ($E=\{e_1,...,e_m\}$) denote the communication routes between the sensor nodes. That is two nodes see each other, are in each other's scope of action, or putting it in a different way, they can be called neighbours if there is an edge between them. Directivity sets communication from where to where, so we can speak of sending and receiving nodes. The cost function interpreted on the edges of the nodes $(c : E \rightarrow R+)$ is considered to be the weight of the communication between the nodes, which carries great significance in developing the routing. In the following a sensor network built of sensor nodes having the same properties and physical parameters is called a homogenous sensor network.

4.1. Communication activity

Let us suppose that in a homogenous sensor network it is registered every time whether a given node participates in the communication or not. This is described by an integer and is registered in an appropriate database. It is further supposed that the sensor network is used for transmitting a simple message or data, the transmission of which takes the same time at each node. Because of the homogeneity, all the nodes show the same power consumption during a change of state, i.e. changing from the sleeping mode into the active mode. If we know how long a cycle time *sleeping* → *active* → *sleeping* is, it can be computed what communication activity (p_{max}) a given node is capable of at a given energy capacity (energy level or energy capacity means the charge level of the power source of the node).
Let the actual communication activity of a node be p and its maximum activity capacity be p_{max}. The term communication activity means the possible number of changes of state *sleeping* → *active* → *sleeping* of a node as a function of its energy level. It can be stated that the activity value is directly proportional to the energy level of the nodes, for the more times a node awakes and becomes active, the more its energy level decreases and thus its activity capacity also decreases. The maximum communication activity registered in a suitably developed database decreases by *1* every time a communication takes place if the node participates in the communication. When the node's communication activity is near *0*, the energy source of the node is practically close to the state of depletion.
By recording the activity value it is possible to monitor what actual energy level characterises a given node and how reliable its operation is. In the following reliability is used to mean whether the node possess the energy sufficient for the change of state *sleeping* → *active* → *sleeping* or not.

4.2. Reliability factor

This activity value makes it possible to introduce the following classification for all the nodes of the sensor network (graph):

- if node v_i is capable of activity p_{max} , it is capable of maximally reliable operation,
- if node v_i shows activity $p_{min} \leq p_i \leq p_{max}$, we can still speak of reliable operation (p_{min} may be the minimal activity value set by the operator),
- if node v_i shows activity $p_i < p_{min}$, we speak of unreliable operation,
- if node v_i has an activity value of $p_i = 0$, the node becomes dysfunctional and becomes depleted.

If the activity values are recorded, we can obtain for every node a value which represents its chance of reliable operation. In the following this value is called the reliability factor (r) of the sensor node. A reliability factor of *1* shows full charging level (100%), so the sensor node can be declared serviceable with 100 % reliability, while a reliability factor of *0* denotes non-serviceability (0 %). The reliability factor of the *i*-th node (r_i) can be easily computed from the activity value as follows:

$$r_i = \frac{p_{\max} - p_i}{p_{\max}} \cdot 100 \ (\%). \tag{1}$$

If the reliability factor is not given in percentage, but the reliability factor is regarded as interpreted along the closed interval $[0 \ldots 1] \in R+$, then by considering them both, it is possible to construe a reliability factor also for the edges of the graph, that is for the communication between the nodes.
Let $0 \le r_i \le 1$ and $0 \le r_j \le 1$. In this case r_{ij} is the probability of node v_i having a reliability factor r_i and node v_j having a reliability factor r_j. The product of the two reliability factors is called the reliability factor of communication between the two nodes. In the following the communication arising between two nodes is called communication edge:

$$r_{ij} = r_i \cdot r_j \,. \tag{2}$$

In view of the fact that all the nodes of the graph are characterised by a reliability factor, a reliability factor can be computed for all communication edges. From here on the concept can be expanded to cover the complete network, that is it can be given what operation reliability characterises the complete sensor network (r_G):

$$r_G = \prod_{k=1}^{|E|} r_k (k \in N^+) \,, \tag{3}$$

where $|E|$ means the number of communication edges of the network, and r_k is the reliability factor of the *k*-th communication edge. Naturally, a reliability value can be assigned to a given part of the sensor network, and this value can have an information content useful in the development of routing as well:

$$r_{\bar{G} \subseteq G} = \prod_{n=1}^{|\bar{E}|} r_n (n \in N^+) \,, \tag{4}$$

where $|\bar{E}|$ means the number of communication edges of a part of the network, and r_n is the reliability factor of the *n*-th communication edge. On the basis of the reliability factor interpreted for the routes derived from the communication edges it is possible to supplement a routing algorithm with a reliability decision, that is which one to choose of the possible communication routes taking the energy level of the nodes into consideration.

4.3. Activity Matrix (AM)

The most obvious way of representing the connections between the nodes is a matrix, i.e. the lines and columns of a rectangular matrix represent the nodes of the sensor network, in the point of intersection of which a *1* is written if the two nodes see each other (are in each other's scope of action), and a *0* in

the opposite case. The principal diagonal of the matrix is filled with zeros, for the connection of a given node with itself is not interpreted (see *Eq. 5* as an example for activity matrix).

$$AM = \begin{bmatrix} 0 & 1 & 0 & 1 & 0 & 1 & 1 \\ 1 & 0 & 1 & 0 & 1 & 0 & 1 \\ 0 & 1 & 0 & 1 & 1 & 1 & 0 \\ 1 & 0 & 1 & 0 & 0 & 0 & 1 \\ 0 & 1 & 1 & 0 & 0 & 1 & 0 \\ 1 & 0 & 1 & 0 & 1 & 0 & 1 \\ 1 & 1 & 0 & 1 & 0 & 0 & 0 \end{bmatrix}. \quad (5)$$

Since we are talking about symmetric communication, the matrix will be also symmetric with respect to the principal diagonal. To visualise the connection between the nodes and to store it, it is sufficient to consider only the upper or lower triangular matrix, for both of them have the same information content. If we wish to store which node was the sender and which the receiver during the communication between two nodes, we can introduce the concept of the momentary activity matrix. The lines of the matrix represent the sending nodes while its columns represent the receiving nodes, that is if the *i*-th node sends a message to the *j*-th, a *1* will be written into the *j*-th column of the *i*-th line of the momentary activity matrix. If the *i*-th node receives a message from the *j*-th node, a *1* goes into the *i*-th column of the *j*-th line of the momentary activity matrix. It can be conceived that in the course of the development of the communication route a given node appears both as a sending and a receiving node; then a loop develops in the graph, which may refer to the non-serviceability and unreliable operation of some of the nodes. This situation may naturally also develop due to momentary interference or some other physical obstacle, at the same time it can also be attributed to the depletion level of the batteries. Thus if the elements *(i,j)* and *(j,i)* of the momentary activity matrix are identical, the given node plays the roles of both the sender and the receiver in the given communications route, which means the message is travelling in a circle, that is the delivery failed. If a resending limit is set and the elements of the momentary activity matrix are incremented, that is on a given communications route a node acts several times both as the sender and as the receiver, the resending limit and the elements of the incremented matrix can be used to establish whether it is a momentary malfunction (e.g. obstacle and interference) or certain nodes of the network are completely out of operation and their operation has become unreliable. If the route keeps developing for the same nodes, the activity matrix will contain *0*-s, *1*-s and values bigger than *1*. If there are values bigger than *1*, it is necessary to examine the neighbours of the given nodes, for there is a high probability of their unreliable operation; they are possibly completely depleted, which may lead to the development of isolated parts in the sensor network. It is possible that because of this there will never develop a sender-receiver scheme between a given node and another node in the network.

4.4. Reliability Matrix (RM)

From the aspect of computerised representation and data storage it may be expedient on the analogy of the activity matrix to store the reliability factors also in matrix form. Let us call this matrix reliability matrix. The reliability factor of the individual nodes will go into the principal diagonal of the matrix while the other elements of the matrix are *0* (see *Eq. 6* as an example for reliability matrix).

$$RM = \begin{bmatrix} 0.35 & 0 & 0 & 0 & 0 & 0 & 0 \\ 0 & 0.82 & 0 & 0 & 0 & 0 & 0 \\ 0 & 0 & 0.93 & 0 & 0 & 0 & 0 \\ 0 & 0 & 0 & 0.72 & 0 & 0 & 0 \\ 0 & 0 & 0 & 0 & 0.35 & 0 & 0 \\ 0 & 0 & 0 & 0 & 0 & 0.86 & 0 \\ 0 & 0 & 0 & 0 & 0 & 0 & 0.17 \end{bmatrix}. \quad (6)$$

It is worth refining the reliability matrix in the following way. The reliability factors of the communication edges will be put into the lower triangular matrix while the upper triangular matrix represents the connections between the nodes, that is if two nodes see each other, we write *1* into the relevant location, otherwise we write *0*. If there is no connection between two nodes, the reliability factor will also be *0*, for there is no communication edge between them. In the development of a route this can be used to reduce the number of cyclically returning computations as well as the complexity of the algorithms and operations, for it will not be necessary to calculate the reliability of the communication edges every time.
Instead of representing the communication connections between the nodes, we can store the activity frequency, that is how many times a given node is involved in the same communication route. In the optimum case this value should remain *1*, that is one node is included in a route only once. In practice the optimum operation does not always materialise, therefore a value bigger than *1* may suggest the malfunction of the neighbours of the node in question. This results in overload and unnecessary use of the batteries. The reliability factor stored in the lower triangular matrix and the incremented values stored in the upper triangular matrix can be used to detect which nodes cause the overload of the other nodes, that is the nodes unreliable in operation, or depleted and malfunctioning can be detected. Due to this detection the necessary intervention can be performed in time, which can prevent the development of isolated parts in the network, network communications malfunctions, further overload, the energy losses caused by them and major maintenance works incurring additional costs.

SUMMARY

The new model introduced can be used to easily implement applications which are able to visualise the connections between the nodes, the reliability of the nodes and communication edges, the potential routes and the most favourable routes from the aspect of energy consumption. The concept elaborated can be further considered in terms of the operation mode of the algorithm, or the data to be stored in the matrix, if not only energy consumption but distance, time or other parameters are intended to be treated with priority. The model introduced carries the disadvantage that is assumes centralised operation, that is a central register, or database is to be used for recording the reliability values, and therefore can only be used in infrastructure-dependent sensor networks. With respect to that fact the model is planned to be refined so that the battery lifetime of the sensor nodes can be monitored also in infrastructure-independent sensor networks that make it possible to plan maintenance works to prevent unexpected network malfunctions.

ACKNOWLEDGEMENT

This research was carried out in the framework of the Centre of Excellence of Mechatronics and Logistics at the University of Miskolc.

REFERENCES

[1] Ajtonyi I.: Ipari kommunikációs rendszerek IV.: Vezeték nélküli ipari kommunikációs rendszerek. 467 p., Miskolc: Aut-Info, 2011. pp. 119-159., ISBN:978-963-08-1516-1
[2] S. Capkun, M. Hamdi, and J.-P. Hubaux, "GPS-free positioning in mobile ad hoc networks", Cluster Computing, 5(2): 157-167, 2002.
[3] J. Blumenthal, F. Reichenbach, M. Handy, and D. Timmermann, "Optimal adjustment of the coarse grained localization-algorithm for wireless sensor networks", Invited Paper, Proceedings of 1st Intl. Workshop on Positioning, Navigation, and Communication WPNC'2004, Hanover, Germany, March 2004.
[4] A. Haeberlen, E. Flannery, A. M. Ladd, A. Rudys, D. S. Wallach, and L. E. Kavraki. (2004). Practical robust localization over large-scale 802.11 wireless networks. In Proceedings of ACM MOBICOM, 2004.
[5] A. Savarese, J. Rabaey, and J. Beutel. Locationing in distributed ad-hoc wireless sensor networks. In IEEE Int. Conf. on Acoustics, Speech and Signal Processing (ICASSP), pages 2037-2040, May 2001.

INTERNATIONAL SCIENTIFIC CONFERENCE ON ADVANCES IN MECHANICAL ENGINEERING

19 November 2015, Debrecen, Hungary

DEVELOPMENT OF A WEB-BASED SYSTEM FOR EVALUATION OF SPEECH SAMPLES OF DEAF AND HARD OF HEARING CHILDREN

VARGA Attila K., CZAP László PhD

Department of Automation and Infocommunication, Institute of Electrical Engineering, Faculty of Mechanical Engineering and Informatics, University of Miskolc
E-mail: varga.attila@uni-miskolc.hu, czap@uni-miskolc.hu

Abstract
The aim of this paper is to present a web-based evaluation system developed as part of a research has been carried out in cooperation with University of Debrecen and University of Miskolc in the framework of the project TÁMOP-4.2.2.C-11/1/KONV (Social Renewal Operational Programme) called 'Basic and Applied Research for Internet-based Speech Development of Deaf People and for Objective Measurement of Their Progress'. The project is aimed at solving basic and applied research tasks to develop an application to support the speech teaching and understanding of deaf and hard of hearing people more effectively than known methods. The idea of the project has come from an audio-visual transcoder for sound visualization developed at the University of Debrecen, and a three-dimensional head model for articulation presentation, called 'talking head' developed at the University of Miskolc. [1] The most important goal of the project is to create a complex system to provide audio-visual speech recognition by visualization of images of speech and articulation, setting up an educational framework. In addition, the system has many other features (prosody display, automatic evaluation and knowledge-based systems implementation), which subsequently allow individual practice not only on computers but also on mobile devices. The module performing the required audio-visual transcoding is language-independent, the talking head and automatic qualification can be made language-independent by training new neural networks. Development of automatic qualification has been required the evaluation of recorded speech samples by surdo-pedagogues and lay students. The online system developed for this purpose is shown in this paper.

Keywords: *hard of hearing and deaf people, audio-visual, recorded speech samples, web-based software development, online evaluation system, PhP, Mysql, reference speech database*

1. INTRODUCTION

The theoretical basis of the research is that studies have shown that integration of acoustic and visual modality in human brain is optimal for producing maximum clarity. For the hearing impaired people, the stronger the acoustic signal distortion, the more they rely on the visual signal. Combination of acoustic signal and visual modality is proven to help the speech detection. If one modality detection is difficult, the perception strongly relies on the other. Since the speech production is based on the perception, thus an obvious assumption is that visual modality will promote the beneficial effect of acquiring productions. Image information processing and sensing of hard of hearing people is smooth and even more experienced than in case of the normal hearing people. Human brain integrates acoustic and visual signals – in both of hearing impairment and normal hearing people – for maximum clarity The poorer the quality of the acoustic signal, the more we rely on the visual modality. Technical development enables the use of more and more intelligent appliances. The latest generation of hearing aids provides individual characteristics

adjusted to the specificities of hearing impaired people promoting the understanding and learning of their speech. Additional help is needed for learning the speech in case of distortion or lack of acoustic perception. The developed client-server service and Internet access allow the deaf and hard of hearing people to practice their speech anytime and anywhere.
One of the objectives of the project TÁMOP-4.2.2.C-11/1/KONV has been to create a method for automatic qualification of speech samples. First of all, the speech samples of children recorded and stored in the server of the University of Miskolc have had to be subjective rated by the surdo-pedagogues and native students involved in the project. Whereas available evaluation systems have been considered unsuitable for our goals (e.g. integration problem with our own database, data archiving and long-term storage), we have to develop our own application to provide user specific features, customized functions and tools for data management, as well as to allow creating unique reports, statistics and trends for further research aims.

2. CONCEPT OF THE SPEECH ASSISTANT SYSTEM

Development of the speech assistant system began in September 2013, with the participation of 14 surdo-pedagogues (each of them deals with deaf and hard of hearing pupils) and hard of hearing children of different ages and stages of development. The methodology of using the system is constantly changing and expanding. Before the start of the development work children had to speak various words and sentences that we recorded from microphone and stored in a high storage capacity and backup server. The same words had to be recorded again beyond one academic year of the development work. [3] Before using the system registration is required, during that only some basic information must be entered to get a full access to use the speech assistant. After logging in, surdo-pedagogues have the opportunity on the home page to select who they want to deal with and what words the child has to practice.

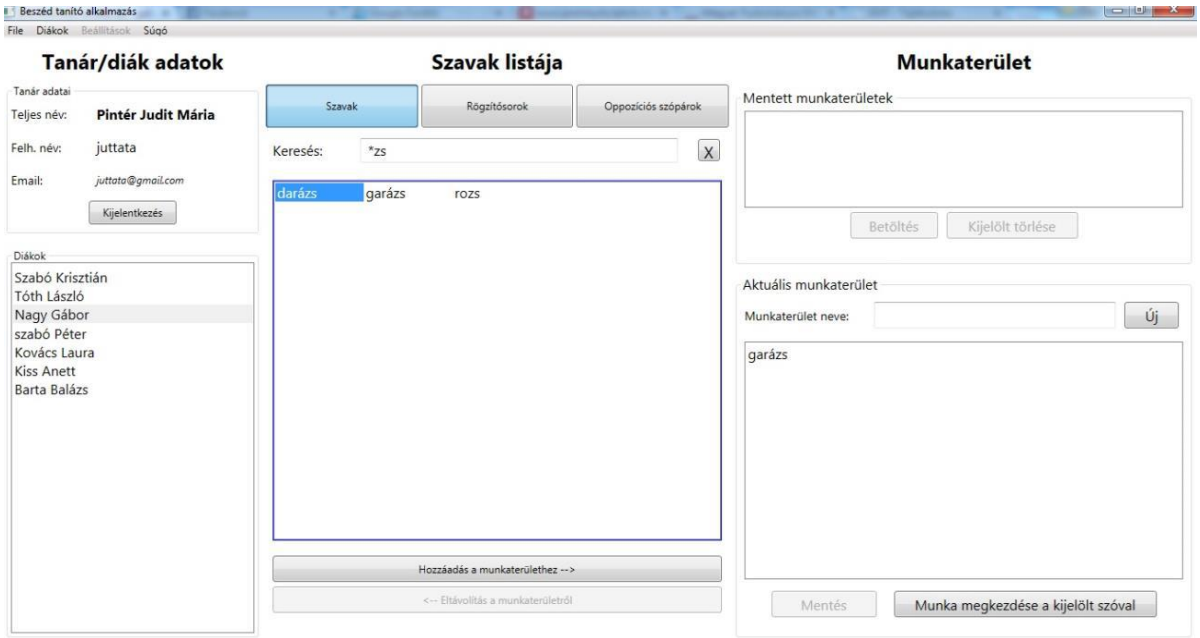

Figure 1 Speech Assistant System

On the initial page (Figure 1) potential new students can be registered with unique identifier and important notes, older students in the system can be deleted , as well as previously saved workspaces can also be loaded again. Patterns recorded during the exercise will be automatically uploaded to the

server dedicated to the pupils for the purpose of carrying out further investigations and research. In case of a pupil is deleted, the samples are not automatically deleted on the server. In the following, the paper is going to show in details the online system developed for evaluating the words and sentences recorded and stored on the central server of the Department of Automation and Infocommunication, University of Miskolc.

3. DEVELOPMENT OF AN ONLINE EVALUATION SYSTEM

3.1. The Concept of the Evaluation System

In the course of learning the pronunciation of the reference is produced by the server or the teacher. The pupil tries to imitate by his/her current announcing. By the analysis of different highlighting and distance calculation methods, a similarity measure can be defined in accordance with the subjective assessment method. This is the basis for progress assessment and feedback generation. The evaluation can apparently be formed by comparing the earlier results, since the same pronunciation can be one pupil's success or the other's failure as well. Verification of the automatic evaluation can be performed by investigation of clarity, for which purpose a client-server based online system had to be developed for storing the ratings of speech samples given by the evaluating users (sudo-pedagogues and lay students). As regards the implementation of the system, primary goal has been to ensure accessible from anywhere online, thus web based development has been the most obvious solution, that provides a 24-hour 'anywhere and anytime' access Development of the system has been done by using combination of PHP and MySQL support for submitting and storing data into database. Thus, the HW and SW infrastructure necessary for the operation has been provided by a central server at the University of Miskolc as follows:

- PHP module: for running PHP based program codes on the server side,
- MySQL module: for centralized data storage and performing filtering and searching operations.

PHP (Hypertext Preprocessor) is an open-source computer scripting language, which can run on any server-side operating systems in cooperation with most of the server software. Its main application field is creation of dynamic websites. [5]
MySQL is a very popular database management system, which is famous for its simplicity and effectiveness. The simplicity is due to among others - as the name implies - that is based on SQL commands. The SQL (Structured Query Language) is a standardized language with the help of different types of databases can be treated in the same way. [6]
Various features are implemented through their own PHP functions. Users can be managed entirely by an administrator, who having supervisor rights can perform such operation as: creating new user account, disable users, deleting user account, managing user rights, changing user profile, etc.

3.2. Structure of the Reference Database

For creation of automatic evaluation, first of all, speeches of hearing impaired children have been recorded as reference data. The initial main database, which consists of 3,000 words, has been systematized by the members of a research team at the University of Miskolc using several criteria: classification of speech; topic classification; number of syllables; number of voices; vowel-consonant formula, etc.
The current database consists of exactly 2,355 words (some words occur multiple times, but the announcers and their intelligibility are different), which have been evaluated by 13 teachers (surdo-pedagogues) and 23 lay students. The basis of the five-scale rating for evaluation is determined by the surdo-pedagogues. All teachers have rated only the students of the other schools to avoid bias

resulting from the recognition of the speakers. Results have been recorded via the web application developed for this purpose. [4]
Given that the speech samples have been recorded in 3 different schools (Budapest, Eger, Debrecen) educating deaf and hard of hearing children, it has been reasonable to store them in three different directories on the server with the following structure (Figure 2).

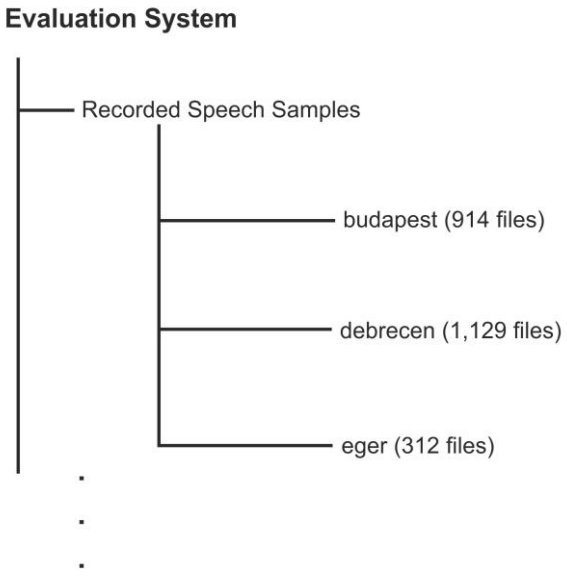

Figure 2 Directory Structure of the Speech Samples Stored on the Server

Database established for storing evaluations of speech samples is shown in the following figure (Figure 3).

ratings

datafield type	datafield name
id	int(5)
speech_sample_id	varchar(5)
user_id	varchar(5)
score	varchar(10)
date	varchar(15)
remarks	varchar(1000)

indexes

key	type	unique	packed	column	cardinality	join	NULL
PRIMARY	BTREE	YES	NO	ID	21273	A	NO

Figure 3 Data Table for Storing Evaluations

Structure and scheme of tables within the database can be described by data fields, in which the following additional parameters have to be defined:

- type of data field: number, char, string, boolean,
- date, etc.,
- length of data field: necessary number of characters for digital storing of data,

- integrity conditions binding to data fields: an inner rule system, the accuracy of the information stored (for example, can be left blank in the data under recording, whether it is a primary key, etc).

Definition of data fields has been done by entering a name and selecting the type of them. Since structures do not clearly identify tables, as more tables may exist with the same structure, and on the other hand defining structures may take long time, thus unique identifying name has been assigned to each table within the database. This name is used to clearly identify a table during operations. Therefore, the name of the tables within the database, and that of the data fields within a table must be unique.

4. FIVE-SCALE EVALUATION

One of the speech assistant system features is the automatic rating and feedback for the hearing impaired pupils to practice the sample words. In the course of learning each pupil's pronunciation is compared to the reference produced by the server. For verification of clarity, the following scale has been defined and used:

- Unintelligible (1): articulation is completely distorted; the vowels and consonants are unrecognisable; the reproduction of the syllable number is not adequate or discernible; breathing and management of breath is faulty; tempo and rhythm are incorrect; the utterance is unmelodious, non-dynamic or too tense.
- Difficult to understand (2): grave distortions, omission of sounds, sound replacement; only some of the vowels can be discerned; distortions due to insufficient breathing, e.g. too breathy or choked; characterised by irregular, disturbing tonality, rhythm and tempo.
- Moderate to understand (3): the articulation of vowels is correct, the number of syllables is appropriate; serious speech defects may occur, e.g. dyslalia (the speech impediment in which certain vowels are incompletely formed, nasality, head voice, etc.), prosodic inadequacies.
- Easy to understand (4): slight speech defects; slight prosodic inadequacies.
- Understandable at the same level as the speech of the hearing (5): at most 1-2 sound defects may occur.

Before evaluators submitted their own scores, they had been able to listen speech samples repeatedly, eliminating this way the loading problems caused by loss of network or a narrow bandwidth Internet connection, moreover private notes about samples can be put into a textbox to indicate any type of problems.

5. DEVELOPED EVALUATING SYSTEM

On the login interface, users must submit the user name and password of their account created by the supervisor, after that user data is loaded. When the supervisor creates a new user account, he/she specifies which speech samples have to be evaluated by the user.

The system performs a check and after success authentication loads the profile on the basis of user accounts defined in the user profiles. After a successful login, the current speech sample for evaluation is loaded. Evaluation process can be interrupted at any time, and be continued until a specified deadline has expired. When a user scores each sample, the system indicates it to the user, and closes his/her account. During listening the current sample, it is displayed in a textbox which word or sentence is concerned. The system indicates to the user how many samples he or she has already rated. Teachers in Budapest have evaluated 1,441 speech samples, teachers in Eger have evaluated 2,043 samples and teachers in Debrecen have evaluated 1,226 samples. Lay students have had to score all the samples, which means 2,355 evaluations for a student.

Figure 4 Developed System for Evaluation of Speech Samples

The evaluation consists of the following steps (Figure 4):

- Clicking on the play button the current speech file loaded for rating can be listened. Each sample can be played multiple times.
- Rating of the audio file can be performed by clicking on a radio button next to the scores.
- If the evaluator wants to record notes to the speech sample currently scored, the textbox can be used for this purpose.
- The evaluation of a speech sample is completed by clicking on the 'Submission of scores', after which the next audio file is loaded for rating.

SUMMARY

The user-friendly interface has been of high priority during the development of the system in order to interconnect the appearance and users' expectations. Due to this goal a comfortable, easy to use system has been resulted facilitating users' work and reducing errors in data entry and data management. We have summarized and averaged the scores given by the students and the surdo-pedagogues. The results show that the students have given higher scores than the teachers. This is due to the teachers' qualifications and experiences, they have taken much more attention to a vocal error too, over which the lay students overlook above. Complex statistic reports and trends, further in-depth analysis of stored ratings are going to be performed in the next two months. In the future, according to user needs changes, the emphasis is going to be placed on the development of additional comfort features, as well as faster and more efficiently function. In order to promote the tasks performed by the administrator, to make easier the management of users, further aim is to develop a web based easy to use administrator interface. Another goal is to implement such functions that are capable to perform various statistical and trend statements, diagrams automatically without exporting data fields from the database to an external data management application, speeding up data handling and processing.

ACKNOWLEDGEMENT

This research was carried out in the framework of the Centre of Excellence of Mechatronics and Logistics at the University of Miskolc.

REFERENCES

[1] L. Czap., I. Sziklai, "Feasibility Study", TAMOP-4. 2. 2. C-11/1/KONV-2012-0002 (Social Renewal Operational Programme)
[2] Czap, L. , Varga, A.K. ; Illés, B.: Concept of a Speech Assistant System, Proceedings of 2013 Fourth World Congress on Software Engineering (WCSE), 3-4 December 2013, Hong-Kong, Chnia, IEEE Computer Society-Conference Publishing Services, ISBN 978-1-4799-2882-8, pp. 207-211
[3] VICSI, K., SZASZÁK, GY.: Automatic Segmentation of Continuous Speech on Word Level Based on Supra-segmental Features. International Journal of Speech Technology, Vol. 8, Num. 4, 2005, pp. 363–70.
[4] VICSI K., KOCSOR A., TELEKI CS., TÓTH L: Hungarian Speech Database for Computer-using Environment in Offices, II. Magyar Számítógépes Nyelvészet Konferencia kötet, 2004, pp. 315–318.
[5] R. Nixon: Learning PHP, MySQL & JavaScript: With jQuery, CSS & HTML5., ISBN 978-1491918661, 2014.
[6] L. Ullman: PHP and MySQL for Dynamic Web Sites: Visual QuickPro Guide, ISBN 978-0321784070, 2011.

INTERNATIONAL SCIENTIFIC CONFERENCE ON ADVANCES IN MECHANICAL ENGINEERING

19 November 2015, Debrecen, Hungary

"DOES" THE SIZE REALLY MATTER?", OR HOW THE HELICOPTER TURBOSHAFT ENGINES ARE PENALISED BY THEIR OWN SMALL SIZE

[1]VARGA Béla PhD, [2]PÁSZTOR Endre DSc, [3]ÓVÁRI Gyula CSc

[1,3]Department of Aircraft and Engine, National University of Public Service
E-mail: varga.bela@uni-nke.hu, ovari.gyula@uni-nke.hu
[2]Department of Aeronautics, Naval Architecture and Railway Vehicles, Budapest University of Technology and Economics

Abstract
The answer for the question in the title is obvious. The size is extremely important. Examining the thermal efficiency (TE) and specific net work output (SNWO) of gas turbine engines, it is well proved that the above mentioned performance indicators of helicopter turboshaft engines are greatly lower than the average of other gas turbine categories, which are today at takeoff power over 40% and 400 kJ/kg, meanwhile 30% TE and 150-250 kJ/kg SNWO are considerable at helicopter turboshafts. This negative effect mainly comes from the small size of their compressor and the accordingly low blade length, especially in the rear stages (higher relative blade tip clearance) and the low Reynolds number of the flow. In this paper the compressor size and its correlation with the above mentioned performance indicators are examined.

Keywords: *helicopter turboshaft engines, specific net work output, thermal efficiency,*

1. INTRODUCTION

The evolution of turboshaft engine category is connected to the rapid development of helicopters in 1950s. The first helicopters in 40s and early 50s were powered mainly by radial engines which allowed relatively low maximum take-off weight and payload. The urgent need for increasing transport capacity claimed new solution to power the helicopters. Obvious choice was the then relatively new gas turbine engine being converted it for shaft power production.
In the early 1950's, General Electric was awarded a 3 million dollar contract by the US Government to develop a next-generation lightweight, affordable and reliable power plant for rotary winged aircraft. Under a secret program named the XT-58, this "baby gas turbine" powerplant was to weigh a mere 400 pounds and was required to produce 800 shp.
On 20th February 1958 the Council of Ministers of the USSR adopted a directive calling for the development of the V-8 helicopter with a cargo-carrying capacity of 1.5 to 2.0 tonnes, powered by a helicopter version of the Ivchenko AI-24V engine. The single-engine V-8 took to the air for the first time on 24th June 1961. Recognizing the disadvantages of AI-24V, the Izotov Engine Design Bureau was ordered to develop the first dedicated helicopter engines. The TV-2VM and D-25V engines used on the Mi-6 were derivatives of engines originally designed for fixed-wing aircraft. The new TV2-117 engines and the VR-8 main gearbox developed by Izotov were delivered in the summer of 1962. The engines had a take-off power rating of 1,500 shp each and possessed relatively good specific performance data.
Helicopter engines, like the other fields of aviation have gone through huge evolution. The increased compressor overall pressure ratio, turbine inlet temperature, the FADEC system highly improved their performance, while the long-term reliability and maintainability has also increased. However some performance indicators of helicopter turboshaft engines, like TE and SNWO are

greatly lower than the average of other gas turbine categories, which is today at takeoff power over 40% and 400 kJ/kg. Meanwhile 30% TE and 150-250 kJ/kg SNWO are considerable at helicopter turboshafts.

2. STATISTICAL ANALYSES OF EXISTING TURBOSHAFT ENGINES

In this part of paper we statistically analysed far not all, but numerous helicopter engines. *Figure 1* and *Figure 2* display the results, where using excel diagrams we created specific fuel consumption (SFC) and SNWO vs. shaftpower curve.

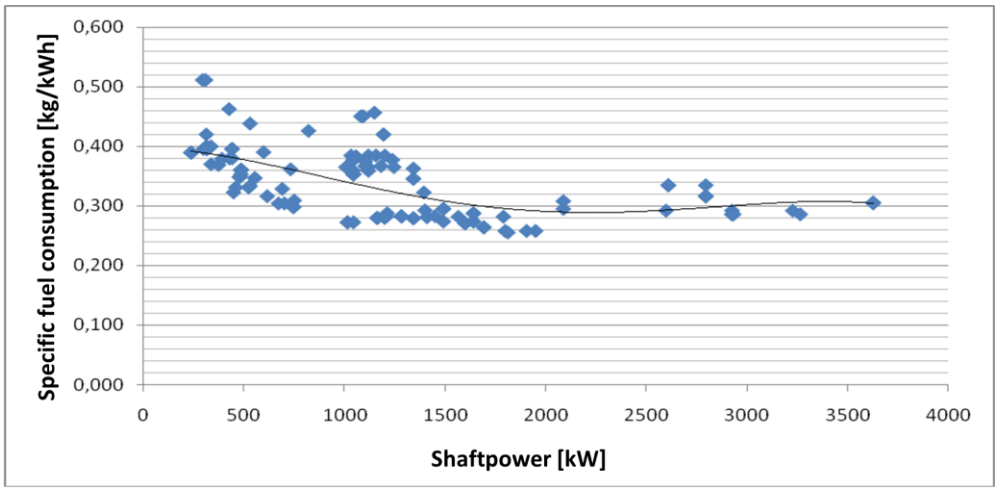

Figure 1 SFC vs. shaftpower diagram [1]

Analysing the diagram in *Figure 1* we can recognise some interesting phenomenon. First, that the examined engines can be separated into three groups by their shaftpower among them with significant power gaps. The smallest category provides about 200-800 kW shaftpower. The next category ranges from 1000-2200 kW, while the large category gives 2500-3700 kW takeoff power. The last one contains the fewest number of engines. Of course actually there are more engines in this category like displayed here, but anyway the smaller number of heavy helicopter types and the fewer piece per types explains the less data comparing to the small and medium category.
But what is more interesting the nature of the average SFC vs. shaftpower curve. Considerable change can be seen at higher shaftpower. The average SFC decreases from about 0.4 kg/kWh to 0.3 kg/kWh. Converting them, the related TEs are 21% (0.4 kg/kWh) and 28% (0.3 kg/kWh) (there are direct relation between the SFC and TE). Today (by my information) the RTM 322-04/08, RTM 322-01/9 and RTM 322-01/9A give the better SFC values with 0,258 kg/kWh which is a bit higher than 32% TE.
The next important quality indicator is the SNWO in *Figure 2*. Creating this diagram we had much fewer data than in *Figure 1*, but the trend is obvious in this case, too. The average SNWO increases from about 150 kJ/kg to nearly 250 kJ/kg. Concluding it, with increasing shaftpower both indicators provide better engine performance (lower weight and lower SFC). But their relation to the shaftpower is indirect. Higher shaftpower is mostly means larger engine, so the better TE and SNWO is rather related to the size of the engine. One of the problem is just rooted in this fact. If we increase the SNWO consequently less mass flow rate is needed for the same shaftpower. It results smaller size which actually worsen the opportunity for achieving better SNWO and TE according to *Figure 1* and *Figure 2*. Of course, even considering nearly the same shaftpower output there is significant difference in SNWOs, which means it is not impossible achieving higher SNWO and TE, but it has to do in “headwind”.

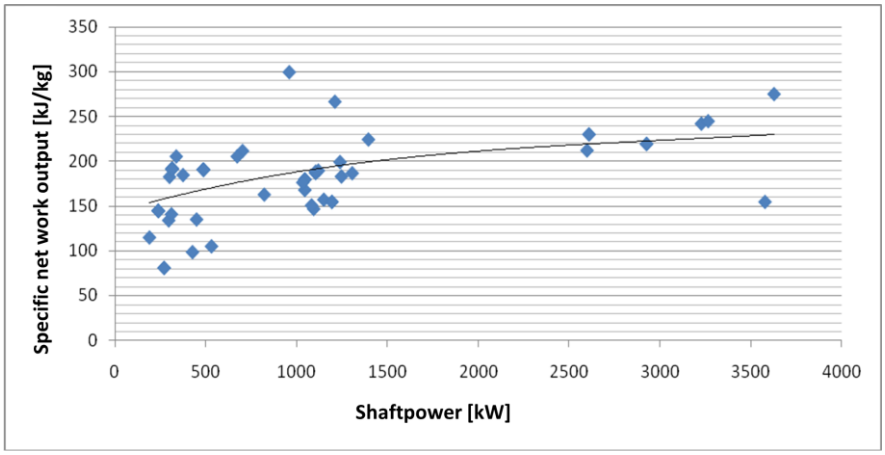

Figure 2 SNWO vs. shaftpower diagram [1]

It is something like "catch 22". In accordance with it we can make a preliminary statement that the size, yes indeed does matter.

3. ANALYSES WITH THERMAL MATHEMATICAL MODEL

Creating thermal mathematical model, we intended to answer numerous questions arisen with the work of gas turbine engines, mainly turboshaft engines. To get these answers we examined the TE and SNWO which are suitable for the evaluation of any kind of gas turbine engines.
The model produces:

- The characteristic curves of the TE and SNWO in turbine inlet temperature versus compressor pressure ratio diagram for any kind of combination of engine component efficiencies;
- Calculates the distinguished compressor pressure ratio values;
- Creates SNWO, TE web in compressor polytrophic efficiency versus compressor pressure ratio diagram;
- It takes into consideration the change of compressor polytrophic efficiency as a function of blade length giving possibility to evaluate its effect on the distinguished compressor pressure ratios, TE and SNWO;
- It provides the analyses and evaluation of existed turboshaft engines.

To process the above listed examinations, Microsoft Excel was used with Visual Basic programming. Microsoft Excel Worksheet provides the communication platform of the created Visual Basic programme [2].
Producing the parameter sensitivity examination, we realised that all engine component efficiencies and losses influence the maximum SNWO and TE but their influence is different. Here we try to reflect how significantly each one effects the above mentioned engine properties. In *Figure 3* it can be seen one examples for 1450 K Turbine Inlet Temperature (TIT or T_3). Initial values of engine component efficiencies and losses are in the top left corners of pictures in *Figure 3.* At first each component efficiencies and losses was worsen individually by 1% and the deterioration of the chosen performance indicators (SNWO and TE) are also given in [%] in *Figure 3.* It is clearly evident that the gas turbine engines are especially sensitive for the compression and expansion polytrophic efficiencies. Considering the SNWO and TE values together, the compressor efficiency influences them most significantly. Furthermore examining the related researches in this field it became clear that the compressor blade length has significant effect on compressor polytrophic efficiency. Shorter blades deteriorate the compressor polytrophic efficiency.

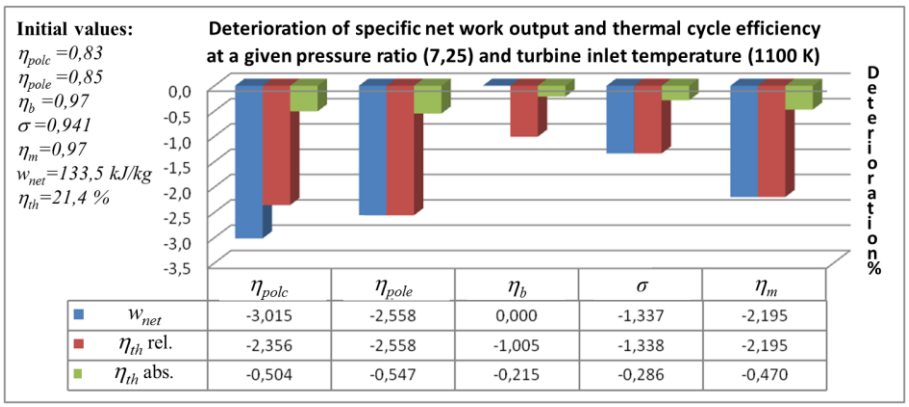

Figure 3 Results of parameter sensitivity examination

Taking into consideration this effect we used equation 1, which was created by Professor Endre Pásztor and it is based on the researches and measures of some foreign scientists (Andenburg, Brown-Boveri, Kirillov, Stepanov). This equation correctly simulate how the blade length of compressors effects the compressor polytrophic efficiency [3].

$$\eta_{polk(i)} = \eta_{polk(0)} \left(1 - K_k \left(\frac{l_r}{l_{(i)}} \right)^{m_k} \right) \tag{1}$$

Where:

$\eta_{polk(i)}$: compressor polytrophic efficiency of stage number "i" [%];

$\eta_{polk(0)}$: compressor polytrophic efficiency considering 0 blade tip clearance [%];

K_k: experimental constant for compressor based on measures (1) [–];

m_k: experimental constant for compressor based on measures (2) [–];

l_r: absolute bade tip clearance (can be constant for all stages in a given compressor) [m];

$l_{(i)}$: compressor blade length of stage number "i" [m];

CONCLUSIONS

In *table 1* I collected the most important data of the analysed seven turboshaft engines, which provide easier comparison. The first six are helicopter engines, while the seventh is power generator or powers ships and provides considerable higher shaftpower. The first three represent the engines from 60s and 70s, the second three are the new generation of helicopter turboshaft engines.
The used symbols in *Table 1*:

- P_{sh}: provided shaftpower;
- T_3: turbine inlet temperature (TIT);
- $\dot{m}$: mass flow rate through the engine;
- π_{wh}-$\pi_{\eta t}$: compressor pressure ratio related to the maximum SNWO and TE;

π: the actual compressor pressure ratio;

- η_{pole}: efficiency of polytrophic expansion;
- η_{polc}: efficiency of polytrophic compression;

- η_t: thermal efficiency (TE);
- w_{net}: specific net work output (SNWO);

All date in *Table 1* refers to the takeoff rate of power.

Table 1 Most important data of examined turboshaft engines

		TV2-117A	**TV3-117VM**	**T58-GE-100**	**MTR 390E**	**T800-LHT-801**	**RTM 322-01/9**	**LM 2500**
1	P_{sh} [kW]	1103	1699	1118	1043	1166	1799	24000
2	T_3 [K]	1168	1250	1269	1627	1444	1507	1504
3	$\dot{m}$ [kg/s]	6,8	8,75	6,35	3,6	4,53	5,79	70,3
4	π_{wh}-$\pi_{\eta t}$ π [-]	6,24-9,97 6,6	7,18-12,2 9,45	6,52-10,22 8,4	9,45-16,73 14	8,92-16,41 15	10,36-20,81 14,7	12,38-29,64 18
5	η_{pole} [-]	0,848	0,846	0,824	0,815	0,849	0,857	0,872
6	η_{polc} [-]	0,824	0,824	0,798	0,774	0,808	0,822	0,858
7	η_t [%]	22,58	25,66	22,59	27,83	29,85	32,26	36
8	w_{net} [kJ/kg]	162,3	190,8	176	303,47	257,3	310,8	341,451

The average turboshafts provide about 250–2500 kW shaft power with 2–12 kg/s air mass flow rate. Accordingly their compressors are relatively small, which causes short blade length, especially in rear stages of compressor (or centrifugal stage is used as last stage). As we mentioned earlier the short blade length has strong negative effect on compressor and turbine polytrophic efficiency. This effect has been heightened by the development trend to increase the specific net work decreasing the engine dimensions and weight. It can be done by either improving the component efficiencies or raising the TIT and compressor pressure ratio together. Choosing the last one it is very hard to avoid the deterioration of polytrophic efficiencies.

It is the reason that in some cases compressor and turbine polytrophic efficiency not significantly higher (5th and 6th row of *Table 1*), what is more sometimes lower, although the engine is much younger. This phenomenon at least partly annul the hoped SNWO and TE improvements. This fact means the compressor pressure ratio is usually not higher than ~15 and the TIT is mostly not much higher than 1500 K, and the resulted maximum TE is less than 35%, while at bigger (new) gas turbine engines (where air mass flow is over 30 kg/s) the TE is usually over 40%. Good example is the LM 2500, which does not achieve 40% thermal efficiency, but its TE is considerably higher than the efficiency of the much smaller turboshaft engines.

The better component efficiencies and the high pressure ratio and TIT of the new generation RTM-322-01/9 presents the best overall features. This is clearly shows us that good performance indicators cannot be achieved only by increasing the compressor pressure ratio and turbine entry temperature. To keep the component efficiencies, especially compressor polytrophic efficiency as high as possible, has a same importance.

REFERENCES

[1] Engine Manufacturers, Helicopter Annual, 2009, p. 57-63
[2] Varga, B.: Gázturbinás hajtóművek teljesítmény és hatásfok növelésének műszaki technológiai háttere, és ezek hatása a katonai helikopterek korszerűsítésére, PhD értekezés, Budapest, 2013, http://uni-nke.hu/downloads/konyvtar/digitgy/phd/2013/varga_bela.pdf, p. 47-81
[3] Pásztor, E.: Szállító repülőgépek gázturbinás hajtóművei nyomásviszonya növelésének termikus problémái, 2007, Repüléstudományi Közlemények, p. 36-45

INTERNATIONAL SCIENTIFIC CONFERENCE ON ADVANCES IN MECHANICAL ENGINEERING
19 November 2015, Debrecen, Hungary

MODELLING QUESTIONS OF METAL FOAMS

[1]VARGA Tamás Antal, [2]KOZMA István, [3]BUDAI István PhD, [4]MANKOVITS Tamás PhD

[1,4]Department of Mechanical Engineering, Faculty of Engineering, University of Debrecen
E-mail: tomivarga27@gmail.com, tamas.mankovits@eng.unideb.hu
[2]Department of Material Sciences and Technology, Széchenyi István University
E-mail: kozma@sze.hu
[3]Department of Engineering Management and Enterprise, University of Debrecen
E-mail: budai.istvan@eng.unideb.hu

Abstract
The development of an efficient procedure for 3D modelling and finite element simulation of metal foams is one of the greatest challenges to engineer researchers nowadays. Creating 3D CAD model from its structure is alone a demanding engineering task due to its extremely complex geometry, and the proper finite element analysis process is still in the center of the research. In this paper the evaluation of the records of the X-ray computed tomography inspection is introduced for the investigated specimen. These results will be used to establish the idealized CAD model of the metal foam.

Keywords: *metal foam, modelling, computed tomography*

1. INTRODUCTION

Metal foams are relatively new and advanced materials with high stiffness to weight ratio, good thermal conductivity, good acoustic insulation and excellent energy absorption capability which make them ideal materials for a variety of applications [1-3]. Therefore, they have increasingly been employed for a wide range of applications, such as structural elements, automotive parts, sound and vibration absorbers or even biomedical implants [4-9]. Basically, the mechanical properties of metal foams are influenced by three dominating factors, namely the property of the solid phase, the relative density of the solid phase and the spatial arrangement, that is, the structure of the metal foam (cell distribution, cell shape). To understand the structure property correlations in metal foams is required for optimizing its mechanical performance for a given application [10].
Although metal foams are popular they are still not sufficiently characterized thanks to its extremely complex structure which is highly stochastic in nature. In the last few years, several researchers focused on the finite element modelling of metal foams with more or less success, but it is still one of the greatest challenges. Instead of modelling the complex internal structure directly, idealized structural approaches (unit cell, statistical models, etc.) are often used where the cells are represented by miscellaneous two- or three dimensional models according to the structure behaviour [11-15]. 3d model created by the help of X-ray tomography (beam model, voxel and tetrahedral element methods) [16,17] is another possibility. In detail, different numerical approaches for the simulation of metal foams were proposed [11-17].
In this paper a closed-cell aluminum foam is investigated. The aim of this research is the preparation for the finite element simulation of the metal foam under compression using 3D CAD model. In order to reach this target the records of the computed tomography analysis are evaluated.

2. METHODS

X-ray computed tomography has recently proved to be a very efficient and powerful tool mapping the complete structure of materials in a non-invasive and non-destructive way [18, 19]. This imaging process allows the visualization of complex structures. However, this equipment thanks to its high-cost level is not always available. The CT tomograms were made in the laboratory of the Materials Science Department of Széchenyi István University with a YXILON CT Modular industrial CT system, with a 225kV micro focus X-ray tube and a resolution of 7μm.
Computed tomography (CT) scanning, also known as computerized axial tomography (CAT) scanning, is a diagnostic imaging procedure that uses X-rays in order to present cross-sectional images of the investigated specimen. Cross sections are reconstructed from the measurements of attenuation coefficients of X-ray beams in the volume of the object studied.
CT is based on the fundamental principle that the density of the tissue passed by the X-ray beam can be measured from the calculation of the attenuation coefficient. CT allows the reconstruction of the density of the specimen, by two dimensional section perpendicular to the axis of the acquisition system. The operation of the industrial CT inspection system can be seen in *Figure 1*.

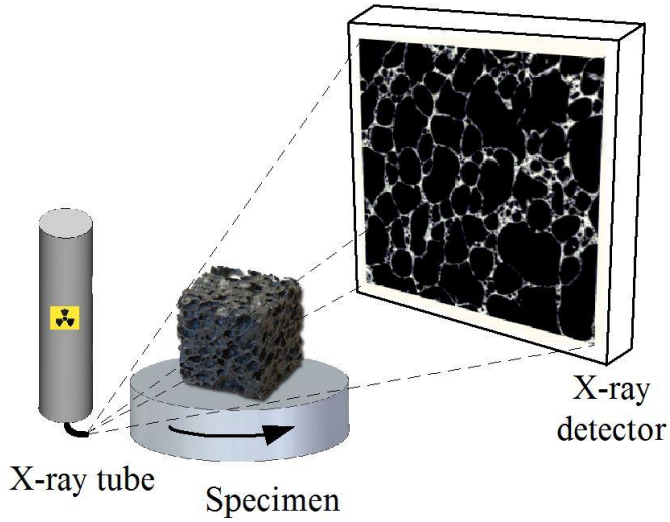

Figure 1 The operation of an industrial CT inspection system

3. RESULTS

Using special purpose software the internal structure of the investigated foam specimen can be mapped. This software allows us to establish the following important structural properties, e.g. geometrical data of the cells (surface, volume, radius, sphericity property) and the location of the cells. The internal structure of the metal foam can be seen in *Figure 2*.

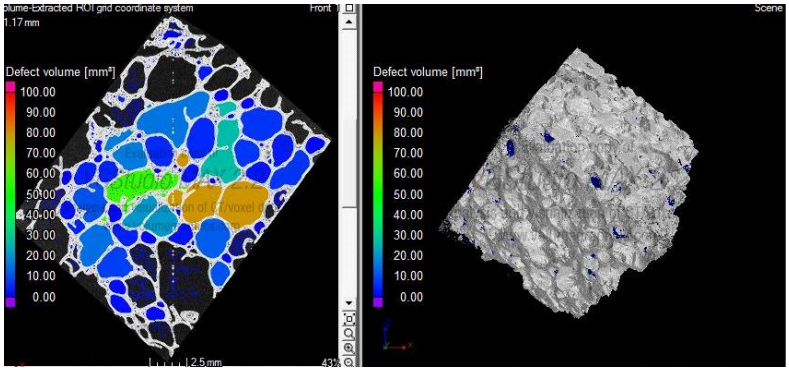

Figure 2 The analysis of the internal structure of the foam

The metal foams are built from several cells and their shape and size are not equal, see in *Figure 2*. Using special purpose software the volume of the cells can be determined and evaluated. The frequency distribution of the cell's volume can be seen in *Figure 3*.

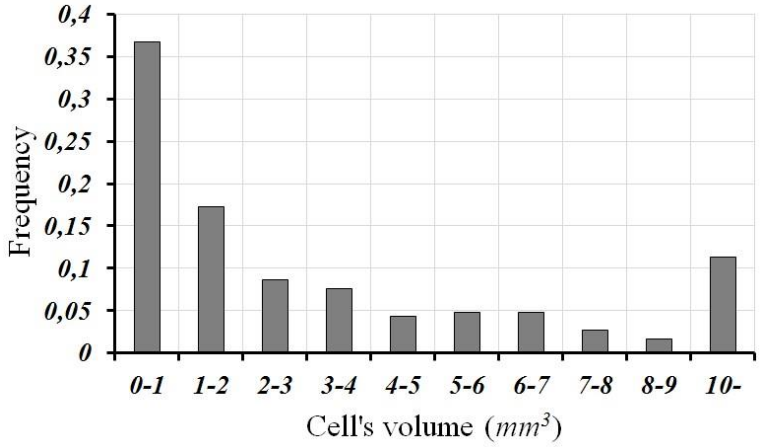

Figure 3 The frequency distribution of the cell's volume

The same software is able to determine the diameter of the circumscribed sphere of the investigated cell. This data gives the greatest size of the cell which is useful during the design procedure of the idealized foam model. The frequency distribution of the circumscribed sphere of the cells can be seen in *Figure 4*.

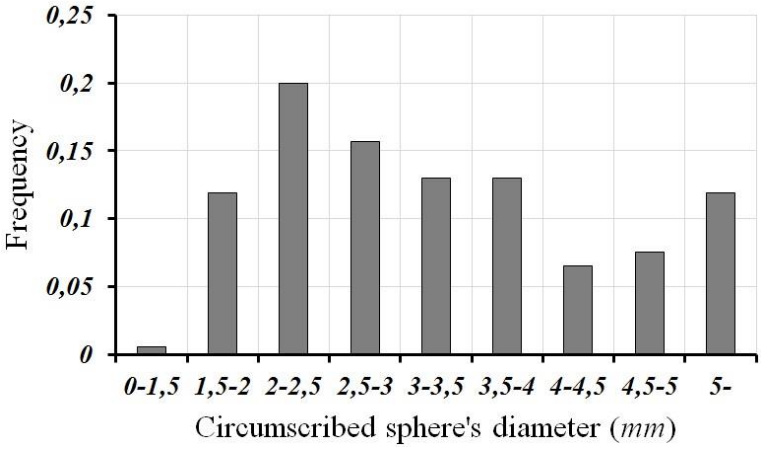

Figure 4 The frequency distribution of the cell's circumscribed sphere diameter

Due the outstanding shape of the metal foam cells the so called sphericity property of a cell is also determined and evaluated. The sphericity is a measure for the ration between the surface of a sphere with the same volume as the cell and the surface of the cell. The frequency distribution of the sphericity can be seen in *Figure 5*.

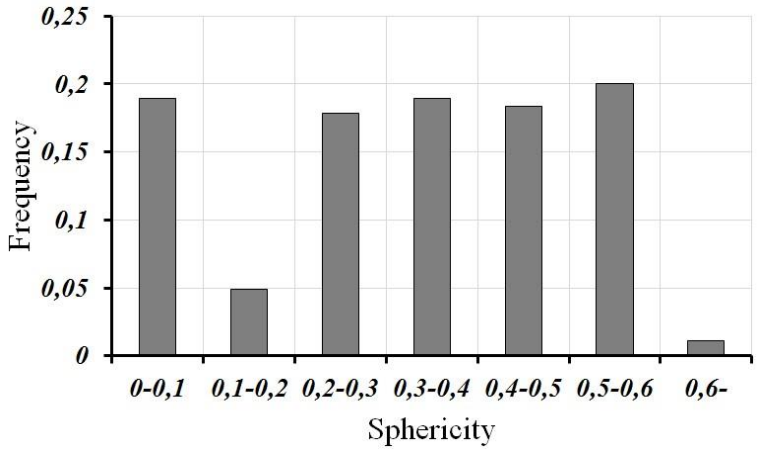

Figure 5 The frequency distribution of the sphericity of the cells

CONCLUSIONS

Although metal foams are popular they are still not sufficiently characterized due to their extremely complex structure which is highly stochastic in nature. Based on CT images numerous parameters of the cells within the metal foam were analyzed by volume analysis using special purpose software. These results are used for establishing the realistic CAD model which can be investigated appropriately in numerical way.

ACKNOWLEDGEMENT

The described work was carried out as part of the Custom Development Grant project in the framework of the National Talent Program (NTP-EFÖ-P-15). The realization of this project is supported by the Ministry of Human Capacities.

REFERENCES

[1] Ashby, M.F., Evan, A.G., Fleck, N.A., Gibson, L.J., Hutchinson, J.W., Wadley, H.N.G.: *Metal Foams: A Design Guide*. Butterworth-Heinemann, 2000.
[2] Czekanski, A., Attia, M.S., Meguid, S.A., Elbestawi, M.A.:*On the Use of a New Cell to Model Geometric Asymmetry of Metallic Foams.* Finite Elements in Analysis and Design, 41(13), 1327-1340, 2005.
[3] Banhart, J.: *Manufacture, Characterization and Application of Cellular Metals and Metal Foams.* Progress In Materials Science, 46(6), 559-632, 2001.

[4] Vendra, L.J., Rabiei, A.: *Evaluation of Modulus of Elasticity of Composite Metal Foams by Experimental and Numerical Techniques.* Materials Science and Engineering: A, 527(7-8), 1784-1790, 2007.
[5] Tuncer, N., Arslan, G.: *Designing Compressive Properties of Titanium Foams.* Journal of Materials Science, 44(6), 1477-1484, 2009.
[6] Kádár, Cs., Chmelík, F., Rajkovits, Zs., Lendvai, J.: *Acoustic Emission Measurements on Metal Foams.* Journal of Alloys and Compounds, 378(1-2), 145-150, 2004.
[7] Djebbar, N., Serier, B., Bouiadjra, B.B., Benbarek, S., Drai, A.: *Analysis of the Effect of Load Direction on the Stress Distribution in Dental Implant,* Materials&Design, 31(4), 2097-2101, 2010.
[8] Kashef, S., Asgari, A., Hilditch, T.B., Yan, W., Goel, V.K., Hodgson, P.D.: *Fracture Toughness of Titanium Foams for Medical Applications.* Materials Science and Engineering: A, 527(29-30), 7689-7693, 2010.
[9] Mankovits, T., Tóth, L., Manó, S., Csernátony, Z.: *Mechanical Properties of Titanium Foams, a Review.* Proceedings of the 1st International Scientific Conference on Advances in Mechanical Engineering, 10-11 October, Debrecen, Hungary, 2013.
[10] Saadatfar, M., Mukherjee, M., Madadi, M., Schröder-Turk, G.E., Garcia-Moreno, F., Schaller, F.M., Hutzler, S., Sheppard, A.P., Banhart, J., Ramamurty, U.: *Structure and Deformation Correlation of Closed-cell Aluminium Foam Subject to Uniaxial Compresion.* Acta Materiala, 60(8), 3604-3615, 2012.
[11] Hodge, A.M., Dunand, D.C.: *Measurement and Modeling of Creep on Open-cell NiAl Foams.* Metallurgical and Materials Transactions A, 34(10), 2353-2363, 2003.
[12] Hasan, A.: *An Improved Model for FE Modeling and Simulation of Closed Cell Al-Alloy Foams.* Advances in Materials Science and Engineering, Article ID 567390, 12 pages, doi:10.1155/2010/567390, 2010.
[13] Kou, D.P., Li, J.R., Yu, J.L., Cheng, H.F.: *Mechanical Behavior of Open-cell Metallic Foams with Dual-size Cellular Structure.* Scripta Materialia, 59(5), 483-486, 2008.
[14] Filice, L., Gagliardi, F., Umbrello, D.: *Simulation of Aluminium Foam Behavior in Compression Tests.* The Arabian Journal for Science and Engineering, 34(1), 129-137, 2009.
[15] Miedzinska, D., Niezgoda, T.: *Initial Results of the Finite Element Analyses of the Closed Cell Aluminium Foam Microstructure under the Blast Load.* CMM-2011 Computer Methods in Mechanics, 9-12 May, Warsaw, Poland, 2011.
[16] Adziman, M.F., Desphande, S., Omiya, M., Inoue, H., Kishimoto, K.: *Compressive Deformation in Aluminium Foam Investigated Using a 2D Object Oriented Finite Element Modeling Approach.* Key Engineering Materials, 353-358, 651-654, 2007.
[17] Jirousek, O., Doktor, T., Kytyr, D., Zlámai, P., Fíla, T., Koudelka, P., Jandejsek, I., Vavrik, D.: *X-ray and Finite Element Analysis of Deformation Response of Closed-cell Metal Foam Subjected to Compressive Loading.* Journal of Instrumentation, 8 C02012, doi:10.1088/1748-0221/8/02/C02012, 2013.
[18] Banhart, J., Borbély, A., Dzieciol, García-Moreno, F., Manke, I., Kardjilov, N., Kaysser-Pyzalla, A.R., Strobl, M., Treimer, W.: *X-ray and neutron imaging - Complementary techniques for materials science and engineering*. International Journal of Materials Research 101(9), 1069–1079, 2010.
[19] Redenbach, C., Rack, A., Schladitz, K., Wirjadi, O., Godehardt, M.: *Beyond imaging: on the quantitative analysis of tomographic volume data.* International Journal of Materials Research, 103(2), 217-227., doi: 10.3139/146.110671, 2012.

INTERNATIONAL SCIENTIFIC CONFERENCE ON ADVANCES IN MECHANICAL ENGINEERING

19 November 2015, Debrecen, Hungary

CONSIDERATION REGARDING THE APPLICATION OF NEW TECHNOLOGIES FOR IMPROVEMENT OF INTERNAL COMBUSTION ENGINE

[1] ZELEA Ionatan Teodor, [2]ACHIMAȘ Gheorghe, [3]GYENGE Csaba, [4]LAZE Daniel

[1,4]PhD student: T.U. Cluj-Napoca
E-mail: ionatanzelea@yahoo.com,
[2,3]Professors at Department of Manufacturing Engineering from T.U.Cluj-Napoca (RO)
E-mail: gyenge_cs@yahoo.com

Abstract
The endurance and liability of motor vehicle engines depends on the tribological behavior of the components and on the specific regimes of lubrication. The effeteness' process of the vehicles' shafts (arbors) means the undesired modifications in the dimensions, quality of the surfaces and in their geometrical form and position. The thermal spraying is one of the technological reconditioning processes for shafts, which permits obtaining new surfaces that will meet new requirements. Throughout thermal spraying we got a new surface by laying down a material coat on the substrate (under layer). Thermal spraying can be obtained by the means of: flame, plasma, flame arc, etc. More advanced methods use the LASER as a power source and as additional materials either wire or powder. The notion of reconditioning always refers to a fixed mark while the notion of repairing refers to an assembly taken as one entity.

Keywords: *reconditioning, shaft, maintenance, tribology*

1. INTRODUCTION

Among the main running indexes, that characterize the technical state of a vehicle, we emphasize the developed force and pull power , the fuel and oil consumption, the power necessary for engaging, etc. This way we are facing the necessity of some maintenance interventions so the vehicle can be re-stated to a good running state for a well-determined period of time. After each repairing the power of the vehicle are growing.
We can sum up that the issue of the "4Rs" that are responsible for the prolongation of the vehicle's life cycle, that are: reusing, repairing, reconditioning combined with modernization and recycling – represents a heightened importance worldwide.
The prolongation of the vehicle's life cycle through actions from the 4Rs range is a problem that is integrated in the modern conception of "durable" development, that once resolved assures:

- on one hand, avoidance of pollution that would be determined by the products' abandonment,
- on the other hand, a cut down of the materials extracted from nature, and so preventing their depletion.

The modernization of the reconditioning procedures, application of terotechnology, of the terological operations, assures the prolongation of the vehicle mains shaft's life cycle, reduction of spares stock, decrease of labor costs, etc.
The remanufacturing and reparation require and modernization of the machinery, so that they incorporate new components within.

2. THE KINEMATICS OF THE CONNECTING ROD-CRACK MECHANISM AT INTERNAL COMBUSTION ENGINES

The construction elements of a connecting rod-crack mechanism of a thermal engine are presented in *Figure 1*.

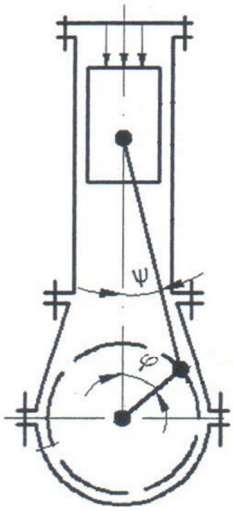

Figure 1 The connecting rod-crack mechanism

The characteristics of the connecting rod-crank mechanism is the relation $\lambda = \frac{r}{l} (\lambda \leq \frac{1}{5})$, where r is the crank's ray and l is the connection rod's length. The kinematics parameters of the mechanism are:

$$\begin{cases} s = r\left[(1 - cos\varphi) + \dfrac{\lambda}{4}(1 - cos\varphi)\right], \\ v = r\omega\left(sin\varphi + \dfrac{\lambda}{2} sin2\varphi\right), \\ a = r\omega^2(cos\varphi + \lambda cos2\varphi). \end{cases} \quad (1)$$

During the functioning cycle of the engine, onto the nodding rod-crank mechanism are engaged the following forces: the force generated by the cylinder's gas pressure, inertia forces, friction forces and forces generated by the system's weight.

The force generated by the cylinder's gas pressure, applied on the head of the piston is:

$$F_p = \frac{\pi D^2}{2}(p_g - p_o) \quad (2)$$

where:

D - is the cylinder's diameter,

p_g - is the indicated pressure of the gases $\left[\frac{daN}{cm^2}\right]$,

p_o - is the indicated pressure of the environment $\left[\frac{1daN}{cm^2}\right]$.

The resulting force transmitted to the piston will be:

$$F = F_p + F_i \quad (3)$$

where:

F_i - is the inertia force

The moment will be given by force F and has value:

$$M_t = F\,\frac{ds}{da} = Fr(sin\alpha + \frac{\lambda}{2}sin2\alpha) \tag{4}$$

An immediate result of the periodical variation of the motor moment (4) is the solicitation to weariness of the mechanism's components.

3. THE FORMS IN WHICH WEARINESS APPEARS

The physical weariness of vehicles are being shown though:

- unwanted modification of composing elements' dimensions;
- unwanted modifications in the quality of the surfaces;
- position of surfaces;
- the geometrical form of the surfaces.

The limits of the weariness/fatigue can be appreciated basing on the following criteria: the technical criterion, the technological or functional criterion, the economic criterion, the recondition-ability criterion and the criterion of safety during functioning.
The materials used in the manufacturing of spares have major influence on the way active surfaces act, in all forms of weariness.
The weariness itself can be appreciated based on several criteria as follows: linear weariness, volumetric or gravimetric (weighing). It is important to mention that until the present, the above mentioned parameters have no established logical theoretical relations, but only empirical, for certain limited conditions.

4. SPARES RECONDITINING METHODS

Are considered as methods of reconditioning the following: restating initial dimensions, adaptation to steps of repairing, application of weariness' compensators and reconstruction trough replacement of a part of the spare.
Reconditioning to the initial dimensions is assured by laying down of metal or other materials, compensation of the weariness and mechanical remaking to the initial dimensions and precision.
The laying down of metal can be obtained through welding (electric manual , semiautomatic under protecting layer, with vibrant electric arc, etc.), through laying down of micro sprayed alloys or through the electric spraying method or by flame, laying down by the means of plasma, galvanic deposits, through sintering, etc.
After the laying down adaptation is realized trough splinting (turning, rectification, etc) so that the initial precision and quality of the surfaces are acquired at the new spare.
The modernization of the reconditioning procedures assures the prolongation of the life cycle of the vehicles' spares, the diminution of invested funds into spare parts, a cut down of labour costs and accidental stops of vehicles.
The characteristic malfunctions of the main shaft are: dirt deposits on the lubrication oil passages, fissures and cracks, bending, twisting, fatigue of crankpin journals and crankshaft journals, deterioration of threads, fatigue of key wholes and of the holes of the flange. In the case of the

fatigue of the crankpin journals and crankshaft journals of the main shaft usually we are dealing with a geometrical deformation that causes the journals to get some oval shaping and some cone shaping.

In *Figure 2* we present the measurement of oval-shaping in the journals of a main shaft .

Figure 2 The measurement of oval-shaping in the journals of a main shaft in a Renault engine

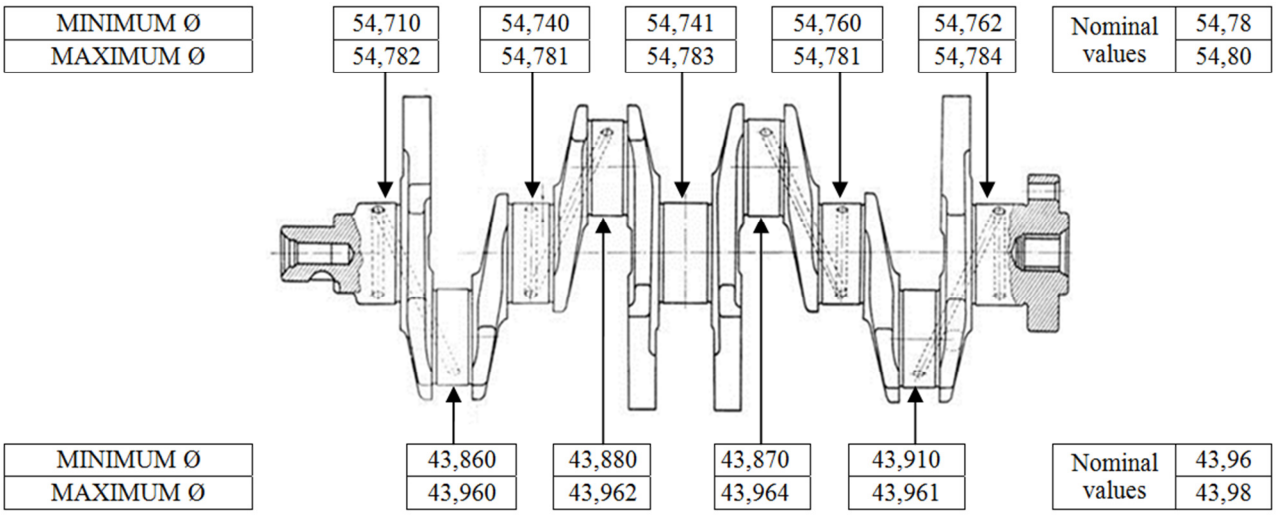

Figure 3 Measured values of oval-shaping of the main shaft's journals, in a Renault engine

In *Figure 3* we present the measured values of oval-shaping of the main shaft's journals , in a Renault engine.

In order to determine the deviation of the geometrical form (oval shaping and conical shaping) is necessary the measurement in three different cross sections and in each section on four directions , respectively a journal or a section of the shaft that will involve twelve measurements from where will result d_{min}, d_{max}, d_{med} oval-shaping and conical-shaping.

Figure 4 represents the measured values for conical—shaping of the shaft on a Renault engine. Comparing the measured values of the oval-shaping (*Figure 3*) and of the conical shaping (*Figure 4*) we can determine that admissible values are exceeded, that imposes the need for reconditioning of the journals. In this case it is considered as a limit of weariness the moment in which grow over

certain values: the oil consumption of the engine, energy consumption etc. that generate exaggerated growth of exploitation costs.

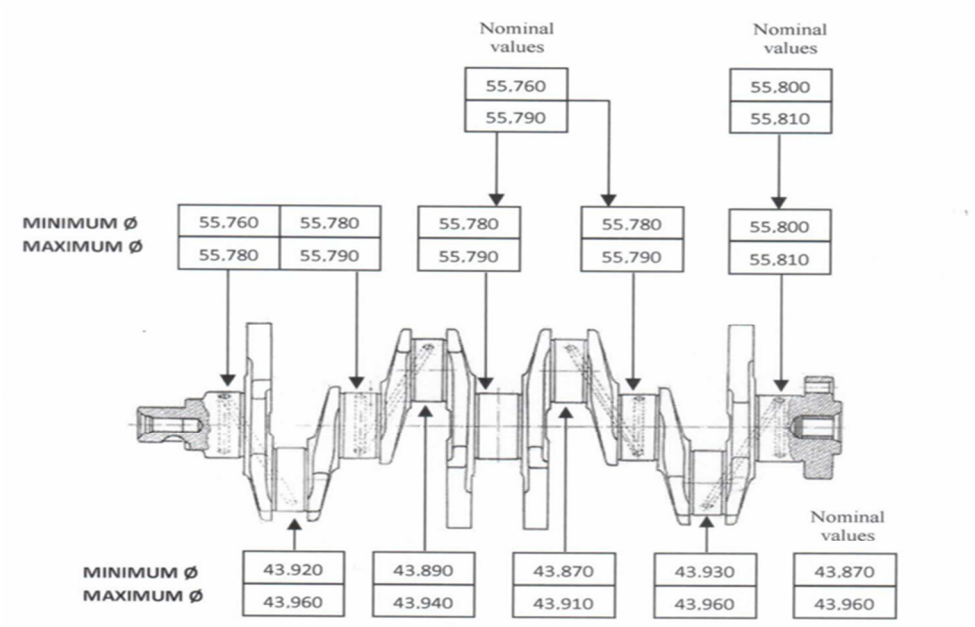

Figure 4 Measured values for conical shaping of the shaft on a Renault engine

CONCLUSIONS

The reconditioning of the shafts is practiced on large scale because of the big expenses these involve. The reconditioning methods that are used for remaking the initial dimensions may be:

- metallization,
- loading through welding,
- electrolytic coating (smooth chromium coating, porous chromium coating, steel coating, copper coating),
- through special methods.

Metallization of the shaft can be executed with a METCO 10E Hard metal spray gun, with flame, that gives economical coatings and of high quality, using metallization wires. It is recommended that the metallization is being made with Molybdenum wires with the additional use of some other material that will give the surface a stronger resistance to solicitations.

The adhesion of the layers depend on the following factors: way of preparing the surface, the surface's ruggedness, the nature of the additional material, temperature, thickness of the deposited layer etc.

REFERENCES

[1] Bejan, V.: *Tehnologia fabricării şi a reparării utilajelor tehnologice.* Editura O.I.D.I.C.M., Bucureşti, 1991.

[2] Cebotărescu, D., ş.a.: *Repararea şi întreţinerea utilajelor din industria alimentară.* Editura Univers, Chişinău, 1993.

[3] Ciolacu, F.G.: *Procedee de generare a suprafetelor*. Universitatea din Craiova, Facultatea de Mecanica, Craiova, 2000.

[4] Ionut, B.,ş.a.: *Mentenanţă, mentenabilitate, tribologie şi fiabilitate.* Editura Sincron, Cluj Napoca, 2003.
[5] Mazilu, D., Crăciunoiu, N., Ciolacu F.G.: *On the Cutting Forces and Tool Wear for some Powder Metallurgy Materials.* Developments in Theoretical and Applied Mechanics – Southeastern Conference on Theoretical and Applied Mechanics, Volume XX, April, 16-18, 2000.
[6] Mureşan, A.: *Contribuţii privind elaborarea unor tehnologii moderne pentru recondiţionarea unor repere din ansamblul motor-transmisie de la locomotivele diesel.* Teză de doctorat U.T.C.-N., Cluj-Napoca, 2010.
[7] Nagy, T.,ş.a.: *Fiabilitatea şi terotehnica autovehiculelor.* Editura Universitaţii Transilvania din Braşov, Braşov, 2010.
[8] Popa, M.A.: *Diagnoză şi reparaţii.* Editura Casa Cărţii de Ştiinţă, Cluj-Napoca, 2003.
[9] Ravai-Nagy, S., Lobonţiu, M.: *Tendinţe moderne în tehnologia aşchierii metalelor.* Conferinţa Naţională cu Participare Internaţională NORDTECH 2004. În: Buletin ştiinţific. Management Tehnologic. Universitatea de Nord din Baia Mare, ISSN 1584 – 7306, 137-142, 2004.
[10] Rusu, T.: *Protecţia mediului şi a muncii.* Editura Mediamira, Cluj-Napoca, 1999.
[11] Vuşcan, I.: *Mecanica proceselor de recondiţionare.* Editura Risoprint, Cluj-Napoca, 2007.

SUPPORTING COMPANIES

THE ISCAME 2015 CONFERENCE AND THE 3rd MECHANICAL ENGINEERING INDUSTRIAL EXHIBITION, DEBRECEN

Company name	Website	Location
Aventics Hungary Kft.	www.aventics.hu	Eger
Coloplast Hungary Kft.	www.coloplast.hu	Nyírbátor
Diehl Aircabin Hungary Kft.	www.diehl.com	Nyírbátor
Enterprise Communications Kft.	www.enterprise-group.hu	Budapest
FAG Magyarország Ipari Kft.	www.schaeffler.hu	Debrecen
FlexLink Systems Kft.	www.flexlink.com	Budapest
HAJDU Autotechnika Ipari Zrt.	www.hajduautort.hu	Téglás
HAJDU Hajdúsági Ipari Zrt.	www.hajdurt.hu	Téglás
Hoya Magyarország Zrt.	www.hoya.hu	Mátészalka
Lego Manufacturing Kft.	www.lego.com	Nyíregyháza
Linamar Hungary Zrt.	www.linamar.hu	Orosháza
Manz Hungary Gépgyártó Kft.	www.manz.com	Debrecen
MSK Hungary Gépgyártó Bt.	www.msk.hu	Nyírbátor
Nyomda-Technika Kft.	www.nyt.hu	Debrecen
Robert Bosch Automotive Steering Kft.	www.bosch-automotive-steering.com	Eger
S&T Consulting Hungary Kft.	www.snt.hu	Budaörs
Seco-Tools Kft.	www.secotools.com	Budapest
SPM Instrument Budapest Kft.	www.spminstrument.com	Budapest
Szimikron Ipari Kft.	www.szimikron.com	Kecskemét
TAKATA Safety Systems Hungary Kft.	www.takata-miskolc.hu	Miskolc
Unilever Magyarország Kft.	www.unilever.hu	Nyírbátor
Werth Magyarország Kft.	www.werth.hu	Monor
ZF Hungária Kft.	www.zf.com	Eger

AVENTICS HUNGARY KFT.

Address: 3300 Eger, Bánki D. u. 3.
Phone: +36 36 531 600
Webpage: www.aventics.hu

Main activity: **M**anufacturing and sales of pneumatic equipment
References:
In commercial vehicle manufacturing: MAN, Daimler, Scania, Volvo, DAF, TATA;
In parts manufacturing: ZF, EATON, GT
Products and services: Mechanically-, electrically- and pneumatically operated valve systems, quick-relief valves, single-acting cylinders, clutch valves, integrated actuators, spare parts, air preparation systems, hoses, connectors
Certificates: ISO TS 16949, ISO 14000, ISO 9001, MEBIR MSZ 28001:2008
Founded in: 2014

ABOUT THE COMPANY

A former subsidiary of the Bosch Group, AVENTICS has been operating independently as a manufacturer of pneumatic systems since 2014 and is currently one of the world's leading suppliers. Its products are used among others in food and beverages industry, packaging and print techniques, as well as metal machining.
Aventics Hungary Kft. is one of the most prominent companies of Heves county. It has a leading position in cylinder manufacturing and assembly and produces valves and marine parts. Beside all these, it is also a supplier of driveline solutions and valve control systems for commercial vehicles. The company pays special attention to the integration of electronic systems in pneumatic components and offers configured and tailor-made solutions in addition to its established product line. As opposed to largeseries manufacturers, AVENTICS is capable of fulfilling orders for small batch orders with short deadlines, selling over 25,000 different types of products every year to more than 10 thousand customers.

COLOPLAST

Webpage: www.coloplast.com

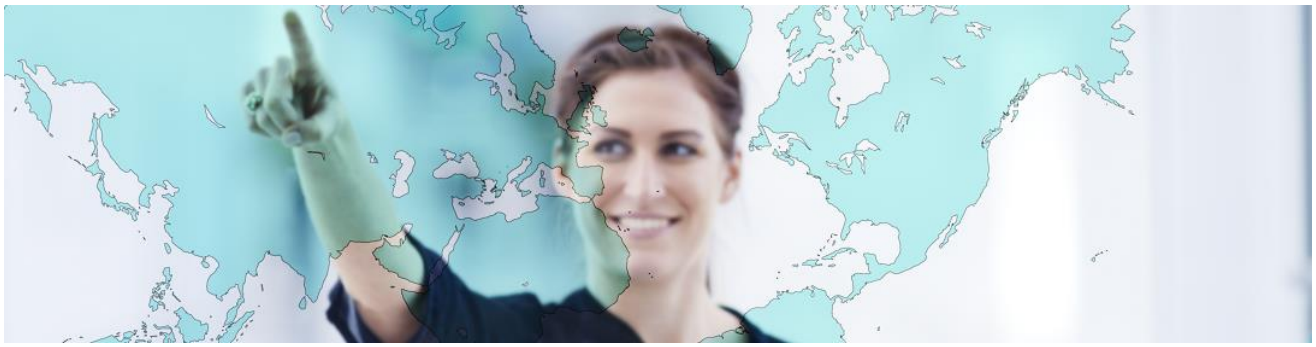

About Coloplast

Coloplast is a Danish international company that develops products and services that make life easier for people with very personal and private medical conditions. Working closely with the people who use our products, we create solutions that are sensitive to their special needs. We call this intimate healthcare.
Our business includes ostomy care, urology and continence care, and wound and skin care. According to Forbes, Coloplast is among the 35 most innovative company in the world! We employ over 10,000 people from 100+ countries. In 2017 we expect to be 11,000 people globally.

Our mission, vision and values

Closeness to all customers makes this possible. We listen to better understand needs, and respond by finding new ways to do things better together. We lead the way by bringing the best ideas first and fast to market in the form of medical devices and service solutions. Deeply private and personal medical conditions are our focus. Our passion to make a real difference to people's lives is what drives and unites us. Our culture supports high ambitions, and releases the full potential of our own people to achieve them. We welcome the broader responsibility that comes with leadership - a responsibility to the environment, to society, to our shareholders, and to act with integrity in all we do.
Coloplast was built on the fundamental ability to listen and respond. Nurse Elise Sørensen listened to her sister's concerns, she understood her needs, and responded by inventing the world's first disposable ostomy bag. An invention that has made life easier for thousands of people. Ever since, listening and responding has been an integral part of all we do. Only by listening, can we understand the world of our consumers and act accordingly by developing the right products and services. Over decades, we have gained invaluable knowledge through working directly with healthcare professionals and the people who use our products.
We will be a trusted guide for consumers in a world of information overload – and a stronger partner with clinicians who are the experts in caring and healing. At Coloplast, we strive to be a greater resource for everyone by setting the global standard for listening and responding.
Our values define the way we think and act, both as individuals and as a company.

Coloplast in Hungary

Coloplast employs more than 2800 people in Hungary. There are 2 factory sites in Tatabánya and Nyírbátor and Postponement and Distribution Center in Tata. We are continuously growing! Join us!

When you get a job here, you get much more than just that – you get a career! We'll push you, stretch you and reward you. Performance here goes a long way, you drive your own career development. Be ambitious and deliver results, and you'll thrive.

Coloplast Hungary Kft Tatabánya
2800 Tatabánya, Búzavirág u. 15.
34/520-500

Coloplast Hungary Kft Nyírbátor
4300 Nyírbátor, Coloplast u.2.
42/886-300

Coloplast PDC Tata
2890 Tata Barina u.1.

DIEHL AIRCABIN HUNGARY KFT.

Address: H-4300 Nyírbátor, Ipari Park utca 9.
Phone: +36 42 510 720
Webpage: www.diehl.com

Welcome to Diehl Aircabin Hungary Kft.

Diehl Aircabin Hungary Kft. is a 100% subsidiary of Diehl Aircabin Gmbh., based in Laupheim Germany, and a member of the Diehl Aerosystems syndicate through the parent company.
Diehl Aircabin has established itself as a preferred partner in the international aviation industry. With its cabin modules, crew rest compartments, and air ducting, Diehl Aircabin provides an array of highly specialized aviation solutions under the general umbrella of Diehl Aerosystems.
The area of expertise of Diehl Aircabin GmbH includes product and process development, design, predevelopment, construction, and the production and qualification of cabin elements. The integration of system components such as in-flight entertainment, oxygen systems, and electrical equipment also forms an important part of the company's broadly based portfolio.
The story of the Hungarian company started in February 2011, when the growing pace of the German parent company made it necessary to establish a new production plant, where they could move a portion of the existing Single Aisle and Long Range airplane part manufacturing. After analyzing multiple sites globally, they choose Hungary: more precisely, Nyírbátor.
In its Nyírbátor plant, Diehl Aircabin Hungary Kft. manufactures three important parts of the passenger cab for the Airbus A319/320/321, A340, A350 and A380 planes: the sidewalls, the door doorframe casing and the air-conditioning pipes that provide the air supply. In our plants, we employ 350 employees. This August we opened our second and brand new production hall in our plant. Till 2018 our headcount will nearly double. Currently, 75% of our employees work in production.
For the production of these mostly handmade parts, the production of which can also be called almost “manufactorial”, a highly special knowledge is required which cannot be matched completely with any current school education. Therefore, beginning with the 2016/2017 school year, our company will also join the Dual Vocational Training system which, according to our plans, will provide education linked to practice in professions that we specifically need. At the same time, the training aims at improving the best skills and abilities of the individual. Students who graduate with good results can count on stable, long term employment. For engineers and people with a higher level of education, we offer more than fix and stable work: we offer a career opportunity. Positions in important areas such as production preparation, process engineering, quality assurance, logistics and economy-finance are expanding in size and responsibility. When launched, our comprehensive trainee program will be adjusted to our future improvements. Our headcount will nearly double after the construction of the new plant hall, and the range of product will widen. As the first step of this process, we would like to fill the engineering positions mentioned above. We are simultaneously hiring entrant engineers, trainees and more experienced colleagues. Moreover, we are counting on colleagues with unique qualifications, such as airplane designers or engineers who have the special certification required for airplane manufacturing. We hope we have been able to increase your enthusiasm for the airplane industry.

Fly with us to the safe future!

ENTERPRISE COMMUNICATIONS MAGYARORSZÁG KFT.
Address: H-1138 Budapest, Váci str. 117-119.
Phone: +36 (1) 471-2380 / ext. 2
Webpage: www.enterprise-group.hu

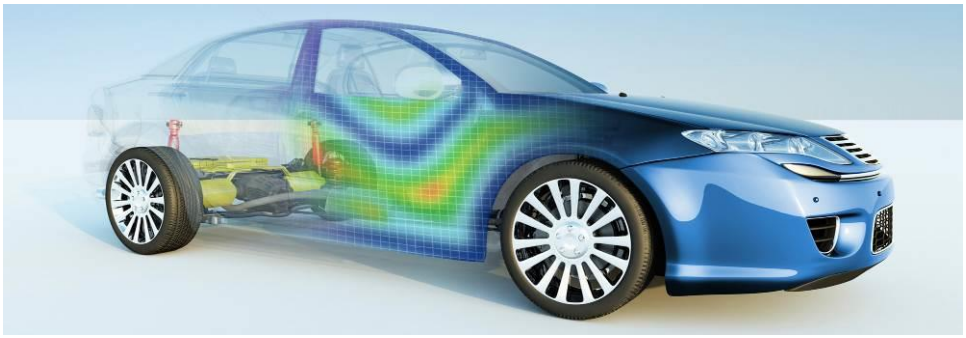

Enterprise Group PLM Business Unit – Engineering Solutions

CAD/CAM solutions and product lifecycle management (PLM) from design to implementation

Our PLM division provides complex engineering solutions and IT services for companies that operate in the field of industry. The market-leading solutions of Siemens PLM and Vero Software cover the entire lifecycle of products - from the original concept, through the design process, all the way to manufacturing - and also support product development and recycling. Our team of experts, with decades of experience in the industry, coupled with the stable corporate background of the Enterprise Group, ensures that our clients will always receive reliable solutions that are customised to meet their own particular requirements.

PLM is a complex process which facilitates the management of a product's entire lifecycle. It includes computer aided design (CAD) and manufacturing (CAM) solutions, but it is more complex than that, as it encompasses the full lifecycle of products. PLM offers advantages such as time-to-market acceleration, product quality improvements, prototype production cost reductions, rapid identification of potential sales opportunities and overall cost savings by recycling previously obtained data and by fully integrating engineering work processes.

Our PLM division supplies the well-known products developed by Siemens PLM Software, as well as their connected services. The division is ready to serve existing and future clients as a distributor of Solid Edge, NX, Tecnomatix Teamcenter and Femap.

With solutions from Vero Software, the world's largest CAM-oriented CAD/CAM developer, the division is capable of comprehensively satisfying all the requirements of manufacturing companies. Among these solutions, Edgecam is recommended for machining, Radan for sheet metal manufacturing tasks, and Alphacam for the wood and stone industries.

Besides supplying the market's well-known Siemens PLM products and solutions, Enterprise Group's PLM division also helps partners with the introduction of new software, as well as support and updates, training programs and constant availability. Our staff, consisting of experts with decades of experience in engineering, IT and industry related projects, can also call on the knowledge of Enterprise Group's other divisions and rely on the smooth operational background of the company when implementing their own projects.

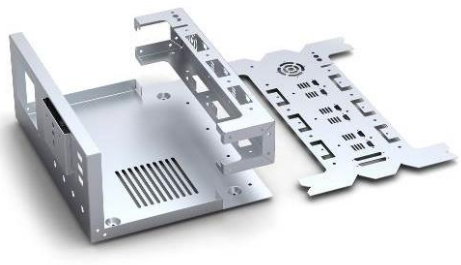

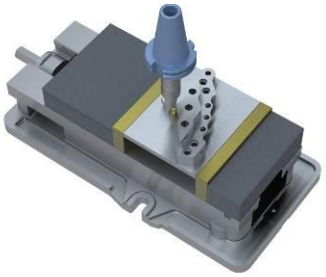

FAG MAGYARORSZÁG IPARI KFT.

Address: 1/D Határ Road/Street, 4031 Debrecen, Hungary

Phone: 00 36-52-581-700

Webpage: http://www.schaeffler.hu

A leading global technology company

The Schaeffler Group is a leading global integrated automotive and industrial supplier. The company stands for the highest quality, outstanding technology, and strong innovative ability. The Schaeffler Group makes a key contribution to Mobility for tomorrow with high- precision components and systems in engine, transmission, and chassis applications as well as rolling and plain bearing solutions for a large number of industrial applications. The company generated sales of approximately 12.1 billion Euros in 2014. With around 84,000 employees, Schaeffler is one of the world's largest technology companies in family ownership and, with approximately 170 locations in 50 countries, has a worldwide network of manufacturing locations, research and development facilities, and sales companies. As a global development partner and supplier, Schaeffler maintains stable long-term relationships with its customers and suppliers. The Schaeffler Group follows a growth strategy aimed at profitable above-market growth. At the core of this growth strategy are top quality, outstanding technology, and strong innovative ability, in doing business with customers as well as in the group's internal processes. Schaeffler identifies key trends early on, invests in researching and developing new, forward-looking products, takes them to volume production, and defines new technology standards.

Divisions and business divisions

Schaeffler develops and manufactures precision products for approximately 60 sectors around the world. Its technologically advanced components and systems are used in applications in vehicles, machinery, plants, as well as in aerospace applications. The group distributes its products and services to numerous auto- motive manufacturers and industrial customers.

Mobility for tomorrow

Globalization, urbanization, digitalization, scarcity of resources, renewable energy, and the growing demand for affordable mobility are leading to changed, much more dynamic market requirements and business models. Based on these megatrends, the Schaeffler Group has developed its "Mobility for tomorrow" strategy concept, under which the company focuses on four areas across divisions and regions: eco-friendly drives, urban mobility, interurban mobility, and the energy chain.

Schaeffler plays an active part in shaping these focal areas through its own research and development activities and, as a leading expert in innovation and technology, offers an attractive product range to its customers and business partners.

The group's broad portfolio of products and services ranges from components and systems for automotive drive trains to products for high-speed trains and from rolling bearings for solar power plants to innovative solutions for aerospace applications.

FLEXLINK SYSTEMS KFT.

Address: HU-1131 Budapest, Rokolya str. 1-13.
Phone: (+36) 20 666 7008
info.hu@flexlink.com

Webpage: www.flexlink.com

FlexLink is the Market leader in conveyors products

FlexLink serves a wide customer base, ranging from local producers to global corporations, and from end-users to machine manufacturers.

We are a leading provider of high-end solutions to manufacturing industries such as: food, beverages, personal care, healthcare, automotive and electronics.

Customers are served through our own operational units in 30 countries and a global network of Strategic Partners.

The partner network has been an important strategic element of FlexLink's business model since the start in 1980, enabling the company to enhance efficiency at factories in more than 60 countries worldwide.

- 840 **employees**
- 30% of employees are **women**
- 50% have a **university degree**
- **Operating units** in 30 countries
- **Partner network** in more than 60 countries
- More than **8000 installations** worldwide; many for leading brands within FMCG, healthcare, automotive and electronics.

FlexLink is a company of COESIA Group. Coesia is a group of innovation-based industrial solutions companies operating globally, headquartered in Bologna, Italy and fully owned by Isabella Seràgnoli.

Coesia's companies are leaders in the sectors of:

- Advanced automated machinery and materials
- Industrial process solutions
- Precision gears

Coesia's customers are leading players in a broad range of industries, including Consumer Goods, Tobacco, Healthcare, Aerospace, Racing & Automotive and Electronics.

Coesia Group consists of fourteen companies:
ACMA, ADMV, CIMA, CITUS KALIX, FLEXLINK, G.D, GDM, HAPA, IPI, NORDEN, R.A JONES, SACMO, SASIB, VOLPAK. The Group has 90 operating units (54 of which with production facilities) in 33 countries, a turnover in 2014 of approx. 1,429 million Euro and over 6,165 employees.

www.coesia.com

HAJDU PUBLIC LIMITED COMPANY

Address: 4243 Téglás, külterület 135/9. hrsz.
Phone: +36 (52) 582-700
Webpage: https: //www.hajdurt.hu
Facebook: https://www.facebook.com/hajduzrt/

Company History

HAJDU Hajdúsági Ipari Zrt.'s forerunner Hajdúsági Iparművek was founded by the Hungarian government in 1952 for the purposes of military industry. In 1957 the company started to build household appliances whose assortment as well export were constantly growing. By manufacturing its own developed as well as licensed products and setting up corresponding machinery it managed to grow into a medium-sized enterprise by the 1980s. After 1998 – with a purpose of using up its free capacities – and after 2002 (primarily due to parts produced by sheet metal forming) the company also opened up to a car industry. In 1993 it was transformed into an incorporated company and in 1994 it was privatized by Hungarian investors. The ISO 9001 quality assurance certification was introduced in 1993, whilst the ISO 14001 environmental management certification was implemented in 2001. In October 2005 HAJDU Hajdúsági Iparművek Rt. split into three separate companies. HAJDU Hajdúsági Ipari Rt. continued to produce traditional products such as hot water storage tanks, washing machines, and spin dryers.

The other two companies

HAJDU Autotechnika Ipari Zrt. deals with metalworking – it characteristically manufactures metal sheet produced automobile parts – and designing as well as manufacturing machine tools.
HAJDU Infrastruktúra Szolgáltató Zrt. operates an Industrial Park which also hosts both of the other HAJDU companies. It occupies quite an extensive area and offers a number of services to the enterprises that have settled there.

In 2006 HAJDU Hajdúsági Ipari Rt. was transformed into a private limited company. In 2008 new branch of business was established, focusing on developing products that use renewable energy as well as launching them onto Hungarian market. This orientation has become one of the company's main strategies. In the same year the company began realizing a two-year investment program, partly financed by European Union, which enabled a significant technological development of the production process. Between 2010 and 2015 HAJDU brand received several awards thus getting recognition for the quality of its product development and business process.

Our mission, philosophy, plans

HAJDU Hajdúsági Ipari Zrt. meets customer demands by providing environmentally friendly household appliances and complex systems that offer a natural helping hand to families, public institutions as well as enterprises. Our goal is to strengthen HAJDU brand's position on regional market and to meet customer demands in Europe as well as in other parts of the World. In order to achieve that we have started following ISO 9001 quality assurance standards in 1993 and ISO 14001 environmental management standards in 2001. Excellent and constant quality of our products as well as their regular development are guaranteed by systematic on-site controls performed by various accredited – both domestic and international – testing institutes (TÜV Rheiland InterCert, VDE, LCIE, etc.) Our company puts a lot of emphasis on environment protection and on minimizing negative impact on the environment. We thus strive to employ an environmentally friendly technology and use resources (materials, energy) in an economical way.

HOYA LENS MANUFACTURING HUNGARY PRIVATE CO.

Address: H – 4700 Mátészalka, Ipari út 18.
Phone: +36-44-418-200
Webpage: www.hoya.com

HOYA Corporation is a diversified, multinational company and leading supplier of innovative and indispensable high-tech and healthcare products. HOYA is active in two main business segments: The Life Care segment encompasses health care areas such as eyeglass lenses and the operation of contact lens retail stores, as well as medical related areas such as intraocular lenses for cataract surgery, medical endoscopes, surgical equipment and artificial bones and implants. HOYA´s Information Technology segment focuses on electronics products for the semiconductor industry and LCD panels, glass disks for HDDs and optical lenses for digital cameras and smartphones. The HOYA Group comprises over 100 subsidiaries and affiliates and over 34,000 people worldwide.

Life Care

HOYA has diversified its business portfolio with its optical technologies providing indispensable products to people´s lives. We strongly believe that by providing enduring solutions that meet needs in areas closely connected to people's lives, such as endoscopes, eyeglass lenses and intraocular lenses, it will be able to bring about changes in the quality of those lives.

Life Care Segment, Health Care

HOYA provides products and services to care for that most important sensory organ- the eye. HOYA started manufacturing eyeglass lenses in 1962 and contact lenses in 1972. Based on the optical and material technologies acquired since 1941, HOYA continues to contribute quality high value-added vision products to people around the world.

Eyeglass lenses

As a global manufacturer of eyeglass lenses, HOYA has passionately driven optical technology innovation with the aim of finding only the best vision solutions.

HOYA´s unparalleled technology creates a profoundly clear vision experience for the progressive lens wearer.
Integrated Double Surface Design (iD), HOYA´s patented, award-winning design technology, separates the surface geometry of progressive lenses into two components: vertical and horizontal, positioned individually on each of the two lens surfaces. Thanks to this technology, HOYA´s premium progressive lenses can be individually designed; each patient´s unique visual and lifestyle requirements can be integrated in the lens design to provide them with the most comfortable and accurate vision, tailored to their individual needs.

HOYA Vision Care Company is a global organization covering 52 countries with a network of over 12,000 employees and over 64,000 active accounts globally.

HOYA Lens Manufacturing Hungary private Co., Mátészalka

HOYA Lens Manufacturing Hungary private Co. is the largest unit of Hoya group in Europe based on the headcount and production volume as well. The past of the company and the nearness of the European market give a geopolitical advantage and stabile future for the company. A Belgian investor bought 50% of Optikai Művek factory's unit in 1991. In 1994 with total ownership the enterprise with mass production has been called Buchmann Optical Művek for 8 years. Hoya has bought the Buchmann-group in 1994, so the plant in Mátészalka also became a member of the japan lens production company. By now the company do partial serving of all affiliated companies in Europe.

LEGO MANUFACTURING KFT.

Address: 4400 Nyíregyháza, LEGO utca 15.
Phone: 0642/505-000

Webpage: www.lego.com/careers

We produce the creative toys of the future in Nyíregyháza

Our new factory has been handed over in 2014, and ensures a secure income for hundreds of families and brings joy to millions of children through the toys manufactured here. One of five LEGO factories of the globe is situated at LEGO street 15 in Nyíregyháza – a site which is not only high-tech and extremely environment-friendly, but its look&feel reflects the world of LEGO toys as well.
The LEGO Group reached a global growth in return of more than 10% yearly in the last decade, year after year. This shows that the world is getting more and more open to high-quality creative play experiences, which moves the fantasy of kids and adults alike.
Our mission is to live up to the ever-growing demand, whilst ensuring the high quality we set for ourselves. As our motto from the 1930s says: Only the best is good enough!

Capacity extended

With our new factory we almost doubled our output – the number of moulding machines grew from 356 to 768, while our production area increased from 38 000 square meters to 122 000 m^2. As of today we have about 2 500 employees.
The biggest part of DUPLO toys have been produced at the Nyíregyháza site since years (we even can say to mould all the DUPLO bricks of the planet), but with the new factory, we do already produce LEGO boxes as well.
As demand rises quickly, we have to expand our capacity further. That is why we set up a new moulding module in an external facility, and therefore we do double our Processing and High-bay Warehouse capacity as well. Should market conditions remain the same, doubling all other production areas are likely to follow next: this would mean more than an additional 1 000 jobs by 2020.

Green Factory

According to our Planet Promise we think it is extremely important to preserve our environment for future generations, thus leave the smallest possible traces with our production activities. Several technological solutions help us save drinking water, electricity and make the environment of the factory and work conditions more liveable.

For detailed information about job opportunities at our factory,
please visit our career site at www.lego.com/careers.

LINAMAR HUNGARY ZRT.

Address: HU-5900 Orosháza, Csorvási street 27.
Phone: +36 68-514-600
Webpage: www.linamar.hu

The Canadian owned Linamar Hungary PLC. is one of the largest agricultural equipment manufacturing companies in Bekes country, in the Great Plain, Hungary. It is famous for its own developed agricultural manufacturing.

There are 3 divisions in Hungary, 2 of them are located in Orosháza, one of them is in Békéscsaba.

The here made own developed products are sold on international markets. Even the components which are produced by us are built into the most famous auto-brands.

We need new colleagues with higher and medium technical qualifications thanks for our growing orders.

Who are we waiting for?

- *Skill-men with higher technical qualifications*
- *CNC programmer, set up for line*
- *Skill-men with tech*

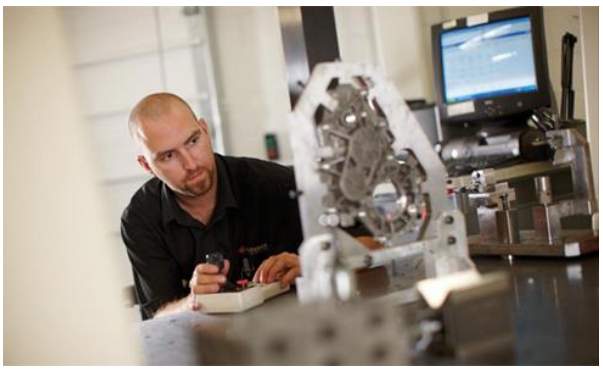

What are we offering for?

- *Competitive payment and other benefits*
- *Interesting job in international workplace*
- *Carrier building and different trainings abroad and in Hungary*

Opportunities at Linamar in the future

Completion of the professional practice:

Our company provides possibilities for students who are studying at university or college. They can also get practice and many experience beside their studies in a real factory environment.

The engineer students make their professional practice according to a planned program, which is offered by our company.

Opportunity for thesis writing:

The engineer students have opportunity for writing up their thesis based on professional and special themes offered by our company. The students can write their thesis work with the help and control of a senior mentor.

As our employee:

The new hired engineers for Linamar take part in an on-boarding program in every case. During the 20 weeks program they get a comprehensive picture about most of the process of the company. Also they can get acquainted with the procedures, instructions according ISO and ISO/TS standard. This program is closed by an exam in front of the division's management.

Our vacant job can be found on this website: http://www.linamar.hu.

If you want to share in our success, let's join in it!

MANZ HUNGARY GÉPGYÁRTÓ KFT.

Address: 4031 Debrecen, Határ út 1/c
Phone: +36-52-530-798

Webpage: www.manz.com

As one of the world's leading high-tech equipment manufacturers, Manz AG, based in Reutlingen, Germany, is a pioneer for innovative products in fast-growing markets. The company, founded in 1987, has expertise in seven technology sectors: automation, metrology, laser processing, vacuum coating, wet chemistry, printing and coating, as well as roll-to-roll processes. Manz deploys and further develops these technologies in three strategic fields, the "Electronics," "Solar" and "Energy Storage" business segments.

The company, led by founder Dieter Manz, has been listed on the stock exchange in Germany since 2006, and currently operates production facilities in Germany, Slovakia, Hungary, Italy, China and Taiwan. Manz AG also has sales and service branches in the USA, South Korea and India. In the middle of 2015, Manz AG had approximately 2,000 employees, 900 of which work in Asia. Revenue in the past financial year amounted to more than EUR 305 million.

With its slogan “passion for efficiency”, Manz is making a promise to offer its customers – all companies active in important future markets – increasingly efficient production equipment. Like this, the company contributes significantly to reduce the production costs of end products and thereby making them available for a broad range of buyers worldwide. Therefore, Manz is continuously optimising its product portfolio. The aim is to achieve highly reliable production processes on the customer side while steadily improving performance parameters for products manufactured on Manz equipment. This makes the Manz Group an important driver of innovation, helping to achieve breakthroughs in key technologies of our times, such as sustainable power generation, displays for global communication needs and e-mobility.

Manz founded its Hungarian subsidiary in 2004. Today 99 highly qualified employees work at the production facilities in Debrecen and the number is growing.

The main profile of Manz Hungary is manufacturing unique equipment for machines. The factory consists of a welding shop, a processing shop with a large portal machine, allowing parts with large dimensions to be processed, a small parts processing shop with CNC (computer numerical control) milling and turning machines as well as an assembly shop where we electrically and mechanically assemble components and machines.

MSK HUNGARY GÉPGYÁRTÓ BT.

Address: 4300 Nyírbátor, MSK tér 1.
Phone: +36 42 511 100
Webpage: www.msk.hu

MSK Covertech Group: The future is what we make it

Innovation is built on tradition. As a family managed business, MSK Hungary Bt, with a headcount of about 350 employees, is a team member of the MSK Covertech Group. MSK offers product-specific packaging and palletizing solutions to a number of industries.

All of our employees are respectful of our customers. We are positive that motivation and flexibility are the key components of successful participation in international competition and that is why we are one of the leading international manufacturers of heavy duty packaging machines and palletizing systems through our worldwide operations.

Value-orientation and an innovative spirit are two of the key factors that have kept the business of the Hannen family of Germany on a growth trajectory for the last 40 years. MSK offers its customers the treasure of its unique experience accumulated during the production of almost 5 000 units of packaging equipment sold. Driving innovation in our work requires us to keep expanding our current limits. MSK has experienced and creative project teams also in the field of product development who rely on their comprehensive industry competence to develop unique and outstanding packaging solutions. Owing to our state-of-the-art manufacturing methods (particularly at the central site in Nyírbátor) and continuous investments MSK stands for quality, productivity and relentess improvement.
MSK's factories count among the most modern in the industry. Accordingly, in 2010, we expanded the production area at the Nyírbátor site by approximately 5,000 m2 thus reaching 21,000 m2, we installed a modern and environment-friendly powder disperser unit and we consistently renewed our CNC equipment fleet. We have recently invested approximately HUF 1 billion including the purchasing of new manufacturing equipment and the extension of our office building. Further development projects, such as the enhancement of our production capacity and the construction of a modern training center, are in the pipeline. MSK is a pioneer in a number of areas demonstrated by the high number of international patens registered by us that are exemplary for the entire industry.

MSK Hungary Bt. – Nyírbátor: The magic of mechanical engineering

Our relentless search for quality, innovation and reliability has made MSK one of the leading international experts of packaging and logistics systems.
MSK means the following:

- customer-specific palletizing and packaging machines
- proprietary corporate software
- complete equipment and system solutions
- development, production, servicing: all from one supplier

Information about our most recent news, development initiatives and open positions is available at:

- www.msk.hu

ROBERT BOSCH AUTOMOTIVE STEERING KFT.

Address: H-3300 Eger, Kistályai str. 2., Hungary
Phone: +36 36 510 930
Webpage: www.bosch-automotive-steering.com

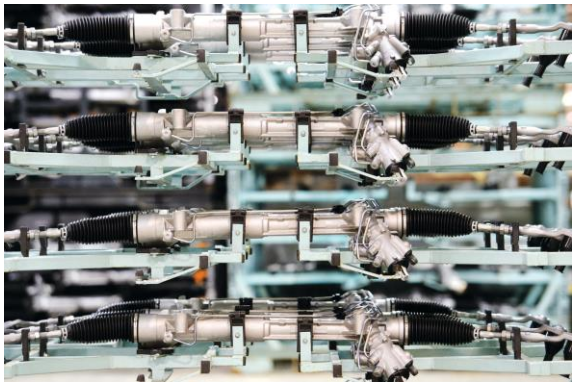

ZF Lenksysteme Hungária Kft. was founded in 2003, with a 50-50% holding by Robert Bosch GmbH and ZF Friedrichshafen AG.
In autumn 2014, the two parent companies announced that ZF is selling and Bosch is buying ZF Lenksysteme as a whole, that is, the 20 subsidiaries operating in 8 countries. The integration was completed in 2015. The Hungarian joint venture was registered in April 2015, under the name of Robert Bosch Automotive Steering Kft. With this, we have become a member of the family of the Hungarian Bosch plants, with a total headcount of nearly 10,000, including us.

Our company was operating in Eger between 2003 and 2014, expanding every year. Up to this point, the initial headcount of 35 has risen to 1000, in line with market demands and the ever-increasing order volume. As an automotive supplier, we produce steering gears, steering columns, I-shafts and reconditioned parts to 109 vehicle manufacturers worldwide, both for passenger cars and commercial vehicles.

Since its founding 2003, for more than 10 years, the company was involved in the assembly and reconditioning of components. Based on our solid production results, in 2012, the international company leadership decided to go beyond hydraulic gears, and expand the subsidiary's scope of activities with the assembly of electric steering gears and parts manufacturing. Following the decision, in 2013, preparations started for the manufacturing and assembly of the EPSapa electric steering gear.

As there were insufficient space to expand at the Eger site to manufacture the new product, another location had to be found. Situated only 10 kilometers from Eger, Maklár turned out to be an ideal choice, thanks to its favorable infrastructural features, and the proximity of the Eger plant and the motorway. The opening ceremony of the new plant was held on September 5, 2014. With this, we have expanded into a dual-based company with locations both in Eger and Maklár.

The new manufacturing activities were set up at the new Maklár plant. 2014 was spent with the implementation of the production hall and the installation and the alignment of machines.

The extensive work has born fruit in 2015: in May, the plant started the serial production of the racks and steering nuts for the electrical steering gear.

SECO TOOLS KFT

Address: 1115 Budapest, Bártfai u. 54
Phone:+36-1-267-6720
Webpage:www.secotools.com

WHO WE ARE.

FOUNDED IN SWEDEN.

Our origins can be traced back to the Swedish mining industry, when Fagersta Bruks', a helve hammer, was established by the river Kolbäcksån in 1611.
The 400 years since were spent developing and applying expertise. In 1932, Fagersta Bruks AB introduced a new product called 'Seco', the Latin phrase for 'I cut'.
Four years later, Seco was established as a separate company unit and has since grown to become the global provider known in today's market. Since 2012, Seco has been part of Sandvik, a Swedish global engineering group dedicated to your productivity and profitability.

GLOBALLY SUCCESSFUL.

Seco operates in more than 40 countries, and with distributors and agents in an additional 35 countries, Seco has a truly global presence. And with 5,000 employees worldwide, it goes without saying that being close to you is the key to providing the advanced solutions you need.

A SYNONYM FOR ADVANCED METAL-CUTTING TECHNOLOGY.

We use our comprehensive know-how to provide advanced technology and tool solutions. On average, we invest approximately 3% of our turnover in R&D – which means that innovation is a part of our corporate culture. Our solutions enable you to succeed in your own markets by ensuring the optimisation and efficiency of your production processes.

SHARED VALUES: UNITING THE SECO FAMILY.

5,000 people are members of the global Seco family, united by our shared values. First comes our family spirit. This means that we maintain an open and friendly workplace and share our knowledge. Next is a passion for you. Which means that we always focus on you, not us. And number three: personal commitment. This means that we ensure you always see our dedication in your individual Seco contact person.

A GLOBAL FAMILY

Seco is a global family present in more than 75 countries and originating from Fagersta in Sweden.

HOW WE THINK.

TOGETHER, WE MAKE IT EASIER.

We make things easier for you by being more than just a cutting-tool provider. We provide advanced products and services and are fully dedicated to understanding your operations, in order to deliver the best solutions for your specific needs.

CONTRIBUTING TO YOUR SUCCESS.

We understand that success in today's manufacturing environment requires more than a focus on tools. We are dedicated to also understanding and identifying with your challenges, and providing the unique personal engagement that results in a true and lasting partnership.

TWO FACETS, ONE VISION

We always aim to combine the best of both worlds: the commitment to expertise and our advanced tool solutions.

WHAT WE PROVIDE.

PRODUCT PORTFOLIO.

With our extensive range of products, we provide solutions for all sizes and scopes of metal cutting applications. Our comprehensive offering includes solutions for milling, turning, grooving and parting off, threading, drilling, reaming, boring and advanced materials. And our array of toolholders provides optimum performance in every type of application through a variety of tooling solutions.

SERVICE PORTFOLIO.

Our advanced services ensure that we comprehensively meet all machining challenges. Component Engineered Tooling tailors solutions to your operations, while our Custom Products ensure that you always get the ultimate tool for your unique application. The Seco Technical Education Programme provides effective training to increase product-competences for every level of expertise. Additionally, the SecoPoint™ system supports you in managing your inventory. 'My Pages' puts the power of Seco at your fingertips. From product availability to cutting data to test reports, all of this information and more is available anytime, anywhere through this comprehensive digital portal.

COMPREHENSIVE SERVICES

Reaching your goals includes advanced services.

SZIMIKRON LTD

Address: H-6000 Kecskemét, Szegedi út 49. HUNGARY
Phone: +36 76 484 100
Webpage: www.szimikron.com

Szimikron ltd. designs and manufactures linear systems and ballscrews offering solutions for different sectors of industry, e.g. machine-tools, automotive, medical industry, automation.

BALLSCREWS

The ballscrew is the motion transmission unit of machine tools and several machinery structures, transforming the rotational motion into linear motion with a high rate of efficiency, ensuring in addition high accuracy, loadability, rigidity and durability.

TRAPEZOID SPINDLES – ACME SCREWS

Serving for the actuation duties at traditional machine tools and devices, for the general requirements of machine production, where simple and reliable motion transmission is required.

LINEAR MOTION SYSTEMS

Our compact modules are the most modern representatives of today's Linear Motion Systems. They can be integrated as a finished module without the effort usually needed for balancing the guide and drive element during installation into the machine. This ease of mounting applies to all our linear motion systems.

HYDRAULIC POWER CHUCKS

Patented innovation: **TAF…** type **programmable power chucks** are the result of a developement project led by Szimikron with Miskolc University machine-tool faculty according to the innovation of prof. Dr. Tajnafői.
The major advantages of the new automatic jaw adjustment chucks:

Novelty: no such hydraulic chucking machine has appeared on the market yet up to now that could safely perform these duties without the significant modifacion of the machine.

Automated: changeover to different diameters requires no manual interaction.

Fast: the adjustment of the three jaws takes place at the same time, so the operation requires three times less time as a minimum related to any previously applied methods.

Universal: the chuck makes automatic changeover possible within its entire diameter range.

Interchangeable: it is simply installable into the place of other traditional hydraulic chucks, the necessary additive elements are provided together with the chuck.

Productive: the dynamically balanced chucks make high cutting speed possible.

TAKATA SAFETY SYSTEMS HUNGARY KFT

3516 Miskolc, Takata út 1.
06-46-407-900
www.takata-miskolc.hu

Our dream

At Takata, we dream of a world with zero fatalities from traffic accidents. We understand the importance of every individual, and hope to one day experience a global community where everyone recognizes the true value of human life.

Takata is a leading global supplier of automotive safety systems, (products include steering wheels, airbag systems, seat belts, electronics, sensors, interior trim, child restraint systems) and supplies all major automotive manufacturers in the world. Headquartered in Tokyo, Japan, Takata is currently operating 56 plants in 20 countries and employs more than 43,680 people, every one of whom is committed to turning innovative ideas into reality.

Our common goal is to reduce the number of fatalities in road traffic accidents to zero. We develop and manufacture products that help keep people safe when travelling on today´s roads, aiming to provide optimum safety on the move, with a range of products for occupant and pedestrian protection. For many decades, we have been pioneering innovative technologies – producing our first seat belts in 1952 and starting the development of airbags as early as 1969. TAKATA's mission is the development of innovative products according to high quality standards, which helps to meet the highest satisfaction of the customers.

„Our mission – your safety."

There is no end to thinking about safety in today's automotive society. As a company that makes seat belts, airbags, child seats and other products that protect life, we are aware of our responsibilities to society and want to contribute to attaining the goal of creating a world that is safe. To do this, we will continue creating and further evolving safety products and systems that people can rely on. At Takata, we would be delighted developing our safety products in a world where they never had to be used, where traffic accidents do not occur anymore. That is the dream that drives us every day.

TAKATA at Miskolc

The latest step toward realizing our dream has been the establishment of Takata Safety Systems Hungary Kft. in October, 2013. This new plant is our first in Hungary and the 17th in Europe and it is located in the city of Miskolc, at the Miskolc South Industrial Park. Takata Safety Systems Hungary Kft. started production of airbag technology at this new facility in October 2014. The company's investment in the new plant is € 68.3 M, with a 25 hectares big ground and up to 60.000 sqm built-in area.

The number of the new employees at Miskolc will be around 1000, who produce lifesaving automotive technology products, such as complete airbag modules, airbag components and inflators for car manufacturers across whole Europe. The new facility also features state-of-the-art systems for product development, testing, quality control and customer service.

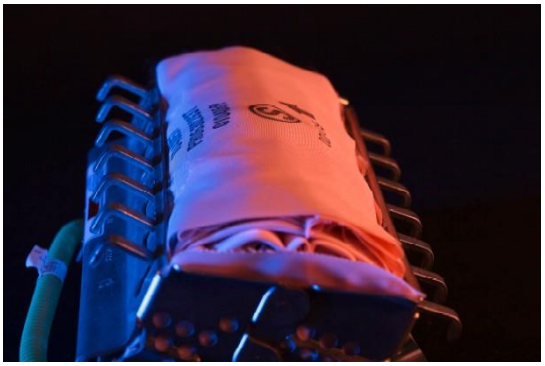

UNILEVER HUNGARY

Address: 182. Váci street, 1138 Budapest
Phone: +36 1 465 93 00
Webpage: www.unilever.hu, www.unilever.hu/careers-jobs/

BRIGHT FUTURE - MADE BY YOU

LOVED THE WORLD OVER

Unilever is one of the largest fast-moving consumer goods (FMCG) companies in the world. We take care of the whole supply chain of our products, from development and sourcing right through to production, marketing and distribution. Over 172 000 employees around the world bring this operation to life – HR, Customer Management (Sales), R&D, Finance, Marketing, Supply Chain and more all working together towards a common vision. Our loved brands, like Dove, Axe, Lipton or Knorr, to name a few are sold 190 countries, and are used by two billion people daily.

AMBITIOUS – FOR THE PLANET

Unilever has a clear purpose: to build a brighter future for our world. We believe that being ambitious in business goes hand in hand with being ambitious for humanity and the environment. Business has a fundamental role in caring for the future of the planet. Unilever's vision is to double our size, while reducing our environmental footprint and increasing our positive social impact. Brands can be powerful influencers of behaviour and positive drivers of change. We can look deeply into what ours can mean for people and the world. This way it becomes not just about washing clothes, for example, but doing so using less water at lower temperatures. It is not just about how personal hygiene can make you clean and healthy, but how it can improve your self-esteem. Brands like Omo and Dove do exactly these things.

MAKE A DIFFERENCE

We have big ambitions about how our business can help create a bright future for our world, but to make it happen we need great people who can challenge the way things are done, bring new ideas, and dare to make big decisions. If you want to make a difference, Unilever is the place to come:

Unilever Future Leaders Programme (UFLP): The Unilever Future Leaders Programme is about developing tomorrow's leaders, today. It's designed to grow you into a manager, through hands-on learning alongside world-class experts. You'll be hired into a function and develop your leadership skills by working on live projects which offer you all the experience you need to become ready for your first management role.

Unilever International Internship Programme (UIPP): This is a world-class 6-month internship in one our Marketing, Finance, or Supply Chain functions.

Local Internship Programmes: We also offer local Internship Programmes across Europe in a broader range of functions: Marketing, Finance, Supply Chain Management, HR Management, Customer Management (Sales)

UNILEVER IN HUNGARY

Unilever was one of the first major international investors which appeared in 1991 in Hungary where it has three factories: the Nyírbátor household chemical factory, the Veszprém ice cream factory and the Röszke food factory. The company employs a total of 1,751 employees, its net sales last year exceeded HUF 83 billion, and its profit after tax in 2014 was over 1.8 billion Hungarian forints.

THE NYÍRBÁTOR HOUSEHOLD CHEMICAL FACTORY is one of Unilever's largest and most cost-effective European factories in the household chemical sector. 85% of the production, that is daily 90 truckloads of product is exported, shipped to a number of countries. Popular brands produced in Nyírbátor include, among others, Domestos, Cif, Floraszept or Coccolino. Local Internship Programmes open for university technical students throughout the year. www.unilever.hu/careers-jobs/

WERTH HUNGARY LTD.

Address: H-2200 Monor, Zólyom u. 80/B. (Office: Petőfi u. 4.)
Phone: +36 29 611 020; +36 20 824 3124
e-mail: info@werth.hu
Webpage: www.werth.hu

COMPANY INFORMATION

General Management: Tamás CSONTOS / General director
Activities: distribution and maintenance of 3D coordinate measuring machines, portable measuring machines, contracted measurements, reverse engineering and measurement services with computed tomography.

ABOUT THE COMPANY

Werth Hungary Ltd. (aka.Werth Magyarország Kft.) started activity in 2010 as affiliate of ***Werth Messtechnik GmbH***. Our parent company provides solutions from 2D profile projectors to complex 3D – requiring multiple sensors at the same time (optical, touch probe, laser or CT X-ray) - complex measuring tasks, while maintaining the exceptionally high quality as fundamental value.

Owing to our cooperation with ***ABERLINK*** from the United Kingdom we provide small, medium and large measurement range, manual or CNC coordinate measuring machines with easy-to-use graphical software and free version updates.

Our portable devices are made by ***CREAFORM***. This Canadian company is the cutting edge in the field of portable coordinate measuring machines. Scanners and CMMs are truly portable with large measurement range. In terms of their use they provide the greatest help to the users in measuring, modelling, medical technology and reverse engineering tasks.

Our relationship with customers does not end with handing over the CMM machine. Our service portfolio contains: CMM installation, cyclical calibration and planned preventive maintenance; training; programming; inspection service; solving complex measurement tasks and retrofitting coordinate measuring machines.

ZF HUNGÁRIA KFT. COMPANY NAME

Address: H-3300 Eger,
2. Kistályai street
Phone: +36 36 520-100

Webpage: http://www.zf.com/

ZF HUNGÁRIA KFT.

ZF is a global leader in driveline and chassis technology as well as active and passive safety technology. The company, which acquired TRW Automotive on May 15, 2015, is now represented at about 230 locations in some 40 countries. The two companies, which were still independent in 2014, achieved a sales figure exceeding €30 billion with 134,000 employees. As in previous years, both companies have invested approximately 5 percent of their sales in Research and Development (recently €1.6 billion) in order to be successful with innovative products. ZF is one of the top three automotive suppliers worldwide.

The company was founded in 1915 for the development and production of transmissions for airships and vehicles. Today, the group's product range comprises transmissions and steering systems as well as chassis components and complete axle systems and modules. As stockholders, the Zeppelin Foundation - which is administered by the City of Friedrichshafen - holds 93.8 percent and the Dr. Jürgen and Irmgard Ulderup Foundation Lemförde holds 6.2 percent of shares.

We have developed ZF Hungaria Kft. consistently in the years since its establishment in 1995. In our factory the parts are made on semiautomatic machining centers. We have one of the largest and most modern heat treatment shop in Hungary, one part of our capacity is utilised by other companies as well. On our new assembly lines a special IT system helps the employee in performing work processes precisely and in quality conrol. In the automatic high shelf warehouse of our logistic center we do storing in and storing out with robot technology. The material supplying is carried out in pull system, the delivery of parts is managed by the work rhythm of assembly work, so the whole process is in optimal rhythm. Parallel with modernization of production also the product development takes place in Eger. There are also an engineering centre, workshop and test-bench on the location, so the creations designed by engineers on the computer can be realized in practise and can be tested in laboratory and highway conditions. With our products and knowledge of our specialists we represent Hungary all over the world and with our purposeful improvements we provide for that, this representation should be high level and worthy of recognition.

PHOTO GALLERY OF THE ISCAME 2015 AND THE EXHIBITION

THE ISCAME 2015 CONFERENCE

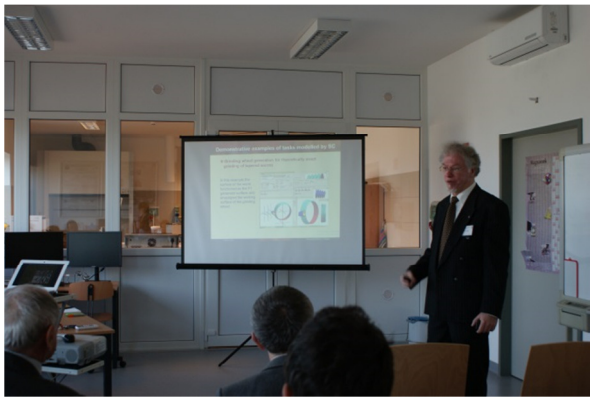

PHOTO GALLERY OF THE ISCAME 2015 AND THE EXHIBITION

THE ISCAME 2015 CONFERENCE

PHOTO GALLERY OF THE ISCAME 2015 AND THE EXHIBITION

THE 3rd MECHANICAL ENGINEERING INDUSTRIAL EXHIBITION

PHOTO GALLERY OF THE ISCAME 2015 AND THE EXHIBITION

THE 3rd MECHANICAL ENGINEERING INDUSTRIAL EXHIBITION